THE EFFECT OF THERMOPLASTIC MELT FLOW BEHAVIOUR ON THE DYNAMICS OF FIRE GROWTH

BY

JO SHERRATT
(BENG(HON), MSC, AMIMECHE)

DOCTOR OF PHILOSOPHY

UNIVERSITY OF EDINBURGH

2001

For Wend

Alice went on, "would you tell me please, which way I ought to go from here?"

"That depends a good deal on where you want to get to," said the Cat.

"I don't much care where....." said Alice.

"Then it doesn't matter which way you go" said the Cat.

".....so long as I get somewhere," Alice added as an explanation.

"Oh you're sure to do that," said the Cat, "if you only walk long enough."

(Lewis Carroll)

ABSTRACT

The UK Health & Safety Executive are responsible for advising on ways to ensure the safety of employees within the workplace. One of the main areas of concern is the potential problem of unwanted fire, and it has been identified that within the area of large-scale storage in warehouses, there is an uncertainty posed by large quantities of thermoplastic. Some forms of thermoplastic exhibit melt-flow behaviour when heated, and a large vertical array exposed to a fire may melt and ignite forming a pool fire in addition to a wall fire.

This project is largely experimental, and aimed at quantifying the effect of a growing pool fire fuelled by a melting wall on overall fire growth rate. The pool fire has been found to increase melting and burning rates, producing a much faster growing fire. It has also been found that ~ 80% of flowing and burning material will enter a potential pool fire, with only 20 – 25% of total mass loss actually burning from the original array.

During the project 400+ small-scale tests and several medium-scale experiments have been undertaken at both Edinburgh University and the HSE's Fire & Explosion Laboratory, Buxton. The experiments have confirmed the main parameters governing pool fire development are molecular weight degradation rate and mechanism, which control flow viscosity. There have also been investigations into other influences, the most significant of which was found to be flooring substrate.

These parameters then form the basis of a simple 1-D model. A semi-infinite heat transfer approximation is used to determine temperature profile through a thermoplastic exposed to its own flame flux, with extrapolated temperature dependant material properties. The derived profile is then inserted into a gravity driven flow model, to produce estimates of flow rate and quantity for plastics undergoing either random or end chain scission thermal degradation processes. The model identifies property data which are required to permit its use as a hazard assessment tool.

ACKNOWLEDGEMENTS

The author gratefully acknowledges the help and support received from the following people during the course of this research:

DOUGAL DRYSDALE

for his supervision, patience, advice and encouragement

ALAN TYLDESLEY, HSE BOOTLE,

for his support, advice and suggestions.

GRAHAM ATKINSON, HSL BUXTON,

for his help, ideas and encouragement.

DAVE BAGSHAW AND ED BELFIELD, HSL BUXTON,

for their technical support, making the larger scale experimental work possible.

KEVIN BROUGHTON & NEIL WOOD, EDINBURGH UNIVERSITY,

for their technical support and help with small & medium scale experiments

(sorry about the eyebrows Neil!)

WEND

for her proof reading, endurance, coffee supply, being there...

and for keeping the dogs distracted and me vaguely sane

MY FAMILY

for their support & putting up with the phone calls

OUR FRIENDS IN CO'PATH

in particular Sheila, Diane, Pat & Dawn

– help with Brodie & Fin, lending of scanners and time out were really appreciated

THIS WORK WAS FUNDED ENTIRELY BY THE UK HEALTH & SAFETY EXECUTIVE.

ABBREVIATIONS

ABS	*– acrylobutadiene styrene*
ADC	*– analogue digital converter*
AIT	*- automatic ignition temperature*
ASTM	*- American Society for Testing & Materials*
BP	*- British Petroleum*
BPF	*- British Plastics Federation*
BRE	*- Building Research Establishment*
BS	*- British Standard*
BSI	*- British Standard Institute*
CIMAH	*- Control of Industrial Major Accident Hazard Regulations, 1982*
CO	*- carbon monoxide*
CO_2	*- carbon dioxide*
CoG	*- centre of gravity*
COMAH	*- Control of Major Accident Hazards Regulation, 1999 (repl. CIMAH)*
CVL	*- centre vertical line*
DD	*- draft document*
DIN	*- Deutsches Institut fur Normung*
dpt	*- differential pressure transducer*
DSC	*- differential*
ECS	*- end chain scission*
EPS	*- expanded polystyrene*
EHC	*- effective heat of combustion*
EU	*- European Union*
FB	*- fire brigade*
FIGRA	*- fire growth rate (SBI terminology)*
FIT	*- flash ignition temperature*
FMRC	*- Factory Mutual Research Corporation*
FP	*- Fire Prevention Journal*
FPA	*- Fire Protection Association*
FR	*- flame retardant*

FRS	*- Fire Research Station*
Fs	*- flame spread (SBI terminology)*
FSC	*- flame spread classification (Steiner Tunnel terminology)*
FSJ	*- Fire Safety Journal*
GPC	*- gel permeation chromatography*
GRP	*- glass reinforced plastic*
HDPE	*- high density polyethylene*
HF	*- heat flux*
HSC	*- Health & Safety Commission*
HSE	*- Health & Safety Executive*
HSL	*- Health & Safety Executive Fire & Explosion Laboratory (Buxton)*
ICI	*- Imperial Chemical Industries*
IMS	*- Industrial methylated spirit*
IRI	*- ignition response index*
ISO	*- International Standards Organisation*
LCP	*- liquid crystal polymer*
LDPE	*- low density polyethylene*
LFS	*- lateral flame spread (SBI terminology)*
LLDPE	*- linear low density polyethylene*
LOI	*- limiting oxygen index*
MFI	*- melt flow index*
MGR	*- mass gain rate*
MLR, mloss	*- mass loss rate*
MW	*- molecular weight*
N_2	*- nitrogen*
NBS	*- National Bureau of Standards (now NIST)*
NFPA	*-National Fire Protection Association*
NHS	*- National Health Service*
NIST	*- National Institute for Standards & Technology*
O_2	*- oxygen*
ODE	*- ordinary differential equation*
PBT	*- polybutylene terepthalate*

PC	*- polycarbonate*
PCS	*- growth calorific potential (SBI terminology)*
PE	*- polyethylene*
PET	*- polyethylene terepthalate (polyester)*
PMMA	*- polymethylmethacrylate*
PP	*- polypropylene*
PPE	*- polyphenylene ether*
ppm	*- parts per million*
PPS	*- polyphenylene sulphide*
PS	*- polystyrene*
PTFE	*- polytetrafluoroethene*
PU	*- polyurethane*
RAPRA	*- Rubber & Plastics Research Association*
RHR	*- rate of heat release*
RS / RCS	*- random chain scission*
RSR	*- rate of smoke release*
SBI	*- single burning item test*
SEA	*- specific extinction area*
SMOGRA	*- smoke growth rate (SBI Terminology)*
SP	*- Statens Provnongsanstalt*
t_f	*- duration of flaming (SBI terminology)*
TGA	*- thermogravimetric analysis*
THR	*- total heat released*
TSP	*- total smoke produced*
TSR	*- total smoke released*
UL	*- Underwriters Laboratory*
UV	*- ultraviolet*

SYMBOLS

α	- thermal diffusivity, $k/\rho c$ (m^2/s)
χ	- combustion efficiency factor
c, c_p, c_v	- heat capacity (constant pressure or constant volume) (J/kg.K)
C_D	- discharge coefficient
D,$\varnothing$	- diameter (m)
$\delta(t)$, $S(t)$	- thermal layer thickness (m)
ε	- emissivity
$E\eta$	- activation energy (J/mol)
γ	- heat capacity ratio (c_p/c_v)
g	- gravity (9.81 m/s^2)
G	- mass flux ($kg/s.m^2$)
Δh_c	- heat of combustion (kJ/g)
k, λ	- thermal conductivity (W/mK)
L	- latent heat (kJ/kg)
Lv	- latent heat of vapourisation (kJ/kg)
m	- mass (kg)
Δm	- mass loss (SBI)
η	- viscosity (Ns/m^2)
p,P	- pressure (N/m^2)
q,Q	- heat (W)
Q_v	- flow rate
R	- universal gas constant (8.3143 J/K.mol)
ρ	- density (kg/m^3)
σ	- stress (N/m^2) or
σ	- Stefan Boltzmann constant ($5.67x10^{-8} W/m^2 K^4$)
θ	- temperature difference
ΔT	- temperature rise (SBI)
T	- temperature (K, ℃)
t, τ	- time (sec)
v,V	- volume (m^3)

TABLE OF CONTENTS

APPENDIX A

CONE CALORIMETER: THERMOPLASTIC TEST RESULTS DATABASE

EXACT SOLUTION FOR MELTING OF A SEMI INFINITE SLAB

PAPER: "THE EFFECT OF THE MELT FLOW PROCESS ON THE FIRE BEHAVIOUR OF THERMOPLASTICS" PRESENTED AT: INTERFLAM 2001 (17 – 19TH SEPTEMBER 2001, EDINBURGH CONFERENCE CENTRE, UK) PUBLISHED IN: PROCEEDINGS OF "INTERFLAM 2001 (THE 9TH INTERNATIONAL FIRE SCIENCE & ENGINEERING CONFERENCE)" INTERSCIENCE COMMUNICATIONS LTD 2001

LIST OF TABLES

CHAPTER 1

CHAPTER 2

CHAPTER 3

CHAPTER 4

CHAPTER 5

CHAPTER 6

LIST OF FIGURES

CHAPTER 1

CHAPTER 2

CHAPTER 3

CHAPTER 4

CHAPTER 5

CHAPTER 6

1 Chapter 1

1.1 Introduction

According to the UK Fire Statistics over the last five years unwanted fires have caused an average of 697 deaths each year and approximately 10,000 injuries (HMSO, 1998). Each year ~110,000 indoor fires are reported, 60 - 65% of which occur in dwellings. Associated with these fires is a cost, including building damage and loss of stock, estimated to be between £0.5 and 1 billion (Price, 1998).

To attempt to reduce these losses, researchers have been investigating fire growth and spread mechanisms to provide a scientific basis for the progression of fire safety engineering. Research has shown that rapid fire growth is dominated by upward flame spread (Magee & McAlvey, 1971). Further work found this growth rate is exponential for vertical surfaces of combustible materials of semi-infinite thickness (Alpert & Ward, 1984). Unfortunately, this [worst case] orientation is commonly encountered in warehouses and storage facilities. Storage presents particular challenges to fire safety because large quantities of combustible stock are often stored in vertical configurations separated by narrow aisles and pathways. This is widely recognised as a 'high risk' arrangement in terms of fire escalation potential (Ward, 1985, Foley, 1995).

There are several published studies looking at the hazards associated with storage fires, including problems related to vertical flame spread (Grant & Drysdale 1995). The studies provide a basis for semi-empirical mathematical models. The models are used to develop more accurate methods of predicting material behaviour in a fire scenario, providing data for use in risk assessment.

This approach is increasing in significance as the legislature moves away from the traditional prescriptive approach, towards goal setting and performance based codes. A UK framework for performance based fire safety is contained within Draft Document DD 240 (BSI, 1997), the basis of forthcoming BS 7974. When performance based codes are eventually fully adopted, complete risk assessments incorporating fire safety will be required for every project. Risk assessments are formulated by combining hazard identification with the probability of occurrence and severity of potential outcome.

The project sponsor, the UK Health & Safety Executive, (HSE), is concerned with assessing and reducing risks in the workplace to an acceptable level. A previous HSE funded study (Foley, 1995) identified that a particular material behaviour, thermoplastic melt-flow, had been largely overlooked by previous research. Understanding how melt-flow effects fire growth will greatly help in assessing the fire hazard posed by many thermoplastics.

1.2 Materials Which Exhibit Melt-flow Behaviour

There are three main polymer classifications; *thermoplastics, thermosets* and *elastomers (synthetic rubbers)*. All three types consist of small molecules, formed into larger repeating structural units of the original molecules during polymerisation reactions. If the polymerisation process produces a cross-linked structure, the result is a thermoset, which decomposes rather than melting when heated. If the molecular structure is not cross linked, the result is a thermoplastic which when heated will soften and perhaps start to melt and flow. It is the tendency to melt-flow when heated that results in this fire spread mechanism, which by definition only involves thermoplastics.

Heating above a particular temperature will cause polymers to decompose, evolving smaller volatile species. Due to the structural difference, this occurs at higher temperatures for thermosets than thermoplastics. The actual combustion of polymers is a complex process, with the possible routes illustrated in Figure 1-1 (Drysdale, 1999).

Pyrolysis is an endothermic reaction requiring sufficient energy input to dissociate the molecular bonds. Therefore, molecular composition dictates both the decomposition temperature range and mechanism.

The melt-flow behaviour is often complicated by the incorporation of various additives[1] during processing. This implies published material properties are either

[1] **Additive** – any material mixed with a polymer to modify processing or end use properties. The resulting mixture is usually called a 'plastic' to distinguish it from the base polymer. ***Common additives*** – dye, pigments, fillers, plasticisers, lubricants, UV stabilisers, anti-oxidants, flame retardants, fibres, mould release agents.

product *and* manufacturer specific, or else related to a pure polymer rather than a commercial material.

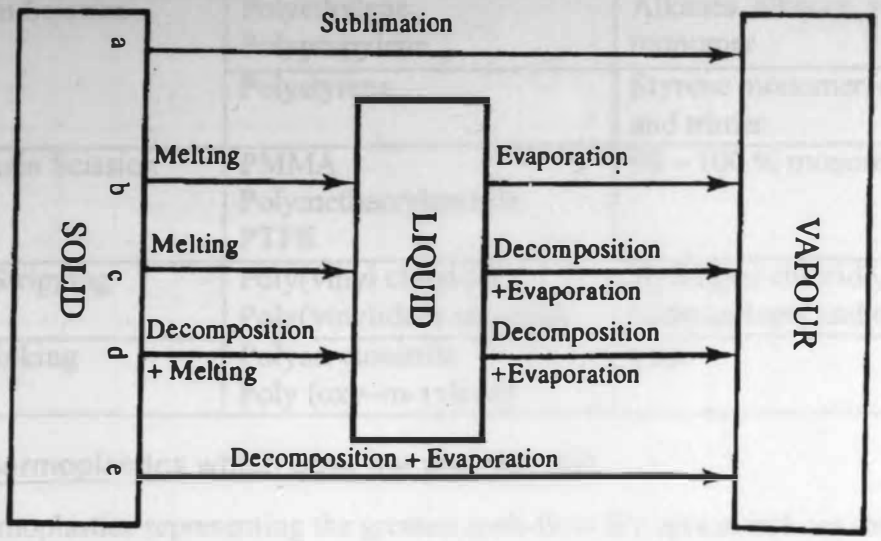

Figure 1-1. Modes of plastic thermal decomposition (Drysdale, 1999)

The thermal decomposition routes are shown in Figure 1-1. From this, route 'e' is mainly applicable to thermosets, leaving four main decomposition mechanisms for thermoplastics (Cullis & Hirschler, 1981), listed in Table 1-A. Some polymers such as PMMA undergo mainly 'unzipping' or end chain scission, (route 'a' in Figure 1-1), reversing the polymerisation process giving high yields of the original monomer. Others exhibit a mixed decomposition behaviour. The decomposition process is determined by molecular structure, but the decomposition rate is a function of other parameters including molecular weight, degree of crystallinity, amount of surface oxygen present and temperature. A polymer will generally undergo the predicted route of decomposition in a fire, although some low molecular weight polymers may melt as well as unzip.

Generally, polymers which chain strip or cross-link upon heating will form a char, and those that unzip will volatise. Therefore the only polymers which are prone to exhibit melt-flow are those which randomly decompose, or exhibit a mixed decomposition behaviour, following routes b, c, or d in Figure 1-1.

Table 1-A. Mechanisms of Thermal Decomposition of Organic Polymers (Cullis & Hirschler, 1981)

Mechanism	Polymer (examples)	Products
Random Scission	Polyethylene, Polypropylene	Alkanes, alkenes, very little monomer
	Polystyrene	Styrene monomer, dimer, and trimer
End Chain Scission	PMMA Polymethacrylonitrile PTFE	90 – 100 % monomer
Chain Stripping	Poly(vinyl chloride) Poly(vinylidene chloride)	Hydrogen chloride, aromatic hydrocarbons and char
Cross linking	Polyacrylonitrile Poly (oxy–m-xylene)	Char

1.3 Thermoplastics which pose the greatest risk

The thermoplastics representing the greatest melt-flow fire spread risk are the most widely available. In Western Europe, the quantity and type of thermoplastics consumed are shown in Table 1-B (Dufton, 1998). This clearly shows the most widely encountered commercial thermoplastics are polyethylene, polypropylene, poly (vinyl chloride) (PVC), and polystyrene.

PVC decomposes by chain stripping, and is inherently flame retarded by its halogenated molecular structure. In contrast, polyethylene, polypropylene and polystyrene all undergo random scission, which will result in melt-flow behaviour. The generic structures for these and some other commonly encountered polymers are shown in Table 1-C.

Thermoplastics are increasingly encountered inside dwellings, industrial and retail premises as well as recycling depots, as both products and packaging. The kaleidoscopic range of thermoplastic applications ensures some level of thermoplastic contribution to the fuel load of most unwanted fires. The main thermoplastic applications are illustrated in Figure 1-2, and show 35% of thermoplastics produced to be used for packaging, 23% in building construction and 11% in electric / electronic applications.

Table 1-B. Polymer consumption in Western Europe, 1997 – 2002 (Dufton, 1998)

Plastic Type	1997 '000 tonnes	Estimated growth p.a.	*1999 '000 tonnes	*2002 '000 tonnes
LDPE/LLDPE	6200	1% LDPE 6 – 7% LLDPE	6500	6900
HDPE	3850	3%	4085	4460
Polypropylene	5800	6%	6520	7760
Polystyrene	2000	2%	2080	2200
EPS	720	0 – 2%	735	780
PVC	5575	3 – 4 %	5945	6500
Acrylics	250	2 – 5%	265	290
ABS	655	2 – 3 %	690	745
Polyamides	540	4 – 5 %	590	670
Acetals	140	3 – 4%	150	165
Polycarbonate	500	7 – 8%	575	730
PC Blends	155	6 – 8%	170	220
PET	1100	15 – 20%	1520	2300
PBT & Blends	90	3 % & 6 %	100	115
Mod PPE	70	5 – 7 %	80	92
High Performance (PPS, LCP etc)	45-50	2 – 4%	60	80
Polyurethanes	2050	2 – 4%	2150	2300
Thermoset Resins				
Polyesters	450	2 – 4%	475	515
Amino's	75		80	85
Phenolics	220		225	235
Epoxy	60		65	71

** predicted volumes*

Further examination of the fire statistics (HMSO, 1998) shows an average of 323 fires annually over the past decade in premises involved in rubber and/or plastics processing, and ~110 fires per year in recycling plants. Reported fires involving plastic manufacturers are shown to be a daily event, whilst 2 or 3 fires will be expected weekly in recycling facilities across the UK. Although not comprehensive, these statistics seem to indicate the fire risk posed by thermoplastics is not constant through the product life cycle. There are further statistics (although not published) from the HSE, focusing on large fires, although the limited number investigated mean that few are of direct relevance to this study.

Table 1-C. Generic Polymer structures, (Mills, 1986)

Generic structure		Name
$\begin{bmatrix} X & & X \\ C & - & C \\ X & & X \end{bmatrix}$	X = H	Polyethylene
	X = F	PTFE
$\begin{bmatrix} H & & X \\ C & - & C \\ H & & H \end{bmatrix}$	X = CH_3	Polypropylene
	X = Cl	PVC
	X = C_6H_6	Polystyrene
	X = CN	Polyacrylonitrile
$\begin{bmatrix} H & & X \\ C & - & C \\ H & & X \end{bmatrix}$	X = Cl	Polyvinylidene chloride
	X = F	Polyvinylidene flouride
	X = CH_3	Polyisobutylene
$\begin{bmatrix} H & & X \\ C & - & C \\ H & & Y \end{bmatrix}$	X = CH_3	PMMA
	Y = $COOCH_3$	

The fire risk posed by thermoplastics is difficult to quantify further only from the literature. As already noted, a variety of thermoplastics are commercially available, incorporating any number and combination of possible additives. The additives are incorporated to fulfil a specific end use or processing requirement and often affect the decomposition behaviour of the thermoplastic. To compound this further, commercial sensitivity usually prevents manufacturers from providing the exact composition of a product.

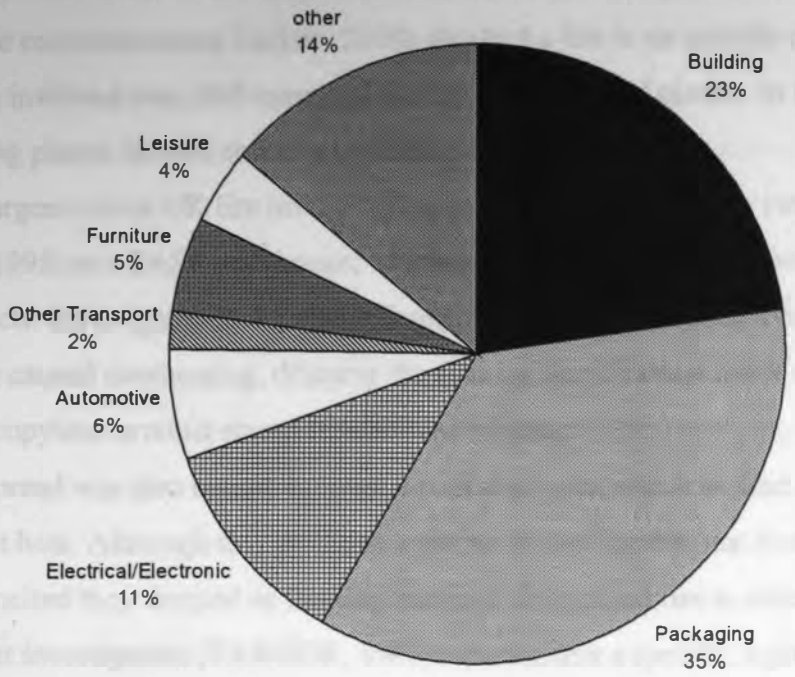

Figure 1-2. Thermoplastic usage by application in the UK (BPF, 2000)

Having overviewed the materials and mechanisms involved, there are several published fire reports, quoting melt-flow behaviour as a contributory mechanism to escalation and fire spread. Some of these are summarised in the following section.

1.4 Some large fires involving melt-flow as a contributor to fire spread

'*Polypipes*' (FP No 238; private communication Wilson, 2000)' suffered a fire in 1999, in a 4550 m^2 storage yard, containing polyethylene and PVC pipes stacked between 2 and 6m high, causing £750k of damage. Burning molten plastic flowed and spread the fire across the stock stored in the yard. Further damage was caused during the post incident clean up - the molten material had become embedded in the asphalt floor, which was pulled up along with the plastic residue.

Two years previously, '*Integral Ltd.*' endured a fire in an outdoor storage area, heavily loaded with polyethylene piping stored on timber drums and pallets (private communication Lamb, 1997). Escalation was caused by piping liquefying, spreading fire beneath other pallets aided by the lack of separation measures. Six months prior

to this, *Milton Keynes Borough Council Recycling Facility* (Bucks F&RS, 1997; private communication Tucker, 2000) also had a fire in an outside storage area, which involved over 500 tonnes of closely piled bales of plastic. In this case, molten burning plastic flowed and blocked drains as it solidified.

The largest recent UK fire involving thermoplastics happened in 1995 (FP No 288; Fire, 1995) at a BASF warehouse, which stored 11,000 tonnes of polypropylene products. Investigation (Cleveland County FB, 1997) concluded a failure in a light fitting caused overheating, dripping the flaming acrylic sheet cover onto the polypropylene product stored beneath and igniting it.

Fire spread was also caused by plastic roof skylights, which melted upon exposure to radiant heat. Although this provided a means of venting the heat from the fire, as they melted they dripped as flaming material, and spread fire to other areas.

Further investigation (TARGOR, 1997) reported that a specific light fitting could develop a fault, producing enough heat to ignite the acrylic cover without blowing the fuse, as the electrical gear train was in direct contact with the cover. Further tests showed that a match could readily ignite the acrylic cover, which would fall as flaming molten droplets, presenting a potential flame spread mechanism.

NB. This hypothesis for explaining the ignition source and flame spread mechanism is disputed (Discussion with Dr Tyldesley & Dr Atkinson, HSL, 1999)

There were several other factors contributing to escalation, for example;

- The previous occupant of the building had a safety monitoring policy, where staff walked through the warehouse hourly, (discontinued by BASF).
- A fire door was left propped open as normal practice for forklift truck access.
- Since the storage area was perceived as 'low risk' by the occupier, there had been no formal risk assessment carried out. Consequently, there was no established inventory of contents, which would have helped the authorities dealing with the incident.

Other thermoplastic-fuelled fires include;

Cressdale Ltd a single storey factory storing a large quantity of polystyrene containers and packaging (private communication Jones, 2000). The building was steel framed, with brick clad walls. During the fire, thermal expansion of the steelwork caused the walls to collapse. Prior to fire brigade arrival flames broke

through the factory roof (corrugated steel with plastic skylights), which collapsed soon after. Escalation was due to a combination of combustible stock and the time delay in discovering and reporting the deliberately started fire.

At a *Plastics Recycling Plant* (FP No 247) an open sided site was used to store plastic products prior to recycling. About 1000 tonnes of mixed plastics, piled in rows up to 4.5m high were ignited. Prior to this other small fires had been started, and the local fire prevention officer had become concerned with the amount of plastic stored, and the lack of water supplies to the area.

After the fire started, burning molten plastic prevented the movement of other plastic and machinery from the area by rapidly bonding everything together. The flow of material also spread flame and created difficulty for the fire brigade to access the fire with hoses. High stacks with narrow gangways also restricted access to the fire. Toxic gases from the incident combined with the weather created further problems, by forming a smoke containing hydrogen chloride. The rain falling onto the area was then contaminated, which when combined with the smoke forced withdrawal of Brigade personnel from the site. This allowed the fire to grow further until weather conditions had improved and operations could resume.

A *plastic products factory* (FP No 247) in Nottinghamshire, suffered a large fire. The factory stored around 1600 tonnes of polyethylene outside in piles up to 4m high. Post-incident work estimated that the fire had begun at least an hour before the fire brigade was called, and it was well established by the time of their arrival. Materials were also stored piled against factory walls, baled in plastic sheeting which was impervious to water, but allowed fire spread beneath the bales. Of the materials stored there were a wide range of products, with over a hundred 45 gallon [2] drums of flammable liquids and two 800 gallon tanks of diesel sited close to the premises. The drums were distributed amongst various unidentified plastics with no firebreaks. Further fire spread (private communication Sisson, 2000) was caused by rivers of burning molten plastic, which forced the fire brigade to create ladder bridges across the 'rivers'. Burning plastic granules had burst from the bales and floated along the

[2] 1 gallon = 4.54609 dm^3 (Kaye & Laby, 1975)

run off water, spreading flame in other directions. Molten plastic then blocked the drains.

A *Derbyshire injection moulders* (FP No 215) suffered a fire in 1988, in a sprinkler protected finished goods warehouse, which escalated out of control due to stock overloading. Gangways in the warehouse were restricted by stored goods, preventing access for the fire brigade.

This sample of reported fires shows that polyethylene, polypropylene, PVC and polystyrene are common fuels, which is predictable since, as shown in Figure 1-2, they have the largest commercial volumes. There are several factors contributing to fire spread, some are applicable to many storage facilities, such as large undivided quantities with extensive vertical surfaces, and breached or overridden fire protection, such as fire doors left open. There are other factors highlighted related to melt-flow, e.g.;

- burning rivers of plastic restricting fire fighting access,
- flaming material flowing beneath surrounding pallets, igniting them
- flaming thermoplastic floating on runoff water, spreading fire
- radiant heat melting & igniting skylights away from the main seat of fire, possibly creating fire seats in other areas
- molten material resolidifying & blocking drains

Generally, from the survey of fire incident reports, melt-flow is reported as only one of many contributors to fire spread, and there is little detail of the extent of escalation directly resulting from melt-flow.

There seem to be several components effecting the fire development process. After ignition, fire growth is initially slow, with material softening, and perhaps some extensional flow occurring. This may lead to flow or drips onto the floor or material below the burning region. If the fire grows, and local surface and ambient temperatures increase, the material at the base of the fire may start to burn as a pool, supplying an additional flux to the material feeding it. This material could then exhibit surface flow, or possibly (depending on the geometry and loading conditions)

the plastic may soften, and the array structurally collapse, with either mechanism leading to an increase in pool (and potentially burning) area. The pattern of fire growth is complex and dependant on all of these interlinked parameters, with the dominant factor perhaps changing over the fire development.

1.5 Project Objective

Investigation reports and published articles such as those referred to above are written from observations. Although there seems to be consensus that melt-flow often increases fire spread, there is no firm detail of exactly how the melt-flow mechanism effects the dynamics of fire growth. The purpose of this study, is therefore to research the following question:

If a burning vertical array of thermoplastic melts and flows, a larger burning surface area will result than that presented by the array alone. This enlarged burning area may increase the rate of burning, due to the increased level of heat flux supplied to the extended surface area.

Does this mechanism create a feedback loop, where the array melts to supply fuel to the burning pool, which increases the heat supply to the wall, increasing the rate of melting and resultant fire growth?

The next chapter is an assessment of the current level of understanding and hazard assessment techniques used at present to quantify the risk posed by melt-flow thermoplastics.

2 Current awareness of the melt-flow effect on fire growth

After looking at some fires reported as influenced by the melt-flow process, this chapter is an investigation of how the melt-flow fire spread problem has been quantified to date. It is divided into two parts; previous experimental work related to thermoplastic melt-flow behaviour, and the 'standard' test methods available to measure some aspect of the fire hazard posed by materials including thermoplastics.

2.1 Current knowledge of fire behaviour of melting plastics

Thermoplastics exhibit differing patterns of flame spread and burning rate, depending on their degradation mechanism, which determines their behaviour upon heating. However the melt-flow effect on fire behaviour has not been accurately quantified, mainly due to experimental difficulties and a lack of appropriate measuring techniques.

Several studies relating to the effect of melt-flow on potential fire hazard for various thermoplastic commodities have been found, the most relevant of which are outlined below.

2.1.1 Wall Lining Panels

Zhang et al, at the University of Ulster (Zhang, 1997) conducted a study of the behaviour of 0.8m x 2.2m x 3mm thick commercially available sheets of PMMA and polypropylene. The sheets were screwed onto vertical plasterboard backing and ignited by BS 5852 (BSI, 1979) No 7 wooden cribs. Zhang observed that the polypropylene melted whilst the PMMA did not, resulting in differing flame spread patterns.

For the polypropylene panel, after ignition the area of the surface undergoing combustion was localised, with a small fire growing slowly from the panel base, where molten polymer was feeding a growing pool fire. It was observed that the size of the flame from the pool fire controlled the flame spread on the panel, and also that flame height from the pool was a function of pool area, resulting from molten polymer flow from the vertical sheet. For this experiment, the maximum height of flame on the sheet from the pool was around 1m, and the pool fire lasted for 55 minutes.

In comparison, the sheet of PMMA established surface flaming and rapid upward flame spread after ignition, covering the entire sheet within 7 minutes after ignition. The total bum lasted a further 7 minutes, with the panel softening, distorting and bubbling, but not dripping or flowing. For this test, the flame spread was driven by the attached vertical surface flame plume, and was much faster than that observed for the polypropylene panel.

Zhang noted similarities between the upward flame spread behaviour of the PMMA panel and cellulosic vertical burning behaviour, except for the lack of char formation with PMMA. This led to the conclusion that melt-flow behaviour significantly effects burning behaviour, particularly in upward flame spread mode.

2.1.2 Milk Crates

The burning behaviour of stacked milk crates was investigated qualitatively by the 'Western Australian Arson Squad' (private communication DeHaan, 2000) in January 1994. The test was performed outdoors on an extremely windy day, and since no measurements were taken, is useful only as an observational study. The filmed test involved an array of 40 crates, stacked in an array 2 x 2 x 10 high against a steel wall. A small horizontal section was ignited with a standard disposable cigarette lighter. (Ignition was achieved in around 2 ½ minutes, prolonged due to the wind continually extinguishing the lighter flame!).

Immediately after ignition, the flame was localised around a horizontal bar approximately 25mm wide, with the first non-burning black drip recorded 3 min 20 sec after ignition. The dripping started at a frequency of around 0.33Hz, and accelerated rapidly over the next 40 seconds, at which time the original ignition area had dripped and burned away. This left two burning sites either side of the original area, which began to spread flame slowly upwards through the adjoining vertical members. The upright sections had disappeared in around 90 seconds, leaving established flame on five adjoining sites. Thirty seconds after this, the droplets were flaming as they fell.

Ten minutes after ignition, 2 or 3 m from the array a small amount of flame was visible. Within thirty seconds of visible flaming being noted, rapid upward flame spread covered the crates above the ignition zone with orange flame. Twenty seconds later, the stack toppled, falling outwards from the array. The flame height instantly

reduced to approximately double the height of one crate, and some of the fallen crates gradually softened and melted to form a pool fire. Every crate was involved by fifteen minutes after ignition, producing copious amounts of thick black smoke. Burnout finally occurred 25 minutes after ignition.

2.1.3 Stacking Chairs

A 1979 BRE report (Woolley, 1979), gave the results of full-scale compartment fire tests assessing the ignition and burning behaviour of 24 different types of stackable chairs, as described in Table 2-A. Stackable chairs individually carry a low fire load in terms of the quantity of flammable material present. However in places of assembly, the amount of chairs stacked together can total 5000 or more, representing a significant fire load, measurable in tonnes. In addition the geometry of the stack increases the fire hazard over that predicted by combining the hazards posed by individual chairs.

The chairs in the 1979 study comprised a moulded shell on a metal frame, as commonly found where a large amount of seating is required. The investigation aimed to assess the hazards introduced by stacking chairs together.

The chair compositions as shown in Table 2-A, were polypropylene, nylon, ABS, polyphenylene oxide, PVC, beech plywood and polycarbonate, plus flame-retardant versions of polypropylene and ABS.

For the tests, single chairs were exposed to a series of increasing intensity flaming ignition sources, from a match (source No 1) to an equivalent of 4 double sheets of newsprint (source No 7) to determine ease of ignition. The ignition sources, taken from BS 5852 are detailed in Table 2-B.

A single chair was then exposed to a No 7 source inside a 3 x 3m x 2.4m high compartment with a 2.4 x 0.7m vent. Thermocouples positioned 150mm below the ceiling measured temperature, and optical density and rate of smoke production, along with CO and CO_2 concentrations were also recorded.

Table 2-A. BRE Study Chair Material & Ignition Test Result (for single chair)

Chair Type	Material	Ignition Rating***
1*	Polypropylene	0(B)
2	Polypropylene	2(B)
3	Polypropylene	0(B)
4	Polypropylene + 5% DBBE/AT	0(B)
5	Polypropylene + 5% DBBE/AT	0(B)
6	Polypropylene + 10% DBBE/AT	0(B)
7	Polypropylene + 10% DBBE/AT	0(B)
8	Polypropylene + 10% DBBE/AT	0(B)
9	Polypropylene + DBBE/AT	0(B)
10	Polypropylene + DBBE/AT	0(B)
11	Polypropylene + DBBE/AT	6(B) (Min Rating)
12	Polypropylene + DBBE/AT	6(B) (Min Rating)
13	Polypropylene + unknown additive	0(B)
14	Polypropylene + 20% asbestos + DBBE/AT	1
15	Polypropylene + 40% asbestos	0
16	Nylon	6(B) (Min Rating)
17	Nylon	6(B) (Min Rating)
18**	ABS	0(B)
19**	ABS + DBBE/AT	6(B) (Min Rating)
20**	ABS + DBBE/AT	5(B)
21	Polyphenylene oxide	5
22*	PVC	6 (Min Rating)
23*	Beech Plywood	6 (Min Rating)
24	Polycarbonate with glass fibre reinforcement and some DBBE	6(B) (Min Rating)

**Single back & seat; ** chair shell moulded from ABS, supported on metal frame all other chairs – moulded shell supported on a metal frame*

DBBE Decabromobiphenylether; AT Antimony Trioxide;

(B) burning droplets

****Ignition rating: a numerical index where 1 implies the chair survived ignition source 1 but failed ignition source 2 and so on, with a zero implying failure to ignition source 1. Failure to ignite with ignition source 6 registered a minimum rating required.*

Following this, six of the chair types were then tested stacked six high with a chair either side of the stack inside the compartment. The stack was ignited with a No 7 crib beneath it, and parameters measured as outlined above.

Table 2-B. Ignition sources used in stacking chair tests (BSI, 1979)

Ignition source No	Type	Weight or volume	size (mm)	Ignited by	application time (min)	calc energy output (kJ)
1	candle	0.17g	-	match	2	7
2	IMS in tray	2 ml	30 x 30 x 15	match onto IMS in tray	B/O	47
3	IMS in tray	5 ml	50 x 50 x 15	match onto IMS in tray	B/O	117
4	wooden crib	9g	10 sticks 6.5 x 6.5 x 40	match on wood wool packing	B/O	165
5	wooden crib	17g	20 sticks 6.5 x 6.5 x 40	match on wood wool packing	B/O	313
6	wooden crib	60g	10 sticks 12.5 x 12.5 x 80	match on wood wool packing	B/O	1100
7	wooden crib	120g	20 sticks 12.5 x 12.5 x 80	match on wood wool packing	B/O	2200

IMS – industrial methylated spirit; B/O – applied until burnout

2.1.3.1 Ignition Resistance

Polypropylene chairs were the easiest to ignite, and burned with a continuous flow of burning droplets. Nylon proved harder to ignite, but melted with all ignition sources, producing burning droplets when exposed to a No 6 ignition source. ABS ignited easily and produced burning drops, although the flame-retardant version was much harder to ignite, resisting ignition when exposed to a No 6 source. The other chairs all proved difficult to ignite individually, with only polycarbonate producing burning drops when exposed to a No 3 source or above.

Flame-retardant treatments moderated the burning behaviour of the polypropylene chairs. The overall size and structure of the seat were also significant parameters

affecting ignition resistance, particularly the size of the hole in the rear of the seat. This is where dripping often originated, and also the location from which fuel was fed onto the ignition source.

Chairs with a separate back and seat generally burned only the seat unless an intense fire was produced, whereby the back became involved.

As single chairs, the polypropylene versions, with the exception of the asbestos filled type, all demonstrated burning molten droplets, with the flame-retardant versions reducing burning severity. The asbestos filler reduced the amount of polymer in the blend and also held it in place reducing the amount of dripping.

The most smoke produced in any test was shown by untreated ABS.

2.1.3.2 Burning behaviour of stacks

The stacked tests showed that some of the chairs gave rise to severe fires, producing copious amounts of smoke and toxic gases. The standard polypropylene chair stack transferred flame to the two adjacent chairs 6 minutes after ignition, producing a maximum room temperature of 1073 K in 9 minutes. The stack underwent substantial melting, forming a pool of burning liquid beneath the chairs which increased fire intensity.

The test was then repeated above a foam backed nylon carpet, whereby the pool of burning polymer combined with the carpet increasing room temperature to over 1173K, and dramatically increased the smoke yield. The flame-retardant polypropylene stack did not burn to any appreciable extent.

The other stacks showed varying behaviour. Nylon chairs were damaged on the base by the ignition source and melted, but didn't spread flame, whereas polyphenylene oxide chairs burned, producing a maximum temperature of 643 K, igniting one of the adjacent chairs after 6 minutes.

The beechwood chairs burned fiercely registering 671 K at 10 minutes, and ignited the adjacent chairs at 12 minutes, but produced much less smoke than the standard polypropylene stack.

NB the total load (kg) of combustible material is much greater for the wooden chairs than the polypropylene. In contrast, the heat of combustion (MJ/kg) is less for beech

(19.5) than for the other materials: e.g. PC = 29.7; PP = 43.3; Nylon = 29.6, ABS = 36 (Drysdale, 1999).

The polycarbonate versions showed melting and damage on the bottom chair in the stack positioned directly above the ignition source, but showed only a small total extent of burning.

The report concludes that most of the polypropylene chairs tested (including flame-retardant versions) ignited easily, with some flame-retardant treatments slightly improving ignition resistance. Nylon, flame-retardant ABS, polyphenylene oxide, PVC, polycarbonate and beech plywood chairs were all difficult to ignite.

Finally, it was found that the burning behaviour of the stack was not always predictable from observation of a single chair. Stack design, specifically the size and location of gaps in a chair, spacing between chairs, shape and edge effects were found to effect burning behaviour leading to a recommendation for further study.

A subsequent study (Paul, 1980) evaluated the role of thermoplastic softening on fire growth, mainly with regard to stacked chairs. A test rig was developed, which held 7 sheets of 300 x 300 x 3 mm test material horizontally in a rack, with ~50mm between each sheet. The rig simulated horizontally stacked seat panels. Thermocouples were located between the sheets to monitor stack and smoke temperatures during a burn, with the ignition source placed beneath the base sheet in the rack.

The materials tested are shown in Table 2-C.

Paul found the flame-spread mechanism for the melt-flow thermoplastics tested, was the base sheet softening, opening in the centre above the ignition source. This allowed flames to pass through the hole, contacting the next sheet. The softened material from the lower sheet forms a 'curtain' around the flame, creating a chimney. This effect became marked as more sheets become involved, resulting in rapid fire growth. The curtain also flowed into the original fire source, increasing the flame size and severity of the floor fire.

In contrast, the wooden sheets were ignited on the underside of the base sheet, and the resultant flames spread to the edge of the sheet and upward on the outside of the stack. This ignites the other sheet edges, leading to pyrolysis of the sheets and flame spread inwards. A similar mechanism was also initially noted for the glass mat/polypropylene laminate, although as flame and heat generation increased, molten

polymer flowed through the glass mat web and the edge ignition propagation changed to flashing ignition, with flames passing through the open webbing of the mat. The asbestos reinforced polypropylene behaved similarly to plywood, with the asbestos forming a 'felt' holding the polymer in position and physically preventing flame penetration through the sheets.

Table 2-C. Materials tested in Paul's study (all at 3mm thickness)

Polypropylene: unmodified extrusion and moulding grades
Polypropylene (flame-retardant): LOI 26 UL94 V1 and U2 grades
Polypropylene/ glass mat compression moulded laminate
Polypropylene/glass ballotini[3] (40%)
Polypropylene/ glass fibre (40%)
Polypropylene/asbestos fibre: flame-retardant, asbestos fibre LOI UL94 VO grade
Polycarbonate: sheet and moulding grades
Polycarbonate flame-retardant sheet grade
Polystyrene: high impact
Polymethylmethacrylate
GRP standard resin, chopped glass mat, 2: 1
Hardboard: standard grade
Plywood: 5ply laminate

The effect of softening was then further investigated by exposing horizontal sheets, supported around the outer edge, to a predetermined level of heat flux on one side. A hemispherical follower contacted the sheet, coupled to a dial gauge for small deflections and an indicating slide for large deflections, which were measured and recorded. The values of applied flux were increased until either the follower passed through the sample, or the sample ignited.

It was found that polystyrene and polypropylene softened at low flux levels with rapid distortion. Polycarbonate behaved similarly but required higher fluxes to

[3] glass ballotini: small glass spheres

soften, whilst PMMA exhibited a two stage pattern of behaviour, initially softening and remaining in a rubber like state until relatively high fluxes, when the follower penetrated the specimen.

The effect of fillers and fibrous additives with polypropylene was to increase the softening point without altering the basic deflection characteristics. However, with the glass mat laminate, the mat remained in place supporting the follower, whilst the polymer flowed away. Asbestos fibre reinforced polypropylene gave an initial deflection which remained constant and finally self ignited.

From the study, an approximate linear correlation was found between the mean softening point and time to burn to the top of the stack, reproduced in Figure 2-1.

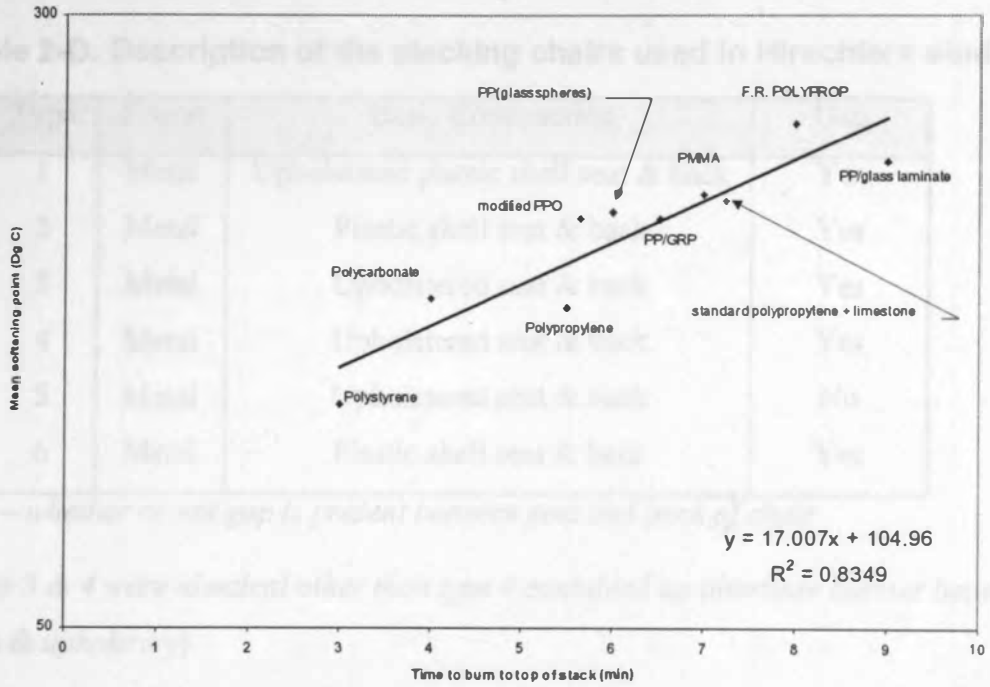

Figure 2-1. Correlation between softening point and burn rate of a stack (Paul, 1980)

This led to the conclusion that the fire behaviour of some thermoplastic sheets is largely dependent upon their softening characteristics. The softening characteristics are in turn, a function of decomposition and heat transfer through the bulk mechanisms. It is also apparent that the form of an additive within the thermoplastic structure can effect the softening behaviour and fire propagation mechanism.

These studies lead to the development of a standard test, ASTM E1822 which was evaluated, with the results for six types of commercial chair, as described in Table 2-D, published in 1997 by Hirschler (Hirschler, 1997).

A vertical stack of five chairs in one of three possible configurations is placed on a load cell. The stack is exposed to flames from a propane gas burner at 12 l.min^{-1} for 80 seconds, and the rate of heat release measured. The three configurations are;

(a) in a test room 2.4 x 3.7m x 2.4m high;

(b) in a test room 3.7 x 3.1m x 2.4m high; and

(c) below a hood.

Table 2-D. Description of the stacking chairs used in Hirschlers study.

Type	Frame	Basic Construction	Gap
1	Metal	Upholstered plastic shell seat & back	Yes
2	Metal	Plastic shell seat & back	Yes
3	Metal	Upholstered seat & back	Yes
4	Metal	Upholstered seat & back	Yes
5	Metal	Upholstered seat & back	No
6	Metal	Plastic shell seat & back	Yes

Gap – whether or not gap is present between seat and back of chair

(*types 3 & 4 were identical other than type 4 contained an interliner barrier between foam & upholstery*)

Over the duration of the test, peak rate and total heat release, peak rate and total smoke released, mass loss, and time to peak rate of heat release are measured. The sample frequency was 0.167Hz, and the test results are shown in Table 2-E.

From Table 2-E, the peak rate of heat release for the stacks ranged from below 300 kW to > 1 MW, with the chairs losing between 4 and 40 % of their original mass during the test. Of the six stacks tested only the Type 4 stacks consistently failed to produce flashover when tested in configuration (a) or (b). Use of the room tests also

showed that re-radiation from the upper part of the room is an important factor for stacks releasing a large amount of heat in a short time.

Table 2-E. Results of Hirschler's stacked chair tests (Hirschler, 1997)

Stack / Test	Mass kg	RHR kW	THR MJ	RSR m^2/s	TSR m^2	mloss kg	t peak minutes
1/a	55.74	982	39	12.6	678	1.41	6.1
1/b	54.79	1624	110	13	1377	3.98	11
1/c	55.49	1602	81	13.2	923	1.81	9.9
2/a	32.35	714	269	5.1	1679	5.74	9
2/b	32.61	661	270	4.5	2066	6.1	7.5
2/c	31.5	1057	288	5.9	1760	4.94	5.6
3/a	30.04	1089	101	2.7	818	5.04	10.1
3/b	30.24	567	303	1.7	734	12.10	12.8
3/c	29.74	603	320	1.2	799	13.15	9.1
4/a	30.44	278	324	0.9	689	12.88	29.5
4/b	30.74	323	339	1.2	1128	13.52	17.5
4/c	30.19	258	321	0.7	1032	12.75	22.2
5/a	42.32	1048	366	3	769	19.78	14.9
5/b	41.49	1082	296	1.8	525	15.16	13.9
5/c	39.70	942	237	1.9	617	14.61	13.3
6/a	36.74	1150	300	7.4	2074	7.58	7.5
6/b	37.29	1099	314	8.2	2425	7.24	9.5
6/c	36.67	963	291	7.5	2255	7.37	7.3

Poor correlations were found between heat and smoke release rates and also mass loss and heat release. The lack of correlation between mass loss and heat release rate indicates that the heterogeneous composition of the chairs produces variations in the

effective heat of combustion (EHC[4]) through the test, and for this reason the EHC values are not tabulated.

The overall conclusion is that in over half of the tests, the heat release rate was great enough to cause flashover in any room in which the stack had been placed. Therefore the potential fire hazard of stacked chairs is high.

2.1.4 Wheelie Bin

A burning polypropylene 'wheelie bin' was the subject of a 1998 investigation undertaken in a Californian car park (private communication DeHaan, 2000). Some crumpled newspaper was ignited inside the bin, and the lid propped open by a piece of wood. Some white smoke was observed after a minute, presumably from the newspaper, followed thirty seconds later by visible blistering on a small area of the side of the bin.

Some ten minutes later, distortion and a colour change of the bin from blue to blue/white could clearly be seen at the base. A small amount of flame burned through the material twelve minutes after ignition. Due to the distortion at the base, the bin lost its geometrical rigidity and slumped forwards onto the ground. The smoke turned black at this point, and within a minute the flame height had grown to be visible from a distance. There was no rapid flame spread into the solid area of the slumped bin, which gradually softened, and melted into a liquid pool.

Sixteen minutes after ignition, a slow moving burning river of molten polymer was evident, and 90 seconds later there was no discernible solid material other than the rubber wheels remaining. The flaming pool area began to recede approximately two minutes later, burning out completely 25 minutes after ignition.

---

[4] $EHC = \left(\frac{\dot{q}}{-\frac{dm}{dt}} \right)$

2.1.5 Computer Tapes

Harwell Laboratory conducted some tests in 1988 (Hiles 1989) to investigate the effectiveness of smoke detectors in computing environments. Reported in Fire Prevention, they found that the layout and equipment found in some rooms rendered optical beam smoke detectors ineffective due to patterns of air turbulence created, which lead them to further investigate the potential hazard posed by storage of computer tapes. A fire test on 1000 open reel computer tapes, made from polyethylene terepthalate and encased in a polycarbonate shell, was conducted in a disused 12 x 12 x 4.5 m high building.

The concrete and brick building was provided with high level windows on three sides, a door and two low level openings, deemed to be representative of an air conditioned storage area. The tapes were stored in three high level racks, with ignition achieved by using a match to light a small amount of combustible debris at the foot of one rack.

Rapid fire growth was observed, with the first rack becoming flame engulfed fairly quickly. The plastic tape cases melted, with drops, progressing to streams of burning plastic falling to the floor and creating blazing puddles, spreading the fire. Little smoke was observed at this stage, with flames at ceiling height, although 5 minutes later thick black acrid smoke was noted, with the smoke layer filling the room to within 30cm of the floor within 3 minutes.

Structural damage to the building was observed with expanding steelwork pushing out the walls and concrete spalling in the roof, leading to a decision to abort the test fifteen minutes after ignition. Two fire fighters tackled the blaze with water spray, which washed the air of the smoke, after which the fire increased in intensity.

The burning racks could be observed with the smoke reduced, and it was noted that the catches holding the racks had burned out, allowing the tapes to fall on the floor, spreading the area of firebase.

High expansion foam was then used to extinguish the fire, but 8 minutes later it re-ignited, and took a further ninety minutes to completely extinguish. Examination of the debris showed that when the soft molten plastic outer shell contacted either foam or water, it solidified into a waterproof shell, protecting any flaming beneath it.

2.1.6 'Polyblock' Scaffolding

This is an expanded polystyrene block scaffolding system, identified as a potential fire hazard by the UK HSE, and tested in 1995 (Atkinson, 1995). The system provides a platform of 1.3 – 2.5m heights, covered in plywood decking and scaffolding boards for use in fitting out operations.

The reasons for HSE interest in this material were that:

- The decking forms a low roof, with potential for smoke logging and rapid fire development beneath it.
- Large quantities of polystyrene foam are present, with potential routes for fire spread through the system

The samples tested were 1300 x 600 x 600 mm, mass 11.2 kg, and consisted of an expanded polystyrene block covered with 2.5mm thick polypropylene.

It was found that the material (tested on a concrete floor) ignited easily with a match or a blowlamp. After ignition, fire spread vertically and horizontally on the cover with pronounced melting and dripping. A pool of molten polymer was observed to form on the floor near the point of ignition, with the foam regressing from the flame creating a cavity in the block, into which the pool spread. After 9 minutes, a rapid increase in burning rate and flame spread led to complete flame engulfment of the block, which rapidly melted down into the pool.

Atkinson concludes that after ignition, for some 5 – 8 minutes, the fire is small enough to be easily tackled by a hand held extinguisher, although may be difficult to detect. After this period, there is rapidly accelerating burning, which will produce strong flame impingement on other blocks and the decking above. The growth period from small, localised flames to strong impingement on the ceiling was approximately 100 seconds, with corresponding rapid smoke logging of the area.

These findings lead to 'Polyblock' being withdrawn from the market due to the level of fire hazard being considered unacceptable by the HSE.

2.1.7 Plastic Bottles (Containing Flammable Liquids)

The Swedish National Testing & Research Institute (SP) presented a paper at Interflam 99 (Milovancevic, 1999) looking at sprinkler protection of plastic bottles storing petrol or alcohol. Petroleum products are sold in thin polyethylene

terepthalate (PET) bottles, with alcohol based products in thicker walled polyethylene bottles. The fire behaviour of the two bottles differs, with PET shrinking on exposure to heat and polyethylene undergoing melt-flow.
Heating has been found to result in concurrent expansion of the flammable liquid, and shrinking of the PET bottle resulting in a build up of internal pressure. This causes cracks around the bottle cap and liquid sprays from the cracks up to 4m radius from the bottle. These sprays are easily ignited.
In contrast, the polyethylene bottle softens, forming a bubble just above the internal liquid surface. The bubble bursts to form a hole, acting as pressure relief for the expanding liquid, although the vapour from the liquid can ignite around the bottleneck.
Therefore the packaging material can effect the fire hazard posed by the product.

2.1.8 Polyethylene Pallets

The Loss Prevention Council undertook some tests in 1999 (Fire Engineers Journal, Nov 2000), where they ignited an array of four HPDE storage pallets, loaded with three levels of empty oil drums. The test was repeated with standard wooden pallets for comparison. It was found that when the ignition source had burned out, the wooden pallets did not sustain the fire. In contrast, after 7 ½ minutes, the entire stack of plastic pallets were burning, resulting in collapse of the stack. Ignition tests found the pallets could be ignited by exposure to a cigarette lighter for < 30 seconds, and once lit, a single pallet would sustain fire growth. Flames then spread laterally to consume the pallet and a pool fire was formed at the base of the array.

2.2 Comment

It is apparent from some of the product tests described above, that softening and loss of rigidity are important factors in fire growth. Softening temperature is reached before the thermoplastic liquefies, and structural collapse into the resulting pool fire is an important additional feeding mechanism governing pool size, in addition to the gravity driven flow of molten material. The collapse mechanism is a function of factors including chemistry, geometry, thermoplastic wall thickness, load level and distribution through the stack, as well as rate of heat transfer into the actual material.

Therefore, the softening mechanism effect on pool size will not be observed during a small-scale test, and is likely to prove difficult to scale.
However, the gravity driven, downward flow pool feeding mechanism is measurable, and the next stage of this chapter is to investigate test methods available for looking at this.

2.3 Existing Fire Test Methods for Plastics

In terms of thermoplastic fire behaviour, since plastics always burn in a fully developed fire, only behaviour in the growth stages, prior to flashover[5] need be considered in a hazard assessment. This can be subdivided into several parts: ignition, flame spread, heat release and contribution to flashover, along with other parameters including smoke, toxicity and corrosivity of combustion products (Troitzsch, 1990).
There are numerous test methods available, which aim to assess some flammability characteristic of a specimen, which although varied in approach, generally fall into two main categories;

Flammability Tests – these are further subdivided into:

standard fire tests which monitor the response of a specimen during a test, but give only a ranking order; and

reaction to fire tests which attempt to determine parameters such as ignitability, rate of heat release and smoke production potential of a specimen, resulting in data capable of further analysis.

Fire Resistance Tests – these are usually performed on physical barriers to fire and load bearing elements such as doors or walls respectively, to establish load bearing capability during fire and any contribution made to reducing fire spread.
Since this thesis is concerned with a specific type of material behaviour, the latter class of fire tests is not considered relevant, and is mentioned only for completeness

[5] "Flashover" – the transition from a localised fire to the general conflagration within the compartment when all fuel surfaces are burning. (Drysdale, 1999)

2.3.1 Current Flammability Tests

A flammability test is generally carried out on a material in order to determine its behaviour under defined conditions. The two main types of test are developed either as a result of discussion by a committee, or (more recently) designed along more scientific principles. The standard tests are focused on achieving reproducible and repeatable results, confirming a specimen meets certain criteria, and generally produce either ranking orders or a pass/fail grading. These tests suffer from a high apparatus dependency. In comparison, the 'scientific' reaction to fire tests, are intended to produce quantifiable parameters for further use in risk assessments. The relative advantages of these methods tend to be low cost and simplicity for the first type, which are often used during product development, whilst the latter produces more detailed information, valuable in understanding specimen behaviour in different fire scenarios.

The traditional legislative 'prescriptive' approach to fire safety was a direct result of the sole availability of tests designed to produce ranking orders. The problem with these tests is that they are usually not related to material behaviour in an actual fire. This problem was highlighted in the 1970's, following some high life loss fires, where rapid fire growth was largely attributed to rigid PU foam being used as a wall covering. The foam passed the standard 'Steiner Tunnel' Test (ASTM 84-84a) for wall covering materials, as the hot combustion products from the impinging gas flame caused the foam to char, releasing vapours without igniting them. This behaviour prevents flame spread along the tunnel, and the material therefore receives a low flame spread rating.

The tendency of the drips to continue burning on the floor below does not effect the test result, and the foam was therefore accepted for use as a wall covering. The tunnel test specification is outlined in Table 2-F. A Federal Trade Commission report (FTC, 1975) investigating why this product had been accepted for use found;

"*..the aforesaid ASTM test standards are neither reliable nor accurate tests for determining, evaluating, predicting or describing the burning characteristics of plastics under actual fire conditions...*" (National Materials Advisory Board, 1979)

Table 2-F. Steiner Tunnel (ASTM 84-84a) Test Specification

Specimens	at least one sample, 0.51m x 7.32m x usual thickness
specimen position	horizontal, underneath tunnel roof
ignition source	2 gas burners with a 88.3kW output, located 190mm below specimen, 305mm from and parallel to the fire end of the test chamber
Test Duration	10 min
Conclusion	Determination of flame spread and 'flame spread classification (FSC)*', measurement of smoke density

**FSC – obtained by plotting distance travelled by flame front vs time. If area under curve (A_T) <97.5 ft/min, FSC = 0.515A_T, otherwise FSC = (4900/(195-A_T))*

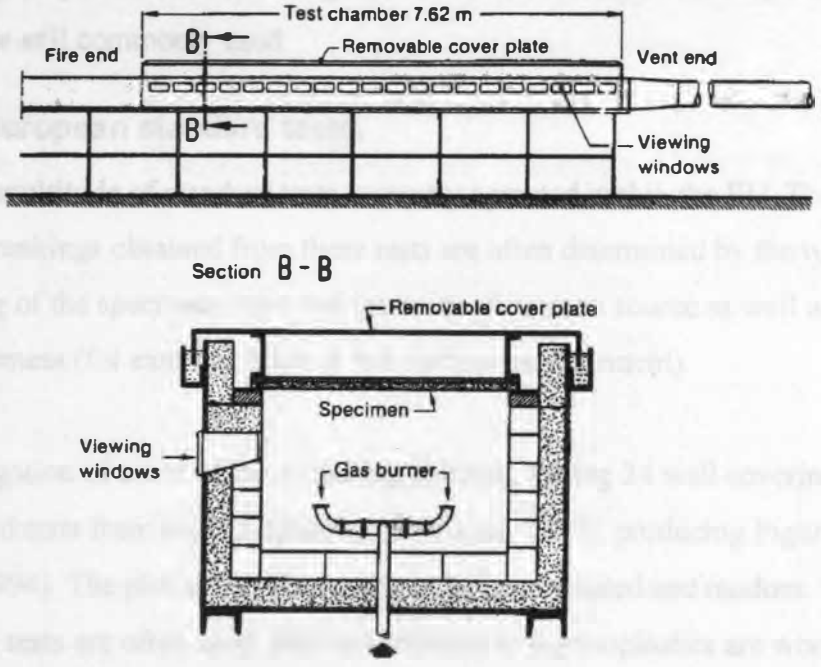

Figure 2-2. ASTM 84-84a (Steiner Tunnel Test) (Troitszch, 1990)

The US courts then forced industry to invest $5m in fire research, eventually leading to development of the 'scientific' tests. The development of a more scientific approach is gradually encouraging engineering solutions to be used in design and construction, for example as outlined by DD 240 (BSI, 1997). However, in the

European Union (EU) there is currently a return to preference for ranking order tests, shown by development of the SBI test, discussed later in Section 2.3.3.

2.3.2 Standard flammability tests

These tests are not assessments of fire hazard, and do not provide 'engineering data' which can be used for quantitative risk assessment. Typically, they are developed as a result of discussion and debate by a committee, such as the American ASTM Committee D-20 for Plastics (Troitzsch, 1990). The intention is to measure response of a specimen to a defined condition. The result is only comparable to other specimens exposed to the same conditions, and does not predict response to an actual fire. There is normally a round robin carried out during the test development process, as reproducibility is a key component to test acceptance. These tests are primarily useful as quality controls, and owing to relative low cost and simple operation, many of these are still commonly used.

2.3.2.1 European standard tests.

There is a multitude of standard tests currently operated within the EU. The specimen rankings obtained from these tests are often determined by the type and positioning of the specimen, type and intensity of ignition source as well as method of impingement (for example edge or full surface impingement).

An investigation of some of these ranking systems, testing 24 wall coverings using the standard tests from six EU countries (Emmons, 1973), producing Figure 2-3 (Fowell, 1994). The plot shows the results to be uncorrelated and random. However, since these tests are often used, the tests relevant to thermoplastics are worth examining. The standard tests used in the round robin are listed in Table 2-G.

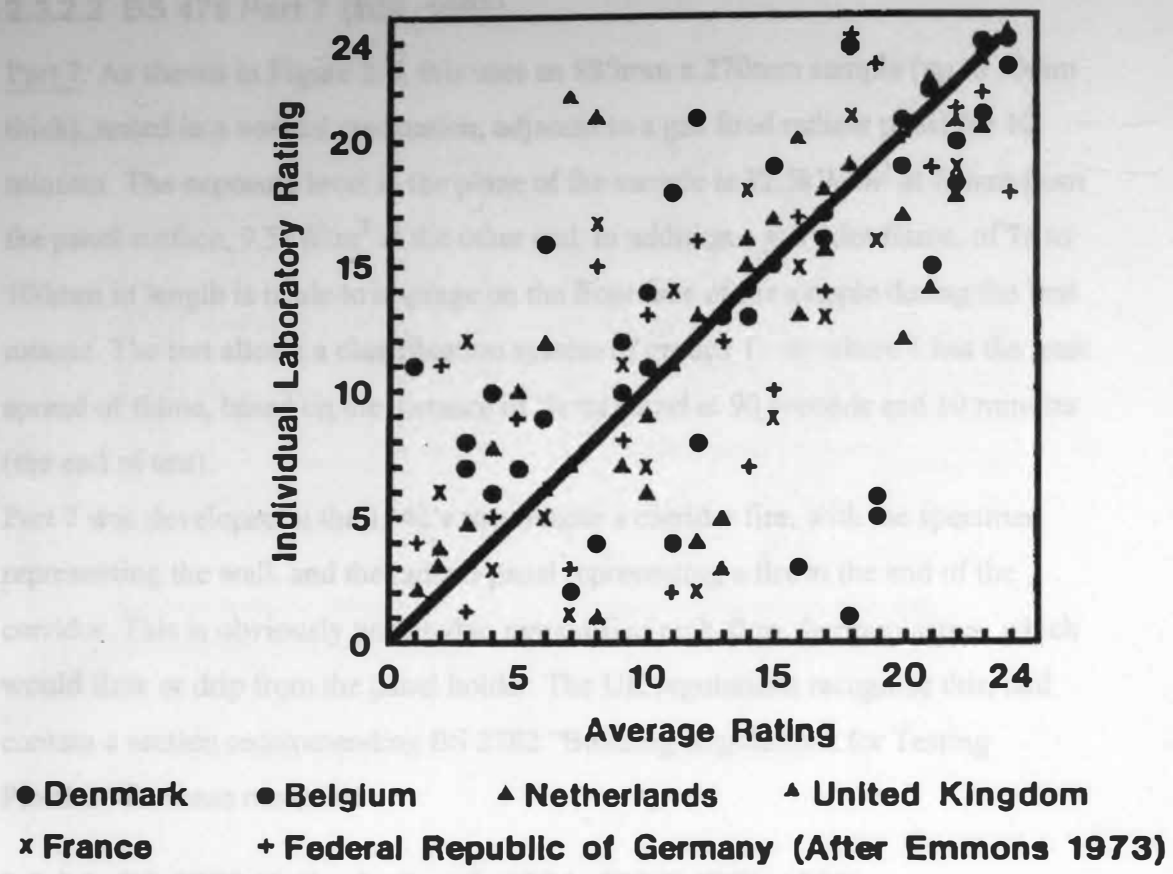

Figure 2-3. Results from Emmons comparison study of EU fire tests

Table 2-G. Tests used in Emmons comparison study

Country	Test
Denmark	slightly modified classification system for BS 476 Pt 7
Belgium	slightly modified radiant panel for BS 476 Pt 7
Netherlands	NEN 3883
UK	BS 476 Part 7 (outlined in Section 2.3.2.2)
France	Epiradiateur (outlined in Section 2.3.2.5)
FDR	Brandschacht (outlined in Section 2.3.2.7)

In the UK, most standard fire tests are grouped within BS 476: Fire Tests on Building Materials and Structures, from which, the tests applicable to thermoplastics are outlined in the following section.

2.3.2.2 BS 476 Part 7 (BSI, 1997)

Part 7: As shown in Figure 2-5, this uses an 885mm x 270mm sample (up to 50mm thick), tested in a vertical orientation, adjacent to a gas fired radiant panel for 10 minutes. The exposure level in the plane of the sample is 32.5kW/m^2 at 75mm from the panel surface, 9.5kW/m^2 at the other end. In addition a gas pilot flame, of 75 to 100mm in length is made to impinge on the front face of the sample during the first minute. The test allows a classification system of groups 1 – 4, where 1 has the least spread of flame, based on the distance of flame travel at 90 seconds and 10 minutes (the end of test).

Part 7 was developed in the 1940's to simulate a corridor fire, with the specimen representing the wall, and the radiant panel representing a fire at the end of the corridor. This is obviously unsuited to unmodified melt-flow thermoplastics, which would flow or drip from the panel holder. The UK regulations recognise this, and contain a section recommending BS 2782 "Building Regulations for Testing Plastics" for these materials.

2.3.2.3 BS 2782 Methods Part 5 (508A, 508D) (BSI, 1970)

BS 2782 Part 5: 508A is used to determine the rate of burning of three specimens (150 x 13 x 1.5mm), which are positioned with the 150mm axis horizontally, and the short (13mm) edge inclined at 45° to the horizontal. A flame of between 13 and 19mm in length is then applied to the free end of the specimen for 10 seconds, as shown in Figure 2-4. A pass is achieved if either the burning rate is less than 50mm/min, or the burn length is 25mm or less.

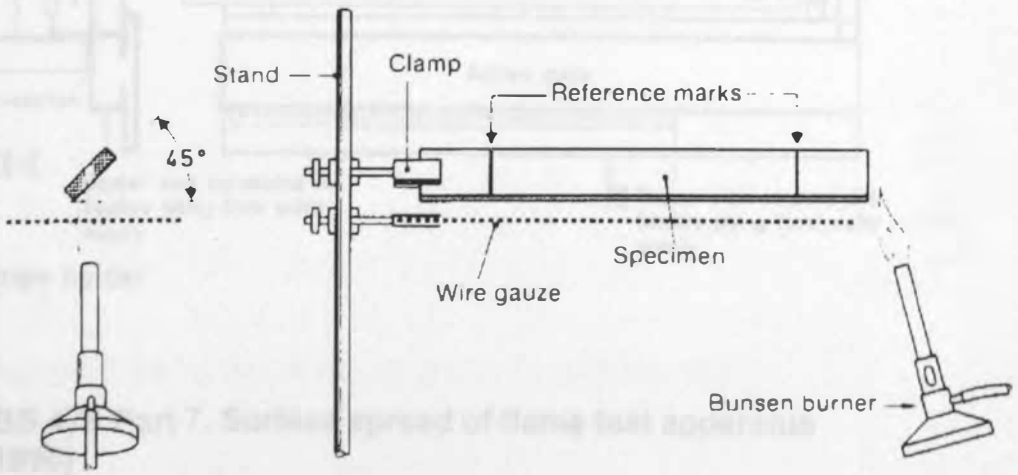

Figure 2-4. BS 2782 Part 5. Rate of burning apparatus (Troitzsch, 1990)

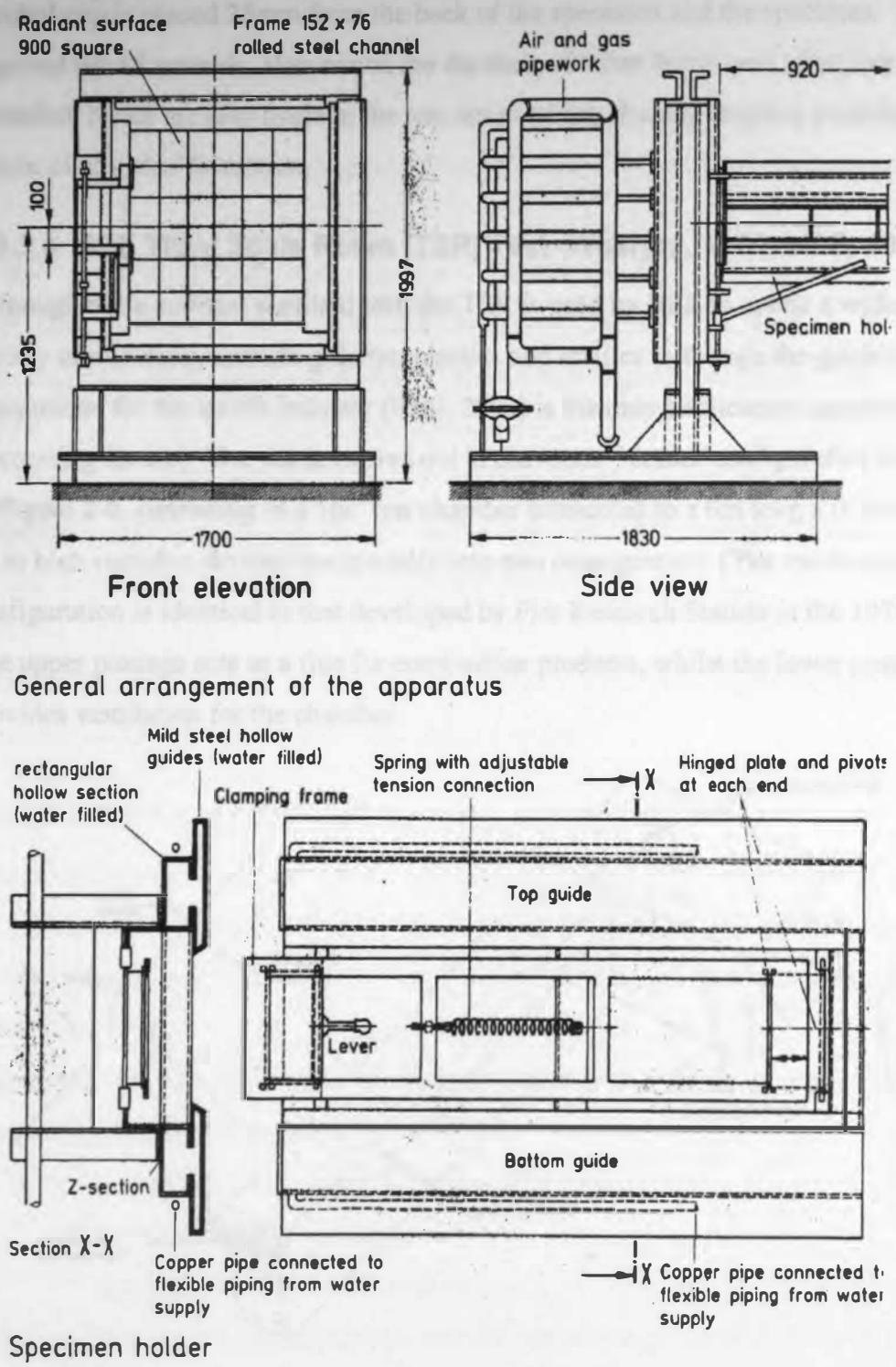

Figure 2-5. BS 476 Part 7. Surface spread of flame test apparatus (Troitzsch, 1990)

BS 2782 Part 5: 508D is used to test the flammability of bulky plastic materials, and has three specimens (150 x 150 x <50 mm), inclined at 45° to the horizontal. An alcohol cup is placed 25mm from the back of the specimen and the specimen exposed for 45 seconds, after which the duration of 'after flame' and afterglow are recorded. Notes are also made in the test report of any flaming droplets produced or extent of any char formation.

2.3.2.4 HSE Third Scale Room (TSR) Test (Wharton, 1990; HSE, 1991).

Although not a national standard test, the TSR is used by HSE to assess a wide variety of materials, including thermoplastics and textiles (although the guide to fire precautions for the textile industry (HSE, 2000) is the only publication currently advocating its use). The test is carried out in the room – corner configuration shown in Figure 2-6, consisting of a $1m^3$ test chamber connected to a 6m long x 0.5m wide x 1m high corridor, divided horizontally into two passageways. (The room-corner configuration is identical to that developed by Fire Research Station in the 1970's). The upper passage acts as a flue for combustion products, whilst the lower passage provides ventilation for the chamber.

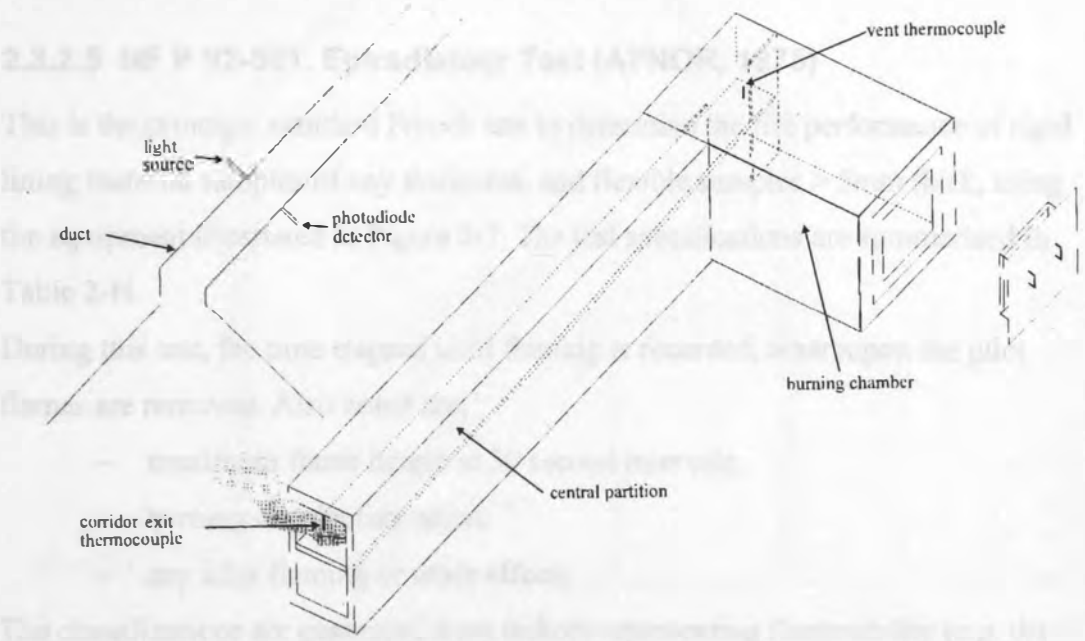

Figure 2-6. HSE Third Scale Room (TSR) Test (HSE, 1991)

A 5kg sample of material is placed in the chamber and ignited by a standard BS No 7 crib, with the test lasting 30 minutes. The test measures rate of rise of temperature at the vent, and also total quantity of smoke produced from the sample collected in the duct from the vent exit, as these are important parameters affecting life safety. A 'hazard ranking order' is then derived from the vent temperature-time curve produced during the test, placing the sample in one of two hazard categories, defined as:

HIGH – maximum rate of vent temperature rise is >700°C/min.

NORMAL - maximum rate of vent temperature rise is <700°C/min.

A further ranking is derived from the amount of smoke produced as:

HIGH - total volume of smoke > $400m^3$ OD ml

NORMAL - total volume of smoke < $400m^3$ OD ml

Materials producing a high ranking in both categories are considered to represent a serious fire risk from both heat and smoke production.

In addition to the UK tests outlined above, there are other tests across Europe, for example the French Epiradiateur test outlined below.

2.3.2.5 NF P 92-501. Epiradiateur Test (AFNOR, 1975)

This is the principal standard French test to determine the fire performance of rigid lining material samples of any thickness, and flexible samples > 5mm thick, using the equipment illustrated in Figure 2-7. The test specifications are summarised in Table 2-H.

During this test, the time elapsed until flaming is recorded, whereupon the pilot flames are removed. Also noted are;

- maximum flame height at 30 second intervals,
- burning droplet formation,
- any after flaming or other effects.

The classifications are generated from indices representing flammability (e.g. the time taken to achieve combustion at the top and base of sample), flame spread (determined as the sum of maximum flame lengths determined every 30 sec), and maximum flame length.

Table 2-H Epiradiateur Test Specification

specimens	4 specimens, 300mm x 400mm x < 20mm
specimen position	inclined at 45°
ignition sources	500W electric radiator (inclined at 45°), 30mm from specimen, producing a surface flux of 3 W/cm^2 2 butane pilot flames to ignite combustion products above and below specimen
test duration	20 minutes
conclusion	classified according to flammability, in classes M1 to M3, or >M3. (M1 if specimen burns <5s).

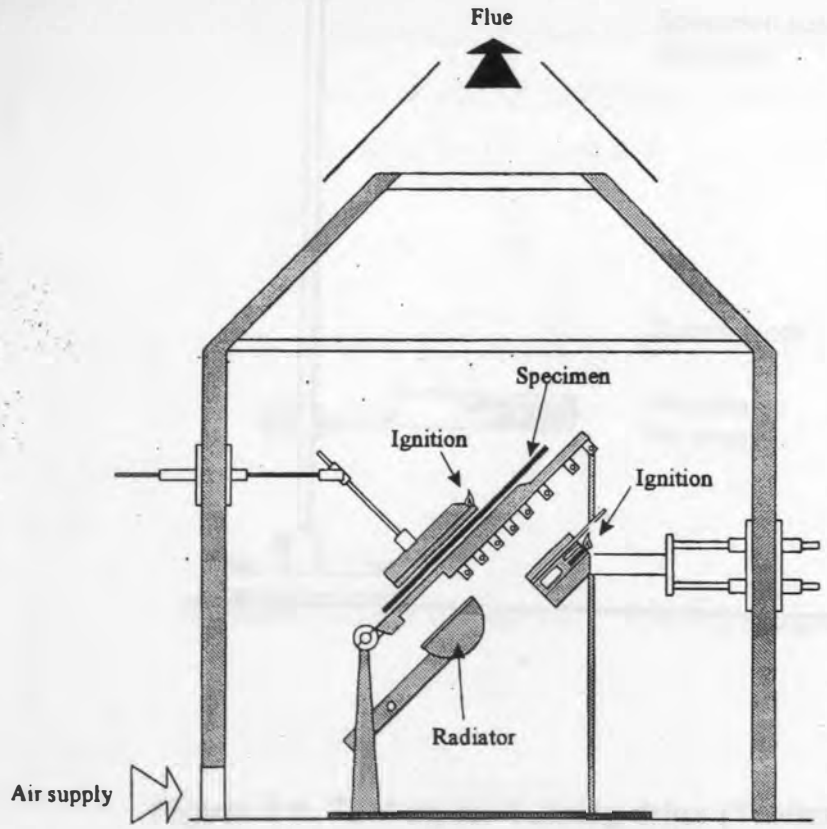

Figure 2-7. Epiradiateur test (Troitzsch, 1990)

A secondary test to this is the dripping test (essai de goutte):

2.3.2.6 NF P 92 – 505.Dripping test (Troitzsch, 1990)

This is carried out if during the previously described test, rapid regression from the heat source, or non-burning drips are observed. Using the equipment shown in Figure 2-8, and removing the radiator 3 seconds after ignition, but replacing it if the specimen extinguishes, classes M1 to M4 are derived. (M4 results from ignition of the cotton wool).

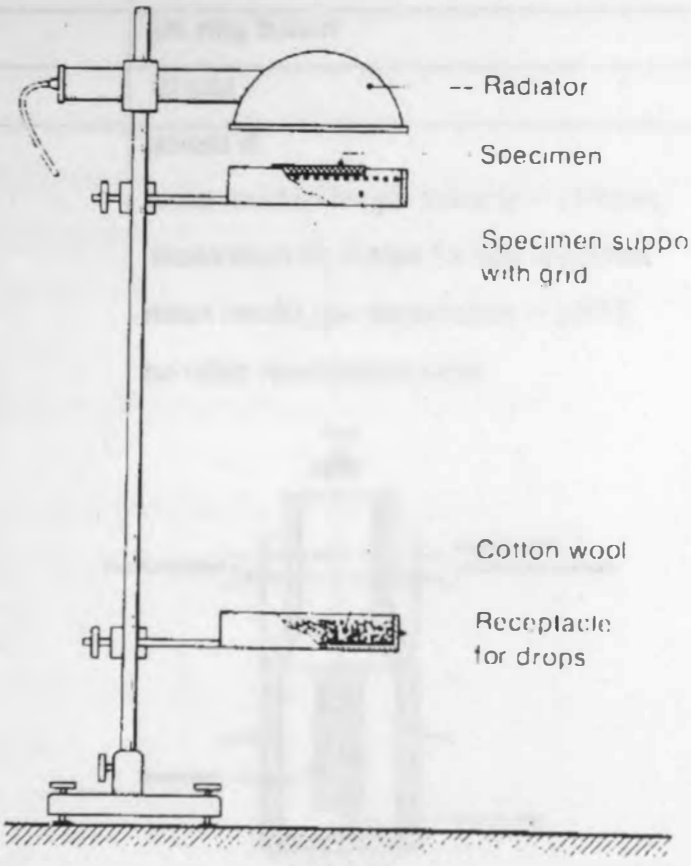

Figure 2-8. Test rig for burning drips (Troitzsch, 1990)

2.3.2.7 Brandschacht Test (DIN, 1978)

This test is the principal German test for building materials, included for completeness. The specifications are shown in Table 2-I, and the equipment illustrated in Figure 2-9.

Table 2-I. Brandschacht Test specification

Specimens	3 x 4 specimens 190mm x 1m x original thickness (max 80mm)
specimen position	vertical, samples at right angles to eachother
ignition source	gas ring burner
test duration	10 min
conclusions	passed if: mean residual length value is > 150mm; mean must be >0mm for any specimen mean smoke gas temperature > 200°C no other reservations exist

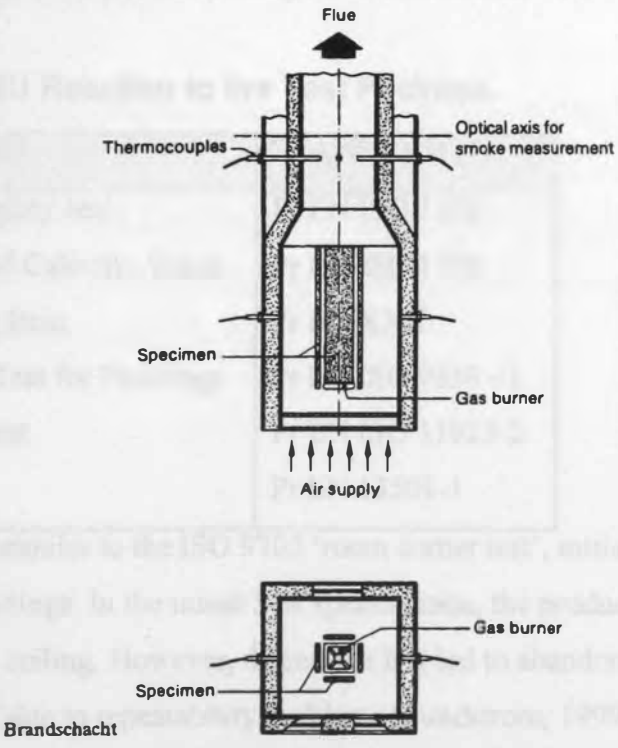

Figure 2-9. Brandschacht Test (Troitzsch, 1990)

2.3.3 Future EU Direction

The discrepancies in ranking system results for products across the EU clearly illustrated by Emmons, have caused problems for both the science and manufacturing communities. To try and redress these problems, the Construction Products Directive (CPD) (EEC, 1989) was formulated to harmonise legislation relating to health and safety, including fire safety, for construction products across the EU. The Technical Committee responsible for fire safety, CEN/TC127 are a 'horizontal' committee producing technical standards for other product committees, such as TC 33 who implement the standards for windows, doors and shutters.
In an attempt to harmonise European fire test methods, a new standard flammability test is being developed, the 'single burning item' (SBI) test (Lukas, 2000). The SBI is part of a package of tests, due to become EU Standards in 2001. The standard tests are intended to reduce the cost of testing to meet standards across the EU for manufacturers, whilst member states will still be able to set their individual required safety levels.
The agreed reaction to fire test package is shown in Table 2-J.

Table 2-J. EU Reaction to fire Test Package.

TEST METHOD	STANDARD
Non-combustibility test	Pr EN ISO 1182
Measurement of Calorific Value	Pr EN ISO 1716
Single Burning Item	Pr EN XXX
Radiant Panel Test for Floorings	Pr EN ISO 9239 –1
Small Flame Test	Pr EN ISO 11925-2
Classification	Pr EN 13501-1

The SBI test is similar to the ISO 9705 'room corner test', initially developed for internal room linings. In the initial SBI specification, the products were mounted on 2 walls and the ceiling. However, discussion has led to abandoning the ceiling as shown overleaf due to repeatability problems (Sundstrom, 1999). The sample walls are then subject to a propane ignition source and the heat release and smoke

production rates are measured. Other effects such as burning droplets will be noted if observed.

The aim is to test products in the form of their end use application in the SBI. Since the SBI is for flat sheet products, pipes, cables, freestanding products etc. are currently excluded from the test as 'exotic products', although this is under consideration to find a solution.

There is a further problem with sheet products, which burn through during the test, resulting in axisymmetric turbulence, reducing reproducibility. This has been observed with polycarbonate glazing panels, which are therefore considered 'exotic'.

The Euroclass system will produce a 7 class ranking system, as shown in Table 2-J. The ranking order is partly based on the Fire Growth Rate (FIGRA), derived from peak heat release rate and time to peak heat release, and also the Smoke Growth Rate, SMOGRA. In order to allow time to adapt to the new system, a five year transition period has been proposed. Over this duration, the Euroclass and national standard are both acceptable.

NB. There are several problems currently associated with the Euroclass package, for example a 1997 round robin exercise covering 15 laboratories and 30 products, found a wide variation in heat flux measured from the SBI burners. A modification has been made to the burner, and the original roof / ceiling has been removed, but there are no plans to repeat the round robin.

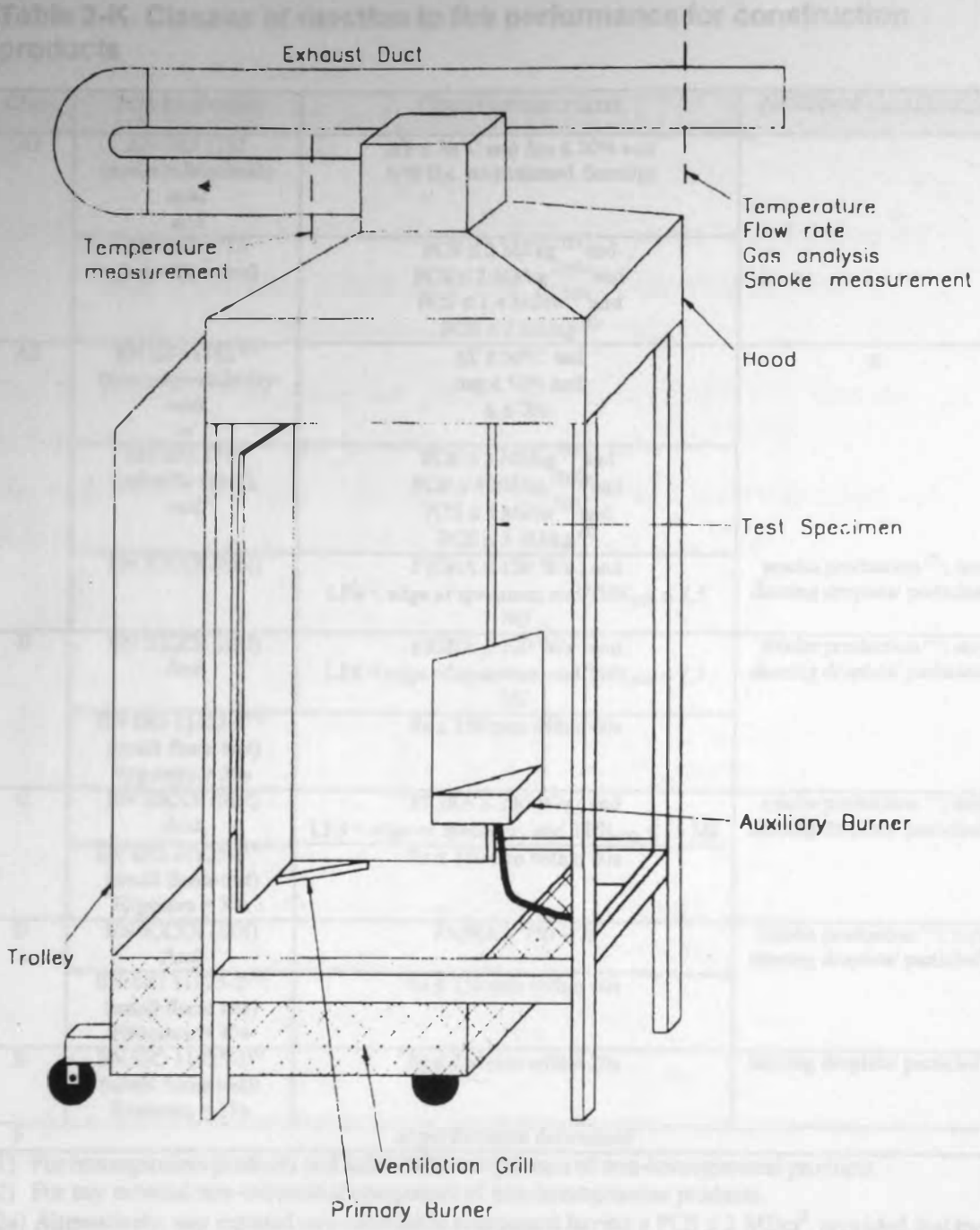

Figure 2-10. SBI Illustration (Briggs, 2001)

Table 2-K. Classes of reaction to fire performance for construction products

Class	Test Method(s)	Classification criteria	Additional classification
A1	EN ISO 1182 (non-combustibility test) and	$\Delta T \leq 30°C$ and $\Delta m \leq 50\%$ and $t_f = 0$ (i.e. no sustained flaming)	
	EN ISO 1716 (calorific value)	PCS ≤ 2 MJ/kg [1] and PCS ≤ 2 MJ/kg [2](2a) and PCS ≤ 1.4 MJ/m² [3] and PCS ≤ 2 MJ/kg [4]	
A2	EN ISO 1182 [1] (non-combustibility test) or	$\Delta T \leq 50°C$ and $\Delta m \leq 50\%$ and $t_f \leq 20s$	≤
	EN ISO 1716 (calorific value); and	PCS ≤ 3 MJ/kg [1] and PCS ≤ 4 MJ/kg [2](2a) and PCS ≤ 4 MJ/m² [3] and PCS ≤ 3 MJ/kg [4]	
	EN XXXX (SBI)	FIGRA ≤ 120 W/s ; and LFS < edge of specimen; and $THR_{600s} \leq 7.5$ MJ	smoke production [5]; and flaming droplets/ particles[6]
B	EN XXXX (SBI) And	FIGRA ≤ 120 W/s ; and LFS < edge of specimen; and $THR_{600s} \leq 7.5$ MJ	smoke production [5]; and flaming droplets/ particles[6]
	EN ISO 11925-2[8]: (small flame test) Exposure = 30s	Fs ≤ 150 mm within 60s	
C	EN XXXX (SBI) And	FIGRA ≤ 250 W/s ; and LFS < edge of specimen; and $THR_{600s} \leq 15$ MJ	smoke production [5]; and flaming droplets/ particles[6]
	EN ISO 11925-2[8]: (small flame test) Exposure = 30s	Fs ≤ 150 mm within 60s	
D	EN XXXX (SBI) And	FIGRA ≤ 750 W/s	smoke production [5]; and flaming droplets/ particles[6]
	EN ISO 11925-2[8]: (small flame test) Exposure = 30s	Fs ≤ 150 mm within 60s	
E	EN ISO 11925-2[8] (small flame test): Exposure = 15s	Fs ≤ 150 mm within 20s	flaming droplets/ particles[7]
F	no performance determined		

(1) For homogeneous products and substantial components of non-homogeneous products.
(2) For any external non-substantial component of non-homogeneous products.
(2a) Alternatively, any external non-substantial component having a PCS ≤ 2 MJ/m², provided that the product satisfies the following criteria of EN XXXX (SBI): FIGRA ≤ 20 W/s; *and* LFS < edge of specimen; *and* $THR_{600s} \leq 4$ MJ; *and* s1; *and* d0.
(3) For any internal non-substantial component of non homogeneous products
(4) For the product as a whole
(5) s1 = SMOGRA ≤ 30m²/s and $TSP_{600s} \leq 50$ m²; s2 = SMOGRA ≤ 180m²/s and $TSP_{600s} \leq 200$ m²; s3=not s1 or s2
(6) d0 = No flaming droplets/particles in EN XXXX (SBI) within 600 s; d1 = No flaming droplets /particles persisting longer than10s in EN XXXX (SBI) within 600 s; d2 = not d0 or d1; Ignition of the paper in EN ISO 11925-2 results in a d2 classification.
(7) Pass = no ignition of the paper (no classification); Fail = ignition of the paper (d2 classification)
(8) Under surface flame attack and, if appropriate to the end –use application of the product, edge flame attack.

SYMBOLS DETAILED IN INTRODUCTION ABBREVIATIONS LIST

In addition to the European situation, there are other tests from other parts of the world applicable to thermoplastics.

2.3.4 USA Test Methods

2.3.4.1 ASTM D568-77 (Reapproved 1985) Standard Test Method for rate of burning &/or extent and time of burning of flexible plastics in a vertical position (ASTM, 1988)

This is a small-scale laboratory test, which compares the relative rate, time and extent of burning for vertical thin sheet or films of plastic.

Ten samples 2.5cm width x 45cm length are tested inside a 76cm high shield, and clamped vertically above a bunsen burner as shown in Figure 2-11.

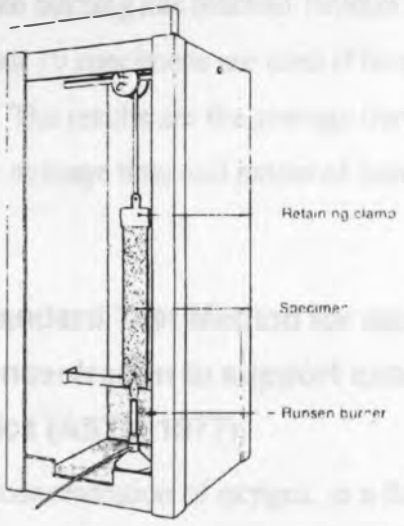

Figure 2-11. ASTM D568-77 Test method for rate, extent & time of burning of flexible plastics in a vertical position (Troitzsch, 1990)

The lower edge of the specimen is exposed to flame until either ignition occurs, or 15 seconds has passed. Upon ignition, the hinged shield is closed and the timer stopped when burning reaches the gauge mark, 38 cm above the initial specimen base. If the gauge mark is reached, then an average burning rate is reported, if not then time and extent of burning are reported. Behaviour such as melting or shrinkage away from the flame invalidates the results of this test.

2.3.4.2 ASTM D 635 –81 Standard Test Method for rate of burning &/or extent and time of burning of self-supporting plastics in a horizontal position (Troitzsch, 1990).

This is a horizontal version of ASTM D568-77, used to test bars, sheets, plates or panels. This system is the same as that used in BS 2782, Method 508A, described in Section 2.3.2.3. The 125mm long x 12.5mm wide specimen is clamped at one end, with a horizontal longitudinal axis and 45° transverse axis, 10mm above a screen of wire gauze. The free end is then exposed to a 25mm high bunsen flame for 30 seconds, the flame is moved if warping, shrinking or melting moves the end away from the flame. The times taken for the flame to reach both 25mm and 100mm from the free end of the sample are recorded, the test stopping when either visible flame or glowing combustion stops or when burning has reached 100mm from the free end. At least 3 specimens are tested, but 10 specimens are used if burning does not reach the 100mm mark at least 3 times. The results are the average burning rate if the 100mm mark was reached, or the average time and extent of burning for samples not reaching the 100mm mark.

2.3.4.3 ASTM D 2863 –87 Standard Test Method for measuring the minimum oxygen concentration to support candle like combustion of plastics (ASTM 1977).

This test measures the minimum concentration of oxygen, in a flowing oxygen/nitrogen mixture that will just support combustion, and has been used on various forms of plastic.

Between 5 and 10 specimens are tested, of dimensions according to type as shown in Table 2-K. The specimen is clamped vertically in the centre of the apparatus column glass chimney as shown, with the sample top at least 100mm from the open top of the column. The initial concentration of oxygen is selected according to previous experience with similar materials, and a gas flow rate of 4 ±1 mm/s through the column is established. The top of the sample is ignited with the ignition flame, which is then removed and the timer started.

The concentration is considered too high, and must be reduced if the specimen burns according to the criteria in Table 2-L, with concentration raised if extinguishment occurs before meeting the criteria.

The critical oxygen concentration is then found as the lowest concentration of oxygen that will meet the criterion above. The concentration, n, is found from:

$$n\% = (100 x O_2)/(O_2 + N_2) \qquad 2.1$$

Some material burning characteristics reduce the reproducibility of the results, in particular charring, dripping or bending of specimens, and a statistical average is the accepted solution to this problem.

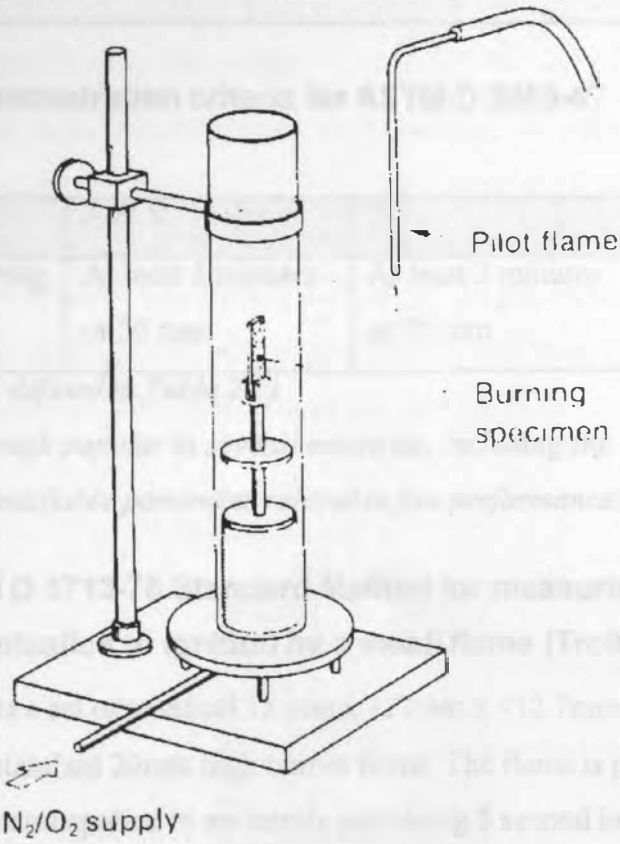

Figure 2-12. Apparatus used in ASTM D2863-87 (Troitzsch, 1990)

Table 2-L. Specimen Dimensions for ASTM D 2863-87.

Type	Plastic Form	Width (mm)	Thickness (mm)	Length (mm)
A	Physically self supporting	6.5 ±0.5	3.0 ±0.5	70 to 150
B	Alternate for self supporting flexible plastics	6.5 ±0.5	2.0 ±0.5	70 to 150
C	Cellular Plastic	12.5 ±0.5	12.5 ±0.5	125 to 150
D	Film or tin sheet	52 ±0.5	As received	140 ±0.5

Table 2-M. Concentration criteria for ASTM D 2863-87

Type	A & B	C	D
Criteria for burning	At least 3 minutes or 50 mm	At least 3 minutes or 75 mm	Past the 100mm reference mark

(Types A – D as defined in Table 2-L)

Curiously, although popular in several countries, including the UK, this test does not measure any identifiable parameter related to fire performance!

2.3.4.4 ASTM D 3713-78 Standard Method for measuring response of solid plastics to ignition by a small flame (Troitzsch, 1990).

This test subjects a set of identical 13 mm x 127mm x <12.7mm thickness horizontal specimens to a standard 20mm high burner flame. The flame is positioned 10mm from the sample and applied in uniformly increasing 5 second intervals, to a maximum 60 second interval, using a new specimen at each increment.

An ignition response index (IRI) is then found from the maximum flame impingement time withstood by a specimen without it being totally consumed, or burning or glowing 30 seconds after removal of the ignition source, or producing droplets that ignite cotton. Owing to the fixed distance between the burner and sample, any sample which drips cannot be evaluated by this method.

2.3.4.5 ASTM D 3801-87 Standard Test Method for measuring the comparative extinguishing characteristics of solid plastics in a vertical position. (Troitzsch, 1990)

This tests a series of 13mm x127mm x < 12.7mm thick specimens by exposure to a standard 19mm high flame for two 10 second flame applications. The flaming time before extinction is recorded after the first flame application, and the times of flaming and glowing extinguishment are recorded after removing the second flame application. The presence of any flaming droplets is also recorded.

This test is purported to examine the effect of material thickness, colour additives and possible loss of volatile components.

2.3.4.6 ASTM 1929-77(1985). Test method for ignition properties of plastics (Troitzsch, 1990)

This uses the 'Setchkin' electric furnace to test plastics. At least five specimens are tested for flash ignition temperature, FIT, in the furnace, as illustrated in Figure 2-13, in a series of three tests. (The furnace differs slightly from the illustration for testing granulated thermoplastics, 3g of which are placed in a pan rather than suspended as a block). The tests are conducted with airflow set to low (25mm/s), medium (50mm/s) or high (100mm/s) rate, and a temperature rise of 873K/h.

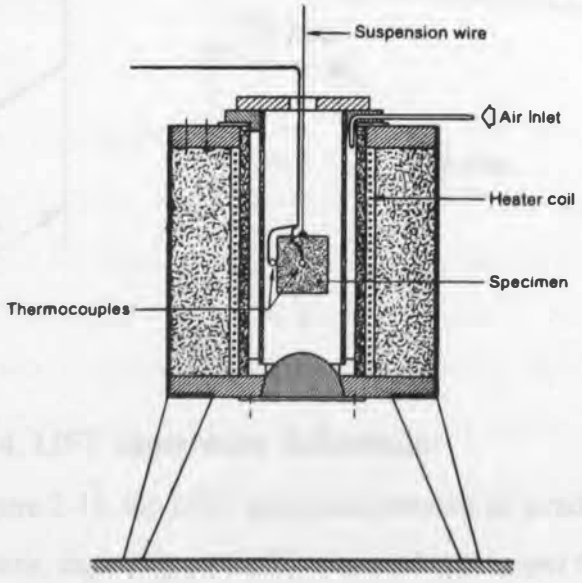

Figure 2-13. Setchkin tube furnace (Troitzsch, 1990)

The air temperature at which the decomposition gases are ignited by a pilot flame is noted, and a further approximation taken with the airflow rate giving the lowest ignition temperature, and a temperature rise of 573K/h.

The actual FIT is then determined at constant furnace temperature, set to 10K below the ignition temperature noted above, and if ignition occurs, the temperature is lowered by 10K, and the test repeated. This is continued until no ignition occurs within 30 minutes. Self-ignition temperature is also measured by this method, omitting the pilot flame from the furnace.

2.3.4.7 ASTM E 1321-93 The Lateral Ignition and Flame spread Test (LIFT)

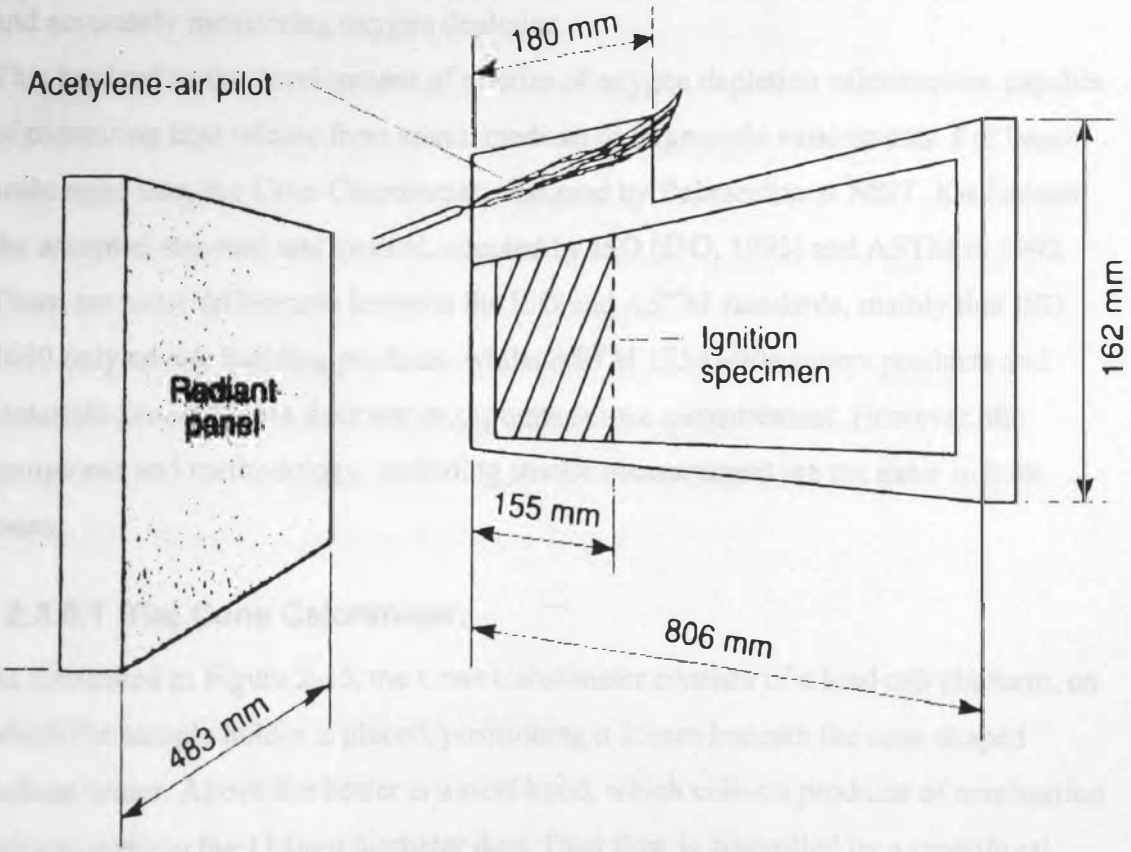

Figure 2-14. LIFT Apparatus Schematic

As illustrated in Figure 2-14, the LIFT apparatus consists of a radiant panel inclined at 15° to the specimens, exposing vertically mounted specimens to a varying level of heat flux across the sample face. The LIFT is used for two procedures, measuring ignition and lateral flame spread. A pilot flame is used for ignition, and flame spread

spread over time as a function of external flux is recorded. Similarly to BS 476 Part 7 and most of the previously described tests, if a plastic melts and collapses from the frame, measurement and thus classification cannot be achieved.

2.3.5 "Scientific" Reaction to Fire Tests.

Heat release has long been recognised (Babrauskas, 1990) as the main reaction to fire parameter, since it defines fire size. However, until the 1980's, it proved difficult to measure effectively. In 1980, Huggett (Huggett, 1980) rediscovered an earlier study of oxygen consumption calorimetry, (Thornton, 1917) showing that for many organic substances, a constant net amount of heat is released per unit mass of oxygen consumed. This allows heat release to be measured by collecting combustion products, and accurately monitoring oxygen depletion.

This has lead to the development of a series of oxygen depletion calorimeters, capable of measuring heat release from small, medium or large-scale experiments. For bench scale apparatus, the Cone Calorimeter, designed by Babrauskas at NIST, has become the accepted standard test method, adopted by ISO (ISO, 1993) and ASTM in 1992. There are some differences between the ISO and ASTM standards, mainly that ISO 5660 only covers building products, whilst ASTM 1354 –90a covers products and materials generally, but does not incorporate smoke measurement. However, the equipment and methodology, excluding smoke measurement are the same in both cases.

2.3.5.1 The Cone Calorimeter.

As illustrated in Figure 2-15, the Cone Calorimeter consists of a load cell platform, on which the sample holder is placed, positioning it 25mm beneath the cone shaped radiant heater. Above the heater is a steel hood, which collects products of combustion prior to entry to the 114mm diameter duct. Duct flow is controlled by a centrifugal fan, set to an ambient flow rate of 24 l/sec, established to provide a factor of safety of around two against spillage of combustion products (Babrauskas, 1992). This also ensures that Cone Calorimeter tests are always well ventilated. At the end of the duct the products are exhausted through the stack to atmosphere.

The heater is preset to the required level of heat flux, measured with a temporarily positioned 1cm^2 heat flux meter, located at the height of the sample face test location. The level of radiant flux can be set to between 10 and 100 kW/m^2.

The test sample, of 100cm^2 area x < 50mm thickness, is wrapped on the back and side faces with tin foil, and mounted on a ceramic fibre pad inside the sample holder, leaving only the uppermost face exposed.

At the start of a test, the holder is then placed on the load cell platform, which registers sample mass for the test duration. The sample is heated, and when the resulting surface temperature exceeds the minimum temperature required for volatile production, volatiles will be emitted from the sample. A 10kV spark ignitor (spark frequency 0.2Hz), placed above the centre of the sample is used for a pilot to ignite the volatiles, with time to ignition recorded by the operator pushing a button.

A pump draws off a sample of combustion products through a line 685mm from the duct inlet, which is passed through a paper filter, cold trap, and silica gel to remove water. The clean and dried line is then split for entry to the oxygen (O_2) and carbon dioxide (CO_2) analysers and further filter of soda lime, to remove carbon dioxide before entry to the carbon monoxide (CO) analyser.

Further along the duct, a 0.8mW Helium-Neon laser beam is passed through the combustion products, monitoring smoke density in the duct prior to stack entry.

In the stack, an orifice plate (which halves the duct diameter), thermocouples and a dpt are used to determine mass flow rate according to:

$$\dot{m}_e = C\sqrt{\frac{\Delta P}{T_e}} \qquad 2.2$$

Where $\dot{m}_e$ = mass flow rate in the duct (kg/s)

C = Orifice plate coefficient (kg$^{0.5}$m$^{0.5}$ K$^{0.5}$)

ΔP = Pressure drop across the orifice plate (Pa)

T_e = Gas temperature at the orifice plate (K)

(*C is a proportionality constant, derived from a 5 kW methane calibration burn and found to be around 0.043* kg$^{0.5}$m$^{0.5}$ K$^{0.5}$).

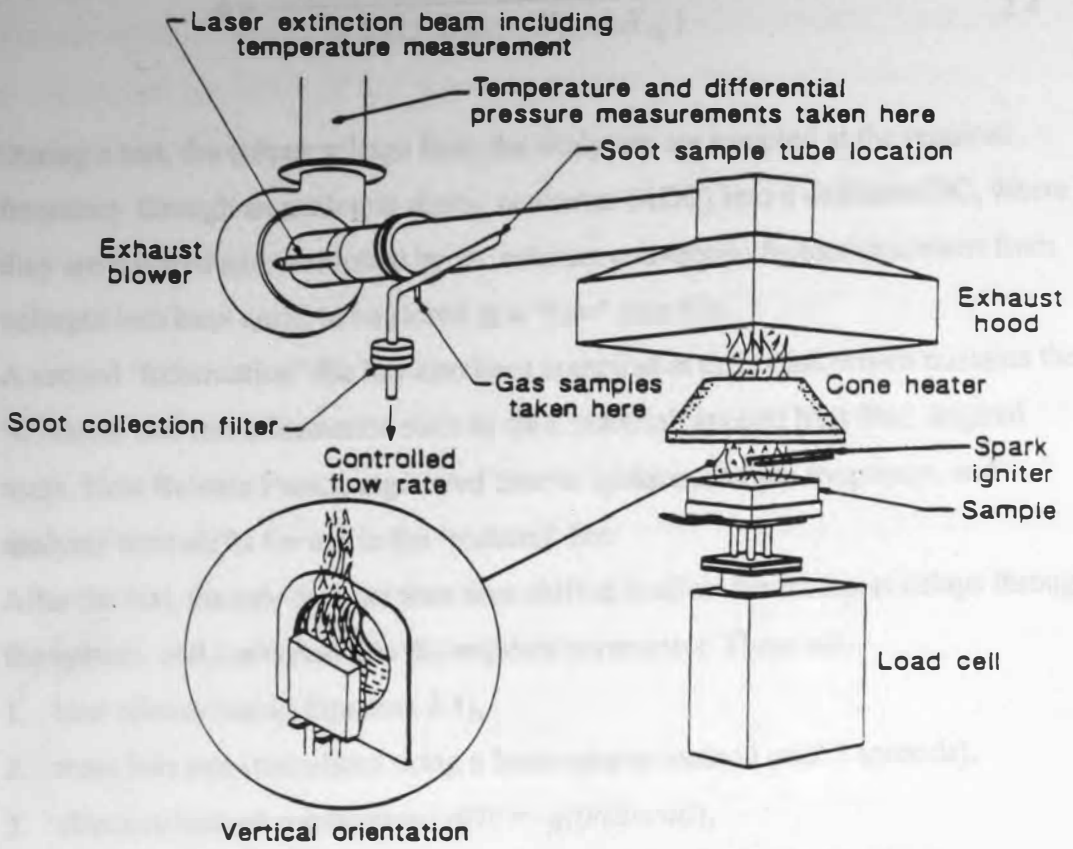

Figure 2-15. Cone calorimeter Test Apparatus

(*NB smoke and soot sampling equipment are optional*)

From the Cone Calorimeter Standard (ISO, 1993), the rate of heat release ($\dot{q}$) can then be determined according to:

$$\dot{q} = 1.10\left(\frac{\Delta h_c}{r_o}\right) X_{o_2}^{o} \left(\frac{\phi - 0.172(1-\phi)\dfrac{X_{CO}}{X_{CO_2}}}{(1-\phi)+1.105\phi}\right)\dot{m}_e \qquad 2.3$$

Where: Δh_c = net heat of combustion (kJ/g)

r_o = stoichiometric oxygen / fuel mass ratio

X = gas analyser output reading

X^o = initial reading prior to test

where the oxygen depletion factor (ϕ) follows from:

$$\phi = \frac{X_{O_2}^{o}(1 - X_{CO_2} - X_{CO}) - X_{O_2}(1 - X_{CO_2}^{0})}{X_{O_2}^{0}(1 - X_{CO_2} - X_{CO} - X_{O_2})} \qquad 2.4$$

During a test, the output voltage from the analysers are sampled at the required frequency through an analogue-digital converter (ADC) into a dedicated PC, where they are collated and multiplied by the relevant conversion factors to convert from voltages into base units, to be stored as a 'Raw' data file.

A second 'Information' file has also been compiled at this point, which contains the 'C' factor and test information such as date, material, applied heat flux, original mass, Heat Release Factor, registered time to ignition, sample frequency, and analyser time shifts for use in the 'reduced' file.

After the test, the raw data are then time shifted to allow for transport delays through the system, and converted into the required parameters. These are:

1. heat release (using Equation 2.3),
2. mass loss rate (calculated using a least squares method over 5 seconds),
3. effective heat of combustion ($\Delta Hc = -q(t)/(dm/dt)$),
4. CO and CO_2 production (per unit mass of sample consumed)

These are finally stored as a 'Reduced' data file. An 'Average' file is also internally generated, which calculates the average to 1, 2, 3, 4, 5 and 6 minutes of the parameters stored in the reduced file. In addition, the maximum and time to maximum values are recorded and the rate of heat release over the test duration is integrated to calculate the total amount of heat released.

For larger scale experiments, which could be undertaken to assess the heat released by furniture, commodities or rooms, the oxygen consumption principle is also used. For furniture, SP (Sweden) developed a calorimeter originally designed by National Bureau of Standards (NBS), which has been incorporated into a NORDTEST Standard, NT FIRE 032. The method uses a wooden crib for the ignition source, mounting the specimen on a load cell platform, 2m below a $9m^2$ hood. The products are drawn into a 0.4m diameter duct, and analysed by a similar method to that used in the Cone Calorimeter.

2.3.5.2 Relationship to fire hazard

Various attempts have been made to translate cone data into a format for use in predicting actual fire behaviour. Since the cone tests are always conducted in well ventilated conditions, and small fires, usually defined as pools < 0.1m diameter, are convection dominated and laminar, Cone data can only be directly related to the initial stages of ignition and fire growth. A study (Ostman, 1988) compared basic parameters from a Cone Calorimeter tests at 25, 50 and 75 kW/m^2, to a full-scale room test (room dimensions 3.6 x 2.4 x 2.4m) for 13 different surface lining materials of varying thickness. The study found no direct correlations between time to ignition, and either total heat released, or peak or average RHR as found from a cone test, and time to flashover from the full-scale test. However, a good correlation was found for the materials tested, although they only include one melting plastic (expanded polystyrene), which is shown below:

$$t_{fo} = a\frac{t_{ig}\sqrt{\rho}}{A} + b$$

Where t_{fo} = time to flashover (full scale)

t_{ig} = time to ignition from Cone Calorimeter data at 25 kW/m^2.

A = heat released by Cone Calorimeter test at 50 kW/m^2 (J/m^2)

ρ = density (kg/m^3)

a = constant (2.76 $MJ(kg.m)^{-0.5}$)

b = constant (-46 s)

The calorimeter developed for the Nordtest standard has been further adapted by Fire Research Station (FRS), who incorporated a natural convection exhaust system and Underwriters Laboratory (UL), who altered the design of the ignition crib. However, the standard test is still the SP version.

For larger items, such as stored commodities, Factory Mutual Research Corp. (FMRC) produced a large-scale calorimeter, with a circular hood of 6.7m diameter, located some 8m above the floor. The flows are channeled through a 1.5m diameter exhaust duct, at a maximum rate of 30kg/s. The maximum capacity of the system is around 5MW.

2.3.6 The unsuitability of current tests for melt-flow thermoplastics.

Melt-flow behaviour of some thermoplastics will result in containment failure by the sample holders. This problem is recognised, and has led to ISO removing the vertical test configuration for the Cone Calorimeter from the standard. It is also recognised as a problem with BS 476, Part 7, where melt-flow thermoplastics receive unclassified ratings because of it. Therefore, for many tests, the assessment criteria simply cannot be completed. In tests where melt flow is noted, such as NF P 92 - 505, the effect of the burning melt on the original sample is neglected, since the distance between drip collector and sample is large. Therefore this can only be used to identify materials exhibiting this tendency.

Adapting sample holders or clamping mechanisms, if it can be made to work, is not always practical. Adaptation may alter parameters such as convection currents over the sample, which invalidates comparisons with other (non melt-flow) materials.

The problem with relying on test results from unsuitable test methodology is clearly demonstrated in a Dow Chemicals paper (Abbott, 1984). There is a requirement for panels used in large agricultural buildings to have a minimum Class 1 rating for BS 476: Part 7 (BSI, 1987). To achieve this with extruded polystyrene (PS) panels, the panels can be laminated with foil on one face, and since the foil stays in position during the test, the classification criteria can be achieved.

Abbott tested laminated and non-laminated PS panels, using them to line the corrugated steel roofs of 4m high x 10m x 10m timber agricultural buildings, inside the barns, 2 bales of straw in a steel box on the floor were ignited. Abbott found the non-laminated boards shrank, retracted from the heat and fell from their supporting mounts onto the floor in a non-burning state. Smoke development was only significant when the boards fell directly onto the fire source, where they continued to burn. The shrinkage of the boards allowed the heat to pass along the corrugated steel roof, exiting at the eaves thereby venting the heat.

In contrast, for the laminated boards, the aluminium foil beneath and corrugated steel above effectively sandwiched the foam. The conductive aluminium liner helped to uniformly heat the foam, which rapidly melted and thermally degraded along with the polyurethane (PU) adhesive used to laminate the panel. The pressure in the

'sandwich' built up, and the PS/PU mix ignited violently when delamination occurred at the joints.

The initial heat release and rise in temperature caused when delamination occurred, ignited of rows of adjacent boards, resulting in rapid fire spread. An external water jet was used to try and control the fire, but instead accelerated fire spread inside the building. At the height of the fire, 5m high flames were observed shooting through holes in the roof, and the building was eventually destroyed.

In this case, the 'safer' material required by the building regulations resulted in uncontrollable fire spread, whereas the unclassifiable material, which would be presumed more hazardous, was actually much safer.

2.3.7 Observations

None of the standard tests are capable of fully assessing the effect of melt-flow behaviour on overall fire growth. Experimentally, pool fire formation at the base of a burning thermoplastic array is well documented, with two main feeding mechanisms: gravity driven surface melt layer flow, and collapse due to softening.

It is apparent that vertical surface flame spread rate is much slower after ignition than for a non-melting thermoplastic. Non-melting materials exhibit a vertical flame spread rate dominated by preheating the surface area ahead of the flame front (Grant & Drysdale, 1995). Preheating reduces the time taken for the surface to rise to the surface volatisation temperature, resulting in an exponentially increasing vertical flame spread rate.

In contrast, for a melt-flow material, preheating ahead of the flame produces a liquid layer, which, at a depth where downward force exceeds yield stress, will flow downward into the flaming area. The low conductivity of plastic produces a temperature gradient through the liquid, and it is possible that the cooler rear face of the flow will act to cool the flaming surface. Therefore, vertical flame spread rate could be a different, initially much slower mechanism, gradually increasing as pool fire formation at the base adds an additional surface flame flux to the wall.

2.3.8 Problems with the approaches taken

The effect of a potential melt upon fire growth is not considered by any test. A burning pool at the base of a melting wall will increase the total area of burning

surface, and supply an additional source of heat flux to the wall. This will increase the heat flux received on the pool surface, along with the rate of fuel supply to the pool. If liquid flow is contained during a test, then the potential rate of increase in burning surface area is restricted. Specifically, since burning rate (kg/m^2s) is partly a function of pool diameter (Zabetakis, 1961), predicted for pools > 0.2m diameter from:

$$\dot{m}'' = \dot{m}''_{\infty}(1 - \exp(-k\beta D) \qquad 2.5$$

where; k = extinction coefficient (m^{-1})

β = mean beam length corrector

D = diameter (m)

$k\beta$= 3.3 m^{-1} (for PMMA[6]) (Babrauskas, 1992)

$\dot{m}''_{\infty}$ = 0.02 kg/m^2s (for PMMA)

This predicts an exponential increase in burning rate until the steady state limit $\dot{m}'' = \dot{m}''_{\infty}$ is reached. This model was developed for radiation dominated pool fires exposed only to their own flame flux. For a pool fuelled by a melting & burning wall, the burning rate will probably be effected by the presence of the burning wall during the growth stage whilst the pool is still relatively small. However, the wall fire is unlikely to affect the burning rate of a large diameter fully developed pool fire.

As mentioned above, there are two main pool feeding mechanisms, flowing and structural collapse. Mounting or otherwise restraining the specimens, as is standard for most tests, (if successful) will modify one or both of these mechanisms. Therefore, results from tests constraining the samples are apparatus dependent, and not likely to be relevant to actual fire behaviour.

None of the test methods account for the effect of the 'flooring' substrate, although it was noted in Hirschler's 'Burning Behaviour of Stacks'experiments that a nylon carpet flooring dramatically increased the overall smoke yield during the test. Flooring material has an important effect on the fire behaviour, particularly for shallow liquid fires such as those generated by burning plastic melts. The material properties for the most common industrial floorings are shown in Table 2-N.

---

[6] PMMA is the only thermoplastic with available & relevant published data

Table 2-N. Material properties of common industrial floorings

	k W/mK	Density kg/m^3	c J/kg K	Typical thickness (mm)	Thermal mass[7] J/m^2 K
Concrete	0.8 – 1.4	1900 – 2300	880	> 150	280 x 10^3
Timber	0.14 – 0.17	640 – 800	2380 – 2850	20	40 x 10^3
Steel deck	45.8	7850	460	5	20 x 10^3

(k, ρ & c taken from Drysdale, 1999)

Table 2-N shows there is a significant difference in thermal mass between the floor types. A high thermal mass indicates a material is slow to heat. For concrete, high thermal mass coupled with low conductivity will produce localised heating and continual removal of heat from a pool fire spreading across the upper surface. This would cool the pool, reducing melt viscosity, and possibly rate of MW degradation. It may be the case that the burning liquid is cooled to below its firepoint, resulting in flame extinction.

In contrast, for steel, the high conductivity and low thermal mass will result in an even temperature distribution in a relatively short time. Initially, steel will remove heat from a spreading pool fire, but once steady state conditions are achieved this will cease. The heated steel will then act to maintain a uniform elevated surface temperature, encouraging pool spread. Steel will also conduct heat ahead of the pool to further assist spread.

Timber floors, commonly encountered in older premises, are combustible. The surface characteristics of timber are a combined function of heating regime, age and environmental conditions. If sufficient heat is applied, the result will be a porous rough, uneven black char. There is also a possibility of burning through the complete thickness during a fire. This provides an additional path for flame spread due to transport by spreading flaming liquid to the area below the fire.

(The extent of the flooring influence on fire growth and behaviour will be a function of various factors, e.g. fire size, duration, floor area and geometry).

[7] thermal mass = (density x heat capacity x thickness)

These parameters and their effects on melt-flow pool fires are experimentally investigated in Chapter 4, and discussed in further detail in Chapter 6.

2.3.9 Practical Problems

There are several reasons for the lack of progress in assessing the melt-flow effect. The experimental problems include:

Tests investigating mass loss, one of the core experimental parameters, suffer problems caused by melt-flow run-off from load cell platforms. This is likely to happen even where panels are successfully mounted on substrates, such as in the SBI, particularly if there is a substantial amount of flow material. The liquid run-off causes two main problems. Firstly, registration of artificially high mass loss data, which will effect any parameters calculated on a '*production per unit mass of fuel consumed*' basis. This is the approach generally used to present heat release, heat of combustion, smoke production and CO & CO_2 production calorimetry test data. Secondly, the molten liquid will often channel itself into the equipment beneath the platform, where it can solidify and physically block the load cells. Alternatively, it may continue to burn; pool fires below equipment are more of a nuisance than a safety hazard during a fire test, as they heat up and alter the resistance of signal cabling, disabling the rig circuitry.

2.4 Conclusion

The fire hazard posed by melt-flow thermoplastics is a function of material properties and external influences. Practically it has proved difficult to assess meaningfully. This is mainly due to the recent massive growth in thermoplastic applications coupled with the focus of previous fire research being on more traditional construction materials such as wood.

This chapter has confirmed that the test and experimental methods currently available cannot be used to address the main question of this thesis; *to what extent does melt-flow behaviour effect thermoplastic fire growth?*

A new experimental technique has therefore been developed, which is described in detail in Chapter 4.

The next chapter is an investigation of specific parameters effecting melt-flow behaviour, divided into external influences and thermoplastic material factors.

3 Factors affecting the fire hazard of thermoplastics

This chapter is a review of factors affecting the level of fire hazard posed by thermoplastics. It is divided into two sections; external factors relevant to production of thermoplastic components, and material factors of the thermoplastics. By definition, the greatest hazard will be associated with the largest volume of material; therefore, the most common processes and materials have been selected for further analysis.

3.1 External Factors; Variation of potential fire hazard over thermoplastic material life cycle

The UK Fire Statistics provide very little detail about the variation of thermoplastic fire hazard through the life cycle. The only relevant information to be gleaned is that thermoplastic processing sites suffer ~ 320 fires/year, whilst thermoplastic recycling premises sustain 100 fires/year. Therefore, the level of fire hazard (DD 240, BSI, 1997) is approximately three times greater for processing than recycling, but it is not known how these levels compare to the hazard associated with other areas within the cycle.

The following section contains a basic product life cycle analysis for polyethylene, the most common thermoplastic, and an investigation of the level of fire hazard posed at each stage. For clarity the approximated life cycle has been produced into the flow chart shown in Figure 3-1.

As shown, the product life cycle overviewed starts with the polymerisation of ethylene, although this is not the primary stage, as ethylene is a product of the naphtha cracking refinery process.

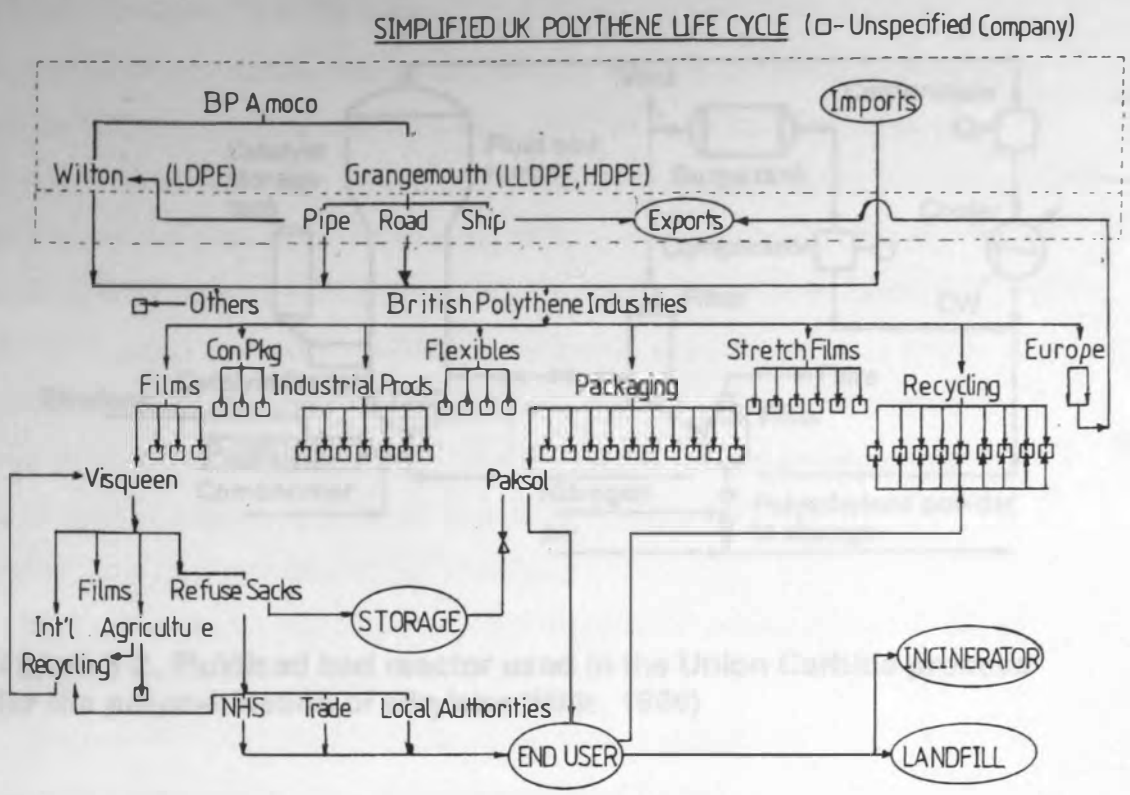

Figure 3-1. Flow chart of simplified PE Life cycle

3.1.1 Stage 1. Polymer production

As illustrated in Figure 3-2, in this process, ethylene gas (C_2H_4) is used as the heat transfer medium to remove heat from the reaction, and solid polyethylene powder is formed in the fluidised bed. A chromium compound catalyst is used for polymerisation, which results in ~ 1ppm chromium in the polymer. During polymerisation, ethylene gas, at around 20 bar is introduced to the base of the fluidised bed reactor, which may be 2.5m diameter x 12m high. Temperature is maintained at 358 – 373 K to prevent conglomeration of polyethylene particles and the catalyst is continually injected into the pressure vessel. Only around 2% of the ethylene is polymerised during each pass through the reactor, the remaining monomer is cooled and compressed prior to re-entering the reactor.

The solid particles of polyethylene sink as they grow. After 3 – 5 hours they will be around 0.5mm diameter and can be removed from the reactor. The granules are then purged with nitrogen before being conveyed into storage in an inert gas stream.

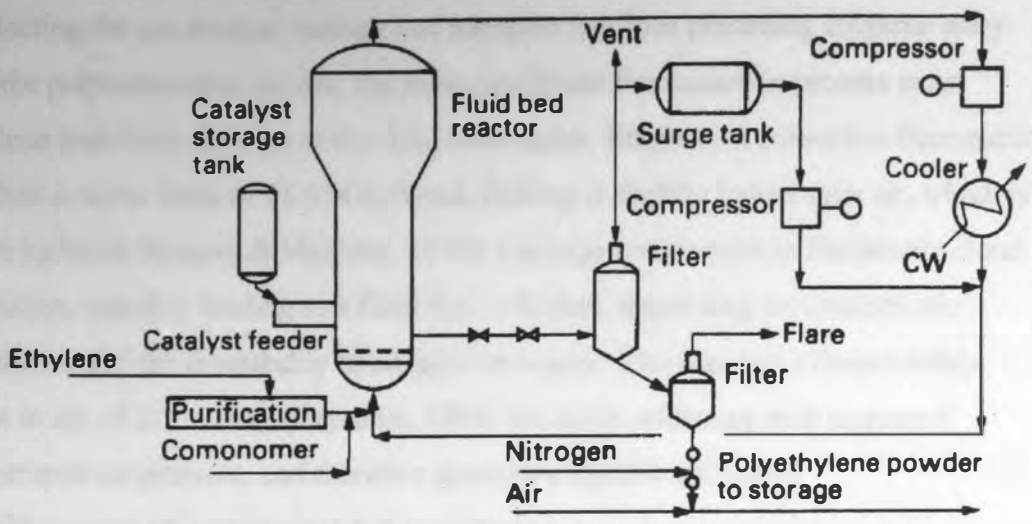

Figure 3-2. Fluidised bed reactor used in the Union Carbide process for the polymerisation of ethylene (Mills, 1986)

The reactor can be used to produce homopolymer or copolymers, usually with butene, the crystallinity being controlled at this point. The molecular weight is controlled by addition of hydrogen, with the width of the molecular mass distribution being controlled by modifying the catalyst.

Table 3-A. Inputs for 1 tonne of polyethylene homopolymer (Cullis, 1981)

Ethylene	1020 kg	
Power	250 kWh	to produce powder
Cooling water	110 m^3	
nitrogen	6 m^3	
catalyst	0.01 kg	
power	300 – 450 kWh	to compound powder into
steam	200 kg	granules
cooling water	40 m^3	

The approximate material and energy inputs to produce 1 tonne of homopolymer are shown in Table 3-A (approximate since they are scale dependant).

3.1.1.1 Process Fire Hazards

Neglecting the production, storage and transport facilities preceding ethylene entry into the polymerisation system, the most significant fire hazard in process is an ethylene leak from the area of the fluid bed reactor. Ethylene, a colourless flammable gas, has a molar mass of 28.054 kg/kmol, making it slightly lighter than air, which is 28.96 kg/kmol (Rogers & Mayhew, 1993). Leakage could result in flammable cloud formation, possibly leading to a flash fire or fireball, depending on atmospheric conditions and the availability of an ignition source. Ethylene has a flammability range in air, of 2.7 – 35%, (Drysdale, 1999) the limits widening with increased temperature or pressure, and therefore presents a significant hazard.

Possible causes of containment failure include;

1. overpressure caused by process malfunction (failure to control reaction due to overheating, excess catalyst etc)
2. physical damage to plant (e.g. due to mechanical impact, etc)
3. faulty plant (leaking seals, stuck pressure relief valves)

Due to the design of pressure vessels, overpressure resulting in tank rupture is much less likely than rupture due to mechanical impact. However, overpressure of pipework or fittings, the weak point of any system, could result in leak sites.

The potential rate of release for this system can be assessed using standard formulae (Lees, 1996):

Critical flow condition is achieved if:

$$\frac{P_2}{P_1} \leq \left(\frac{2}{\gamma+1}\right)^{\frac{\gamma}{\gamma-1}} \qquad 3.1$$

Where P_2 = initial vessel pressure (20 bar)

P_1 = atmospheric pressure (1 bar)

γ = Ratio of specific heats; Cp/Cv = (1.453kJ/kg K)/(1.166kJ/kg K) = 1.246

Mass flux (G) for critical flow:

$$G = C_D\left[\frac{P_1}{V_1}\gamma\left(\frac{2}{\gamma+1}\right)^{\frac{\gamma+1}{\gamma-1}}\right]^{0.5} \qquad 3.2a$$

Mass flux for non-critical flow:

$$G = \frac{C_D}{V_2}[2P_1V_1\frac{\gamma}{(\gamma-1)}\left\{1-\left(\frac{P_2}{P_1}\right)^{\frac{\gamma-1}{\gamma}}\right\}]^{0.5} \qquad 3.2b$$

Where C_D is a discharge coefficient (nominally 0.6)

V_1 is the initial specific volume (i.e.$1/\rho$), found to be $0.0535 m^3/kg$

The resultant potential mass flux is 2411 kg/sm^2. This will be tempered by the leak site area, but presents a high potential hazard.

NB This type of hazard has resulted in previous disasters, most notably Flixborough NYPRO Factory (1974), where a 50cm diameter temporary bypass pipe was installed whilst a cracked reactor was repaired. The pipe failed, and the operating system, running at 423K, 10 bar (gauge), discharged 50 tonnes of cyclohexane (C_6H_{12}), normal boiling point 354K. When the gas cloud ignited the resulting explosion destroyed the plant, killing 28 people, and caused damage to houses approximately ½ mile away.

In the UK, most polyethylene is produced by BP Amoco at Grangemouth, Scotland, and Wilton, Middlesborough (http://www.bpamoco.co.uk/polyethylene). The 500 acre Grangemouth site is the largest, turning over 450,000 tonnes/year of HDPE and 300,000 tonnes/year of LLDPE, whilst Wilton produces 100,000 tonnes/year of LDPE. The ethylene is actually produced in a Grangemouth refinery for both plants, with a production capacity of 1,000,000 tonnes/year.

This level of potential hazard is strictly regulated and monitored. Although ethylene is not a specifically named substance[8], due to its quantity and also other materials and processes on site, the site is designated under COMAH (Control of Major Accident Hazards Regulations, 1999). (COMAH is the updated regulation previously known as CIMAH (Control of Industrial Major Accident Hazard (CIMAH) Regulations, 1984)). Under COMAH, identification of all major hazards (including

[8] COMAH lists substances & minimum quantity, which if present on a site require application of Regulations 7 -12, as it is foreseeable that they would aggravate a major accident – e.g. 50 tonnes of propylene or propane would require a separate safety report.

frequency and consequence assessments), and proof of control and protection systems for hazard reduction have to be produced in a 'safety report'. Therefore, although there is a high potential hazard, the risk has to be reduced to an 'acceptable' level to permit site operation.

3.1.2 Stage 2. Transportation

There are three main transportation systems from Grangemouth;

1. pipelines, which transport excess ethylene to local companies and Wilton (350 km away),
2. ships which move polyethylene granules from Grangemouth port to Europe,
3. road tankers which are the main distribution method for polyethylene within the UK.

There are 6,000 loads/year moved to the continent by sea[9], with a similar volume moved by road tanker to UK destinations (Private communication, Swanson, BP).

3.1.3 Stage 3. Manufacturing

Although the polyethylene granules are transported UK wide to a large number of manufacturers, to be processed into commodities, the largest individual granule processor is Visqueen, who produce ~120 tonnes.day^{-1} of polyethylene products. For further investigation, site visits were undertaken to look at 'typical' industrial practice, focusing on fire safety. Accompanied by Dr Alan Tyldesley from the HSE's Technology Division, visits were made to Visqueen, Yarm Rd, Stockton on Tees and Packaging Solutions, North Tyne Industrial Estate, Newcastle. Both these companies are part of British Polyethylene Industries plc, which is divided into commercial sectors of films, industrial products, consumer packaging, recycling, packaging services, and retail flexibles.

3.1.3.1 Visqueen

Visqueen, the major firm in the 'films division' illustrated in Figure 3-1, manufacture polyethylene granules into film and sheet applications. The site is operational 24 hours a day, with the 350 employees split into three shifts. There are four distinct

[9] 1 load = 25 tonnes

businesses operating within the factory, dealing with agriculture, films, refuse sacks and internal recycling. A short distance from the Stockton site, Visqueen also partner a transportation and haulage firm in a warehousing operation. The company has operated for 10 years at the site, prior to which the company and site were part of ICI.

3.1.3.1.1 Process Layout

Pellets are delivered by road to the site, and either unloaded directly into a steel silo, or delivered packed in 25kg plastic bags, which are unloaded by forklift truck and moved into a storage area.

Packaged pellets are stored mainly outside on wooden pallets, the maximum quantity outside being 500 - 600 tonnes, whilst some formulations which are susceptible to water absorption, (generally >100 tonnes) are stored inside. A typical pallet is loaded with 500 – 700 kg of pellets in 20 or 25kg bags. There are problems with stability of sacks containing pellets, which flow inside the sack, the rate being worsened by heat, light, or pressure. The sacks are also easily ruptured, with leaked granules creating a trip hazard. A ruptured bag will also dislodge the stack, by altering the support base for the material above it making forklift access unsafe, so silos are generally preferred.

Pellets are moved from storage into operations areas when required, and processed by either extrusion or blowing into sheets, which are then either cut and sealed into bags, or rolled onto cardboard tubes. If printing is required, the sheet is electrically charged, which helps the solvent-based print adhere to it.

Any scrap sheet or film from processing is sent to the recycling area and reground into pellets, which re-enter the processing cycle. Final products are then stored in a finished goods warehouse area awaiting shipping to customers.

3.1.3.1.2 Fire Safety

The storage areas for pellets are fitted with smoke alarms, but not sprinklered. Some parts of the operation, i.e. those containing finished products, are sprinklered as

insisted on by the site insurer. The reason for only fitting sprinklers into finished goods areas is that finished goods are worth more money than pellets.
NB the HSE view sprinklers as relevant in reducing the likelihood of structural collapse during a fire, but not relevant to life safety in this type of premises.

The standard of housekeeping through the site was excellent in the storage areas, and reasonable in the process areas. Fire alarms are tested every Friday, and smoke and heat detectors along with portable fire fighting equipment are located throughout the site. The local fire brigade has a tested callout response time of 3 to 5 minutes. Security for the site is maintained by a continual staff presence, and the buildings are single storey concrete floored, prefabricated steel constructions with warehousing / storage areas separated from the rest of the operations. The storage areas have wide aisles and high ceilings. Smoking is banned, other than in specified areas.
Fire safety is the responsibility of the group safety manager, although since the September 2000 advent of the Workplace Health and Safety Regulations, each company must be able to show evidence of undertaking their own workplace fire risk assessment. This has prompted Visqueen's site safety & training officer and the site superintendent to attend courses on risk assessment.
In addition to the above, the site is located close to Wilton, Cleveland, where a major fire occurred in the BASF polypropylene warehouse in 1995, as discussed in Section 1.4. Awareness of this recent event has further reinforced the commitment to fire safety precautions.
After the visit, Dr Tyldesley raised some concerns in particular the siting of charging equipment for electrical forklift trucks inside the warehouse. (When batteries are charged 'gassing off' results, which, depending on ventilation, could present a potential hydrogen hazard). The overall fire precautions for the site were considered reasonable.

3.1.3.2 Overview of Packaging Solutions (PAKSOL).

Packaging Solutions, part of the Packaging Group shown in Figure 3-1, is a company which import polyethylene products, mainly 'rip seal' bags from China, to redistribute to a variety of customers. The single storey warehouse has five staff, working 7.30 – 5pm, 5 days a week. Fifteen members of staff in offices adjacent to

the warehouse undertake sales and administration functions. The company has been operating from the industrial unit for around 3 years, prior to which the unit housed a paint supplier.

3.1.3.2.1 Process Layout

The economics of importing stock result in cheaper bulk buying leading to 'feast or famine' storage conditions. Inside the single storey steel frame unit is a wide mixture of product lines including bubble wrap, cardboard rolls and polystyrene granules housed in one section, and steel racks (4 high), containing wooden or polyethylene pallets covered in polyethylene shrink wrapping covering the rest of the area. Further storage is provided in a warehouse on another site, holding a further 250 pallets. A typical pallet carries 800 – 850 kg of products, often packed in cardboard boxes and shrink-wrapped onto the pallet.

3.1.3.2.2 Fire Safety

As with Visqueen, fire safety is the responsibility of the group Safety Officer, who visits regularly. The site has never received a visit from the fire brigade, and there was no awareness of predicted response times. A local authority building control representative has visited, and was satisfied with the fire precautions.

Security on the industrial estate is a problem, although a guard is employed to patrol the estate at night. There have been several recent burglaries in adjacent units, and due to the security risk, the premises are alarmed and all windows in the unit are barred. There are two means of escape from the unit; one direct to outside and the other from the warehouse through a corridor to outside, which is also the means of escape for the offices.

There are no sprinklers in the unit, but smoke alarms are located in the ceiling. Smoking is banned from the warehouse area, and the general level of housekeeping is satisfactory.

3.1.4 Stage 4. Retail & Distribution

Having manufactured the granules into a diverse range of products, the products are then transferred into a nation-wide warehouse wholesale, retail & distribution chain.

To keep the analysis simple, only refuse sacks, one of the four main areas of output from Visqueen, will be considered from this point.
Of the total refuse sacks produced by Visqueen, according to their sales department, approximately 50% are sold direct to the NHS, with the remainder divided between local authorities and trade sales.

3.1.4.1 NHS

The NHS is currently split into various 'Fund holding Trusts', each being responsible for their own supply procurement. Bulk purchases are cheaper and supplies are stored in warehouses prior to site delivery.

3.1.4.2 Local Authority

Local authority stock control is dictated by operational use, and most authorities carry a month excess supply. The excess is stored with the distribution supply at the single storey operational depots, in cardboard boxes on pallets, 100 bags/box. The stock level varies with demographics, but one month's supply is approximately (private communication, Whitman, 2000) one bag / 0.6 head of population.

3.1.4.3 Trade

'Trade' is mainly divided between wholesalers who then sell on to smaller retailers, and industrial stockists. For retail, the large firms usually carry large stocks in warehouses, delivered to stores when required, whilst smaller stores tend to collect from wholesalers on a weekly basis.

3.1.5 Stage 5. Recycling / Disposal

Most refuse sacks eventually either enter landfill sites, or are incinerated along with their contents. However, many other thermoplastic products can be recycled, and a growing industry sector is concerned with collection and recycling. The collection and storage sites seem, statistically, to suffer a significant fire problem, with a Brigade in England or Wales called out to an incident every 3 days or so. From the reports outlined in Fire Prevention, most of the recycling depot fires are outdoors, and involve large quantities of mixed stock stored in large piles.

Many common problems occurred in the Wolverton depot fire, one of the largest of the recent fires in thermoplastic recycling plants. This occurred in June 1996 in a materials recycling plant in Milton Keynes (private communication,Tucker; 2000; RB Hawkins, 1997; Buck's Emergency Planning Unit, 1999; Bucks F&RS). The fire happened in an outside storage area involving over 500 tonnes of baled plastics. Lack of fire separation between bales and plentiful fresh air made it impossible to fight the fire successfully. Therefore, extra fuel was removed from the area, and the fire was allowed to burn itself out.

Fortunately, weather conditions allowed the smoke to rise vertically remaining within a plume, allowing the plastics to burn at high temperature reducing the production of dioxins[10] and furans[11]. However, there was a problem with the absence of an inventory of plastics within the storage area, and the resulting lack of knowledge of the combustion products and their effects.

A report into contamination aspects of the incident (Hawkins, 1997) detailed

"... the combustion of plastics.. can produce a complex mixture of organic compounds of differing volatilities and toxicities, ...breaking down the polymeric body of the material liberates bound up pigment inks, extenders, fillers, plasticisers and fire retardants, many of which become toxic when liberated from their organic matrices.."

This incident also found other fire spread problems with burning plastics. For example, molten burning plastic flowed into drains, blocking them as it solidified. However, the initial procedure of surrounding the fire with skips to contain it prevented the burning molten liquid causing further fire spread.

3.1.6 Summary of changes in fire hazard through life cycle

1. The most hazardous stage is polymerisation, since large quantities of chemicals are undergoing reaction processes. This stage, being concentrated into only two main locations, has the highest potential fire load density of the life cycle, as supply becomes geographically divided after this stage. This is also the most tightly regulated and controlled part of the life cycle, and with fire safety being

[10] 'dibenzdioxin': $C_{12}H_4O_2Cl_4$ (toxic colourless liquid compound)

[11] 'furan' – colourless liquid compound, C_4H_4O

high priority there should be a lower frequency of occurrence. High staff training and awareness, along with the capability to detect and deal effectively with ignitions, should mean overall fire risk[12] is reduced, although, the potential 'worst case' consequences are very severe.

2. Transport of granulated polyethylene is no more hazardous than transportation of any low flammability load.
3. Thermoforming of plastics is a hot work process, with a high ignition risk, as reflected in the Fire Statistics showing daily Fire Brigade call outs to processors. The statistics are produced by annually collating all Brigade call out records for England & Wales, ('FDR 1' forms), and it is probable many more potential fires are extinguished onsite at an early stage, and thus do not appear in the statistics.
4. Warehousing presents a different set of problems: lower monitoring and staffing levels reduce the probability of early detection by staff, which increases the probability of fire growth and spread after ignition. Stock configuration, particularly vertical stacking, offers a fast potential flame spread mechanism, whilst a high density of combustible materials makes water penetration through the stack by either sprinklers or brigade hoses difficult. In addition to these problems, which are common to most warehouses, thermoplastic storage also has the potential to spread fire through movement of molten burning material.
5. Wholesale \ Retail sites have lower volumes of material than warehouses, as they are approaching the end of the supply chain, but stock 'in situ' is likely to be mixed with other, possibly more hazardous materials. However, staff levels are much higher than in warehouses, so early detection and alarm probability is high.
6. Recycling often involves large quantities of materials, stored outside in unmonitored, relatively unsecured areas with little separation between stock. This, combined with stock ideally configured for rapid flame spread, and detection / alarm often dependant on passers by noticing something, produce a high fire risk in this sector.

---

[12] 'Fire risk': the product of:

a) the probability of occurrence of a fire in a given technical operation or state; and

b) the consequence or extent of damage to be expected on the occurrence of a fire

(DD 240:Part 1:1997, Section 3 Definitions & notations)

3.2 Material Factors Influencing Potential Fire Behaviour.

The previous section looked at how the level of fire hazard & fire risk changes over the thermoplastic life cycle due to non-material factors. Following this, an analysis will now be made of the material factors effecting fire behaviour for the most significant thermoplastic materials.

3.2.1 Polyethylene

Polyethylene is the most important commercial thermoplastic, with current UK consumption of approximately 1,220k tonnes/annum (private communication, McIlwee, 2000). This comprises 740k tonnes of low-density polyethylene (LDPE), and around 480k tonnes high-density polyethylene (HDPE). The main usage of LDPE is in packaging, whilst HDPE is commonly found as pipes, containers, film and tape.

3.2.1.1 Material Preparation & Characterisation

LDPE is formed by the free radical addition of ethylene at high pressure ($1 - 2 \times 10^5$ kPa) and elevated temperatures (< 520 K), with a small but critical amount of oxygen. LDPE has a low fraction of (< 60%) crystallinity, and low softening & melting temperatures (Tm = 378 –388 K), due to the presence of highly branched chains (8 – 40 branch points /1000 main chain atoms). The molecular weight of LDPE is generally less than 5×10^4 g/mole. In terms of mechanical properties, the low crystallinity reduces stiffness and increases impact strength (Encyclopaedia of Polymer Science & Engineering).

HDPE is polymerised in a solution of aliphatic[13] hydrocarbons at low pressures ($10^2 - 10^3$ kPa) and temperatures of 330 – 350 K in the presence of a metal alkyl (e.g. triethylaluminium) and a transition metal halide (e.g. titanium tetrachloride) catalyst. It has limited branching (< 5 branch points / 1000 main chain atoms), and high crystallinity, (about 95%). HDPE has a high molecular weight, up to 3×10^6 g/mole.

[13] alkanes (paraffins), alkenes (olefins) or alkynes (acetylenes)

In addition to these types, other variations such as linear low-density polyethylenes (LLDPE) have been produced. These are ethylene co-polymers containing α-olefins, with a density of 915 – 940 kg/m^3.

A typical distribution of molecular mass plotted against mass fraction is shown in overleaf. From the plot, the Molecular Mass has a log normal distribution.

The published values for crystalline melting temperature vary between 410 and 419K (Brandrup, 1975), with a glass transition temperature of 148K. The crystalline melting point represents the end of a temperature range during which the crystal phase melts. The end-point of the range depends upon mainly upon initial crystal size and volume fraction. The extent of crystallinity also effects mechanical properties; for example, the influence over yield stress is shown overleaf. From this, it is clear that the more crystalline a material, the higher value for yield stress. Since crystallinity reduces with increasing temperature, yield stress is also an indirect decreasing function of temperature.

Material density is a direct function of the degree of crystallinity, where the crystal phase density (van Krevelen, 1976) for polyethylene is 997 kg/m^3 and the amorphous phase density is 854 kg/m^3. The degree of crystallinity can be determined from the material density, using:

$$\rho = V(\rho_c) + (1 - V)(\rho_a) \qquad 3.3$$

Where: ρ = overall material density

V = crystallinity volume fraction

ρ_c = density of crystal phase

ρ_a = density of amorphous phase

Therefore the overall solid phase density of semi crystalline HDPE is generally between 955 and 970 kg/m^3, whilst 910 – 935 kg/m^3 is a typical range for the less crystalline LDPE. There are also medium density polyethylenes marketed at around 940 kg/m^3.

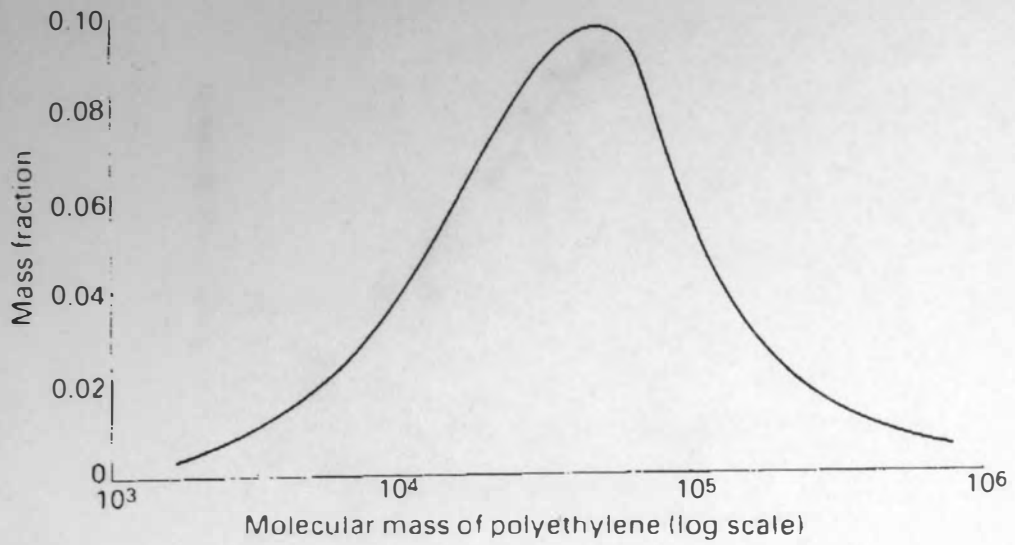

Figure 3-3. Plot of polyethylene MW distribution, determined using GPC (Mills, 1986)

From Figure 3-4, yield stress is a direct linear function of degree of crystallinity. This is important, since although complete thermoplastic melt rheology[14] does not follow any generic viscosity model, there is an initial resistance to flow similar to a 'Bingham plastic' (Kay, 1988). (The Bingham model applies to materials that are rigid until applied shear stress exceeds a critical value, after which point they exhibit characteristic Newtonian flow).

This critical stress is the yield stress, σ_{yield} (MN/m^2) found from Figure 3-4 to be:

$$\sigma_{yield} = 65.686(\text{vol fraction}) - 17.735 \qquad 3.4$$

NB. This approximation will break down for low crystallinity, since there is a crystal concentration limit below which there is no continuous structure of spherulites.

[14] rheology: study of deformation and flow of matter

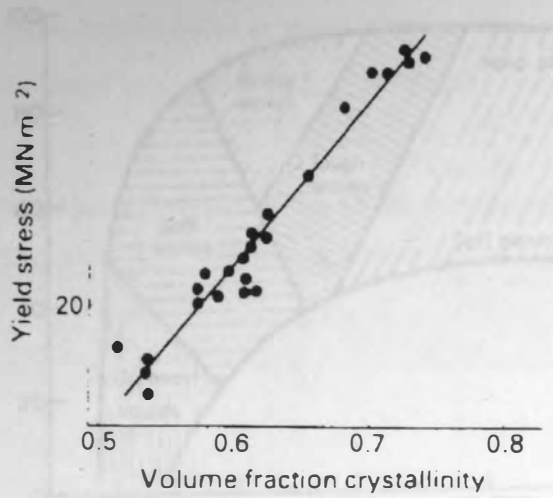

Figure 3-4. Effect of crystallinity on yield stress (at 293K) for PE (Mills, 1986)

The combined effects of crystallinity and molecular weight on physical properties are illustrated in Figure 3-5. From the diagram, it is clear that reducing crystallinity without altering the molecular weight causes reversible material softening. However, if irreversible MW degradation occurs, then the physical structure of the material softens, becomes waxy and then degrades to a liquid, dependant on the degree of degradation.

Previous experimental work, heating high density polyethylene in the absence of oxygen, found that the material was stable up to 563 K, above which molecular weight degraded, resulting in material appearing like a hard polyethylene wax (Madorsky, 1964)

Further work comparing linear & branched polyethylene (Wall & Strauss, 1960), found branching enhances intramolecular hydrogen transfer at expense of intermolecular reactions due to decreased availability of α-hydrogen atoms, therefore thermal stability is diminished. Consequently, increased density of polyethylene produces increased thermal stability.

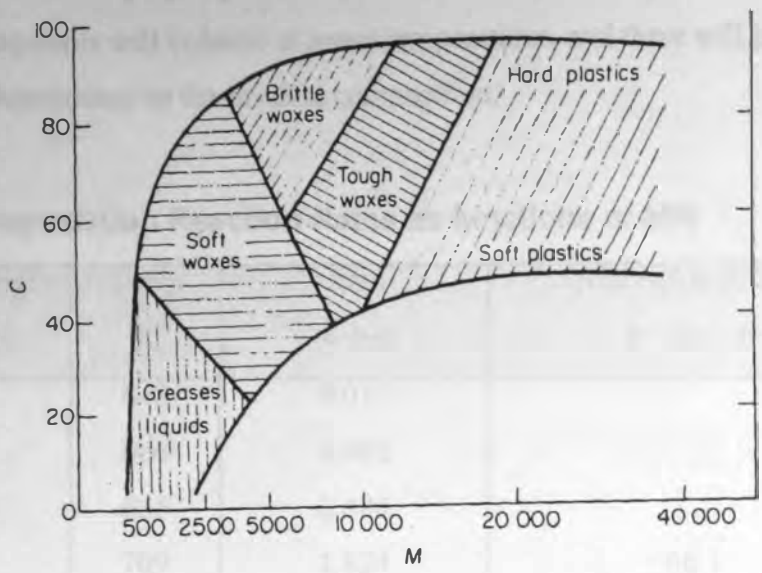

Figure 3-5. The effect of molecular mass (M) and % crystallinity (C) on properties of PE (Mills, 1986)

Jellinek (Jellinek, 1949; Cullis, 1981) studied 3 low molecular weight polyethylenes, (23000, 16000 and 11000) weighing them in a vacuum as they were heated. The results are plotted as Figure 3-6. Inspection shows cumulative weight loss is linear below ~70% volatilization, indicating zero order degradation processes. Reaction rates were then calculated from the curves, as shown in Table 3-B. From this, it is clear that activation energy increases with increasing MW of the polyethylene samples.

The rate of heating, as well as actual temperature will also effect the material properties. The level of applied heat flux supplied to a polymer surface affects the rate of reduction of molecular mass. Support for this is found from experiments carried out to thermally degrade a commercial polyethylene (MW 20,000) in a vacuum (Madorsky, 1964). The results are shown in Table 3-B, comparing temperature, time and amount of material volatized.

The analysis shows that significant volatisation occurs over a range, in this case 673 – 723K, with a small amount of material volatised at lower temperature. Since

thermal degradation of polyethylene is via a random scission process, it is probable that lighter fragments will volatise at lower temperatures, and there will be a temperature dependency to the product composition.

Table 3-B. Degradation Reaction Rates as functions of MW

Molecular weight of Sample	Temp K	Rate %/min	Activation Energy kCal/mole
23000	648	0.011	
	666	0.092	
	685	0.480	
	709	1.824	66.1
16000	649	0.072	
	650	0.078	
	661	0.234	
	676	0.486	
	685	0.744	52.6
11000	647	0.108	
	666	0.270	
	683	0.582	
	693	1.014	
	699	1.248	46.0

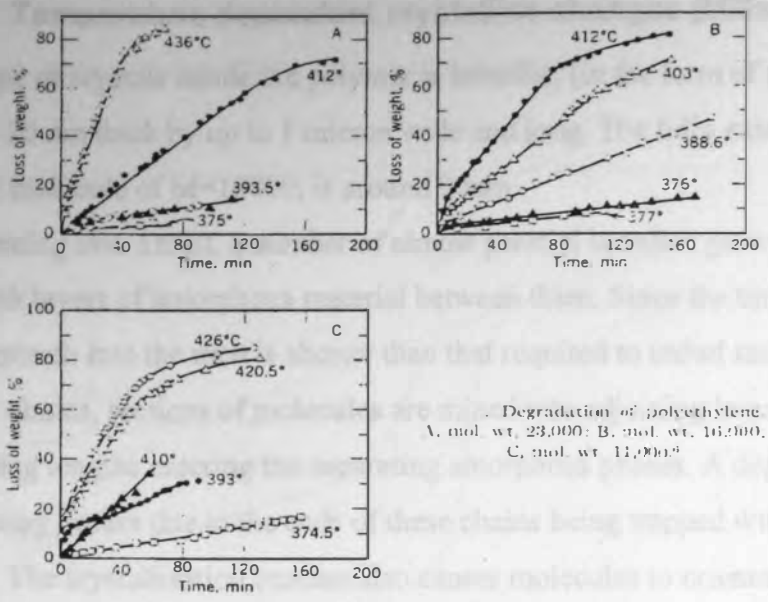

Degradation of polyethylene
A, mol. wt. 23,000; B, mol. wt. 16,000;
C, mol. wt. 11,000.[5]

Figure 3-6. Results from Jellinek's thermal degradation study

Table 3-C. Pyrolysis of low molecular weight polyethylene as a function of temp & time

Exp't	Temp K	Heating duration (min)	Volatisation %	Pyrolysed volatiles (%)
1	608	30	3.4	92.9
2	648	60	12.2	95.1
3	649	30	14.8	93.9
4	653	30	23.5	98.3
5	653	60	17.0	95.9
6	653	30	17.6	95.8
7	653	90	21.1	97.6
8	677	30	70.3	96.6
9	677	30	62.3	98.2
10	678	60	70.6	96.9
11	679	60	88.6	97.2
12	679	90	93.9	97.2
13	723	30	98.6	96.9

3.2.1.2 Temperature dependant crystalline changes (Mills, 1986)

The shape of crystals inside the polymer is lamellar, (in the form of a plate or sheet), and 10 –20 nm thick by up to 1 micron wide and long. The fully extended length of a polymer molecule of M=10000, is around 90nm.

Upon heating into a melt, a number of almost parallel lamellae grow together into the melt, with layers of amorphous material between them. Since the time taken for crystal growth into the melt is shorter than that required to unfurl randomly coiled polymer chains, sections of molecules are mixed into adjoining lamella crystals, with intervening lengths entering the separating amorphous phases. A degree of crosslinking occurs due to the ends of these chains being trapped within different crystals. The crystallisation process also causes molecules to orientate into positions of minimum stress near growth fronts, with some molecules merging to form intercrystal links.

The polymer melt starts to crystallise after formation of heterogeneous crystal nuclei, usually formed on foreign particles, such as residues, pigment or dust. The lamellae grow from the nucleus, and branch into 'spherulites' (small spheres), growing until they impinge on each other. Since the melt contains a range of molecular masses and chain regularity, the spherulitic composition varies through the melt. This variation occurs because the rate of crystallisation is a function of molecular mass.

As the lamellae grow into the melt, short chains have time to diffuse a distance equal to half the lamella thickness, and the lower molecular fraction will crystallise at a lower temperature between the main lamella. Slow melt rates may allow time for diffusion of low molecular mass material ahead of the growing spherulites, forming weak boundary regions. The overall solid phase crystallinity is between 40 – 95%, with some of the amorphous material contained the space between the lamella. Due to variations in molecular mass material, the lowest molecular mass lamella can have a melting point 30K below the overall melt point.

In addition to the crystal effects outlined above, all polymers have high thermal expansion coefficients, due to increased thermal vibration with increased temperature being only weakly resisted by the van der Waals forces between the chains. If molecular orientation is present, then the expansion will be anisotropic, largest in the direction with the smallest fraction of covalent bonding. A comparison of specific

volume increase with temperature for generic polymers in amorphous, semi-crystalline and crystalline states is shown in Figure 3-7.

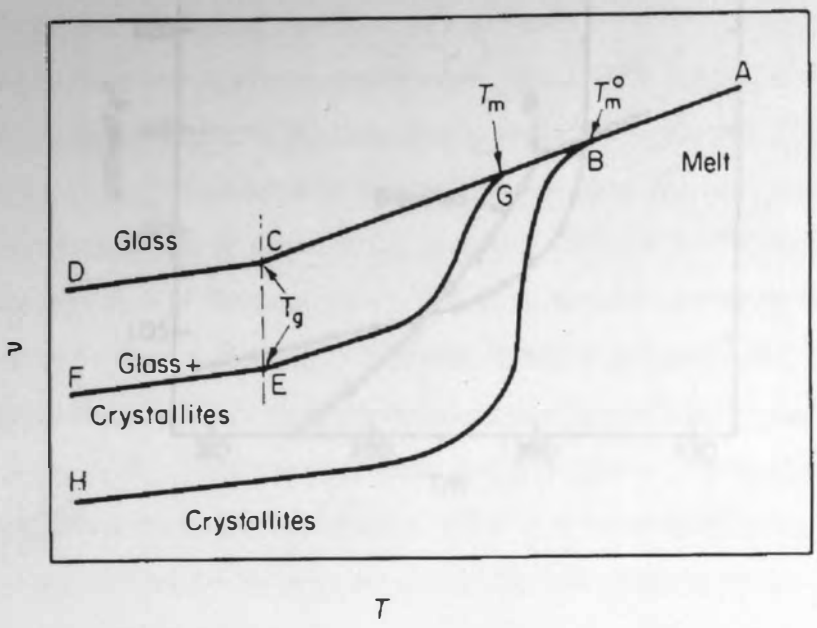

Figure 3-7. Specific volume increase with temperature for generic polymer types (Cowie, 1973)

Figure 3-7 clearly shows that above melt temperature, Tm, all polymers show a gradual linear volume increase with temperature. Below Tm, there is a distinct difference in volume – temperature functions due to the extent of crystallinity present in the polymer. Therefore expansion is related to both thermal vibration stresses overcoming the van der Waals forces, and the amount of crystallinity.
For a semi-crystalline polymer, the greatest increase in specific volume is associated with the melting of the crystal phase. Figure 3-8 is a volume – temperature diagram for polyethylene, showing the difference between high (linear) and low density (branched) material. There is a sharp increase in specific volume at Tm.

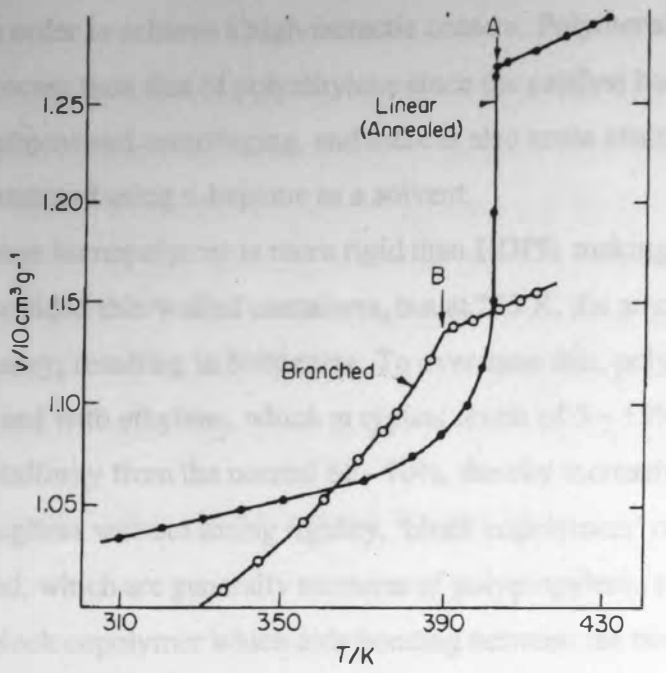

Figure 3-8. The volumetric expansion of high & low density polyethylenes (Points A & B are the respective melting temperatures) (Cowie, 1973)

3.2.2 Polypropylene

Polypropylene is the second most important commercial thermoplastic, accounting for around 20% of the market, ~ 740 ktonnes/annum in Western Europe. Around 30 % of the total produced is used for fibre applications, preferred to HDPE because of its higher melting point, with a further 20% used for oriented film, where good clarity is required, e.g. wrapping for cigarette packets.

3.2.2.1 Material Characterisation & Properties

Polypropylene has a density of between 850 and 940 kg/m^3, and crystallinity of ~ 65 %. The glass transition temperature for polypropylene lies between 238 - 299 K, and melt temperature is around 443 K.

To manufacture polypropylene (Mills, 1986), propylene is polymerised with an organometallic[15] catalyst, such as a mixture of aluminium alkyl and titanium

[15] metal with an atom or ion bound to an organic group

chloride, in order to achieve a high isotactic content. Polymerisation is a more complex process than that of polyethylene since the catalyst has to be removed by solvent treatment and centrifuging, and there is also some atactic by-product which has to be extracted using n-heptane as a solvent.

Polypropylene homopolymer is more rigid than HDPE, making it a better choice for injection moulded thin walled containers, but at 273 K, the amorphous fraction becomes glassy, resulting in brittleness. To overcome this, polypropylene is usually copolymerised with ethylene, which at typical levels of 5 – 15% ethylene, will reduce crystallinity from the normal 60 - 70%, thereby increasing flexibility. To improve toughess without losing rigidity, 'block copolymers' of 5 – 15% ethylene are produced, which are generally mixtures of polypropylene, some polyethylene, and some block copolymer which aids bonding between the two phases. Upon heating, the polyethylene component will melt at lower temperature phase than the polypropylene, as shown by peaks on specific heat plots, as shown in Figure 3-9.

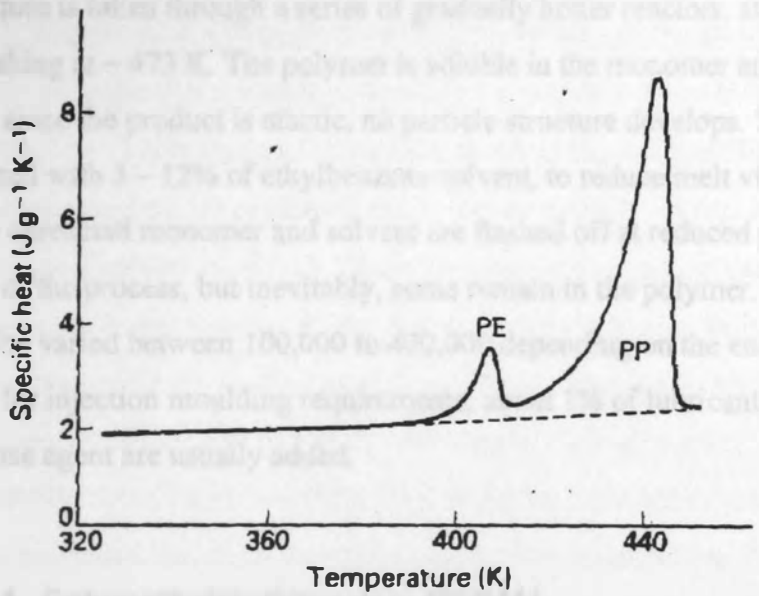

Figure 3-9. Specific Heat - Temperature plot for a PP copolymer

Although polypropylene is less thermally stable than polyethylene, one of the key similarities in terms of decomposition factors, is that molecular weight starts to decrease at temperatures well below those at which weight loss becomes significant (David, 1975).

3.2.3 Polystyrene

This is the fourth largest volume commercial polymer, with a 6.3% market share (private communication, McIlwee, 2000). Polystyrene homopolymer is an optically clear glass, which as oriented film is used for electrical insulation of capacitors. Another use is foamed, for building insulation and shock absorbing packaging. However, polystyrene is brittle and susceptible to UV degradation, and so has been developed into several toughened versions, such as high impact polystyrene (HIPS) which contains an elastomeric additive and is often used for television set housings.

3.2.3.1 Material Characterisation & Properties

Polystyrene has a glass transition temperature of 358 –380 K, a melt temperature of ~513 K and a density of 1050 – 1130 kg/m^3 (van Krevelen, 1976).
Styrene (phenylethene) homopolymers (Mills, 1986) are produced by a free radical polymerisation process. This proceeds to completion as the styrene/polystyrene mixture is taken through a series of gradually hotter reactors, starting at 383 K, and finishing at ~ 473 K. The polymer is soluble in the monomer at all concentrations and since the product is atactic, no particle structure develops. The system is often diluted with 3 – 12% of ethylbenzene solvent, to reduce melt viscosity at later stages. The unreacted monomer and solvent are flashed off at reduced pressure toward the end of the process, but inevitably, some remain in the polymer. The molecular mass can be varied between 100,000 to 400,000 depending on the end use requirement, and for injection moulding requirements, about 1% of lubricant, and 0.3% of mould release agent are usually added.

3.2.4 Polymethylmethacrylate (PMMA)

This polymer is not commercially significant, with only a 0.8% market share. Despite this, this optically clear glassy amorphous plastic has been universally adopted as the favoured thermoplastic for testing within the fire research community, which is the reason for inclusion within this study. The preference for PMMA is because the polymer 'unzips' to monomer when heated to its degradation temperature. The unzipping mechanism (end chain scission), is repeatable and results in a slow decline in molecular weight. It is also generally commercially sold in high

molecular weight form, which does not melt so that it can be used in all the standard test methods and apparatus. Its other uses include lighting diffuser panels, and 'bullet-proof glass'.

3.2.4.1 Material Characterisation & Properties

PMMA is an atactic polymer with a density of 1170 to 1230 kg/m^3, a glass transition temperature of 266 – 399 K and a melt temperature of 433 – 473 K (ICI, 1985). The molecular weight of extruded PMMA at around 10^5 tends to be lower than that of cast PMMA, which is ~10^6. This enables extruded polymer to be injection moulded or further extruded, whilst cast PMMA is best suited to thermoforming techniques. A free radical vinyl polymerisation process produces PMMA, whereby free radicals are formed and react with monomer molecules to form long chains which are substantially unbranched.

3.3 The general effect of material properties on fire behaviour

The most important material parameters for analysis of fire behaviour are generally accepted to be density (ρ), thermal conductivity (k) and specific heat capacity (c). These parameters are combined into terms describing thermal inertia ($k\rho c$) and thermal diffusivity, α, ($k/\rho c$). Thermal inertia is a useful indicator of material response to initial heating. A low thermal inertia indicates a rapid rise in initial surface temperature, as illustrated for different materials in Figure 3-11. Thermal diffusivity is a measure of rate of heat transfer through a solid.

Generally, these values are calculated assuming constant values for k, ρ and c taken from published literature, generally having been measured at 298K. however, for thermoplastics, material properties are not constant over large temperature ranges. A problem then arises, since the only published data available is that used for processing, incorporating a temperature range below that required for a 'fire' analysis. For example, the variation of 'c' is shown for linear and branched polyethylene in Figure 3-10. From the diagram, specific heat increases with temperature, and there is a difference between high and low-density polyethylene. An infinite rise in specific heat occurs during a crystal melt temperature range.

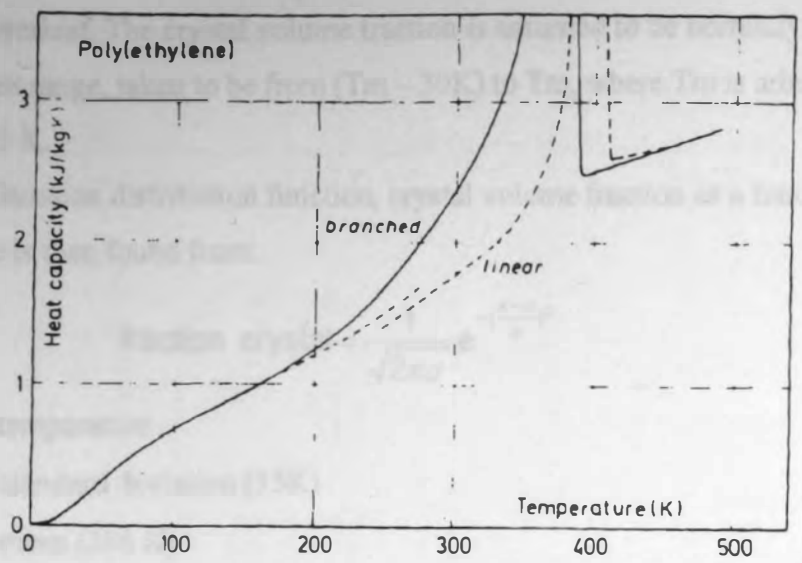

Figure 3-10. Variation in specific heat with temperature for HDPE & LDPE (Brandrup, 1976)

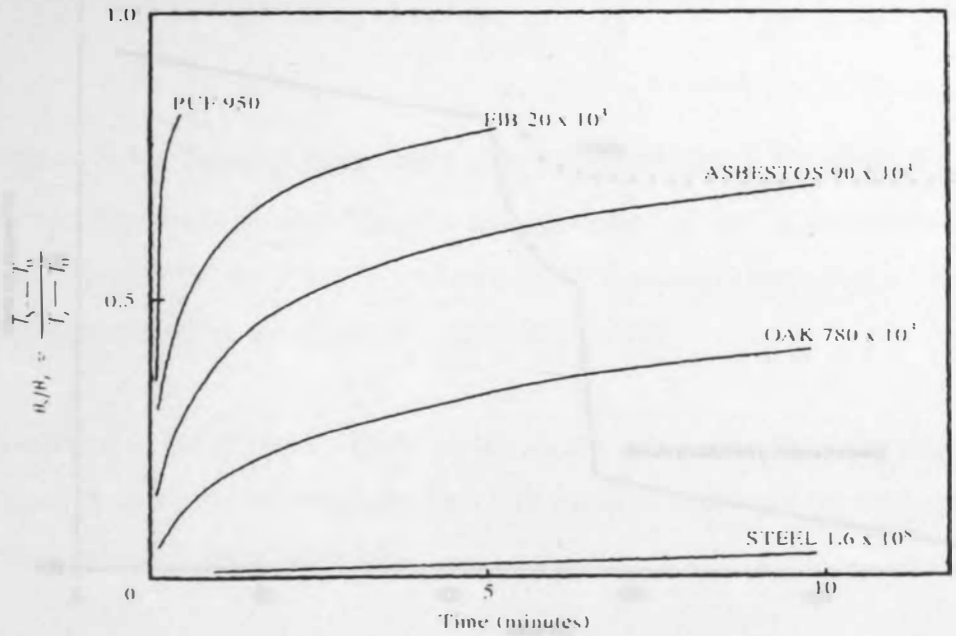

Figure 3-11. Effect of thermal inertia on surface temperature rise (Drysdale, 1999)

In terms of ρ, the reduction generally associated with a solid – liquid phase change will be further modified by the volume expansion. This, as shown in Figure 3-8, can be up to a 30% volume increase, at a temperature of 433 K.

The effect of reduction in crystallinity combined with volume expansion has been estimated overleaf. The crystal volume fraction is assumed to be normally distributed over the melt range, taken to be from (Tm – 30K) to Tm, where Tm is arbitrarily taken as 413 K.

Using the Gaussian distribution function, crystal volume fraction as a function of temperature is then found from:

$$\text{fraction crystal} = \frac{1}{\sqrt{2\pi\sigma}} e^{-\left(\frac{x-\mu}{\sigma}\right)^2} \qquad 3.5$$

Where x = temperature

σ = standard deviation (15K)

μ = mean (398 K)

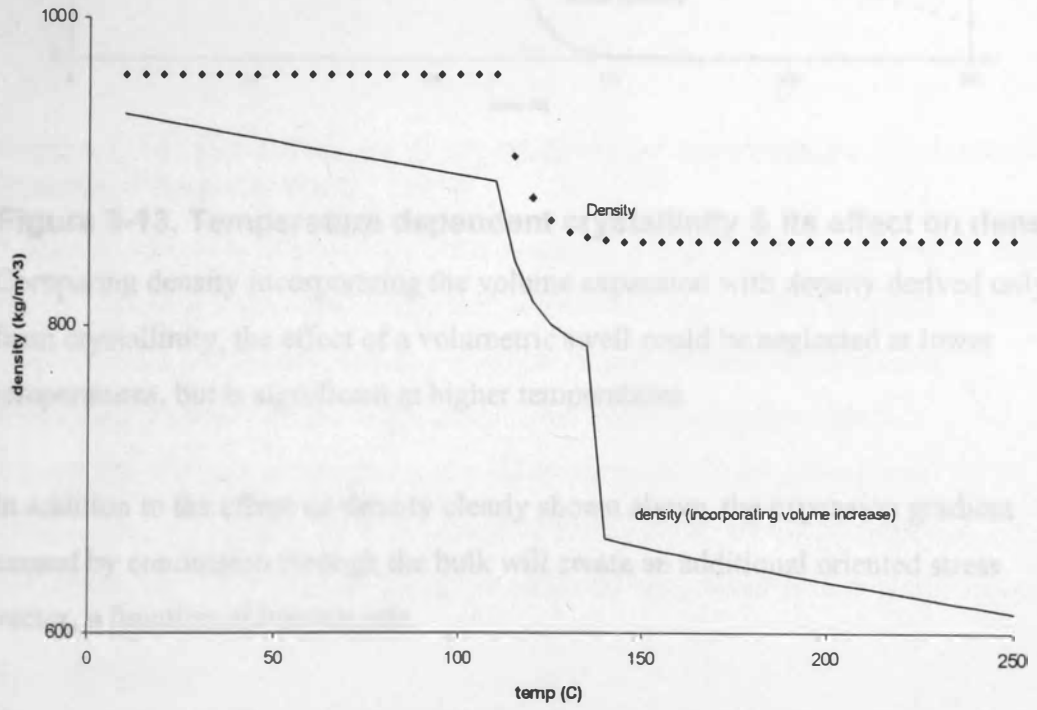

Figure 3-12. Density - temp function (with & without volume swell)

Density can then be calculated directly as a function of crystallinity using Equation 3.4. The increase in specific volume is approximated by two separate linear functions

(T < Tm, and T ≥ Tm); the resultant variations in fraction crystallinity and density as functions of temperature are shown in Figure 3-13.

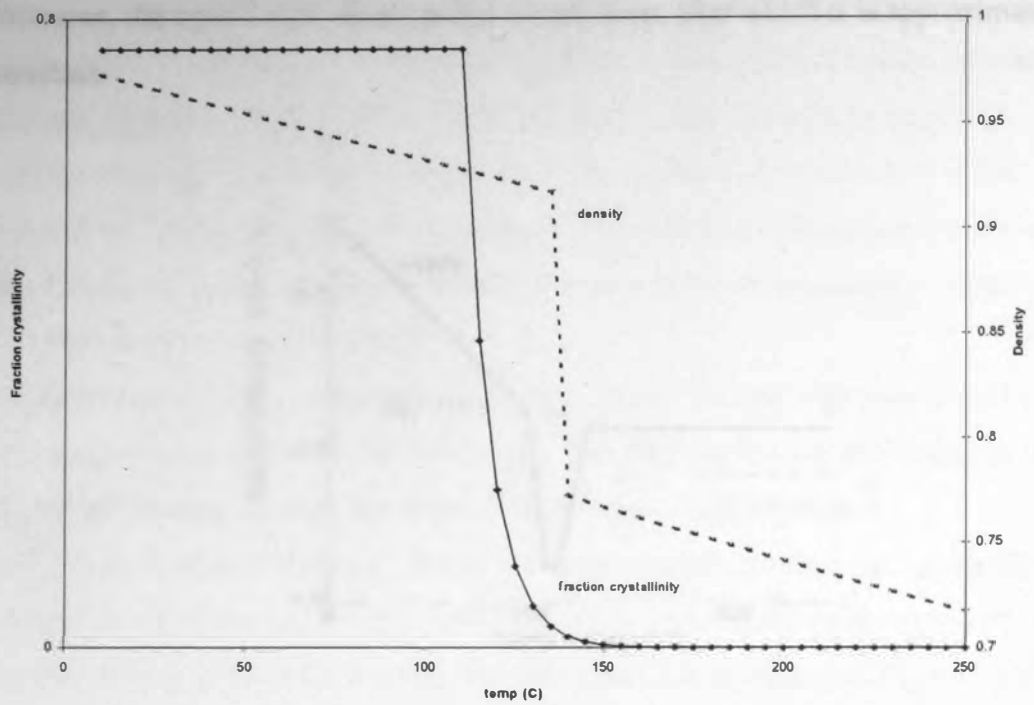

Figure 3-13. Temperature dependent crystallinity & its effect on density

Comparing density incorporating the volume expansion with density derived only from crystallinity, the effect of a volumetric swell could be neglected at lower temperatures, but is significant at higher temperatures.

In addition to the effect on density clearly shown above, the expansion gradient caused by conduction through the bulk will create an additional oriented stress vector, a function of heating rate.

The expansion gradient may be at least partly responsible for the surface protrusions noted in the 'kebab' experiments conducted at Buxton, when large localised surface expansions were the predominant drip sites for the molten flow as illustrated in Figure 4.1.6. These expanded areas were obviously significant parameters affecting melt flow behaviour, adding observational support to the importance of expansion in a flow analysis.

Figure 3-14 compares the thermal diffusivity, α, of semi–crystalline HDPE with amorphous polycarbonate. Whilst in both cases, α decreases as the temperature increases, the crystal melt phase causes a steep drop, after which α is approximately constant.

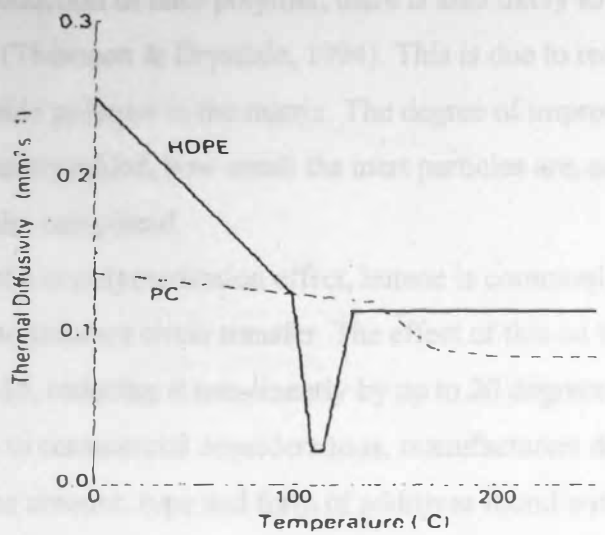

Figure 3-14. The influence of crystallinity on temperature dependant thermal diffusivity (Mills, 1986)

A melt is defined by the loss of crystal structure, which influences properties such as density, internal stress level, and material form. Having lost this structure, which restricts chain movement, molecular weight is then the predominant factor controlling viscosity, which is the main factor determining flow rate.

An additional problem relates to material composition. Base polymers or copolymers, which have been discussed up to this point, are not commercial thermoplastics, the difference being the additives introduced during manufacture.

3.4 Additives

Having looked at some of the factors influencing base polymer behaviour, it must be recognised that commercial plastics are rarely encountered in this form.

Huge ranges of molecular structures based on polyethylene are available, encompassing a range of material properties. The structures are designed to fulfil an end use application, and the composition is commercially sensitive. However, figures for consumption of the main additive groups in 1997 for Western Europe are shown

in Table 3-D. From this, it is clear that the most common additives are fillers. These can serve several purposes, for example cost reduction or increased component rigidity[16].

It is difficult to accurately quantify the general effect of an additive upon fire performance. For example, if inert mineral filler is incorporated to reduce the cost of a plastic by mass reduction of base polymer, there is also likely to be improved ignition resistance (Thomson & Drysdale, 1994). This is due to reduction of the quantity of flammable polymer in the matrix. The degree of improvement however, is a function of quantity added, how small the inert particles are, and how evenly it is distributed within the compound.

As an illustration of a copolymerisation effect, butene is commonly copolymerised with polyethylene to enhance chain transfer. The effect of this on the melting point is shown in Figure 3-15, reducing it non-linearly by up to 20 degrees.

Unfortunately, due to commercial considerations, manufacturers do not generally release details of the amount, type and form of additives found within a product. The general effects on polymer viscosity are summarised as illustrated in Figure 3-16 (Cogswell, 1981).

[16] Although there are many additives listed, some are never added to melting plastics (e.g. plasticiser which is usually incorporated with rigid PVC).

Figure 3-15. Effect of butene on Tm for HDPE

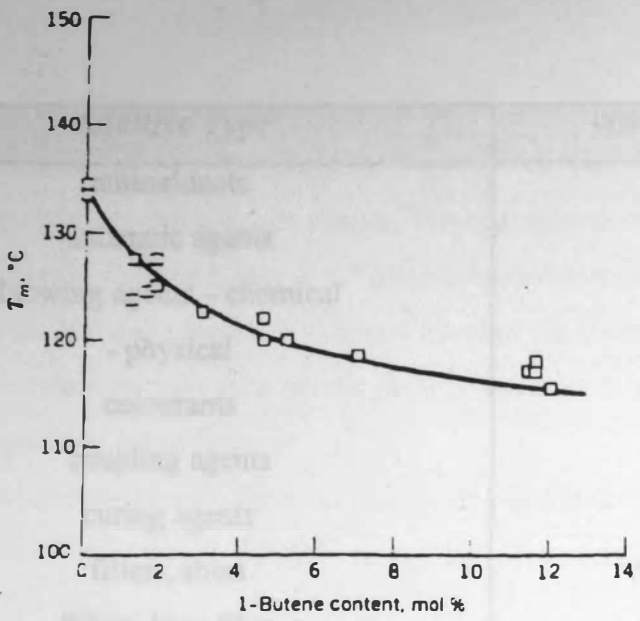

Melting point of HDPE as a function of 1-butene content.

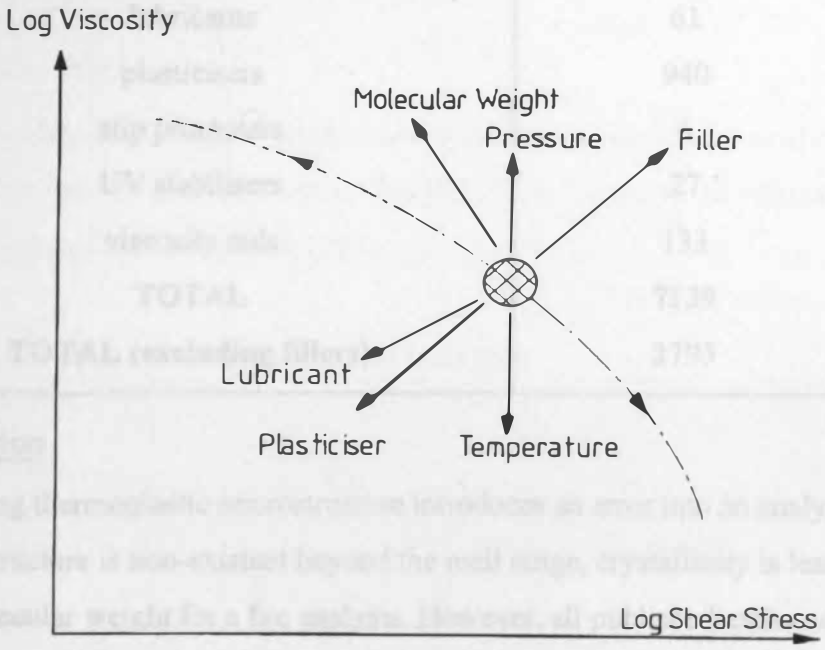

Figure 3-16. Effects of additives on polymer viscosity (Cogswell, 1981)

4 Experimental work

This chapter is subdivided into three main sections:

1. Small-scale work aimed at using the Cone Calorimeter to produce a large database of thermoplastic test results. The materials tested cover all of the thermoplastic decomposition mechanisms described in Table 1-A, Chapter 1. The main uses of the database are to assess whether the Cone can produce meaningful data for assessing melt flow thermoplastics and also to compare different decomposition behaviour.
2. The development process for a medium scale experimental technique (known as the "Sedan Rig") capable of determining the effect of melt flow behaviour on overall fire dynamics
3. Results of experiments carried out using the "Sedan Rig" assessing the influence of melt-flow on fire growth.

4.1 Cone Calorimeter.

4.1.1 Overview.

The Cone Calorimeter was illustrated and described in Section 2.3.4. The level of radiant flux can be set to between 10 and 100 kW/m^2, some of the effects of which are outlined in Table 4-A (Paul, 1994).

Table 4-A. Effects of various levels of heat flux

Surface Heat Flux (kW/m^2)	Effect
10	Unbearable skin pain after 10 sec
13-20	Minimum for pilot ignition of cellulosics
20	Nominal heat flux at floor level for the onset of 'flashover')
40-70	Low ventilation fire
50-150	"Normal" ventilation controlled fire

4.1.2 Method.

A series of commercial thermoplastics were acquired as shown in Table 4-B, covering a range of thermoplastic fire behaviour. None of the thermoplastics supplied contains fire retardant additives, but further detail of their composition has proved commercially sensitive and impossible to obtain. The experiments were designed to test 13 materials at six levels of applied heat flux (20, 25, 30, 40, 50, 60 kW/m^2), with 3 tests / material / flux, making a total of 234 tests. Some additional work was undertaken to investigate the effect of differences in thickness, orientation and molecular weight for the same material, bringing the total to 377 tests.
All samples were trimmed to $100cm^2$ area and weighed, to calculate the average density of each material. Of the 16 material variations tested, twelve were 4mm thick, two were 6mm thick, with one at 3mm and one 5mm thickness. 311 of the tests used horizontally orientated samples with 66 vertically orientated.

Table 4-B. Materials tested in this study.

Material	Thickness (mm)	Behaviour	Density kg/m^3
Durolon Polycarbonate	4	Char	1379
Polypropylene Novolen 1100H	4	Melt	929
HDPE Lupolen 5361A (200L)	4	Melt	967
UPVC Hostalit 2060B	4	Char	1549
Polyman PS 185K (Polystyrene)	4	Melt	1132
Eastman Spectar (Polyethylene Terephthalate)	4	Melt	1323
PS Muster (Polystyrene)	4	Melt	1111
Cyrex 200 (Polycarbonate/Acrylic alloy)	4	Char	1291
Polystrol Hi Natural (Polystyrene)	4	Melt	1055
Polyman Glaskar PC XP 41 RS (Polycarbonate)	4	Char	1268
Polyman PXC 31 (Polycarbonate)	4	Char	1305
Low Molecular Weight PMMA (ICI)	6	Melt	1185
High Molecular Weight PMMA (ICI Perspex)	5	Sublime[1]	1092
High Molecular Weight PMMA	4	Sublime	1371
Polystyrene (supplied by Easter Rd Plastics)	3	Melt	1013
Polypropylene (supplied by Easter Rd Plastics)	6	Melt	896

[1] PMMA degradation – not a true sublimation as the molecular structure changes, but the solid is converted to vapour without passing through a liquid state.

The tests were conducted as described previously, using Edinburgh University's Stanton Redcroft Cone Calorimeter, over a period of 30 months, finishing in January 2000.

4.1.3 The effect of Molecular Weight (MW)

To investigate the effect of MW on fire behaviour, two transparent 5mm thick PMMA materials were tested at 20 and 35 kW/m^2. The sample molecular weights were 196000 (low), and 535000 (high), with densities 1111kg/ m^3 and 1092kg/ m^3 respectively. The relevant averaged data are presented in Table 4-C, with standard deviations in brackets.

Table 4-C. Comparison of Different MW Cone Results

Q_{app} kW/m^2	MW	t_{ig} (s)	Pk RHR (kW/m^2)	t (Pk RHR) (s)	EHC (MJ/kg)	Peak dm/dt (g/s)
20	High	164.5	408.7	425	23.7	0.167
		(11.5)	(5.8)	(30)	(0.3)	(0.003)
35	High	58	614.3	261.7	22.76	0.257
		(0.8)	(11.1)	(2.4)	(1.9)	(0.01)
20	Low	158	456	420	23.96	0.189
		(4.2)	(12.9)	(7.0)	(0.01)	(0.01)
35	Low	60	653.3	258.3	22.08	0.278
		(2.2)	(21.6)	(10.2)	(0.3)	(0.01)

From these results, it is apparent that MW variation has no significant effect on time to ignition or effective heat of combustion. This is expected, since time to ignition is a function of thermal inertia, kρc (as discussed in Section 4.1.6) and the material densities are very similar.

A reduction in MW for PMMA is found to produce a higher peak heat release and higher peak mass loss rate. Therefore, the lower molecular weight material burns faster with an increased rate of heat release in comparison to the higher molecular weight material.

Two different MW polystyrenes were also tested, PS 185K (low MW) and PS Muster (higher MW), with densities 1132 (185K) and 1111kg/m^3 (Muster). Some of the results are shown in Table 4-D.

In comparison to the PMMA results, there is a higher rate of heat release for both polystyrenes. This is due to greater ΔH_c values for PS (39.85 kJ/g compared to 24.89 for PMMA (Drysdale, 1999)). The EHC values shown in Table 4-D are much lower than this. This is partly because polystyrenes produce very low viscosity melts, which are uncontainable with this apparatus. Consequently, the mass loss rate recorded is artificially high since some material is flowing away from the heat source and onto the load cell platform below rather than burning. Therefore high mass loss rates produce low EHC values. The low combustion efficiency is also consistent with the fact that burning polystyrene produces more soot than PMMA, resulting in a much more radiative flame than is found for PMMA.

Table 4-D. Comparison of different MW Polystyrenes

Flux & material	t_{ig} (s)	Pk RHR (kW/m^2)	t (Pk RHR) (s)	EHC (MJ/kg)
20 MUS	181.7(21.7)	555(18)	296.7(6.2)	25.9(1.4)
20 185K	201(2)	540(18)	300(0)	28(4.3)
25 MUS	165.6(5.4)	533(61)	293.3(8.5)	26.7(3.2)
25 185K	163.7(5.7)	554(40)	258.3(15)	28.3(2.9)
30 MUS	90(1.4)	744(11)	186.7(2.4)	26.1(0.3)
30 185	101.3(6.0)	659(9)	190(4)	24.3(0.5)
40 MUS	58.3(2.1)	784.3(4.8)	146.7(4.7)	18.99(2.3)
40 185	59.6(6.8)	736.3(19.5)	143.3(11.8)	18.87(1.5)
60 MUS	35(0)	904.6(95.2)	141.6(2.4)	24.89(2.6)
60 185	36(1.4)	974.1(15.6)	141.7(10.27)	22.68(0.5)

(NB The dm/dt values are excluded from the table due to overspill making them artificially high).

4.1.4 Sample Thickness

Since the thermoplastics investigated are all between 3 and 6mm, a simulated approach was selected to investigate varying thickness. High MW PMMA was selected for testing at 20 and 25 kW/m^2, with thickness varied in 3 ways. Single samples were tested as controls, and then a 2mm steel plate insert used as backing for a single sample inside the foil wrapping, and finally two samples were placed in an oven for at 130°C for 4 hours, compressed by a 5kg mass. This resulted in a thermally fused 10mm thick sample. The results are as shown in Table 4-E, from which it is apparent that the conductive backing reduces the peak heat release and increases time to ignition and peak heat release. The doubled sample also takes longer to ignite, but the peak heat release is increased along with the time taken to achieve it. There are two peaks for heat release and peak dm/dt in this case, where the higher values are found on the second peak.

Table 4-E. Effect of thickness on test properties

Condition (Flux)	t_{ig} (mean) s	Pk RHR kW/m^2	t(Pk RHR) s	dm/dt max g/s
Single (20)	217	352	475	0.145
+steel plate	284	324	610	0.159
Doubled	261	383	883	0.175
Single (25)	119	464.3	360	0.181
+steel plate	134	405.6	436.7	0.144
Doubled	132.67	481.7	735	0.172

This indicates that although a sample is insulated by the ceramic fibre pad it rests on in the sample holder, it is not perfectly insulated. Therefore for thermally thin samples the results are apparatus dependent.

Thermal Thickness

To reduce the property dependence on the equipment, thermally thick samples would be required. The definition of thermal thickness is derived from consideration of a semi-infinite solid, exposed to a uniform heat flux (Drysdale, 1999). The limiting condition relates to when the rear face of the slab is heated to a temperature

arbitrarily set to 0.5 % of (T_s-T_o), where T_s is the surface temperature and T_o is ambient. This is incorporated in Equation 4.1, where $\sqrt{\alpha t}$ is the characteristic thermal conduction length, which can be used to estimate the depth of the heated layer (L).

$$L \approx 4\sqrt{(\alpha t)} \qquad 4.1$$

t = heating time (time to ignition from the cone test results)

α = thermal diffusivity (k/ρc)

From this, a material can be considered thick, and heat losses through the rear classed as negligible providing the thickness > $4\sqrt{(\alpha t)}$. Using published (constant) values of α, this is found to be the case for most of the materials in this study exposed to high values of applied heat flux. *NB It was found in this study, as shown in Figure 4-1, that a material can behave as thermally thick at high heat fluxes, but not at lower heat fluxes, when the assumptions used to derive the approximation break down. Therefore comparisons of results cannot be made for different thermoplastic thicknesses.*

(In practice the use of a constant alpha is not justifiable for a melt flow plastic, as explained previously in Section 3.3.)

4.1.5 Orientation Effects

In the Cone Calorimeter, it is possible to test samples in either horizontal or vertical orientations, using the appropriate sample holder and heater configuration. Due largely to problems with melt-flow thermoplastics, vertical testing is no longer included in the ISO Test protocol, but it has been investigated during this study. For comparison, 5mm thick PMMA (High MW) was selected because it does not melt and flow upon heating, and can be better contained within the vertical sample holder. The results for 25 and 35 kW/m^2 tests are shown, with standard deviations in brackets, in Table 4-F.

Table 4-F. Comparison of horizontal & vertical cone test results

Flux & Angle	t_{ig} sec	Pk RHR kW/m^2	t (Pk RHR) sec	dm/dt (g/s) (10-90%)	EHC MJ/kg
25 Hor	119 (4.5)	464.6 (7.0)	360 (21.2)	0.102 (0.027)	23.02 (3.28)
35 Hor	58 (0.8)	614.4 (11.1)	261.7 (2.4)	0.201 (0.004)	22.77 (1.90)
25 Ver	118 (5.1)	530.6 (26.0)	326.7 (20.9)	0.144 (0.014)	22.23 (0.29)
35 Ver	66.7 (6.3)	665.5 (2.9)	263.3 (4.7)	0.177 (0.024)	22.68 (3.64)

From this, the vertical samples produce a higher peak rate of heat release, slightly faster than horizontal specimens. These differences may be due to the convection currents over the sample, which if the heater is ignored, can be approximated to natural convection for a flat plate in a hot gas stream. These are standard empirical correlations found from (Holman, 1992):

$$h_{hor} = k/l \; 0.54(Gr\,Pr)^{0.25} \qquad 4.2a$$

laminar flow (i.e. $GrPr < 2 \times 10^7$)

$$h_{hor} = k/l \; 0.14(Gr\,Pr)^{1/3} \qquad 4.2b$$

turbulent flow ($GrPr > 2 \times 10^7$)

$$h_{vert} = k/l \; 0.59(Gr\,Pr)^{0.25} \qquad 4.2c$$

laminar flow ($GrPr < 10^9$)

$$h_{vert} = k/l \; 0.13(Gr\,Pr)^{1/3} \qquad 4.2d$$

turbulent flow ($GrPr > 10^9$)

where: k is the thermal conductivity of air,

l is a characteristic length (0.1m for Cone work),

Gr is the Grashof Number[2]

Pr is the Prandtl Number[3]

(all properties evaluated at the mean film temperature)

---

2 $Gr = \frac{gl^3\beta\Delta T}{v^2}$ a ratio of upward buoyancy forces to viscous drag

3 $Pr = \frac{v}{\alpha}$ where v = kinematic viscosity

A preliminary investigation of the effect of sample orientation on ignition (Thomson, 1990) using a rotatable rig containing a cone heater, found time to ignition to be around 35 % greater for vertical samples than for horizontal ones at all fluxes. Thomson also found that ignition temperatures were higher for vertical samples than for horizontal with a greater difference found at low fluxes, which is as expected from the convective loss coefficients shown above. Thomson considers the time to ignition taking longer for vertical than horizontal to be explained by a greater flow of volatiles being required to establish a flame, as the flame is less stable at a vertical orientation. This flame stabilisation sensitivity is a function of the boundary conditions, which may account for the variation between the results from fan assisted Cone Calorimeter flow, with side walls reducing cross flows and Thomson's cone heater in an open rig. Therefore, the vertical cone results are largely a function of the apparatus and experimental conditions.

NB. The buoyancy driven flows generated by the presence of the hot cone heater must also have an effect.

4.1.6 Minimum Flux for Ignition

From the cone results, it is possible to plot time to ignition against applied heat flux for each material in order to estimate the asymptotic minimum flux required for ignition. Alternatively, correlations have been produced (see Drysdale, 1999) based on simplified heat transfer models where a constant surface flux is applied and heat losses are ignored, so that time to ignition can be found from Equation 4.3a (for thermally thick materials) or Equation 4.3b (for thermally thin materials):

$$t_{ig} = \frac{\pi}{4} k\rho c \frac{(T_{ig} - T_o)^2}{\dot{Q}''^2_R} \qquad 4.3a$$

$$t_{ig} = \rho c \tau \frac{(T_{ig} - T_o)}{\dot{Q}''_R} \qquad 4.3b$$

where τ = material thickness.

This suggests that a plot of t_{ig}^{-1} vs applied flux for a thermally thin material will produce a straight line, which can be extrapolated to produce the critical flux for ignition, similarly a plot of $t_{ig}^{-0.5}$ for a thermally thick material will be linear. Both

plots for PP Novolen 1100H are shown in Figure 4-1, from which both straight lines seem to indicate that it is borderline thermally thick/thin, and either criteria could be justifiably applied. Further consideration of the thermally thick plot shows the critical flux for ignition is around zero, indicating the material may be liable to spontaneous heating, which is nonsense and shows why these approximations should be used with caution for these materials.

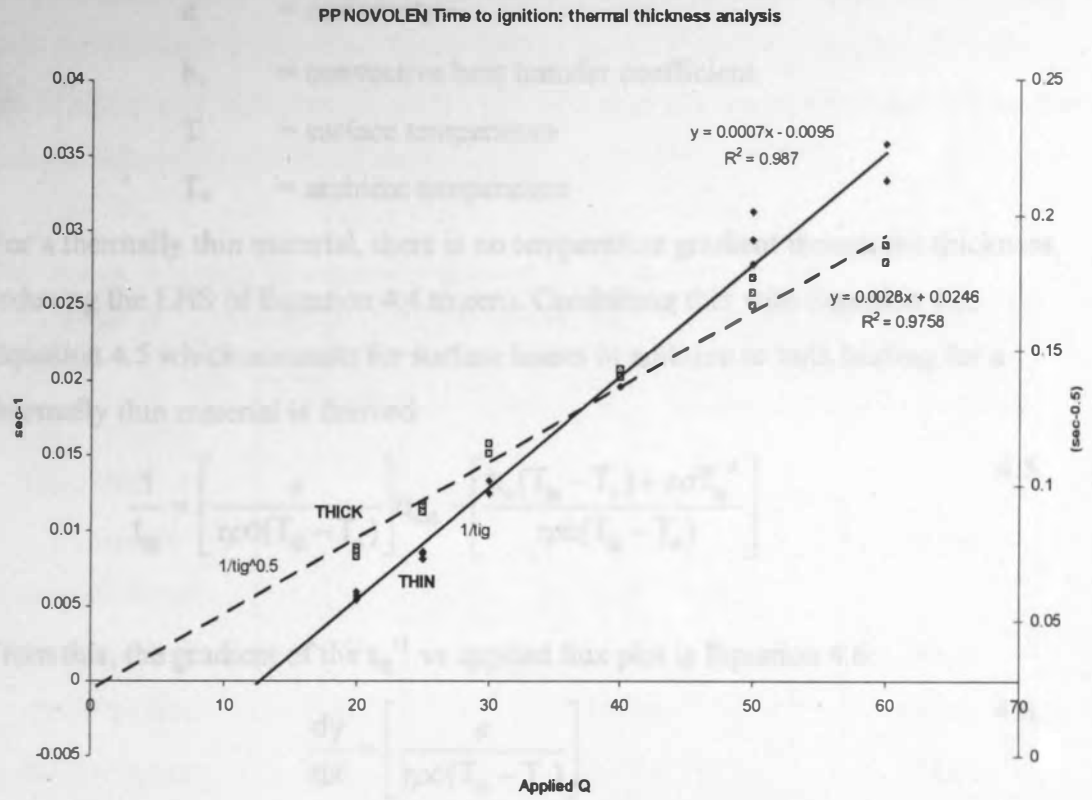

Figure 4-1. Plot of Q_{app} vs t_{ig}^{-1} and $t_{ig}^{-0.5}$ for PP

As outlined above these approaches ignore heat losses, and as the imposed heat flux is reduced, convective losses and also losses through the rear face of thin samples increase in significance. An examination of the significance of losses at low heating rates (for thick fuels) concluded that the critical flux derived in this way is only around 70% of the true value (Delichatsios, 1991).

Further investigation (Quintiere, 1992) of the surface losses from a semi infinite solid, (neglecting rear face losses) showed that convective and radiative losses can be accounted for by;

$$-k\frac{\partial T}{\partial y}\bigg|_{y=0} = \dot{q}'' = \varepsilon\dot{q}'' - h_c(T - T_o) - \varepsilon\sigma T^4 \qquad 4.4$$

Where
- k = thermal conductivity
- ε = emissivity
- h_c = convective heat transfer coefficient
- T = surface temperature
- T_o = ambient temperature

For a thermally thin material, there is no temperature gradient though the thickness, reducing the LHS of Equation 4.4 to zero. Combining this with Equation 4.3, Equation 4.5 which accounts for surface losses in addition to bulk heating for a thermally thin material is derived:

$$\frac{1}{t_{ig}} = \left[\frac{\varepsilon}{\tau\rho c(T_{ig} - T_o)}\right]q_{ext} - \left[\frac{h_c(T_{ig} - T_o) + \varepsilon\sigma T_{ig}^{\ 4}}{\tau\rho c(T_{ig} - T_o)}\right] \qquad 4.5$$

From this, the gradient of the t_{ig}^{-1} vs applied flux plot is Equation 4.6:

$$\frac{dy}{dx} = \left[\frac{\varepsilon}{\tau\rho c(T_{ig} - T_o)}\right] \qquad 4.6$$

Previous work attempting to model cone data in this way (Hopkins, 1995) using thick fuels, has measured ignition temperatures, assumed an emissivity of 1, and rearranged the equation to obtain thermal inertia ($k\rho c$). For thin fuels, if an ignition temperature can be measured then specific heat capacity can be found directly.

4.1.7 Ignition Temperatures

Previous work (Thomson, 1987) has shown that for thermoplastics exposed to constant radiant flux, the surface temperature for ignition (T_{ig}) is independent of the level of applied flux, although this is experimentally difficult to measure. Thomson worked with 6mm thickness x (65mm x 65mm) thermoplastic samples, and

measured the ignition temperatures shown in Table 4-G. This is directly relevant to this study as Thomson's thermoplastics are of similar thickness. Further similar work was undertaken (Hopkins, 1995) investigating ignition times and temperatures of Nylon 6/6, polyethylene, and black cast PMMA using the Cone Calorimeter. In this study, at 25mm thickness the materials are definitely thermally thick and the measured results are shown in Table 4-H.

This shows, however that the average values of T_{ig} for Hopkins' materials are lower than for Thomson's materials. This is largely due to Thomson's results being of much higher precision than Hopkins', but there may also be an effect due to heat loss through the rear face of the thinner samples.

Table 4-G. Average Measured Values of T_{ig} (Thomson, 1987).

Material	Density (kg/m^3)	Range of applied heat flux (kW/m^2)	T_{ig} (°C)
ICI Perspex (cast PMMA)	1190	17-37.5	310±3
Finnacryl (cast PMMA)	1190	18.5-38	309±6
Polyoxymethylene	1420	21-34	281±5
Polyethylene	920	19-34	363±3
Polypropylene	905	21-42.5	334±4
Polystyrene	1040	19-34	366±4

Table 4-H. Measured Ignition Temperatures (Hopkins, 1990)

Material	Density (kg/m^3)	Range of applied heat flux (kW/m^2)	T_{ig} (°C)
Nylon 6/6	1169	20 – 80	≈ 500
Polyethylene	955	20 – 80	315 – 330
Polypropylene	900	20 – 80	250 – 360
PMMA	1190	20 – 80	250 – 355

The scatter in Hopkins results reflects the experimental problems of thermocouple attachment to a melting surface under a continual heat flux, and also bubble formation within the material.

4.1.8 Emissivity

There is some similarity between Thomson's work and this study in terms of comparable materials tested. An approximation of emissivity (ε) can be derived by rearranging Equation 4.6 and using a known target value for T_{ig} (taken from Thomson), achieved by altering ε as shown in Equation 4.7. This was looped iteratively to achieve convergence on T_{ig} using an Excel spreadsheet, and ε calculated for the four similar materials between the studies (PMMA, polyethylene, polypropylene, polystyrene).

$$\left(\frac{q_{crit}\varepsilon}{h_c} + T_o\right) - \left(\frac{\varepsilon\sigma T_{ig}^{\ 4}}{h_c}\right) = T_{ig} \qquad 4.7$$

Where: q_{crit} =value from cone results

h_c = convective heat transfer coefficient (*taken from analysis of flow over horizontal flat plate to be 10 W/m^{2}K.)*

T_o = ambient temp (293K)

The results are shown in Table 4-I (increasing T_{ig} or reducing q_{crit} increase ε).

Table 4-I Derived values for emissivity

Material	T_{ig} (K) (Thomson)	critical flux for ignition (kW/m^2)	Derived ε
PMMA	561	13.7	0.33
Polyethylene	636	14	0.73
Polypropylene	608	13.6	0.54
Polystyrene	639	14	0.73

Whilst no data on thermoplastic flame emissivity for cone samples were uncovered, a study of radiative properties of thermoplastic pool fires (Markstein, 1979) found emissivity generally reduced with increasing height above the burning pool. The

emissivities for the four plastics studied (measured at the heights plotted, directly above the fuel bed) are shown in Figure 4-2 for comparison.

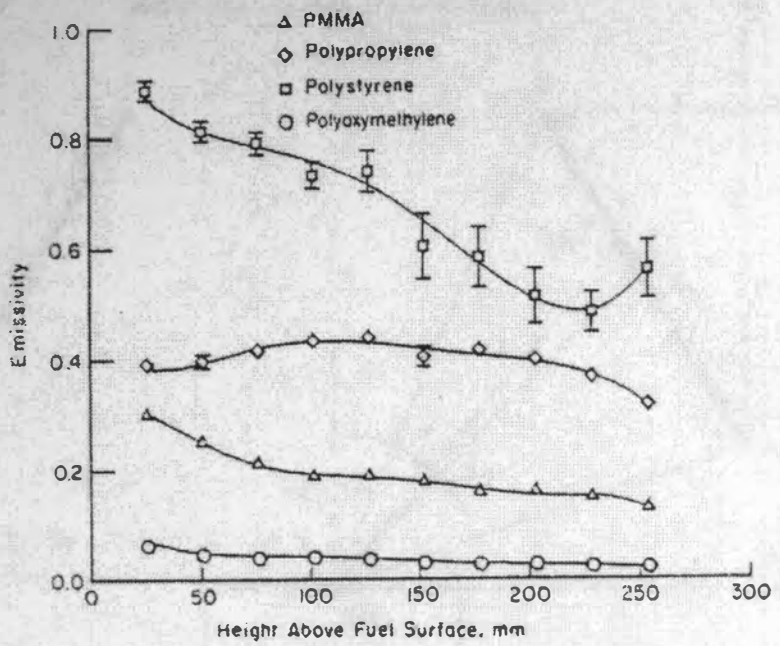

Figure 4-2. Flame emissivity vs height above fuel surface for 0.31x 0.31m pool fires

Char forming Polymers

The materials tested by Thomson & Hopkins looked at burning behaviour including melting and solid – vapour degradation, but not charring. The char formers present a more complex problem, since the char protects the base polymer by forming a hollow carbonaceous structure if the rate of heating is sufficient to initiate the char forming chemical reactions. Some of the problems are outlined below:

1. Char involves expansion, so the outer surface is no longer steady or horizontal therefore the convective heat transfer coefficient (h_c) used above is not applicable.
2. The expansion takes the surface closer to the heater and will therefore be exposed non-uniformly to an increased level of external heat flux on the surface. The effect of raising an element of the surface, (dA_2) is illustrated in Figure 4-3 (Persson, 1997). This analysis was conducted to determine the effect of positioning for a HF meter.

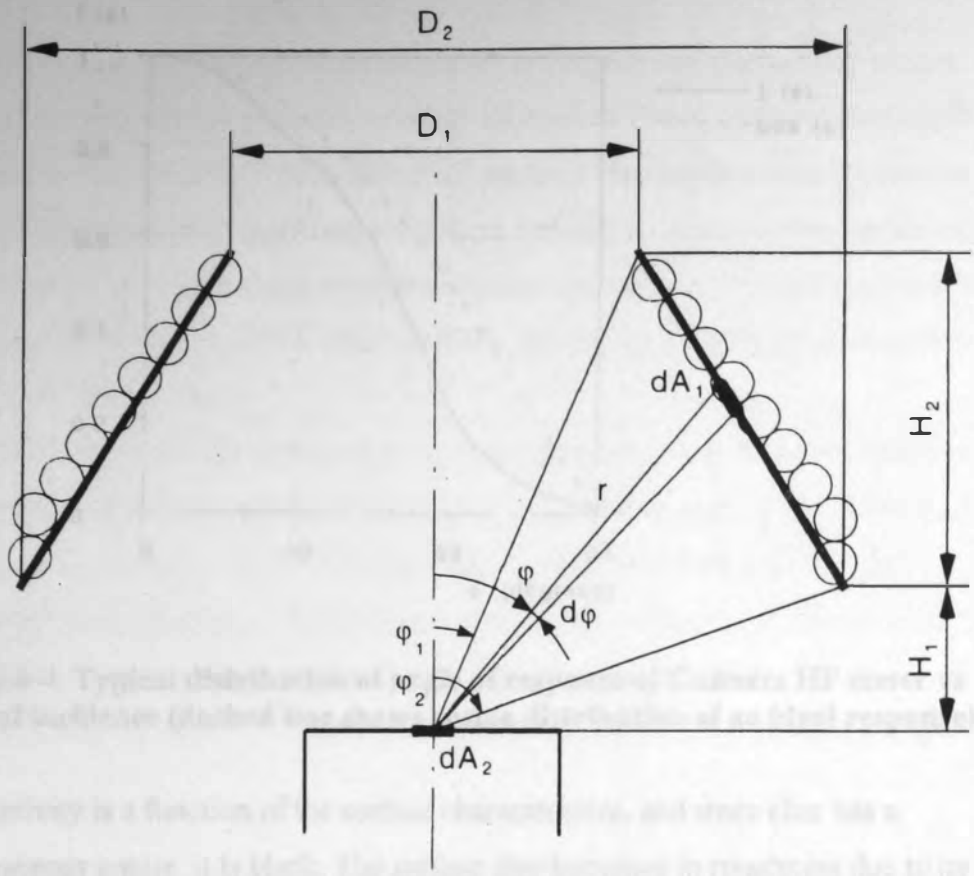

Figure 4-3. Factors determining surface heat flux in the Cone Calorimeter

From Figure 4-3, if a heat flux meter (dA_2) is located at a distance H_1 below the heater base (D_2), where H_1 is normally 25mm, then the level of heat flux received is:

$$q = 2\sigma(\varepsilon_w T_w^4 - \varepsilon_c T_c^4)\int_{\varphi_1}^{\varphi_2} f(\varphi)\sin(\varphi).d\varphi$$

where: $\varphi_1 = \text{arctg}\,(0.5 \times D_1/(H_1+H_2)$

$\varphi_2 = \text{arctg}\,(0.5 \times D_2/H_1)$

T_c = cooling water temp

T_w = heater coil temp

$f(\varphi)$= angle response (*taken from Figure 4-4, showing angle response vs angle of incidence*)

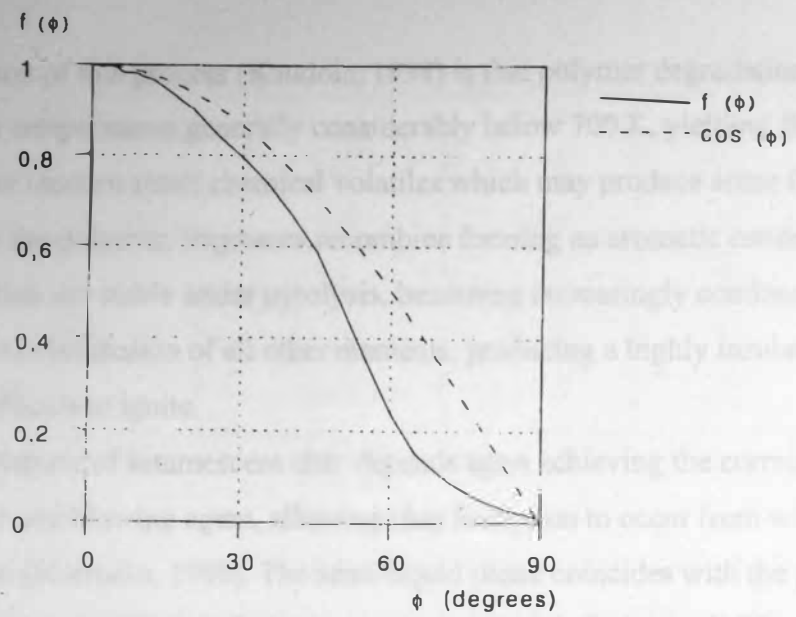

Figure 4-4. Typical distribution of angle of response of Gunners HF meter vs angle of incidence (dashed line shows cosine distribution of an ideal response)

3. Emissivity is a function of the surface characteristics, and since char has a carbonaceous nature, it is black. The surface also increases in roughness due to its evolving porous structure, therefore the emissivity will probably be higher for the char than for the base polymer.

4. Char formation has a lower initiation temperature than the base polymer volatisation temperature as it needs to activate prior to the polymer burning in order to protect it, thus the T_{ig} for the base polymer can't be measured using these techniques.

5. The decomposition mechanisms are a function of heating rate, therefore different mechanisms will result in varying extents of char and different burning behaviour.

For practical use an emissivity of 1 has been assumed for char formers, and the derived emissivity used for the other materials in this study. When this is incorporated into Equation 4.7, the char formers are found to have ignition temperatures of between 700 and 750 K (not accounting for increased surface flux, convective loss or reduced density). These temperatures are much higher than those

for the most common char former, wood, which ignites at 570 – 630K (Drysdale, 1999).

A description of this process (Kandola, 1998) is that polymer degradation occurs early on, at temperatures generally considerably below 700 K, yielding flammable monomer or random small chemical volatiles which may produce some flashing ignition. In the polymer, fragments recombine forming an aromatic condensed ring system, which are stable under pyrolysis, becoming increasingly condensed above 700 K due to elimination of all other elements, producing a highly insulating char which is difficult to ignite.

The effectiveness of intumescent char depends upon achieving the correct balance of char former and blowing agent, allowing char formation to occur from within a semi-liquid phase (Horrocks, 1998). The semi-liquid phase coincides with the gas formation phase, enabling inflation to occur, and with inflation, solidification of the semi-liquid occurs, giving rise to a cellular or foamed char. These processes generally occur between 250 - 400°C, with char oxidation occurring above 450°C.

4.1.9 Specific Heat Capacity

Having plotted t_{ig}^{-1} against applied flux for each material tested, the gradients are listed in Table 4-M. These were inserted into Equation 4.6, along with the emissivity and surface temperatures outlined above to find the specific heat capacity (in kJ/kg K) of each material. These are shown in Table 4-J, compared to published data.

A brief sensitivity check found an increase in density or thickness produced a proportional decrease in heat capacity, whilst a 10% increase in T_{ig} resulted in a 22% decrease in c.

Specific heat capacity depends on both phase and composition of the polymer, which are both dependent on heating rate. The published values generally refer to those for pure polymers measured at constant pressure and 25°C, and are expected to rise with increasing temperature.

Table4-J. Published and Derived Specific Heat Capacities

Material	c* J/kg K	c (Eq 4.6) J/kg K	% difference
POLYSTYRENE	1.051 – 1.2	0.72	36
HDPE	2.315	1.09	53
POLYPROPYLENE	1.789	0.66	63
PMMA	1.388	0.33	76
POLYCARBONATE	1.181	1.12	5.2
UPVC	0.934	0.46	51

(* Brandrup & Immergut, 1975)

If the specific heat for a pure, non-degrading polymer is examined as a function of linearly increasing temperature (Brandrup & Immergut, 1975) as shown previously in Figure 3.14, there is an infinite rise in c during the solid/liquid phase change. A difference is then expected between the derived heat capacity of polymers degrading directly to a vapour (i.e. high MW PMMA) and those exhibiting melt-flow behaviour, due to the differences in latent heat. Inspection shows that PMMA has the lowest measured specific heat capacity of the materials tested. All these derived values are less than the published values, by an average of 47%.

4.1.10 Latent Heat of Volatisation

For a diffusion flame, the rate of burning is directly related to the rate of volatile production, which is a function of the rate of heat transfer to the fuel. The rate of burning ($\dot{m}''$), is generally expressed as follows (Drysdale, 1999):

$$\dot{m}'' = \frac{\dot{Q}_F'' + \dot{Q}_E'' - \dot{Q}_L''}{Lv} \qquad 4.8$$

Where: $\dot{Q}_F'' + \dot{Q}_E''$ =heat flux to the surface (flame + external radiation)

$\dot{Q}_L''$ = heat losses from the surface

L_v = heat required to produce volatiles

From this, a plot of steady state $\dot{m}''$ against applied heat flux shows the gradient represents L_v^{-1}. The 5 point average used to obtain the mass loss rate results in a large

amount of noise in the test results, and so an average value of dm/dt for between 10 and 90% of the total mass lost is generally used.

The latent heats for each polymer degradation behaviour investigated are calculated as follows (Babrauskas, 1992):

Direct solid-vapour degradation, a single phase change, is found from Equation 4.9a:

$$L_v = \Delta H_v + \int_{To}^{Tv} C_p.dT \qquad 4.9a$$

Melt-flow polymers, undergo a two stage vapourisation process, modifying L_v to:

$$L_v = \int_{Ta}^{Tm} (C_p s).dT + \Delta H_m + \int_{Tm}^{Tv} (C_p, l).dT + \Delta H_v \qquad 4.9b$$

Char formation involves three phase changes and a series of chemical reactions, so:

$$L_v = \int_{Ta}^{Tm} (C_p, s).dT + \Delta H_m + \int_{Tm}^{Tv} (C_p, l).dT + \Delta H_v + (C_p, char) + \Delta H_{char} \qquad 4.9c$$

(NOTE: many char formers (e.g. wood) do not liquify).

Comparison with published data for the two most common thermoplastics are shown in Table 4-K. (The slope of the dm/dt vs $Q_{applied}$ graph is the main source of error in the calculations).

Table4-K. Comparison of published and derived mat'l properties for PE & PP

Mat'l	T_m (K)	T_v (K)	*C_p,s (kJ/kg K)	*C_p,l (kJ/kg K)	*H_v kJ/kg	*H_m kJ/kg	L_v (calc) kJ/g	**L_v kJ/g
PP	451	609	2.36	3.29	1.52	1.91	3.13	2.03
PE	419	636	3.86	3	1.56	2.38	3.82	2.32

(published data from (*Brandrup, 1975; **Tewarson & Pion, 1976))

(*specific heat values are taken at mid range temperature*)

A problem with melt-flow polymers, is any melt leaving the load cell to fall onto the platform is registered as mass loss, producing artificially high dm/dt values. Since melt-flow viscosity is a function of temperature, as illustrated in Figure 5-7, higher applied fluxes will generally result in lower viscosity melts, increasing the

probability of overspill, although it was observed to some extent in almost every one of the melting plastic tests. For this reason, this approach is not well suited to melting plastics.

4.1.11 Melt-flow Thermoplastics

This is the most important group investigated for this project, and includes the most common thermoplastics, polyethylene, and polypropylene, as well as polyethylene terepthalate and three formulations of polystyrene.

Polystyrene homopolymer is a transparent, brittle material and is often modified by incorporating elastomers, which result in an opaque material. In this study, PS 185K and PS Muster are both transparent materials, of different molecular weights whilst Polystyrol Hi Natural (PHN) is opaque. PHN has been confirmed by the supplier to contain approximately 10 % styrene butadiene, and is a 'high impact' polystyrene.

Time to Ignition

As previously shown, plots of t_{ig}^{-1} vs applied flux for thermally thin materials are linear, which can be extrapolated to produce the critical fluxes for ignition. t_{ig}^{-1} against applied flux has therefore been plotted overleaf. The slopes and intercepts are tabulated in Table 4-L.

PS 185K and PS Muster have similar slopes, with gradients of 0.0006 kWm^{-2}/sec, which increases slightly to 0.0007 for PHN. The intercepts are similar for 185 and MUS, at 11.55 and 12.67, whilst PHN is higher at 17.71 kW/m^2. Therefore, the additive (including copolymer) appears to influence the time taken to ignite PHN.

For a derived critical flux for ignition, the straight lines are approximately converging, giving an average value of critical flux for these melt-flow plastics of 13.5 kW/m^2, with a standard deviation of 2.2.

As outlined above this approach ignores heat losses, and as the imposed heat flux is decreased, convective and radiative losses from the surface of samples increase in significance. The effect of this is that for short heating times (i.e. high applied fluxes), the material behaves as thermally thick. When the heating times are increased, the material behaviour moves toward thermally thin behaviour.

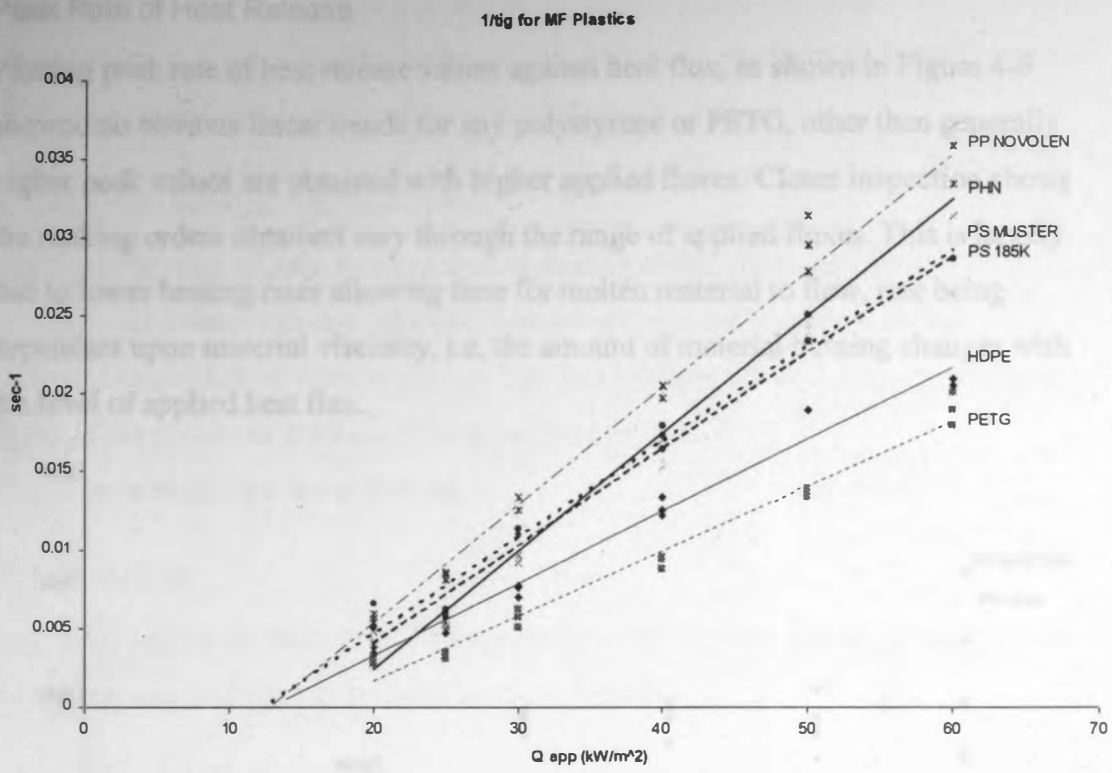

Figure 4-5. Q_{app} vs t_{ig}^{-1} for melting plastics

Table 4-L. Results of (t_{ig}^{-1} vs applied flux) plots for plastics tested

Material	critical flux for ignition (kW/m^2)	Gradient of t_{ig}^{-1} (kWm^{-2}/sec)
HMW PMMA (5MM)	12.8	.0008
HMW PMMA (4MM)	14.6	.0008
LMW PMMA (6MM)	16.6	.0007
PP NOVOLEN 1100H	13.6	.0007
HDPE LUPOLEN	14	.0005
EASTMAN SPECTAR	17.3	.0004
PS MUSTER	14	.0006
POLYPROPYLENE(6MM)	17.5	.001
POLYMAN PS 185K	13.1	.0007
POLYMAN PC XP41 RS	16.2	.0005
POLYSTROL HI NAT	15	.0007
CYREX 200 PC ALLOY	17.6	.0009
DUROLON POLYCARB	17.5	.0004
POLYSTYRENE (3MM)	7.7	.0007
UPVC	21.1	.0008
POLYMAN PXC 31	23.5	.0004

Peak Rate of Heat Release

Plotting peak rate of heat release values against heat flux, as shown in Figure 4-6 showed no obvious linear trends for any polystyrene or PETG, other than generally higher peak values are obtained with higher applied fluxes. Closer inspection shows the ranking orders obtained vary through the range of applied fluxes. This is largely due to lower heating rates allowing time for molten material to flow, rate being dependant upon material viscosity, i.e, the amount of material burning changes with the level of applied heat flux.

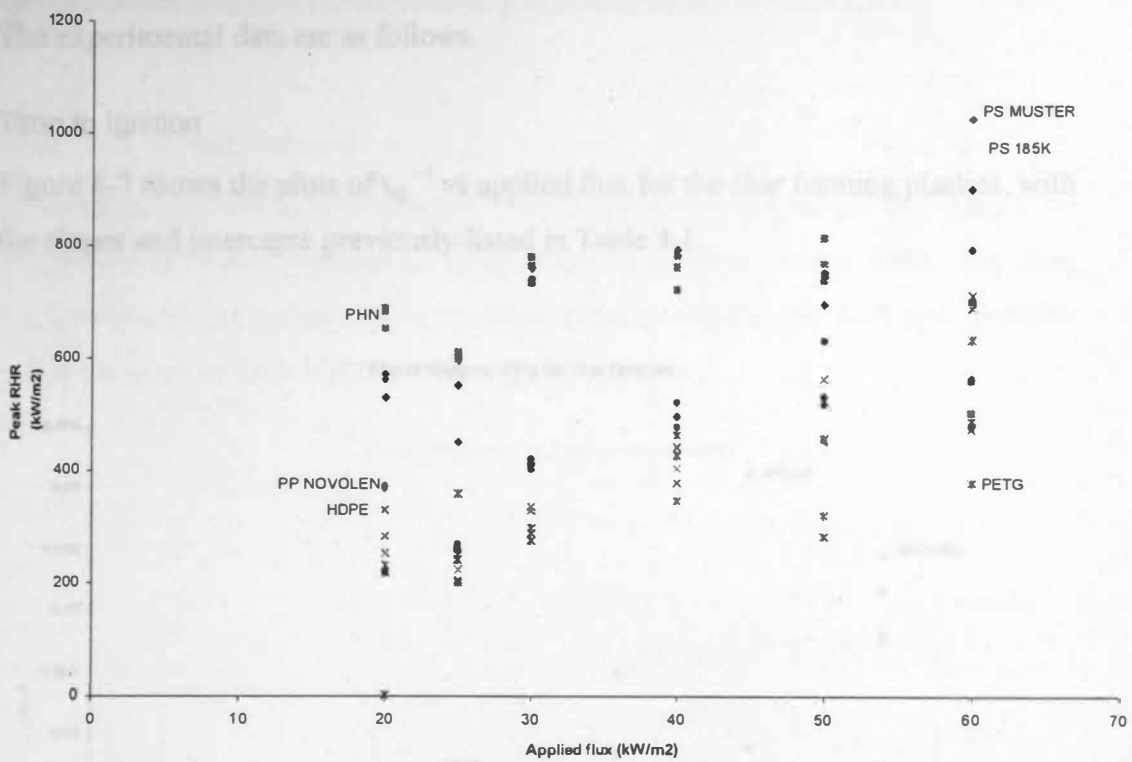

Figure 4-6. Q_{app} vs peak RHR for melting plastics

The polystyrenes are similar and distinct from the other melt-flow thermoplastics, with consistently higher values of peak flux. The general ranking order of heat release as a function of applied flux is:

polystyrene > polypropylene > polyethylene > PETG

This is partly a reflection of the soot volume fraction in the flame, the controlling parameter of radiant flame flux level, which is significantly higher for PS than the other plastics tested. (*NB The values of L_v do not suggest this order*).

Having looked at the melt-flow thermoplastic results, comparison can now be made of char and intumescing thermoplastic fire behaviour.

4.1.12 Char forming thermoplastics

The fire behaviour of char forming thermoplastics differs from melt-flow thermoplastics since the char protects the base polymer by forming a porous carbonaceous structure when sufficient heat has initiated the char forming reactions. Some of the problems were previously outlined in Section 4.1.8:
The experimental data are as follows.

Time to Ignition

Figure 4-7 shows the plots of t_{ig}^{-1} vs applied flux for the char forming plastics, with the slopes and intercepts previously listed in Table 4-L.

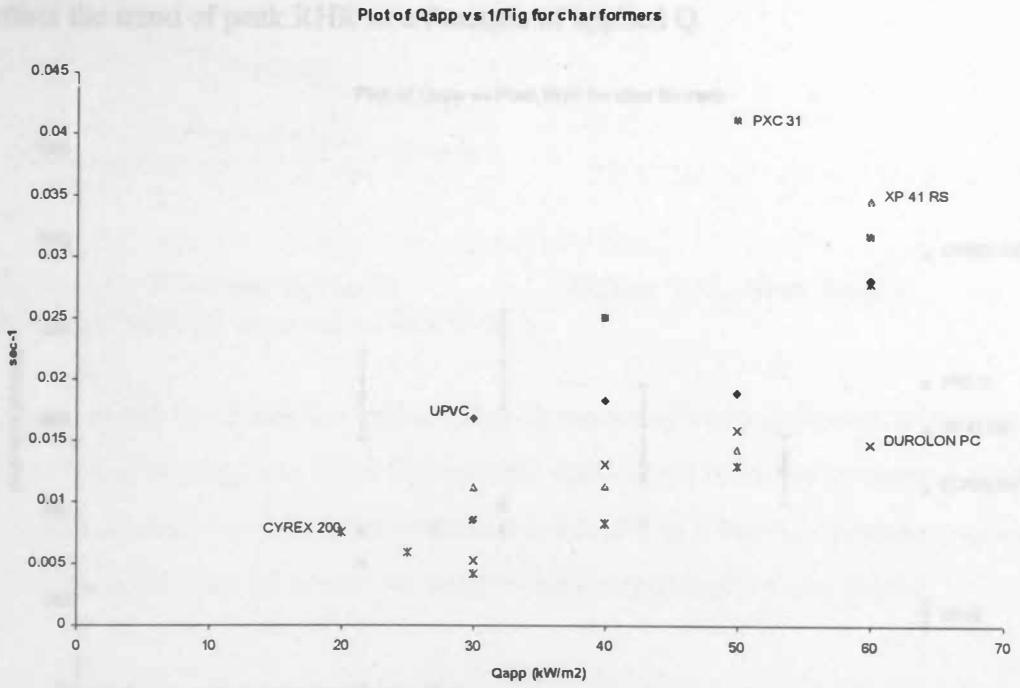

Figure 4-7. Q_{app} vs t_{ig} for char formers

During the tests on the polycarbonate derivatives, some melt-flow behaviour was observed at the lower fluxes, alongside some bubbling and browning of the polymer. This bubbling caused expansion of both the 31 and 41 polymers at 20 kW/m^2, which

then solidified forming transparent brown tinged foamed solids. When removed from the Cone Calorimeter without having flamed, and allowed to cool, the foamed solids were found to be extremely hard and impact resistant. At 25 kW/m^2, the foamed polymer turned into a shiny black char, which eventually turned yellow. Above this level of flux, a white lacy delicate char was the residue for both polymers and the DPC. At all fluxes, the UPVC initially turned brown, foaming with small bubbles which then turned into a matt black / grey rapidly expanding char. The char expanded more rapidly at higher fluxes, with some flashing ignition at early stages of the test. There was no sustained flaming observed in any of these tests.

Peak Rate of Heat Release

Within the range of experimental error, (error bars are shown for UPVC) there is no discernible difference between the polycarbonates in terms of peak RHR. Therefore, the acrylic additive makes the polycarbonate easier to ignite, but does not otherwise effect the trend of peak RHR as a function of applied Q.

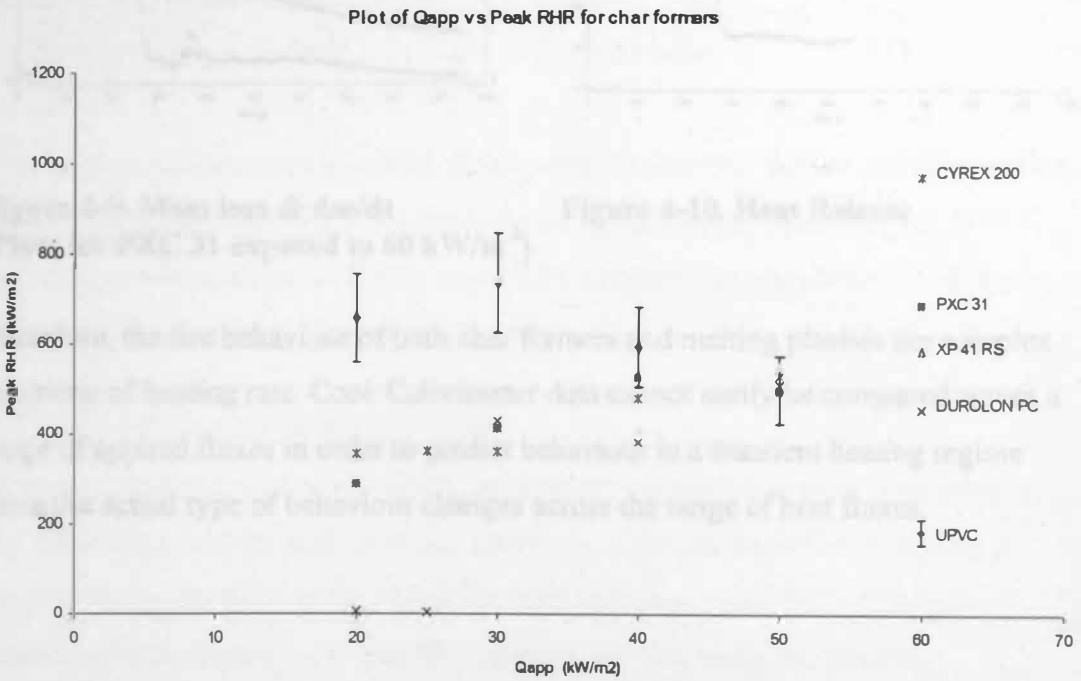

Figure 4-8. Q_{app} vs Peak RHR for char formers

From closer inspection of the mass loss and mass loss rate plots of the char forming polymer group, as shown in Figure 4-9 for Polyman PXC 31 at 60 kW/m^2, it can clearly be seen that there are two distinct peaks for dm/dt. This corresponds to two peaks found on the RHR-Applied Q plot shown in Figure 4-10. It appears that the rapid mass loss to first peak represents the initial stage of burning, the drop in dm/dt may indicate a slowing mass loss as the polymer liquifies, and then a much slower deceleration of mass loss representing final char formation and increased heat absorption. If some of the polymer separates at a lower temperature than the activation temperature for the polycarbonate char mechanism, this will lead to two stage burning behaviour.

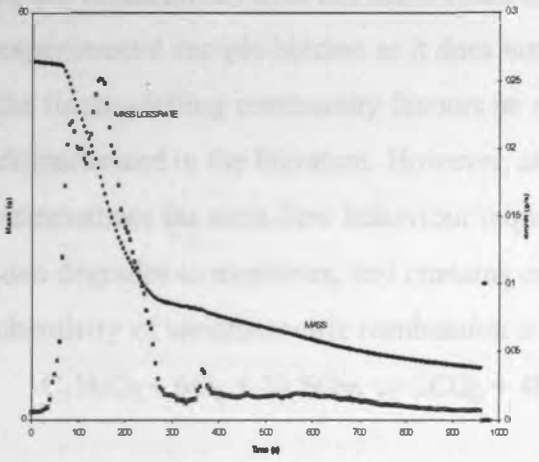

Figure 4-9. Mass loss & dm/dt (Plots for PXC 31 exposed to 60 kW/m^2)

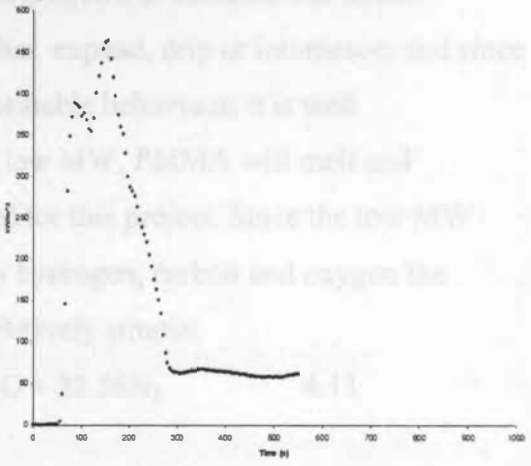

Figure 4-10. Heat Release

Therefore, the fire behaviour of both char formers and melting plastics are complex functions of heating rate. Cone Calorimeter data cannot easily be compared across a range of applied fluxes in order to predict behaviour in a transient heating regime since the actual type of behaviour changes across the range of heat fluxes.

4.2 Developing a technique to assess the melt-flow effect on fire growth

Research outlined in Chapters 1 – 3, and the Cone Calorimeter database described in the previous section demonstrate only certain materials will exhibit melt-flow when heated. These are thermoplastics with either a random scission degradation mechanism, or have a low initial molecular weight (MW) undergoing end chain scission.

The simplest and most reproducible thermal degradation behaviour is exhibited by high MW PMMA. This degrades via end chain scission, yielding over 90% monomer in the volatiles, but does not melt. There is no problem of containment within experimental sample holders as it does not char, expand, drip or intumesce, and since the fire modelling community favours its repeatable behaviour, it is well characterised in the literature. However, at a low MW, PMMA will melt and demonstrate the melt-flow behaviour required for this project. Since the low MW also degrades to monomer, and contains only hydrogen, carbon and oxygen the chemistry of stoichiometric combustion is relatively simple:

$$C_5H_8O_2 + 6O_2 + 22.56N_2 \Rightarrow 2CO_2 + 4H_2O + 22.56N_2 \qquad 4.11$$

Therefore, some high and low MW sheets were obtained for further testing, since any differences in behaviour between them would be solely due to the effect of MW (private communication, Dr I. Robinson, ICI), a controlling parameter for viscosity (where viscosity $\propto MW^{3.4}$) (Cogswell, 1981).

4.2.1 Experimental System Outline

Using 6mm thick samples of PMMA, preliminary experiments were undertaken at the HSE's Buxton Fire & Explosion Laboratory. The area available for testing is situated below the hood at the end of the third scale test rig (TSR) corridor, the hatched area on Figure 4-11. The TSR restricts the area under the hood to approximately 1m x 1.86m, and the rigs have been designed to accommodate this. From the burn area, the combustion products are carried for approximately 5.6m through the small duct (36cm diameter) before entering the fan controlled main duct (68.5cm diameter). At entry to the main duct the products are diluted with additional

air from an inlet hood 7m downstream, and transported 9.5m to cross an orifice plate some 3.5m downstream of the fan, prior to exhausting to atmosphere. The two fan speeds, High and Low, control flow rate in the main duct, varying differential pressure across the plate from 0.16 Pa (Low) to 0.64 Pa (High).

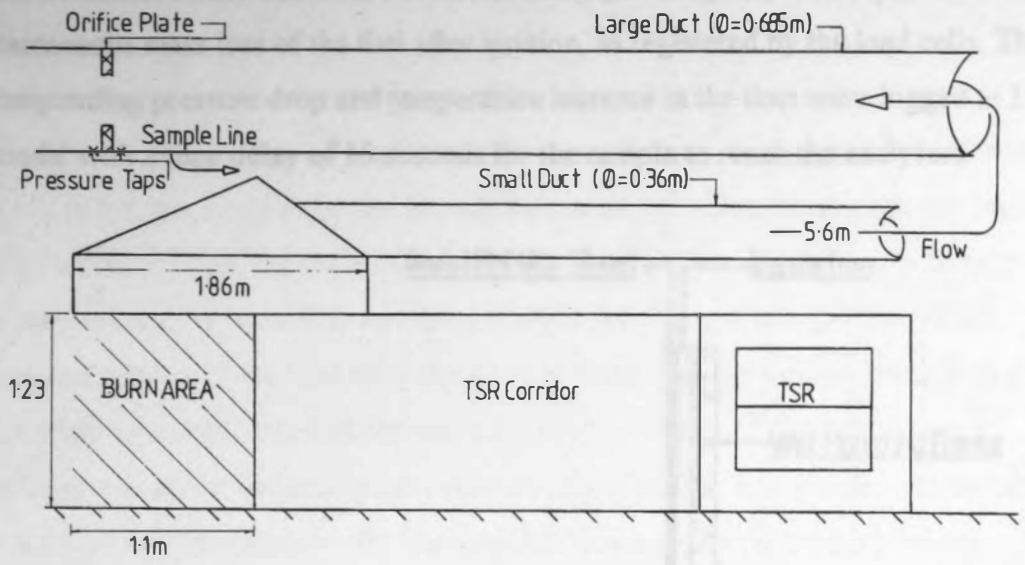

Figure 4-11. Schematic of the third scale rig at Buxton Laboratory

As shown above a sample of combustion products is drawn off before reaching the orifice plate. The measurement system is similar to that for the Cone, as the sample is drawn off through a 10mm pipe, then passed through a filter and drying agent before the pipeline is split into two lines for entry to the CO and CO_2 analysers. A differential pressure transducer (dpt) measures the pressure drop across the orifice plate, with the output voltage converted to Pa by a calibration factor of 1V =19.6Pa. This was derived from comparison of dpt output voltage to inclined manometer readings at both fan speeds for calibration. A sheathed thermocouple is used to monitor the duct temperature.

Transient measurements are taken of pressure and temperature, with the orifice plate area (a) at half the main duct area (A). The Continuity and Bernoulli equations are then applied, from which the flow rate (Q_v) of air through the main duct at room temperature (293K) can be derived (Kay & Nedderman, 1988):

$$Q_v = CA \sqrt{((2\Delta P)/(\rho(A^2/a^2-1))} \qquad 4.12$$

Taking C (discharge coefficient) as 0.6, this yields Q_v =0.06 m^3/s (High fan speed) and 0.03 m^3/s (Low fan speed), showing ambient duct velocity to be either 0.16 or 0.08 m/s respectively.

From a methanol calibration burn conducted at High fan speed, the output data show instantaneous mass loss of the fuel after ignition, as registered by the load cells. The corresponding pressure drop and temperature increase in the duct were logged at 12 seconds, with a time delay of 15 seconds for the sample to reach the analysers.

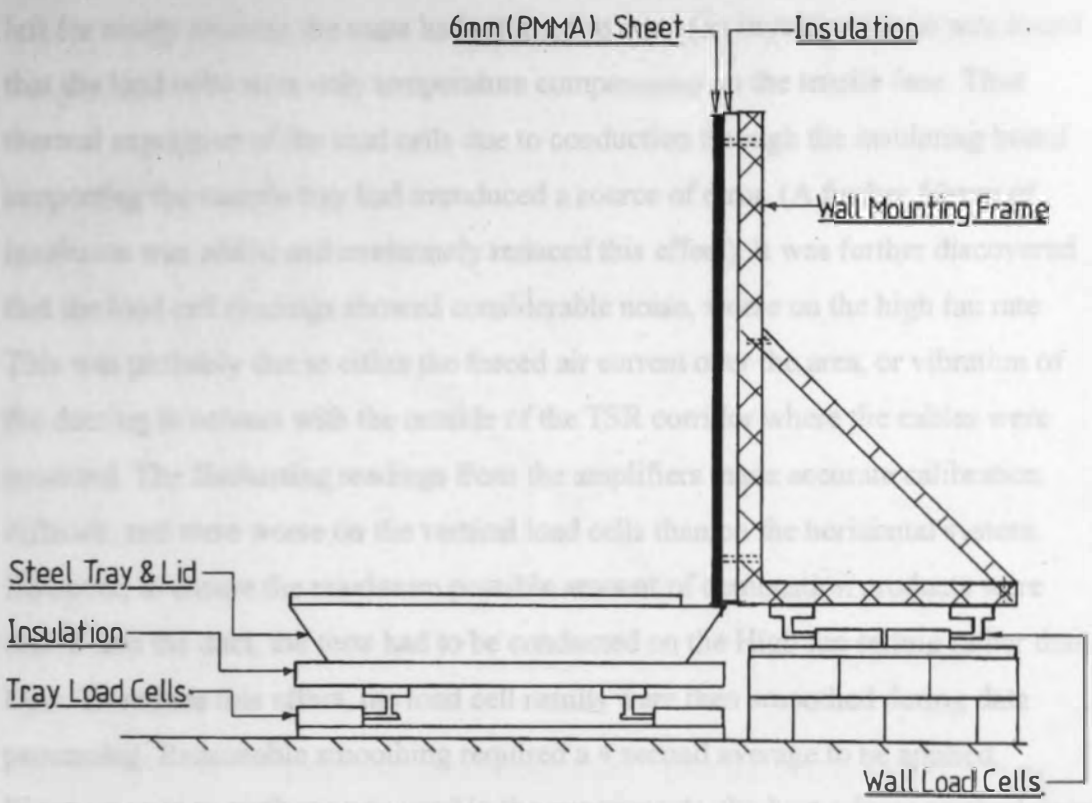

Figure 4-12. Schematic illustration of horizontal & vertical rigs

A sample size of 0.5m x 0.5m was used for each test, and two independent load cell rigs for horizontal and vertical samples were built as shown in Figure 4-12.

This arrangement allowed the measurement of CO_2, CO, mass losses, duct temperature and orifice plate differential pressure for each experiment. Data collection at 1 Hz frequency was performed by a Windmill Data Logger, followed by data processing using Microsoft Excel.

The "Principle of Oxygen Consumption Calorimetry" outlined in Section 2.3.5.1, (Huggett, 1980), was then used to derive the rate of heat release for each test. If this is divided by mass loss, the net (or effective) heat of combustion is calculated. This allows a comparison to be made between the burning behaviour of the various orientations, and also a comparison to published data for verification purposes.

Initial experiences of the system using methanol in a $0.25m^2$ tray showed that the load cells registered a gain of approximately 15 to 20 % of the original fuel mass by the end of the test, despite the fuel having burned away. When the equipment was left for ninety minutes the mass had returned to zero. On investigation, it was found that the load cells were only temperature compensated on the tensile face. Thus thermal expansion of the load cells due to conduction through the insulating board supporting the sample tray had introduced a source of error. (A further 50mm of insulation was added and moderately reduced this effect). It was further discovered that the load cell readings showed considerable noise, worse on the high fan rate. This was probably due to either the forced air current over the area, or vibration of the ducting in contact with the outside of the TSR corridor where the cables were mounted. The fluctuating readings from the amplifiers made accurate calibration difficult, and were worse on the vertical load cells than on the horizontal system. However, to ensure the maximum possible amount of combustion products were drawn into the duct, the tests had to be conducted on the High fan setting rather than Low. To reduce this effect, the load cell results were then smoothed during data processing. Reasonable smoothing required a 4 second average to be applied. Since no oxygen analyser was used in the experiments, the heat release methodology was adapted to calculate heat release based on CO_2 production, monitoring CO to assess combustion efficiency rather than direct from oxygen consumption.

4.2.2 System Calibration (With Methanol)

Methanol was selected as a calibration fuel because of its high combustion efficiency (0.993) (Drysdale, 1999), indicating that over 99% of the fuel oxidises to CO_2 and H_2O during combustion. Since methanol consists only of hydrogen, oxygen and carbon, the only products of complete combustion will be carbon dioxide and water, as shown in the stoichiometric equation:

$$2CH_3OH + 3O_2 \Rightarrow 2CO_2 + 4\ H_2O \qquad 4.13$$

$$(2 \times 32) + (3 \times 32) \Rightarrow (2 \times 44) + (4 \times 18) \qquad \text{(Mol Masses)}$$

This reaction is exothermic, producing water vapour (latent heat of evaporation at 25°C= 44 kJ/mol). The heat of combustion is --635 kJ/mol (Drysdale, 1999) expressed as –(635/32) = -19.84 kJ/g of methanol[4]. Since the size of fire is characterised by the rate of heat release due to combustion of fuel vapour, the main factor is the mass flow rate of fuel, and the heat release can be predicted if this is known. From the calibration burn, the load cell output is shown in Figure 4-13. From this, the steady state mass loss rate, registered between ~100 – 350 seconds, was 0.0032 kg/s.

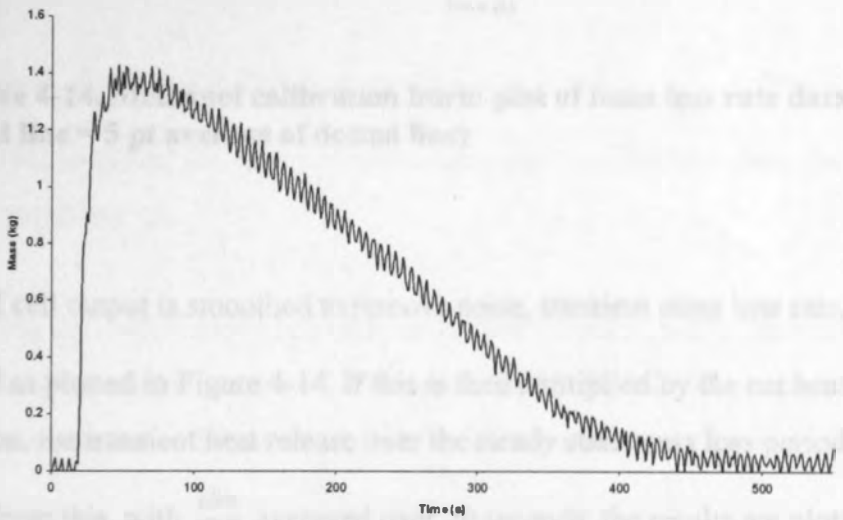

Figure 4-13. Plot of methanol calibration burn; (horizontal) load cell output

$$\dot{Q}_c = \dot{m}\chi\Delta H_c = (0.0032)(0.993)(19.84\text{x}10^3) \approx 63 \text{ kW} \qquad 4.14$$

Where:

$\dot{Q}_c$ = rate of heat release (due to combustion of fuel vapour) (MW)

χ = combustion efficiency (0.993 for methanol)

$\dot{m}$ = steady state mass loss rate of fuel (kg/s),

ΔH_c = heat of combustion (19.84 MJ/kg)

---

[4] 32 is the gram molecular weight of methanol

4.2.3 Method 1 :Heat Release Based On Mass Loss

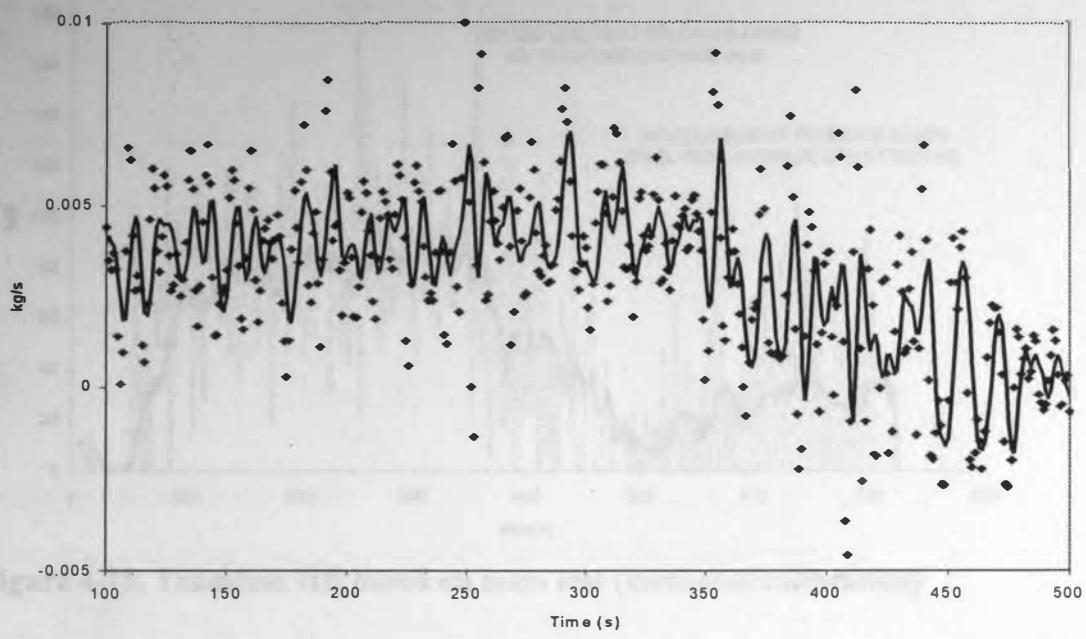

Figure 4-14. Methanol calibration burn: plot of mass loss rate data (solid line = 5 pt average of dotted line)

If the load cell output is smoothed to remove noise, transient mass loss rate, $\frac{dm}{dt}$, is calculated as plotted in Figure 4-14. If this is then multiplied by the net heat of combustion, the transient heat release over the steady state mass loss period can be derived. From this, with $\frac{dm}{dt}$ averaged over 20 seconds, the results are plotted in Figure 4-15. The solid line indicates a further 20 point average. This reduces the peak value of $\dot{q}(t)$ to 100 kW, some 60 % over that anticipated.

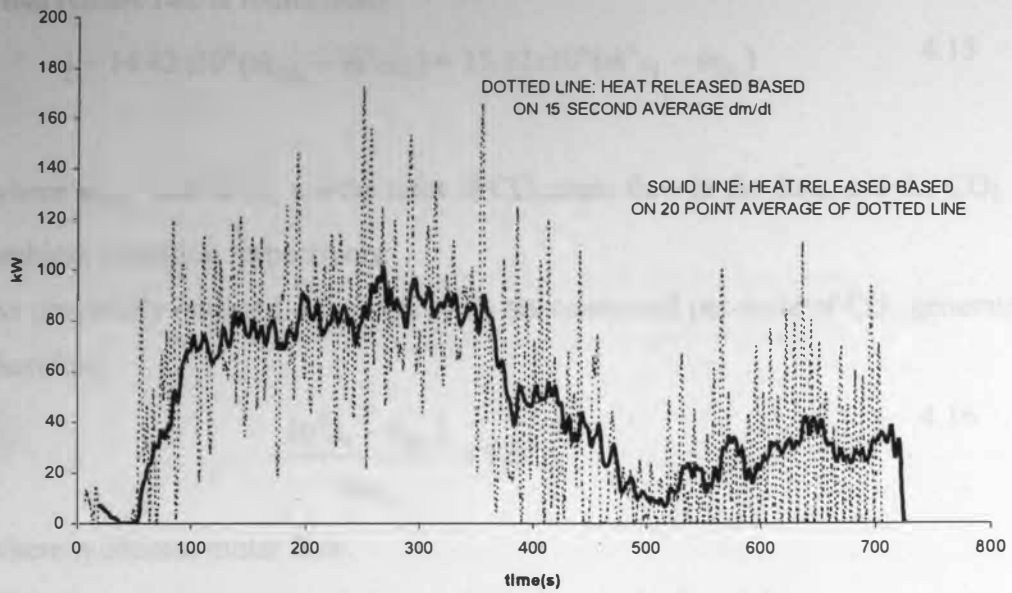

Figure 4-15. Transient HR based on mass loss (methanol calibration)

This approach, due to the differentiation required to produce $\frac{dm}{dt}$, increases the noise on the results, reducing the accuracy when compared to a method using direct instrumentation output.

The resulting amount of averaging required is clearly unacceptable. However, in circumstances where the capture of all combustion products is not possible and the load cell problems outlined above are rectified, this may be an acceptable approach.

4.2.4 Method 2: Heat Release Based On Calorimetry

An alternative method of obtaining heat release from this system is to use the calorimetry equations. The output from the CO analyser recorded CO production varying between 15 and 25 ppm for methanol, which seems negligible and in agreement with the 99 % combustion efficiency for the fuel. From Equation 4.13, it can be seen that 1 kg of fuel will combine with 1.5kg of oxygen, producing 1.375 kg of CO_2, and liberating ($1.5 \times 13.22 \times 10^6$)= 19.83MJ of heat in the process (Drysdale, 1999). Therefore the % CO_2 production measured during the burn is converted to Joules of heat produced, using an effective heat of combustion in terms of CO_2 production of (19.83/1.375) = 14.42 MJ/kg of CO_2.

Heat release rate is found from:

$$\dot{q} = 14.42x10^6(\dot{m}_{CO_2} - \dot{m}^0{}_{CO_2}) = 13.32x10^6(\dot{m}^0{}_{O_2} - \dot{m}_{O_2}) \qquad 4.15$$

where $\dot{m}_{CO_2}$ and $\dot{m}^0{}_{CO_2}$ are the rates of CO_2 mass flow in the duct, and the CO_2 ambient condition respectively.

As previously outlined, 1.5 moles of O_2 are consumed per mole of CO_2 generated, therefore;

$$\frac{(\eta^0{}_{O_2} - \eta_{O_2})}{\eta_{CO_2}} = 1.5 \qquad 4.16$$

where η denotes molar flow.

From this, the percentage of oxygen depletion can be found from:

$$\frac{(\eta^0{}_{O_2} - \eta_{O_2})}{\eta_{CO_2}} = \left[\frac{(X^0{}_{O_2} - X_{O_2})(1 - X_{CO_2})}{X_{CO_2}(1 - X^0{}_{O_2})}\right] = 1.5 \qquad 4.17$$

Since $X^0{}_{O_2}$ (the ambient mole fraction of oxygen) is 0.2095, this can be rearranged to give:

$$0.2095 - \left[\frac{(1.5X_{CO_2} - (1 - 0.2095))}{(1 - X_{CO_2})}\right] = X_{O_2} \qquad 4.18$$

The expansion between exhaust and intake can then be calculated:

$$\frac{(1 + (b-1)X^0{}_{O_2} - b(x_{O_2})}{(X^0{}_{O_2} - 2X_{O_2})} \qquad 4.19$$

where:

$$b = \frac{(\eta_{CO_2} - \eta_{H_2O})}{\eta_{O_2}} = \frac{3}{1.5} = 2 \qquad 4.20$$

Substituting for b and $X^0{}_{O2}$ gives:

$$\left[\frac{(1.2095 - 2X_{O_2})}{0.2095 - 2X_{O_2})}\right] \qquad 4.21$$

A system calibration equation for the orifice plate can then be derived:

$$c = \frac{\dot{q}}{13.22x10^3x1.1}\sqrt{\frac{Te}{P}}\left[\frac{(1.2095 - 2X_{O_2})}{(0.2095 - 2X_{O_2})}\right] \qquad 4.22$$

where;

$\dot{q}$ = 63 kW (from Equation 4.14)

1.1 = MW_{O2}/MW_{air}

Te = duct temperature

ΔP = duct differential pressure

The range of c is then plotted over the steady state region, as shown in Figure 4-16. The average over the steady state region is found to be ~ $0.03 kg^{0.5} m^{0.5} K^{0.5}$.

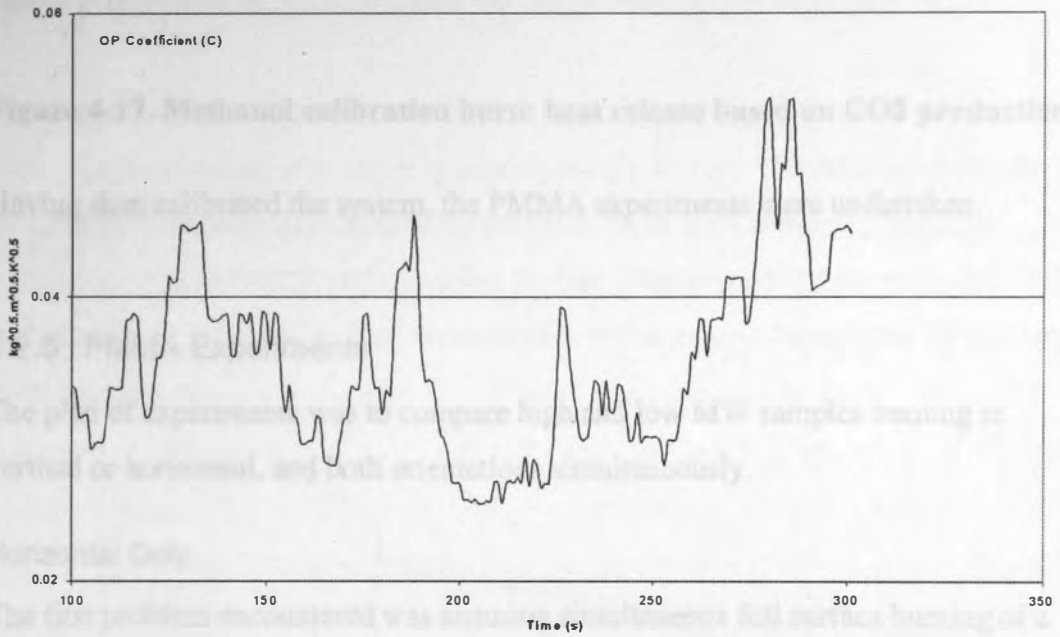

Figure 4-16. Methanol calibration burn: Plot of derived orifice plate coefficient

The coefficient is then used to derive the mass of air entrained into the system as per the Cone Equations described in Chapter 2, using Equation 2.2. Finally, the heat released is found from Equation 2.3. This is plotted in Figure 4-17.

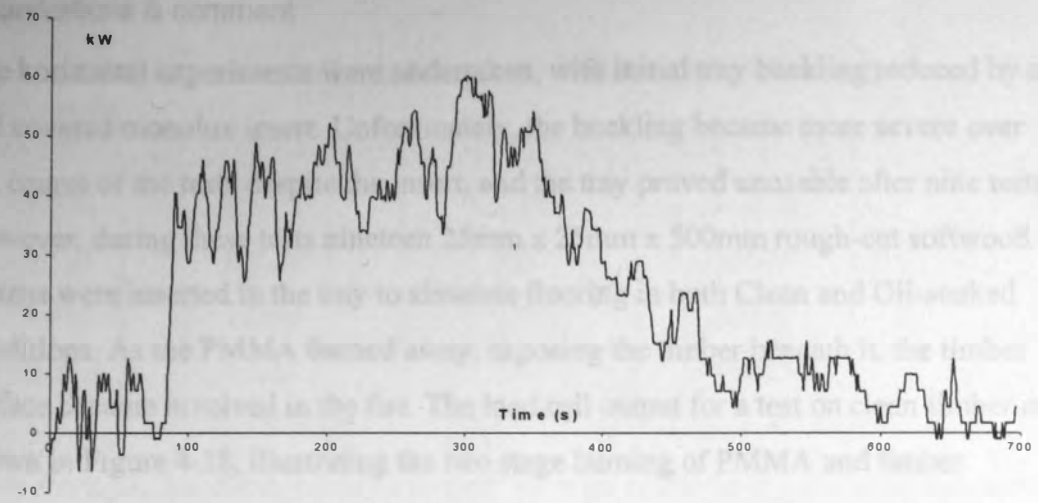

Figure 4-17. Methanol calibration burn: heat release based on CO2 production

Having then calibrated the system, the PMMA experiments were undertaken.

4.2.5 PMMA Experiments

The plan of experiments was to compare high and low MW samples burning in vertical or horizontal, and both orientations simultaneously.

Horizontal Only

The first problem encountered was ensuring simultaneous full surface burning of a horizontal sheet of PMMA. Initial attempts with a propane line burner positioned across the surface showed the surface spread of flame to be too slow to allow this to develop unaided. The sheet also arched upwards by approximately 50mm directly under the burner. The arched region then distorted into a surface 'trough', which, when the sheet eventually softened enough to flatten back into the tray, further restricted lateral flame spread.

After several unsuccessful trials, comparative success was achieved by creating a rig with a pulley and chain enabling the tray to be raised to around 40° from the horizontal. The line burner was then fired across the base of the tray, with the flames hugging approximately 80 % of the surface area. After ignition, the tray was lowered back to the horizontal position with sufficient slack in the chain to prevent interference.

Observations & comment

The horizontal experiments were undertaken, with initial tray buckling reduced by a foil covered monolux insert. Unfortunately, the buckling became more severe over the course of the tests despite the insert, and the tray proved unusable after nine tests. However, during these tests nineteen 25mm x 25mm x 500mm rough-cut softwood battens were inserted in the tray to simulate flooring in both Clean and Oil-soaked conditions. As the PMMA burned away, exposing the timber beneath it, the timber surface became involved in the fire. The load cell output for a test on clean timber is shown in Figure 4-18, illustrating the two stage burning of PMMA and timber.

The original mass of Clean timber was 2.8 kg which, having become involved in the burn, exhibited a final char depth of approximately 10 mm. The oil-soaked timber, which had previously been soaked overnight in 1L of used sump oil, produced copious amounts of black smoke during the test. This overspilled the exhaust system, and resulted in a deeper, uneven depth of char which burned through the 25mm deep battens in places.

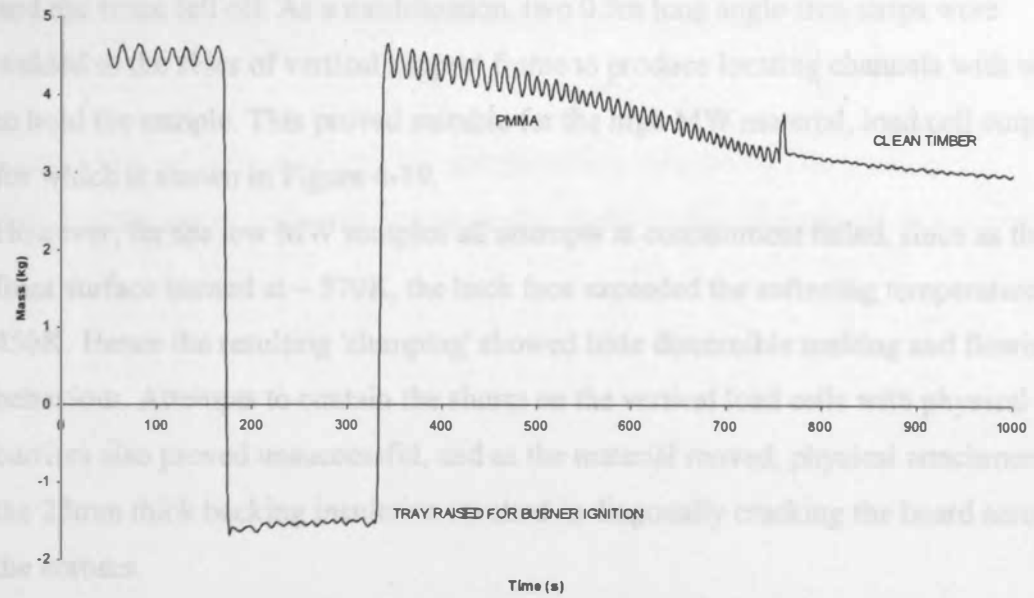

Figure 4-18. Load cell output for burning high MW PMMA sheet resting on clean timber flooring battens.

Comparison

Table 4-M. Comparison of high & low MW PMMA sheets, burning horizontally.

TESTID	High or Low MW	Peak HR (kW)	MLR_{ss} (kg/s)
JO5HPM	HIGH	107	-0.0028
JO7HPM	HIGH	124	-0.0025
JO6LPM	LOW	113	-0.003
JO10LPM	LOW	140	-0.0025

From the table, the average mass loss rate[5] for high & low MW horizontal sheets was 0.0027 kg/s (e.g. 12 - 13 $x10^{-3}$ $kg/m^2.s$), with no significant difference between the materials. The peak heat release averaged 120 kW: there was too much scatter mainly due to noise & averaging, to detect any difference between high & low MW materials.

Vertical Only

The initial method of using 'G clamps' with steel strips up the sides to hold the sample in place was unsuccessful, as the thickness of the sample reduced as it burned and the strips fell off. As a modification, two 0.5m long angle-iron strips were welded to the sides of vertical support frame to produce locating channels with which to hold the sample. This proved suitable for the high MW material, load cell output for which is shown in Figure 4-19.

However, for the low MW samples all attempts at containment failed, since as the front surface burned at ~ 570K, the back face exceeded the softening temperature ~ 450K. Hence the resulting 'slumping' showed little discernible melting and flowing behaviour. Attempts to contain the slump on the vertical load cells with physical barriers also proved unsuccessful, and as the material moved, physical attachment to the 25mm thick backing insulation resulted in diagonally cracking the board across the corners.

[5] average mass loss rate found from applying a linear trend fit over the steady state region

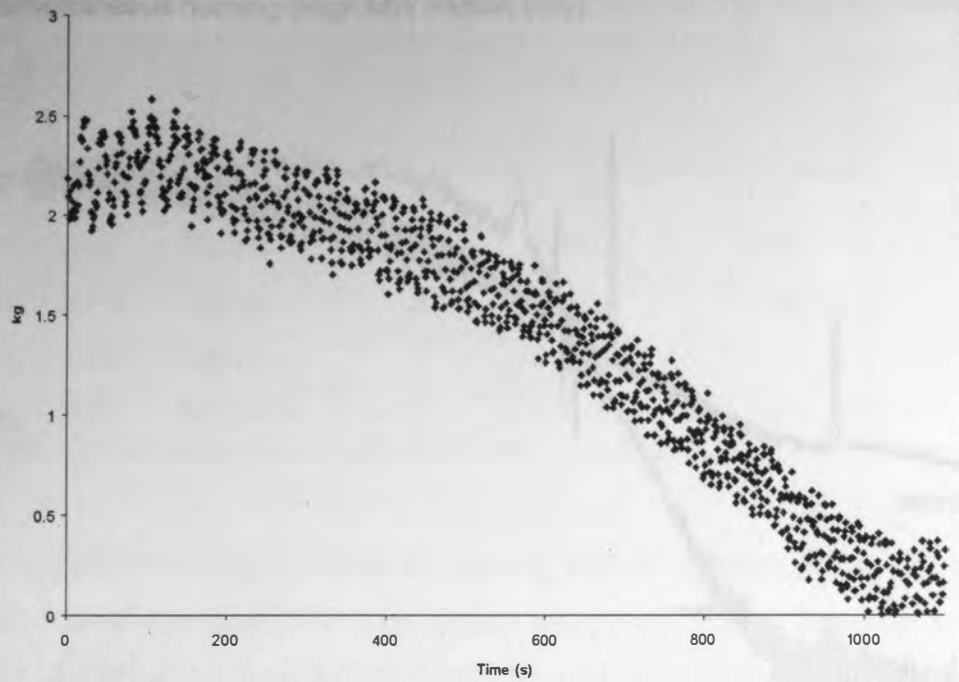

Figure 4-19. Load cell output for high MW PMMA burning vertically.

Table 4-N. Data from High MW PMMA Vertical surface burning

TESTID	High or Low MW	Peak HR (kW)	MLR_{ss} (kg/s)
JO12HM	HIGH	75	-0.0024

Comparison of these data with the horizontal test data shows that it has a significantly lower peak heat release, and a slightly lower average mass loss rate.

Simultaneous burning (High MW PMMA only)

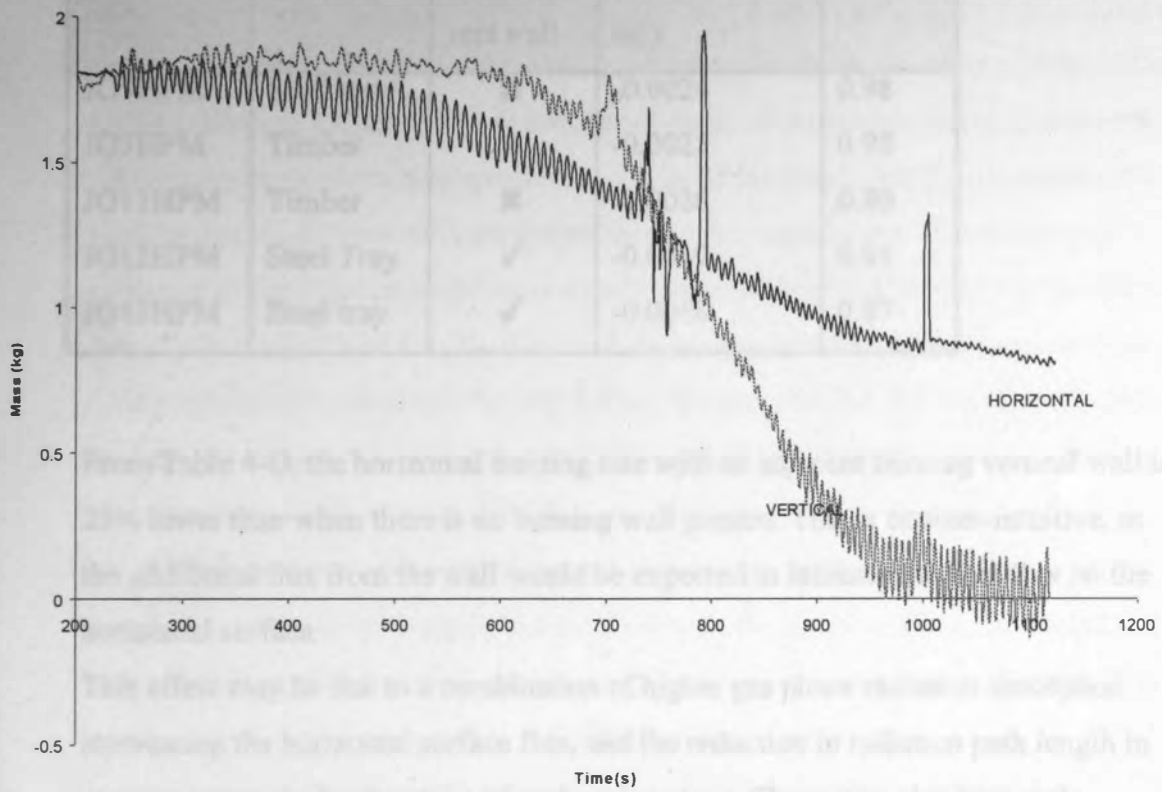

Figure 4-20. Load cell output for high MW PMMA horizontal & vertical samples burning together

A plot of load cell outputs for two samples (horizontal + vertical) burning together is shown in Figure 4-20. It is immediately apparent that the vertical surface is burning faster than the horizontal. The calculated rates from 700 – 900 seconds, are 0.0018 kg/s for the horizontal surface, and 0.0065 kg/s for the vertical. Therefore, the vertical surface is burning ~3.5 times faster than the horizontal.

The peak heat release was ~210 kW, as expected this is higher than for the previous tests since with two surfaces burning, there is double the surface area of the previous high MW tests.

Interestingly, the horizontal surface is burning more slowly than the average of the single horizontal burning sheets, but the vertical surface is burning much faster than previously found. The burning rates for all the horizontal sheets tested are compared in Table 4-O.

Table 4-O.Burning rate comparisons for horizontal high MW PMMA sheets burning with & without adjacent burning vertical surface

TESTID	Substrate	+burning vert wall	Max burn rate kg/s	R^2
JO5HPM	Steel tray	✖	-0.0024	0.98
JO7HPM	Timber	✖	-0.0025	0.95
JO11HPM	Timber	✖	-0.0026	0.80
JO12HPM	Steel Tray	✓	-0.0019	0.91
JO18HPM	Steel tray	✓	-0.0018	0.87

From Table 4-O, the horizontal burning rate with an adjacent burning vertical wall is 25% lower than when there is no burning wall present. This is counter-intuitive, as the additional flux from the wall would be expected to increase the heat flux on the horizontal surface.

This effect may be due to a combination of higher gas phase radiation absorption attenuating the horizontal surface flux, and the reduction in radiation path length in comparison to the horizontal surface burning alone. There may also be a scale influence, as with small fires, the burning rate is increased at the leading edge, and the wall presence restricting oxygen will reduce burning rate toward the rear of the sample. This is discussed in further detail in Chapter 6.

Since vertical burning comparisons between high and low MW material could not be made using this system, the experimental series was terminated at this point for further consideration, and an alternative experiment, the 'Fishtank' was developed.

4.2.6 The Fishtank Experiment

Dr Atkinson suggested that a steep temperature gradient could be achieved by cooling the rear face of a 6mm thick sample of low MW PMMA, which may permit surface flow to occur. This could possibly overcome the slumping problem previously noted. The idea was to make an open-topped, water filled cube, with a steel base, sides and back and PMMA front face. The water would then to cool the back face of the PMMA sample as the front face burned. The temperature gradient

through the thickness might then permit surface burning and flowing to occur simultaneously.

The 50 cm x 50cm x 13cm box was duly constructed and tested, filled with ~ 32kg of water. The PMMA surface was ignited with a propane gas line burner ~25mm above the base. Surface ignition in the immediate vicinity of the burner was achieved after ~ 4 minutes exposure, which spread to the base of the sheet after approximately 20 minutes (the total extent of flame spread during the experiment). However, some distortion of the sheet occurred soon after ignition, which lead to failure of the silicon seal attaching the PMMA to the box, and several small leaks (similar to those from a watering can) were observed. Around 1.5 kg of water was lost through these leaks by the time the sheet had self extinguished after an hour, the water temperature having increased from 290K to around 300K.

Inspection of the remaining PMMA sheet showed that bubbles were present in the burn area to around 1mm depth, and the minimum thickness of sheet was found at the base to be approximately 2 mm. It was also noted that more sheet distortion had occurred in the upper area, where the water had been removed.

At this point, it was felt that this material was not thick enough to exhibit the characteristic behaviour required for the study, and a different approach was required.

A survey of thermoplastic commodities was then undertaken, looking for affordable thermally thick materials to test. Rolls of opaque polyethylene sheeting, of the type used on construction sites were considered potentially suitable.

4.2.7 Polyethylene Rolls

A 1.3m length roll of polyethylene sheet, sheet thickness 0.12mm, roll external diameter ~19cm, internal diameter ~ 10cm, wound onto a hollow cardboard core, was then obtained for an observational trial (no instrumentation). Attached to a vertical support rig and placed in a large steel tray beneath the extract hood, a BS No 7 crib was used to ignite the outer surface of the roll.

Initially the surface slowly regressed into the roll and the crib was pushed further in, the regression forming a 'cave'. After 10 minutes the crib had burned away and a flame height of about 30cm was observed on the roll surface. The roll did not

delaminate. However, when sufficient depth of plastic was burned away to reveal the cardboard core (after around 30 minutes), 25mm or so of thickness appeared to peel away to the sides further away from the pool established in the tray. The tray surface was not level, and so burning was more intense in some places, and the square shape ensured uneven radiant feedback from the sides, but two distinct burning regimes were observed. The pool is estimated to have grown from about 25cm diameter after 11 minutes to around 60cm at 25 minutes.

It was observed that the liquid melt from the roll protected the cardboard centre as it flowed, and also cooled the pool at entry, preventing flame establishment. The melting rate was not uniform over the roll surface, mainly due to the uneven heating regime, and it was also observed that initial flame was blue, getting bigger and turning gradually yellow after around 12 minutes. The test was extinguished after around 35 minutes for safety considerations, as the flames had reached the height of the duct.

This observational test confirmed the usefulness of continuing with commodity items known to cause melt flow problems in preference to PMMA simulations intended to reduce the number of variables. A rig (nicknamed 'The Kebab') was then developed for a larger scale test, carried out in the 'Temple[6]' at HSE Buxton, on a full size polyethylene roll.

Full Polyethylene Roll Test (The 'Kebab' Experiment)

A supply of 'polyethylene' sheet wound onto rolls, ~ 2m long was supplied by HSL for testing. The rolls, total mass ~21.5 kg, have a PE bulk density of 887kg/m^3. The 12μm thick PE sheet is wound around a cardboard core, inside which a scaffold pole welded to a supporting steel disk was inserted. The pole was suspended from a chain incorporating a tensile load cell, above a 25mm thick monolux tray, 2.4m x 1.2m, divided in the centre by an insulated ridge to form two square sections. The tray rested on a separate load cell rig, as shown in Figure 4-21.

---

[6] 'Temple' – a 9m high steel framed building, with plastic sheeting attached to wooden battens forming 7m high walls enclosing an area ~ 5.5m x 3m (a 2m air gap is present below the steel roof)

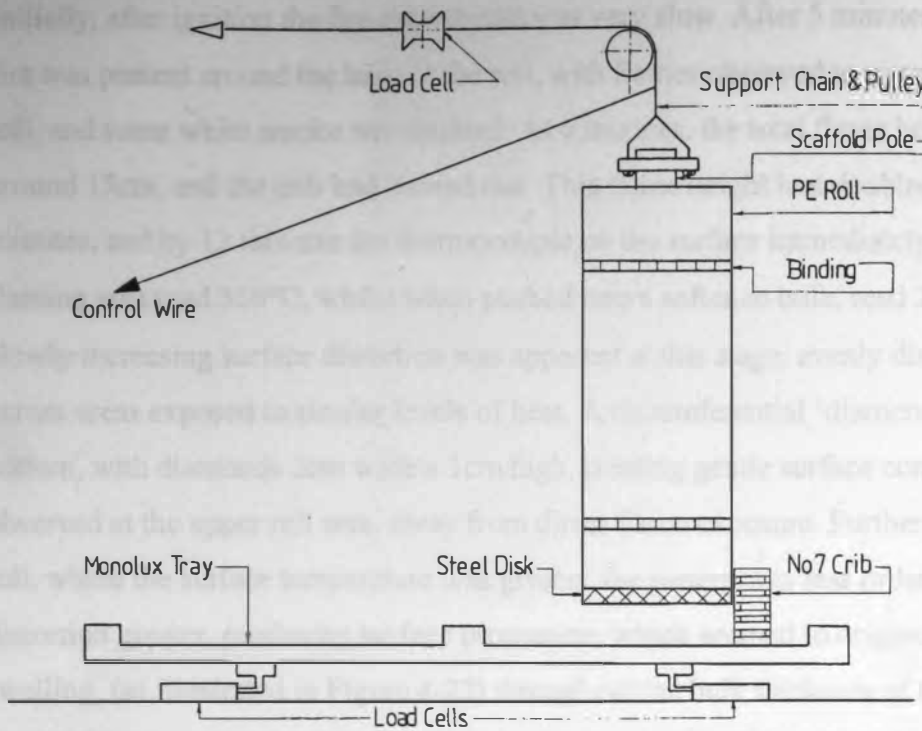

Figure 4-21. The 'Kebab' Experiment

As illustrated in Figure 4-21, the burning roll is suspended above the centre of the tray. A steel line attached above the roll on the supporting steel chain allowed the burning roll to be pulled across into the second area in order to observe the extent of vertical/horizontal burning interaction.

Ignition was achieved by means of a BS No 7 wooden crib, placed in the centre of one section of the monolux tray, contacting the perimeter at the base of the roll.

The instrumentation consisted of the two load cell rigs, static DVD and Infra-Red (IR) cameras and a hand held DVD camera, in addition to a hand held thermocouple. The hand held equipment was used to monitor 'close up' behaviour until the burn area became untenable due to the level of radiant heat. The static cameras were placed outwith the burn area, and monitored through a hole in the shielding wall. All temperatures were recorded using the hand held thermocouple.

Observations

For the first test, the roll was suspended ~ 3cm above the base. This was found to be too close, as thermal expansion of the steel support chain led to contact between the roll and base during the test. A separation distance of 15cm was found satisfactory.

Initially, after ignition the fire growth rate was very slow. After 5 minutes a small fire was present around the base of the roll, with flames observed to wrap around the roll, and some white smoke was emitted. At 6 minutes, the total flame height reached around 15cm, and the crib had burned out. This flame height had doubled by 9 minutes, and by 12 minutes the thermocouple on the surface immediately behind the flaming area read 350°C, whilst when pushed into a softened bulk, read 280°C. Some slowly increasing surface distortion was apparent at this stage, evenly distributed across areas exposed to similar levels of heat. A circumferential 'diamond mesh' pattern, with diamonds 2cm wide x 1cm high, creating gentle surface contours, was observed at the upper roll area, away from direct flame exposure. Further down the roll, where the surface temperature was greater, the pattern was less ordered and distortion greater, producing surface protrusions which seemed to originate from swelling, (as illustrated in Figure 4-22) throughout the bulk thickness of the plastic. Some of the lower smoothly curved protrusions were 20 – 25mm proud of the original surface, and appeared opaque at depth, but transparent near the surface. The transparent surface layer was observed to flow downward.

A small non burning transparent brown liquid pool of approximately the same diameter as the roll started to form at 13 minutes, varying from 310°C in the centre to 190°C at the edge. The pool was fed by drips from the base of the roll, which had regressed to expose some of the steel disk. The liquid on the steel disk registered ~ 400°C on the thermocouple.

Some soot particles from the flame became adsorbed in the molten surface layer, the (varying) downward velocity of which was at most 1 – 2 cm/s. The bulk of the roll was opaque, but the thin moving surface layer and drips had become transparent. By 14 minutes, some burning was evident in the pool centre, but an outside 3 – 5 cm wide 'rim' of non burning material was also noted. This rim was producing small bubbles of volatiles. The burning liquid pool varied between 340°C and 130°C at the outer edge, being 260°C just inside the edge. Pool depth varied between 3- 5mm at the rim, and 1 – 2mm at the centre, covering an extent equivalent to around 60cm (not even). At this time, the flames from the pool were around 20 cm, with 50cm high flames attached to the roll. (This pool structure is consistent with a surface tension driven flow of the molten material).

Figure 4-22. PE roll surface distortion & drip site

By 18 minutes, the vertical flame height had reached 0.7m, the surface protrusions had increased and the smoke had turned black, rapidly increasing in volume. The temperature of the protrusions were found to be ~ 300°C for the main bulk, rising to 350°C for the upper surface, which was at most 2 – 3mm deep. A close up image from the hand held DVD is shown in Figure 4-22.

At 20 minutes, the pool covered around 1/5th of the tray area, with a total vertical flame height of around 1m, unevenly spread across the roll surface. It was noted that the pool depth never became greater than 3 or 4 mm.

At approximately 24 minutes, the area was evacuated due to the level of radiant heat present, and observation continued from the static camera location outside.

With vertical flames over 2m in height, flickering up to 2.5 – 3m, the pool started to exhibit pulsing behaviour at 25 minutes. An area of pool would burn out completely, leading to flame extinction, and then a process of material accumulation, then the surface would eventually re-ignite. This burn off - replenish – re-ignition cycle was unsteady in terms of time taken and also area covered, although it seemed to be within the ever present non flaming rim. By 26 minutes, the pool covered over half the tray area, although the above cycle made accurate estimation difficult.

The roll was fully flame engulfed by 30 minutes, and was then temporarily physically removed from the pool. This clearly showed a large pool fire and a much

smaller fire on the roll, proving the dominant fire to be from the pool (the roll flaming covered mainly the extent of roll surface). The DVD static camera image of this is shown in Figure 4-23.

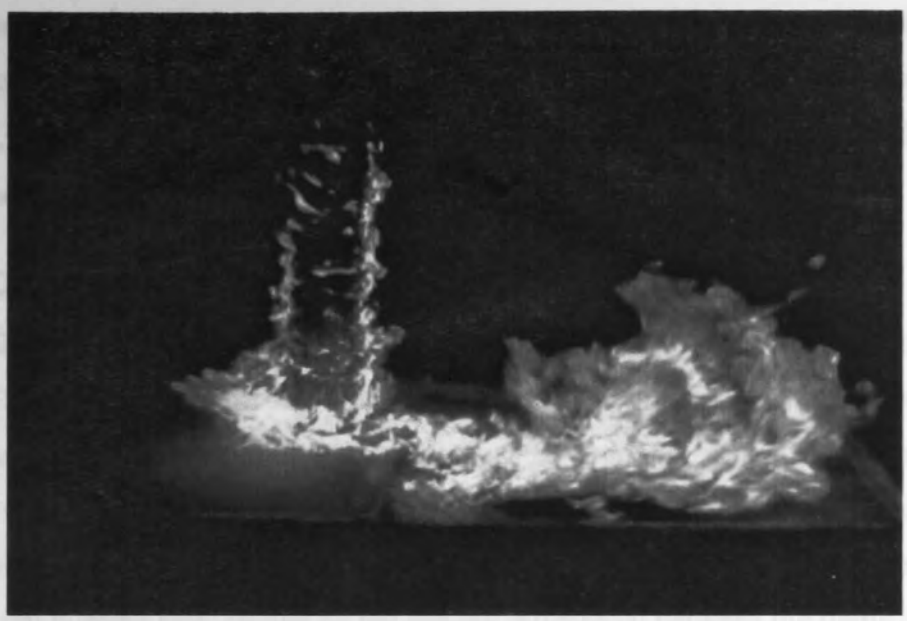

Figure 4-23. DVD Image showing Roll & pool separated (the roll has been pulled over to the left)

A further, smaller pool was formed in the second area as liquid came off the roll, and some spitting of burning material from the roll surface was noted. When the roll was returned to its original position, it caught on the central ridge from where it had to be dislodged (again due to thermal expansion of the steel chain). However when the roll was put back over the pool, the fire grew in size and intensity before stabilising.
By this stage, some pieces fell off the roll, landing in the pool to burn, but maintained the roll curvature on the outer surface. The pool shrunk back to around ¼ of the tray area by 32 minutes, increasing back to ½ the area by 34½ minutes.
The drips feeding the pool could clearly be seen to come from the mid-point of the curved protrusions at several locations, and were 2 – 3mm diameter. The distortions maintained their geometry whilst losing the surface layer, which was continually replaced by the melting surface above. In addition to the surface drip points, there were occasional episodes during which a shower of flaming droplets was produced which burned out prior to reaching the floor.
By 40 minutes, most of the vertical surface had been consumed, larger pieces falling off due to the loss of surrounding plastic which they were previously attached to, and

some of the cardboard core became involved at this stage. It was considered safe to reenter at this point, with the pool covering ~ ½ the tray area, including some non-burning regions.

The cool rim width had reduced to < 1cm wide in places, and the flame height from the pool had reduced to 0.6m. It was found that the base of the transparent pool was 300°C, rising to 350°C through the bulk, and 450°C at the extreme upper surface. The pool finally burned out at 50 minutes.

Load Cell Results

From the suspended roll load cell output shown in Figure 4-24, steady state mass loss was 0.02 kg/s, over about 1000 seconds. Output for the horizontal tray showed the maximum total mass accumulated is 4.2kg, gained over 1000 seconds, accumulating during the steady state region of the vertical roll at 0.003 kg/s. However, there is a problem with the load cell output, due to a buoyancy effect. This is greatest at maximum burning rate, caused by the density differential between the flame column and cooler surrounding air above the tray.

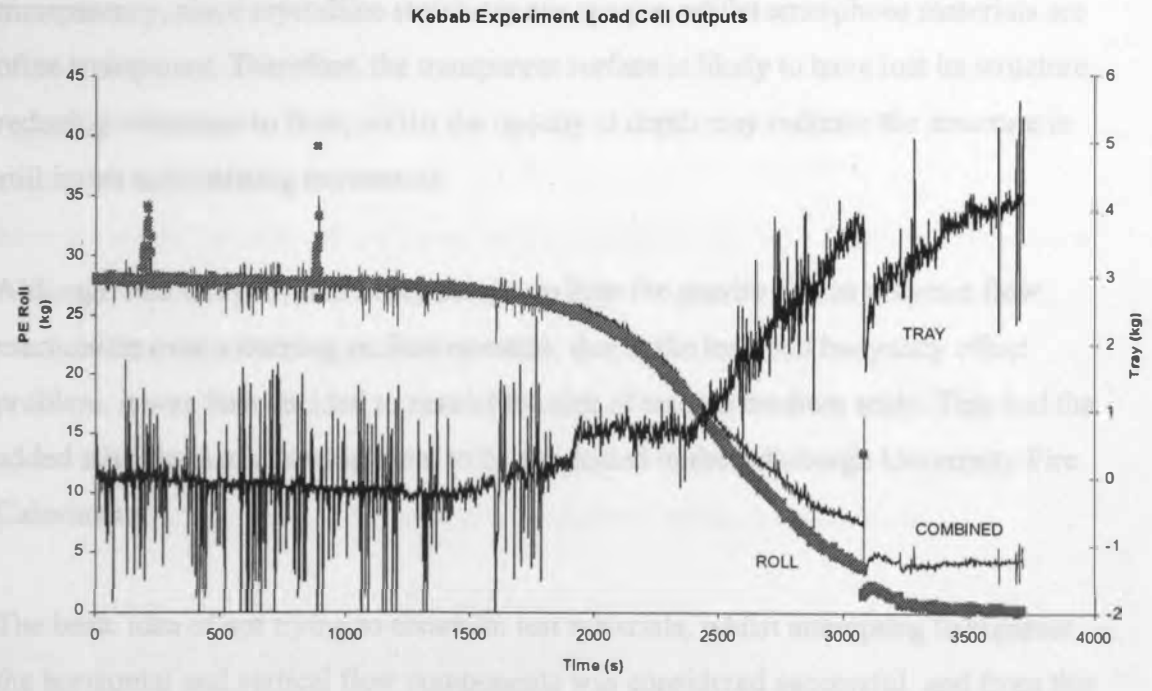

Figure 4-24. Load Cell Output for Kebab Experiment

Using a 'line of best fit', the combined (vertical + horizontal) flow rate, accounting for non burning melt, is then 0.019 kg/s. Therefore, during the maximum burning rate 85% of the mass lost is burning, with 15% being registered on the tray.

Comments

The hand held thermocouple shows the maximum roll polymer surface temperature to be ~ 350°C, with temperature increase resulting in vapourisation of a superficial layer. This should be compared with Thomson's measured piloted ignition temperature of 363°C for polyethylene. In addition to the surface measurements, it is apparent that there is a high thermal gradient through the bulk. Published data indicate that polyethylene softens at 70 – 80°C, with the crystalline phase completely melting by 130 – 135°C. However, during the test, bulk temperatures in excess of 280 – 300°C were taken from inside the soft but geometrically stable and non-flowing plastic bulk. Observation indicates that flow only occurred on a thin superficial layer, the outside of which was also volatising.

A further clue to the flow mechanism may be gleaned from the level of material transparency, since crystalline structures are opaque, whilst amorphous materials are often transparent. Therefore, the transparent surface is likely to have lost its structure, reducing resistance to flow, whilst the opacity at depth may indicate the structure is still intact and resisting movement.

Although this test provided many details on how the gravity driven polymer flow mechanism over a burning surface operates, due to the load cell buoyancy effect problem, it was then decided to restrict the size of tests to medium scale. This had the added advantage of allowing them to be conducted in the Edinburgh University Fire Calorimeter.

The basic idea of not trying to constrain test materials, whilst attempting to separate the horizontal and vertical flow components was considered successful, and from this point, the final 'sedan chair' rig was devised.

4.3 The Sedan Rig

4.3.1 Initial Setup

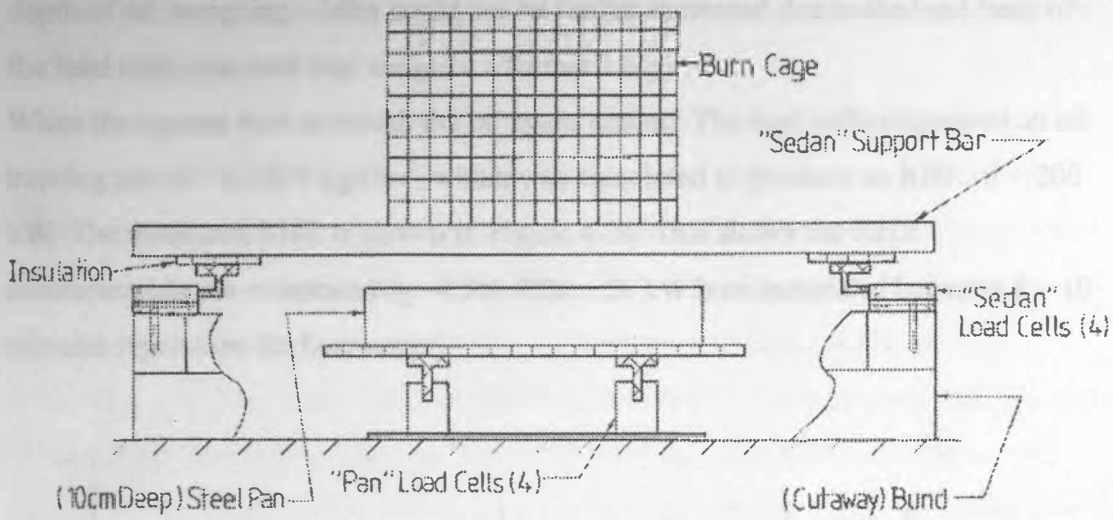

Figure 4-25. Sedan Rig

As shown in Figure 4-25, both ends of the sedan chair rested on load cell platforms, each supported by 2 load cells covered by an insulating board. The 2 load cells were bolted on to a steel plate, which was in turn bolted to the top of the bund wall for rigidity. Bricks were then mortared onto the bund at the sides of the plates to further protect the load cells.

Beneath the sedan chair, was a separate load cell platform, with 4 cells mounted on a steel plate and covered with insulating board. A steel pan was placed on the board, and filled with quenching oil, 'Teresso 100' (normally used in gearboxes).

A beer crate was then placed in the sedan chair, directly above the quenching oil, and ignited. The oil was intended to extinguish the burning molten material, allowing the amount of mass flowing to be separated from the quantity burning 'in situ'.

4.3.2 System Modifications & Development

Initial tests, burning beer crates ignited with a blow-torch, resulted in ignition of the quenching oil in the pan below the sedan chair. The problem was initially thought to be insufficient oil in the 5cm x 0.2025m^2 pan, which was being heated by a

combination of the burning plastic flowing into it and radiant heat exposure from the burning material in the sedan chair ~13cm above the oil surface.

To rectify this, a larger pan was commissioned, 10cm depth x 0.25m^2, and the sedan chair raised by stacking two small bricks under each supporting bar end. The 7.5cm depth of oil, weighing ~16kg could not be further increased due to the load limit of the load cells (the steel tray weighed a further 12kg).

When the system was re-tested, the oil again ignited. The load cells registered an oil burning rate of ~0.0203 kg/s/m^2, which was calculated to produce an RHR of ~ 200 kW. The measured RHR is shown in Figure 4-26. This shows the RHR measurements are overstated by ~25%. (The ~50 kW burn measured between 8 – 10 minutes represents the beer crate!).

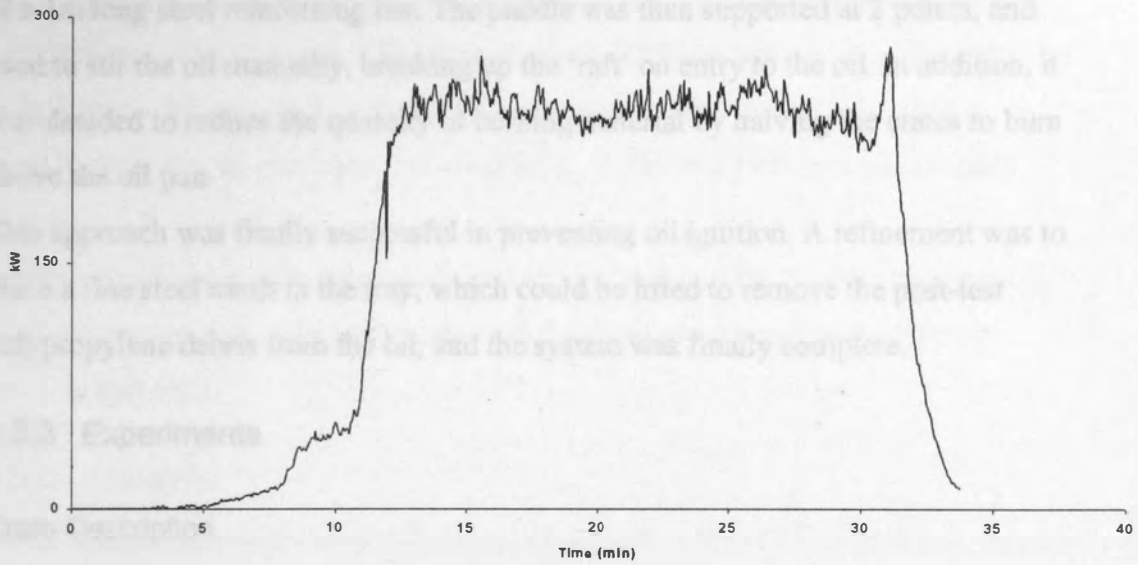

Figure 4-26. Heat Release of Grolsch crate + ignited oil pan

Since no additional mass could be added due to the load cell limitation, an independently suspended cooling water pipe was placed in the oil, to reduce the bulk temperature. The 5mm diameter coiled copper pipe was suspended from two retort stands, and lay around 1cm below the oil surface. Water was fed from a tap into the coil and directed out to a drain. When tested, again the oil ignited.

Observation of the build up to ignition indicated that despite the oil being less dense than polypropylene, the burning polypropylene was forming a 'raft' on the surface.

Initially, this was extinguishing, but when the molten burning material feed rate onto the raft built up, it ignited, eventually igniting the oil.

NB, it was found that a foam extinguisher was not particularly effective at extinguishing this system, mainly due to not having a back plate to direct it off. CO_2 and powder were better, although the powder resulted in a terrible mess throughout the lab!

At this point, the cooling coil was scrapped in favour of a method to prevent the raft build-up on the surface. Filtering and recirculating the oil from the surface, then cooling it before re-entering the tray was considered. This idea was abandoned when an attempt to pump clean, cold oil resulted in instant swelling of the neoprene pump impeller, causing the impeller to impact the housing and seize the pump.

A 'paddle' was then constructed, by welding an 8cm x 2.5cm steel strip onto the end of a 1m long steel reinforcing bar. The paddle was then supported at 2 points, and used to stir the oil manually, breaking up the 'raft' on entry to the oil. In addition, it was decided to reduce the quantity of burning material by halving the crates to burn above the oil pan.

This approach was finally successful in preventing oil ignition. A refinement was to place a fine steel mesh in the tray, which could be lifted to remove the post-test polypropylene debris from the oil, and the system was finally complete.

4.3.3 Experiments

Crate Description

A variety of beer crates were kindly donated for testing by Scottish & Newcastle Brewery, South Gyle, Edinburgh. Further 'Sunblest ' bread crates and 'Robert Wiseman' milk crates were also acquired. Although no material tests have been carried out, the British Plastics Federation state that beer, bread and milk crates are usually injection moulded from polypropylene granules, coloured as required.

Despite having a range of extremely complex geometries, as illustrated in Figure 6-8 there are 3 main design variations, for beer crates, intended to carry either 500/550 ml bottles, 330/275ml bottles or 112 ml mixer bottles. The wall thickness varies between 2mm internal subdivisions, and 3mm walls forming the outer shell. Some crates have single thickness outer walls, whilst others are contained by double skin

2mm walls with a separation air gap. The crate masses vary from 1.6 kg (small 'Schweppes' mixer bottle crates) to 3 kg (large 'Grolsch' bottle crates). Bread crates have no internal divisions.

The overall complete beer and milk crate dimensions are approximately constant (33 x 40cm) for stacking purposes, with a height varying between ~15 and 30cm, depending on bottle size.

Some further 'mushroom' crates were also obtained, which are small, (~ 250g mass) blue crates with no internal divisions and a 2mm thickness diamond meshed floor and wall design, the overall size being ~ (20 x 30 x 5) cm.

4.3.4 Investigations

Tests were carried out to compare burning half crates with the pool fire quenched, and burning half crates with a free burning pool. Some tests were also carried out on fully burning whole crates, with a further test undertaken on the half- length polyethylene roll, as previously tested at HSL, November 1999 and described in Section 4.2.7.

Further investigation was also conducted using crates and PP slabs burning onto a concrete paving slab, a plywood sheet and the steel tray, to look at the effect of flooring material.

4.3.5 Problems

It was found that whenever extinguishers were used, (either CO_2 or powder), that the heat release 'spiked', probably caused by the interference with the combustion process. The results beyond this point are irrelevant, and so the remaining data has been deleted.

The other major problem was caused the lack of temperature compensation on the tray load cells, which required a large amount of insulation and spacers to separate the tray from the load cell platform, minimising the amount of heat conducted through it.

4.3.6 Tabulated Mass loss data

Table 4-P. Mass flow rates of quenched ½ crates

TEST ID	MLR* g/s (sedan)	MGR** g/s (tray)	Burn Rate g/s	% of Mass collected in tray	% burning
BROWN5	-3.33	2.49	-0.84	75	25
HOLST5	-1.66	1.27	-0.39	76	24
MUSH1	-0.37	0.27	-0.1	74	26
RED5	-3.97	3.2	-0.78	81	19

**MLR = Mass Loss Rate, **MGR = Mass Gain Rate*

From these tests, around ¾ of mass lost from a flowing burning crate has been extinguished in the pan.

Table 4-Q. Mass flow rates for completely burning systems

TEST ID	Sedan MLR g/s	Tray MGR g/s	Tray MLR g/s	overall burn rate g/s	% of total burn rate in pool
HOLSTFB	-2.36	2.05	-0.5	-0.23	87
YELLFB	-6.7	2.8	-3.7	-5.08	72
MUSHFB	-0.8	0.8	-0.06	-0.15	39
PEROLLFB[x]	-11.9	-0.6	----------	--------	--------

[x]had to be manually extinguished for safety reasons

The situation with pool + sedan burning is harder to analyse. For example, looking at the load cell results of "HOLSTFB", plotted in Figure 4-27, initially the sedan is losing minimal mass, developing to –0.142 kg/min between 5 and 10 minutes, 0.123 kg/min of which is registering as entering the (burning) pan. This situation continues between 5 and 10 minutes, after which ~ 80% of the sedan mass is lost. The remaining mass then declines at a much slower rate, and the mass entering the pan no longer exceeds mass burning. The pan mass loss rate is then ~ 0.03 kg/min until accelerated burning at the end of the test.

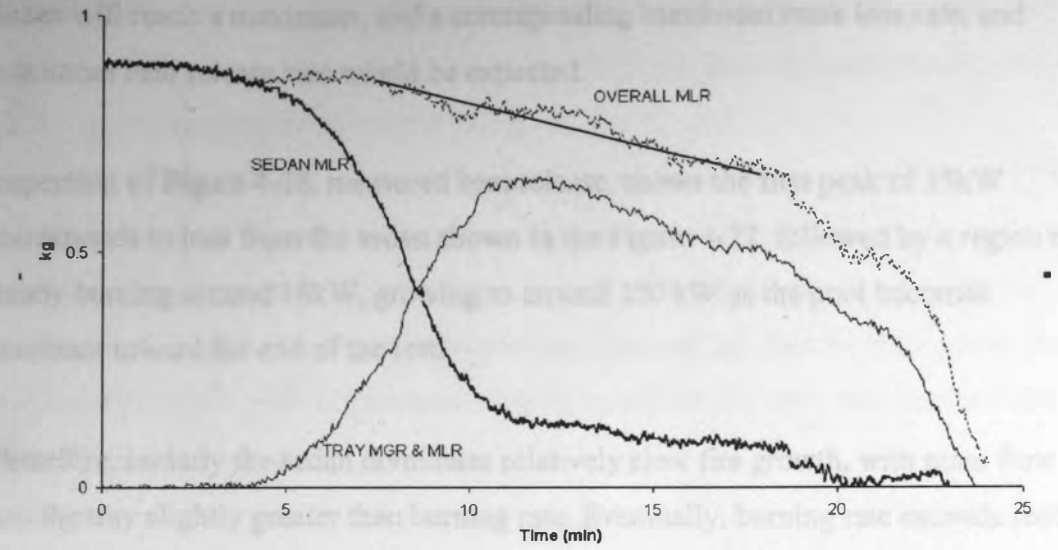

Figure 4-27. Mass flows for full burning Holsten Pils crate (HOLSTFB) (the line shows the overall mlr steady state approximation)

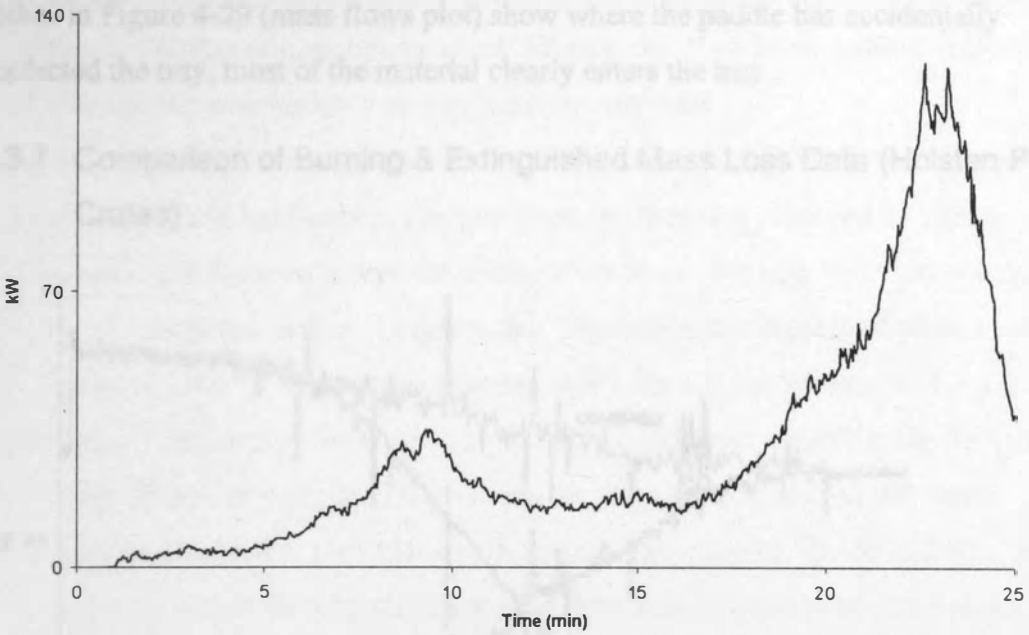

Figure 4-28. Heat release for full burning Holsten Pils crate (HOLSTFB)

Therefore 87% of the material leaving the sedan is entering the pan below. The overall mass loss rate is reasonably constant at 0.014 kg/min for the first 20 minutes of the test, increasing at the end. This is difficult to assess further because the pool supplies an additional radiant flux to the sedan, which also radiates heat from the chair down to the pool. Thus, when both areas are in flaming mode, the surface

fluxes will reach a maximum, and a corresponding maximum mass loss rate, and maximum hear release rate would be expected.

Inspection of Figure 4-28, measured heat release, shows the first peak of 35kW corresponds to loss from the sedan shown in the Figure 4-27, followed by a region of steady burning around 18kW, growing to around 120 kW as the pool becomes dominant toward the end of the test.

Therefore, initially the sedan dominates relatively slow fire growth, with mass flow into the tray slightly greater than burning rate. Eventually, burning rate exceeds feed in rate and the pool produces a fire, with four times the heat release rate of that measured from the initial sedan burning region.
If this is compared to a crate where the pool is extinguished (ie HOLST5) where the spikes in Figure 4-29 (mass flows plot) show where the paddle has accidentally contacted the tray, most of the material clearly enters the tray.

4.3.7 Comparison of Burning & Extinguished Mass Loss Data (Holsten Pils Crates)

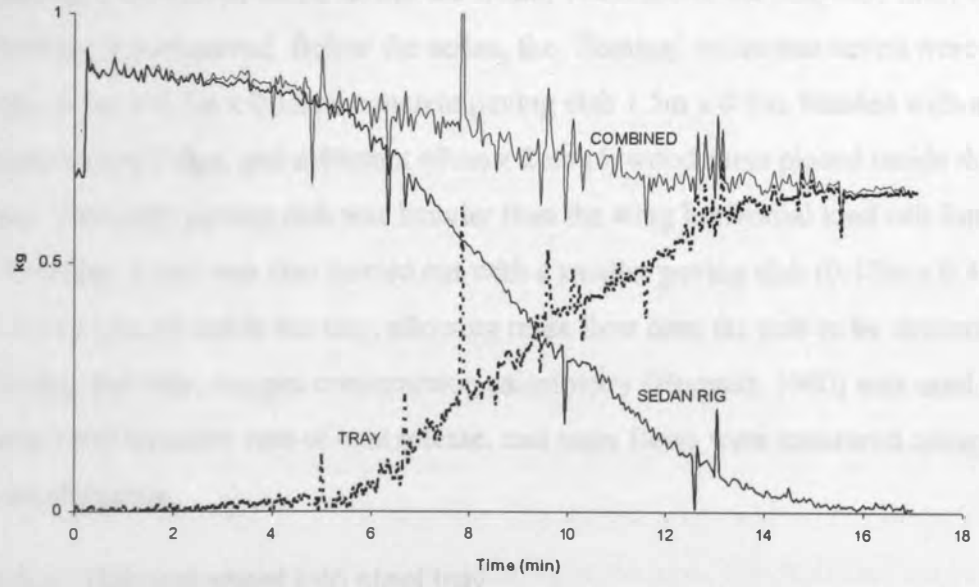

Figure 4-29. Mass flows for HOLST5; (burning melt oil quenched))

Inspection of Figure 4-29 shows the sedan to lose 0.099 kg/min, with 0.076 kg/min entering the pool. Compared to the full burning experiment, where the sedan lost

0.174 kg/min, shows the pool burning below almost doubles the mass loss rate above it. This increased mass loss rate then increases the feed rate to the pool, from 0.076 to 0.113 kg/min, an increase of around 1/3.

If the percentage of burning rate represented by the pool is examined, as shown in Table 4-R, for the mushroom crate, it is only ~ 40 %, but since this is only 250g of fuel it is likely that the steel tray had a cooling effect on this. For the other crates, the pool represented 75 – 85% of the total burning rate. This is clearly the dominant fire after an initial 'fuel feeding' stage.

4.4 Effect of flooring substrate on polymeric pool fire formation.

A series of experiments were carried out using the Sedan Chair Rig, investigating the influence of the nature of flooring material on the behaviour of a pool fire fuelled by a melting & burning polypropylene sheet. Three types of common industrial flooring were selected for investigation: timber, concrete and steel.

Opaque polypropylene sheets, 30cm x 50 cm high x 2.5cm thickness, were bound to a monolux insulating board in the burn cage. Ignition was achieved by slowly passing a blowtorch flame across the width, 10cm above the slab base until sustained flaming was observed. Below the sedan, the 'flooring' substrates tested were a steel tray, 0.5m x 0.5m x 0.1m, a concrete paving slab 1.5m x 0.5m, bunded with a 2.5 cm high cement ridge, and a 49cm x 49cm x 2cm plywood sheet placed inside the steel tray. The large paving slab was heavier than the 40kg horizontal load cell limit. Therefore, a test was also carried out with a smaller paving slab (0.45m x 0.45m x 0.03m), placed inside the tray, allowing mass flow onto the slab to be determined. During the tests, oxygen consumption calorimetry (Huggett, 1980) was used to determine transient rate of heat release, and mass flows were measured using load cell platforms.

4.4.1 Burning sheet into steel tray

Initial fire growth was very slow, the flame spread initially downwards, covering the base 10cm of the sheet after 8 minutes. By 15 minutes after ignition, a 2cm wide non-burning layer of thermoplastic was formed directly below the sheet, which was

¾ covered in flame. The base of the layer had re-solidified, whilst the top remained liquid. This was fed from five main sites, which released burning drips, extinguishing as they contacted the liquid surface. The surface of the sheet was observed to flow slowly, with soot particles taking 20 seconds to flow downward over the lower 10cm of the slab.

Approximately a minute later, a small area ~25mm diameter, fed by a continual flaming dripping stream, began to sustain a small blue flame, around this time, the sheet fire had grown to full surface flaming. Through the flame, it was observed that a transparent depth had formed ~2cm wide, around the sheet sides and base, with surface flow being much faster over this region than over the opaque area.

At 18 minutes, the surface flow rates were 0.6cm/sec over the opaque central area, and 1 cm/sec over the transparent edge zone. By 20 minutes, the pool had covered 30% of the tray, with ~25% of the total pool burning. By 22 minutes, this had increased to ~ 80% of the tray covered, with full tray burning by 23 minutes. Flame height at this point was ~1.6m, behind which the sheet was observed to be still largely opaque. At 26 minutes, the level of radiant heat had increased, making the lab untenable, so the lab was evacuated. The fire finally burned out 35 minutes after ignition. The heat release and mass loss plots are shown overleaf.

Inspection of the heat release (HR) plot, Figure 4-30, shows a very slow developing fire, taking 25 minutes to grow to ~30kW. However, the growth rate then accelerates very rapidly, from 40 to over 450 kW in just four minutes.

Looking at the Figure 4-31, the flow rates are minimal for the first 15 minutes, and then start to increase. By 25 minutes, 1kg has been lost from the sedan, of which 0.6kg has accumulated in the tray at a rate of 0.045 kg/min. By 26.5 minutes, accumulation in the tray has reached a maximum, and the burn rate exceeds the feed in rate. From this point, mass is then lost from the tray at a rate of –0.135 kg/min. At this stage, the sedan mass loss is increased from the rate of–0.011 kg/min shown from 15 –22 minutes, to -0.427 kg/min. The overall mass loss is also increased after 25 minutes, to -0.468 kg/min, corresponding to the peak HR described above.

From comparing the two plots, the peak HR occurs after the point of maximum mass accumulation in the pool, and the tray burning/feeding ratio becomes > 1. Therefore, the burning pool increases the sedan mass loss rate, which must increase the feed rate

into the pool. Since the pool is losing mass despite more material entering it, implying the pool burning rate has increased, this increases the overall mass loss rate. This then dominates the overall heat release mechanism. The total heat released during the test, i.e. the area under the HR curve, was 197 MJ.

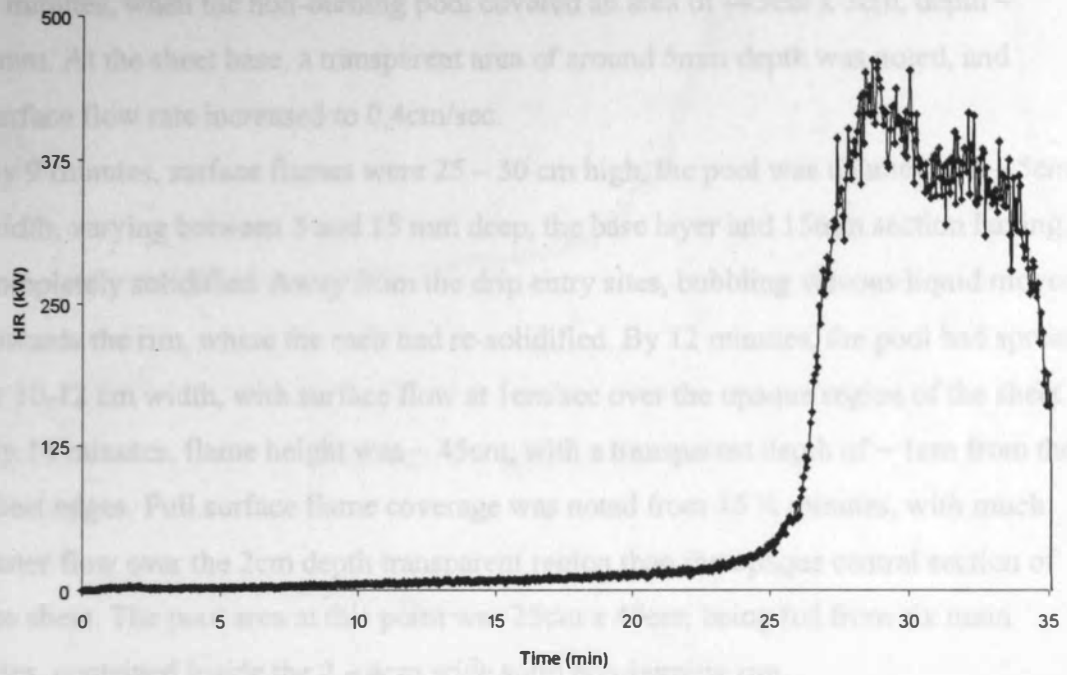

Figure 4-30. Heat released from a PP sheet burning into a steel tray

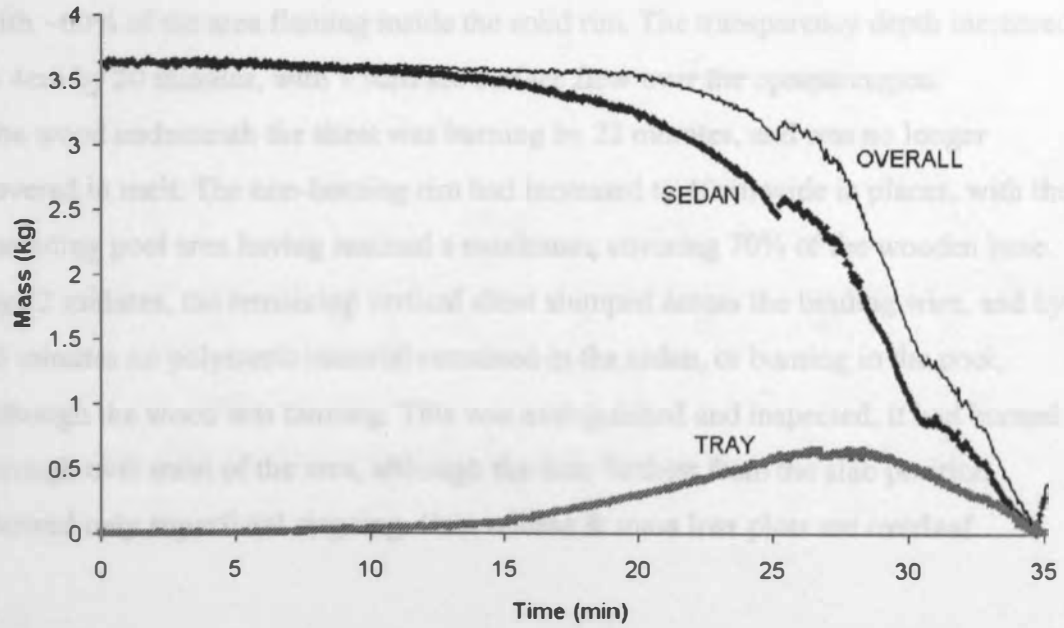

Figure 4-31. Mass flows for PP sheet burning into steel tray

4.4.2 Sheet burning & flowing onto wood

Drips from the sheet were noted two minutes after ignition, frequency ~5Hz. Surface flame covered the lower 15cm of the sheet, all of which was opaque. By 3 minutes, the surface flow rate was 0.3cm/sec. By 5 minutes, there were four drip sites, issuing flaming drips at ~ ½ second intervals. The surface flame had grown to 20 cm high by 6 minutes, when the non-burning pool covered an area of ~45cm x 3cm, depth ~ 3mm. At the sheet base, a transparent area of around 5mm depth was noted, and surface flow rate increased to 0.4cm/sec.

By 9 minutes, surface flames were 25 – 30 cm high, the pool was an uneven 3 – 5cm width, varying between 3 and 15 mm deep, the base layer and 15mm section having completely solidified. Away from the drip entry sites, bubbling viscous liquid moved towards the rim, where the melt had re-solidified. By 12 minutes, the pool had spread to 10-12 cm width, with surface flow at 1 cm/sec over the opaque region of the sheet. By 14 minutes, flame height was ~ 45cm, with a transparent depth of ~ 1cm from the sheet edges. Full surface flame coverage was noted from 15 ½ minutes, with much faster flow over the 2cm depth transparent region than the opaque central section of the sheet. The pool area at this point was 25cm x 45cm, being fed from six main sites, contained inside the 2 – 4cm wide solid non-burning rim.

By 18 minutes, ~1/4 of the wood was covered by melt, with a small burning region ~2cm x 4cm. This had increased to ½ the base area by 20 minutes, about 5mm deep with ~60% of the area flaming inside the solid rim. The transparency depth increased to 4cm by 20 minutes, with 1.5cm/sec surface flow over the opaque region.

The wood underneath the sheet was burning by 22 minutes, and was no longer covered in melt. The non-burning rim had increased to 10cm wide in places, with the spreading pool area having reached a maximum, covering 70% of the wooden base. By 32 minutes, the remaining vertical sheet slumped across the binding wire, and by 35 minutes no polymeric material remained in the sedan, or burning in the pool, although the wood was burning. This was extinguished and inspected. It had burned through over most of the area, although the 6cm furthest from the slab position showed only superficial singeing. Heat release & mass loss plots are overleaf.

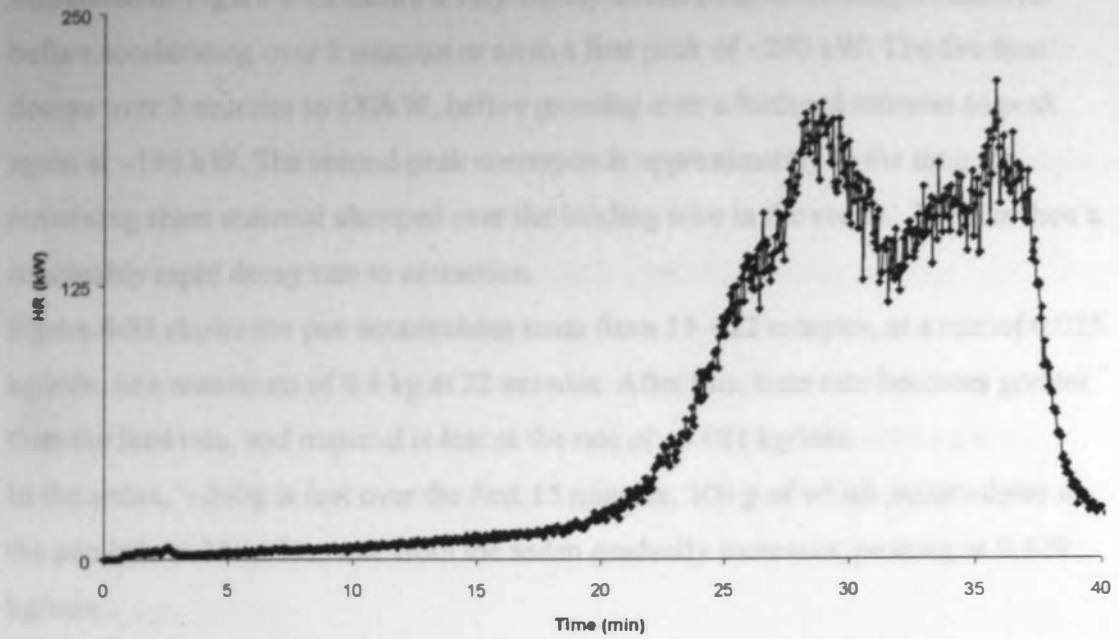

Figure 4-32. HR for PP sheet flowing onto plywood

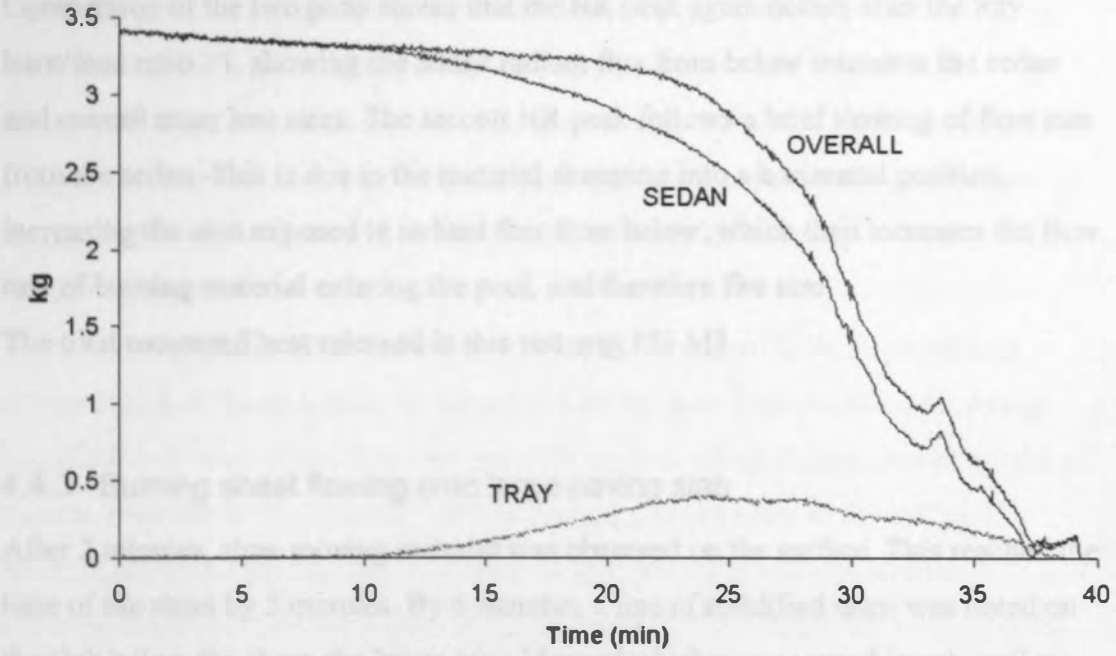

Figure 4-33. Mass flows for PP slab flowing onto plywood sheet

Inspection of Figure 4-32 shows a very slowly developing fire, taking 20 minutes before accelerating over 8 minutes or so to a first peak of ~200 kW. The fire then decays over 3 minutes to 130kW, before growing over a further 4 minutes to peak again at ~190 kW. The second peak corresponds approximately to the time the remaining sheet material slumped over the binding wire in the sedan. There is then a reasonably rapid decay rate to extinction.

Figure 4-33 shows the pan accumulates mass from 15 – 22 minutes, at a rate of 0.025 kg/min, to a maximum of 0.4 kg at 22 minutes. After this, burn rate becomes greater than the feed rate, and material is lost at the rate of –0.081 kg/min.

In the sedan, ~260g is lost over the first 15 minutes, 100 g of which accumulates in the pan below. Mass loss rate from the sedan gradually increases, peaking at 0.329 kg/min.

Overall, the mass loss rate is negligible for the first 20 minutes, building to –0.385 kg/min between 28 – 32 minutes, corresponding to the first and largest peak on the HR plot.

Comparison of the two plots shows that the HR peak again occurs after the tray burn/feed ratio >1, showing the added radiant flux from below increases the sedan and overall mass loss rates. The second HR peak follows a brief slowing of flow rate from the sedan. This is due to the material slumping into a horizontal position, increasing the area exposed to radiant flux from below, which then increases the flow rate of burning material entering the pool, and therefore fire size.

The total measured heat released in this test was 151 MJ.

4.4.3 Burning sheet flowing onto large paving slab

After 2 minutes, slow moving material was observed on the surface. This reached the base of the sheet by 5 minutes. By 6 minutes, a line of solidified drips was noted on the slab below the sheet, the lower 10 – 15cm of which was covered in pale yellow flame. By 10 minutes the flame had turned orange, and was ~10cm high over most of the sheet, rising to 20cm high at the left edge. By 13 minutes, the left edge flame height was ~35cm, with 20cm over the rest of the sheet, with flaming drips issuing from the left edge onto the slab, where they self extinguished. At 15 minutes, edge flame height was 50cm, whilst flame height over the rest of the sheet had not grown

significantly. The non-burning pool was much wider below the flaming edge, ~10 cm compared to 2 – 3cm over the rest of the pool. The sheet flame had grown to 25 – 30 cm by 16 minutes, with a noticeable 1cm deep transparent edge forming by 18 minutes. A burning stream, ~2cm wide was feeding the pool by this stage, although burning was not sustained on the slab. The pool below the flaming edge had grown to 20 cm wide, flaming only where the single burning stream was feeding in.

By 22 minutes, the sheet was ¾ covered in flame, and the pool width varied from 2 to 30 cm. By 24 minutes, a 5 – 10 cm wide burning area was observed in the pool, directly under the burning edge, where the transparent depth had increased to 2 - 3 cm. The burning flow on the flaming edge resulted in the sheet tilting 17° to the left (as illustrated in Figure 6-9). The pool had grown to cover ¼ of the slab, about 20% of which was flaming.

By 25 minutes, the sheet flame coverage increased to ~80% of the sheet, covering all but the uppermost right corner, whilst the pool flaming area had also increased to 30 cm width, ~ ½ the total pool area. At 27 minutes, flame was observed 25 – 30 cm above the initial sheet height, with a pool width of 1m, although the flaming zone was restricted to directly beneath the flaming sheet, which had a 3cm wide transparent edge. Melt was solidified at the pool edge. Pool size increased to the full slab width by 29 minutes, still only flaming below the sheet, and the pool was 4-5mm depth. By 30 minutes, the pool covered over half of the slab, with no increase in flaming area.

Total flame height by 32 minutes was ~50cm, flickering to 70cm.The pool area covered ~3/4 of the slab, with no spread in burning area. The solidified pool edge had lifted 3 or 4mm above from the concrete surface, which further limited spread of molten material, to ~1.1m wide. Further slumping of the sheet to the left by 33 minutes increased the burning pool area slightly, but there was no increase in concrete coverage. The sheet then began to slump forward across the binding wire, which resulted in increased area coverage of the slab below. By 35 minutes there was full burning across the slab width below the sedan, flaming over 30% of the total slab area, although 10 – 15% of the concrete remained untouched. The remaining largely transparent sheet was now 35° from the vertical. By 38 minutes, about 40% of the pool was flaming as the remaining sheet slumped across the burn cage floor. Within

2 minutes, the entire slab had become covered in melt, about 50% of which was flaming. Flame height grew to 1m from the 50 % slab burning area, and the remaining sheet material burned away.

The flame area then died back, with flaming area covering 20% of the slab at 42 minutes, with a flame height of 50 cm, reducing to ¼ of the slab area and 30 cm high flames by 43 minutes. Flame height was <10cm by 45 minutes, with a 10cm wide burning area. The heat release and sedan mass loss plots are shown in Figure 4-34. From Figure 4-34, the peak HR of 117kW occurs at ~26 minutes, and 77 MJ are released during the test. The mass loss after 15 minutes is ~-0.178kg/min, which remains reasonably constant until the fire peaks at 26 minutes, after which is decays rapidly.

The inability to sustain pool burning when the externally applied radiant flux is removed, as shown with the test on the concrete slab was then further investigated using a smaller slab contained within the tray.

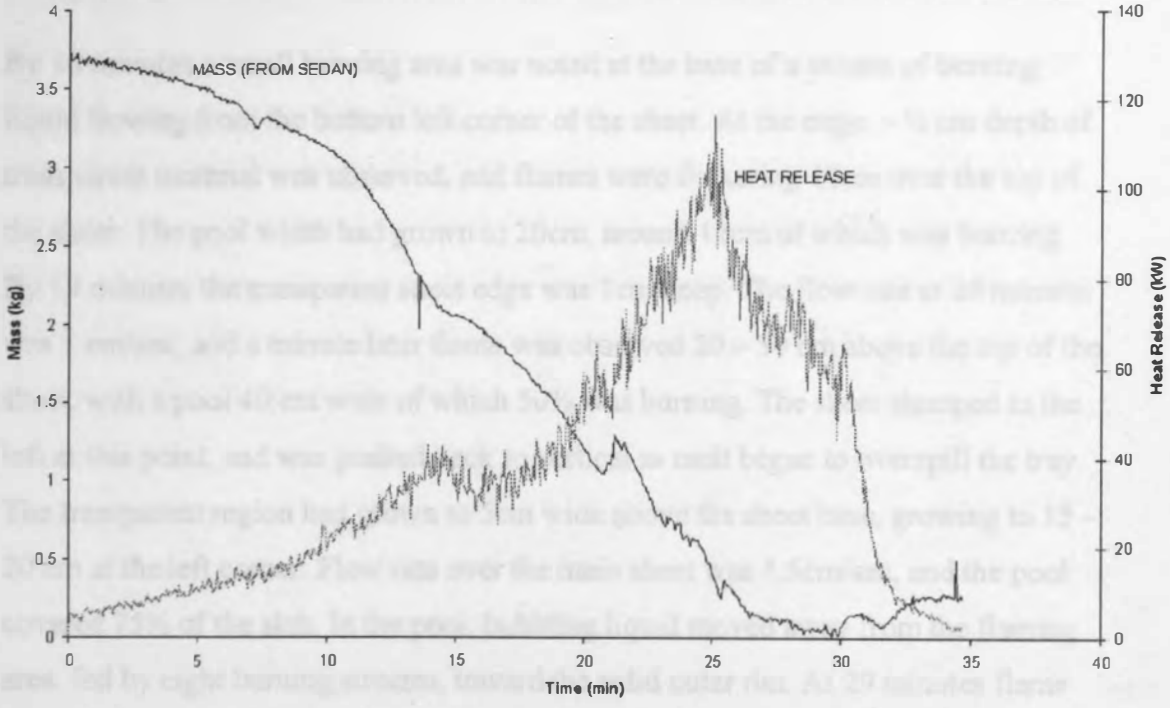

Figure 4-34. HR & Mass loss from sedan for PP sheet onto large slab

4.4.4 Burning sheet flowing onto small slab in tray

90 seconds after ignition, blue flame covered ~5cm of the surface. The first drips to flow the 15cm to the sheet base were noted at 2:05 minutes. By 3.40, some drips had fallen onto the slab, and ~30% of the flame had turned from blue to yellow. By 5 minutes, flame height had reached 20cm from the sheet base.
The first flaming drips were noted at 7½minutes, with ~ ½ Hz frequency. By 8 minutes, three drip sites were issuing burning drips, which extinguished on the slab below. The surface flow rate was 0.2 cm/sec, accelerating toward the base, and ~ 30% of the slab was covered in yellow flame. The drip frequency had increased to 1Hz by 10 minutes, and there were six drip sites formed. By 11 minutes, flow rate had increased to 0.3cm/sec, with 50% of the surface flaming. By 13 minutes, flame permanently covered 75% of the sheet, flickering to the top of the sheet. The non-flaming pool, now fed by nine drip sites, varied between 3 and 7 cm wide and had solidified at the edges. By 14 minutes, flow rate was 0.6 cm/sec, with flame covering 80% of the sheet.

By 16 minutes a small burning area was noted at the base of a stream of burning liquid flowing from the bottom left corner of the sheet. At the edge, ~ ½ cm depth of transparent material was observed, and flames were flickering 10cm over the top of the sheet. The pool width had grown to 20cm, around 12cm of which was burning. By 18 minutes the transparent sheet edge was 1cm deep. The flow rate at 20 minutes was 1 cm/sec, and a minute later flame was observed 20 – 30 cm above the top of the sheet, with a pool 40 cm wide of which 50% was burning. The sheet slumped to the left at this point, and was pushed back to vertical as melt began to overspill the tray. The transparent region had grown to 5cm wide above the sheet base, growing to 15 – 20 cm at the left corner. Flow rate over the main sheet was 1.5cm/sec, and the pool covered 75% of the slab. In the pool, bubbling liquid moved away from the flaming area, fed by eight burning streams, toward the solid outer rim. At 29 minutes flame height had grown to 60 cm above the sheet top. By 30 minutes, the pool area had reached a maximum over ~80% of the slab, and the solid edges bowed up forming a 2 – 4mm deep air gap between polymer and concrete. The bowing created a 'dish' which then contained the melt within a 5 – 8cm solid rim. By 32 minutes, ½ the sheet

had become transparent. Flames from the pool were entrained toward the sheet, with bubbling liquid pushed outward to the solid rim which had formed a ridge 5 – 8mm above the concrete.

By 34 minutes, the burning pool width was 20cm, and a minute later the completely transparent sheet folded over the restraining wires. By 37 minutes the flow viscosity into the pool was comparable to olive oil, and there was a stable flame height noted of ~1m above the pool. The sheet was completely horizontal in the burn cage by 40 minutes, with a 20cm wide burning pool. The horizontal sheet had 10cm of flame above it, around which were 1.1m high flames from the pool. The flow rate into the pool increased, and this resulted in fire growth to 35cm burning pool area. The non-burning rim was still present, and there was no further pool spread after this point, although some melt had entered the gap between slab and tray edge. All material had left the burn cage by 45 minutes, and the flames died back to 30cm height shortly after. By 46 minutes there was only sporadic flame flicker noted, burning out completely by 48 minutes. The HR and mass loss plots are shown overleaf.

Inspection of the Figure 4-35 shows a slow, steadily growing fire taking 45 minutes to reach a peak of 112 kW, followed by a rapid decay over 4 minutes. The total heat released during this test was 85 MJ.

From the Figure 4-36 (load cell outputs), 33% of the initial 3.5 kg, accumulates on the slab as re-solidified melt by the end of the test. The accumulation rate onto the slab is steady from ~ 15 minutes, at 0.035 kg/min. The mass loss rate from the sedan is also reasonably constant from 25 minutes, at –0.133 kg/min. The steady-state overall burning rate is –0.092 kg/min.

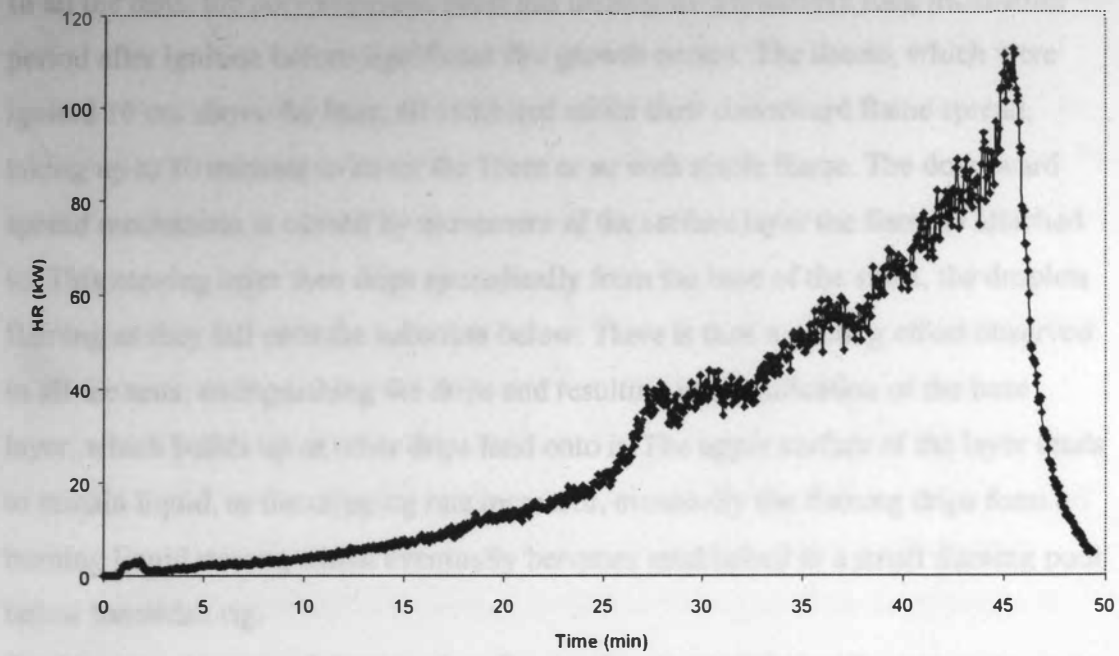

Figure 4-35. HR for PP sheet onto small slab

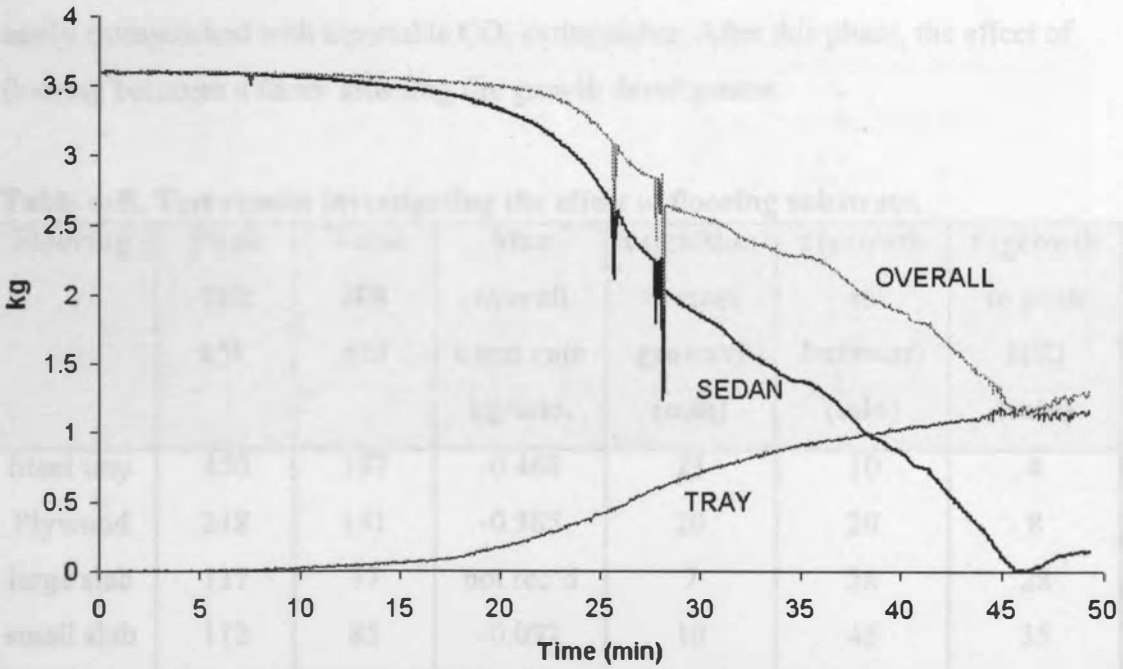

Figure 4-36. Mass flows for PP sheet flowing onto small concrete slab

4.4.5 Analysis & comparison of test results

In all the tests, the polypropylene sheet has undergone a relatively long incubation period after ignition before significant fire growth occurs. The sheets, which were ignited 10 cm above the base, all exhibited initial slow downward flame spread, taking up to 10 minutes to cover the 10cm or so with stable flame. The downward spread mechanism is caused by movement of the surface layer the flame is attached to. This moving layer then drips sporadically from the base of the sheet, the droplets flaming as they fall onto the substrate below. There is then a cooling effect observed in all the tests, extinguishing the drips and resulting in solidification of the base layer, which builds up as other drips land onto it. The upper surface of the layer tends to remain liquid, as the dripping rate increases, eventually the flaming drips form a burning liquid stream, which eventually becomes established as a small flaming pool below the sedan rig.

By this time, the area of sheet surface flaming has increased significantly, not obviously related to any increase in heat flux supplied from the small fire below. This early phase occurred in all the tests, regardless of flooring material, and for practical purposes, for over 15 minutes, the flames from the sheet are noticeable, and easily extinguished with a portable CO_2 extinguisher. After this phase, the effect of flooring becomes a factor affecting fire growth development.

Table 4-R. Test results investigating the effect of flooring substrate.

Flooring	Peak HR kW	Total HR MJ	Max overall burn rate kg/min.	t (ignition to start growth) (min)	t (growth to burnout) (min)	t (growth to peak HR) (min)
Steel tray	450	197	-0.468	23	10	4
Plywood	218	151	-0.385	20	20	8
large slab	117	77	not rec'd	7	38	28
small slab	112	85	-0.092	10	45	35

From Table 4-R, the experiment with the steel tray produces the fastest growing and largest fire of the floorings tested. The total heat released is ~ double that of the fire onto wood, and almost four times that of the fire flowing onto concrete. The peak HR

is 25% greater than for a wood base, and 60% greater than that on the large slab. However, the fire onto steel has the longest incubation period, followed by the fastest growth rate and the shortest fire duration. It was also the only test where the entire 'floor' was covered in flaming material, no melt was left after the test, and the level of radiant heat necessitated lab evacuation.

Comparison of the fires onto the small and large concrete slabs shows the results are similar.

Comparing the pan mass flow rates shown in Table 4-S, finds both the accumulation and loss rates onto steel are almost double those recorded onto wood. The accumulation rate onto steel is thirteen times greater than that onto the concrete slab.

For further comparison, the estimated growth in flame heights and pool areas during the tests described above, are plotted in Figure 4-37. From Figure 4-37, the early flame height growth rates for all floors are similar. This is because flame height is dominated by spread across the sheet surface during the early stage. However, after 15 minutes, the steel tray experiment undergoes an exponential flame growth rate, producing the fastest flame growth rate of the experimental series.

Table 4-S. Flow rates onto & from steel, wood & concrete flooring

Floor	Feed rate into tray – burning from tray kg/min	burn rate from tray (after burn rate exceeds feed rate) kg/min
Steel	0.045	-0.135
Wood	0.025	-0.081
small slab	0.003	condition not achieved

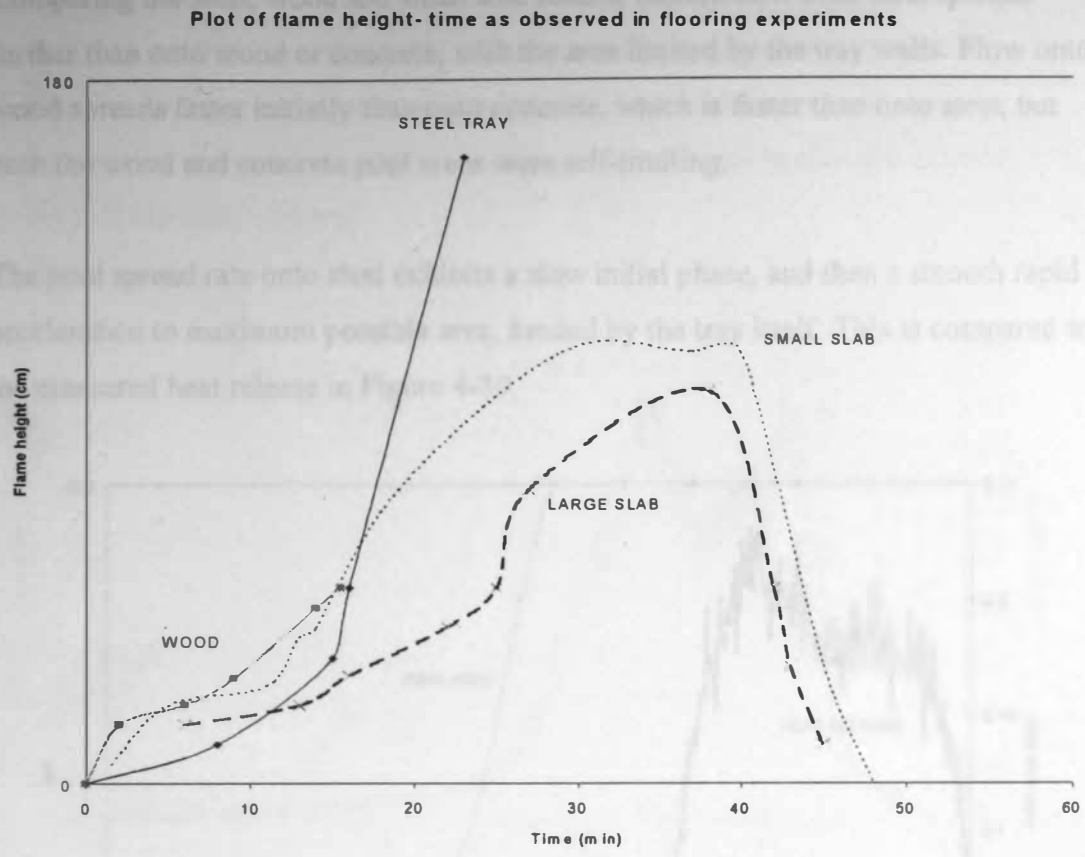

Figure 4-37. Estimated flame height -time correlations

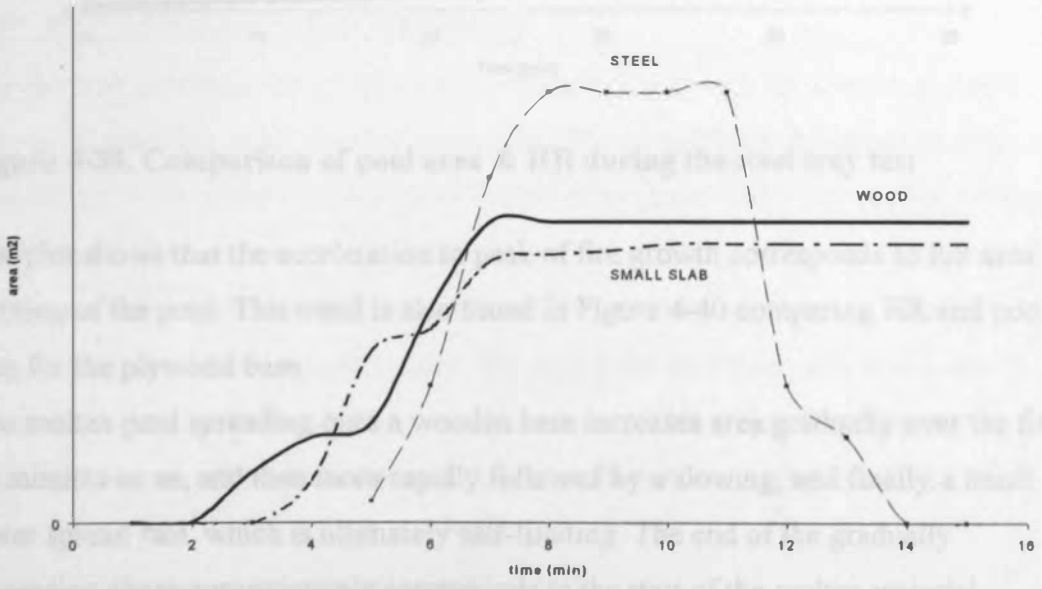

Figure 4-38. Estimated pool area - time correlations

Comparing the steel, wood and small slab results, molten flow onto steel spreads further than onto wood or concrete, with the area limited by the tray walls. Flow onto wood spreads faster initially than onto concrete, which is faster than onto steel, but both the wood and concrete pool areas were self-limiting.

The pool spread rate onto steel exhibits a slow initial phase, and then a smooth rapid acceleration to maximum possible area, limited by the tray itself. This is compared to the measured heat release in Figure 4-39.

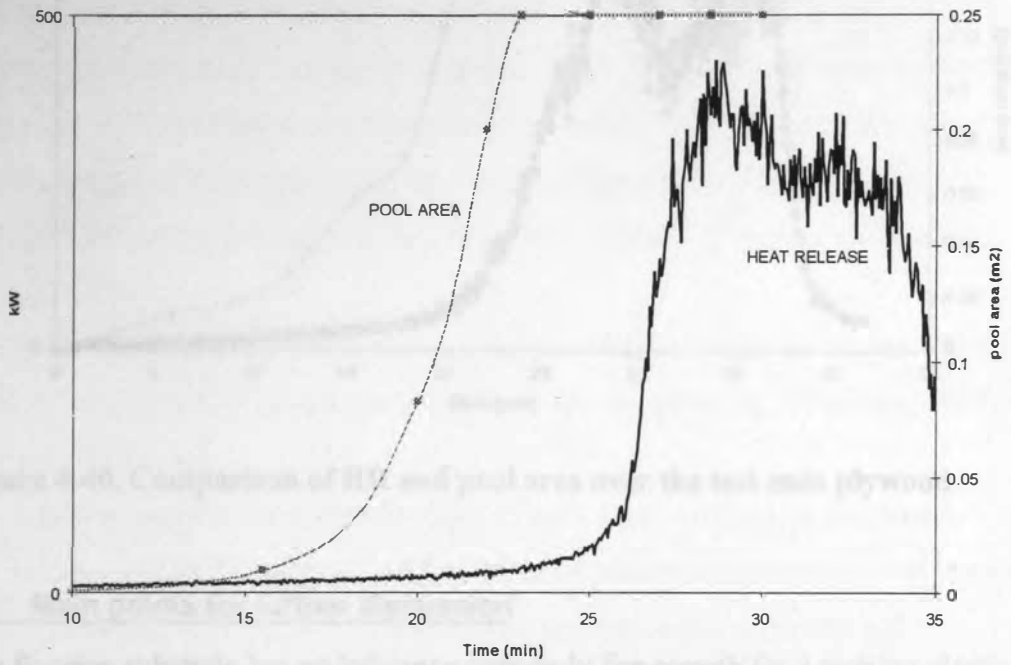

Figure 4-39. Comparison of pool area & HR during the steel tray test

The plot shows that the acceleration to peak of fire growth corresponds to full area burning of the pool. This trend is also found in Figure 4-40 comparing HR and pool area for the plywood base.

The molten pool spreading onto a wooden base increases area gradually over the first 10 minutes or so, and then more rapidly followed by a slowing, and finally a much faster spread rate, which is ultimately self-limiting. The end of the gradually increasing phase approximately corresponds to the start of the molten material burning, and the faster spreading rate corresponds to the time the wood began to burn.

These tests indicate that for a pool formed on a steel base, the extent of spread is controlled by either the amount of material available, or physical containment barriers. In contrast, a combustible wooden substrate may limit spread, whilst a concrete substrate enables spread, but will not sustain burning after the external flame flux has been removed.

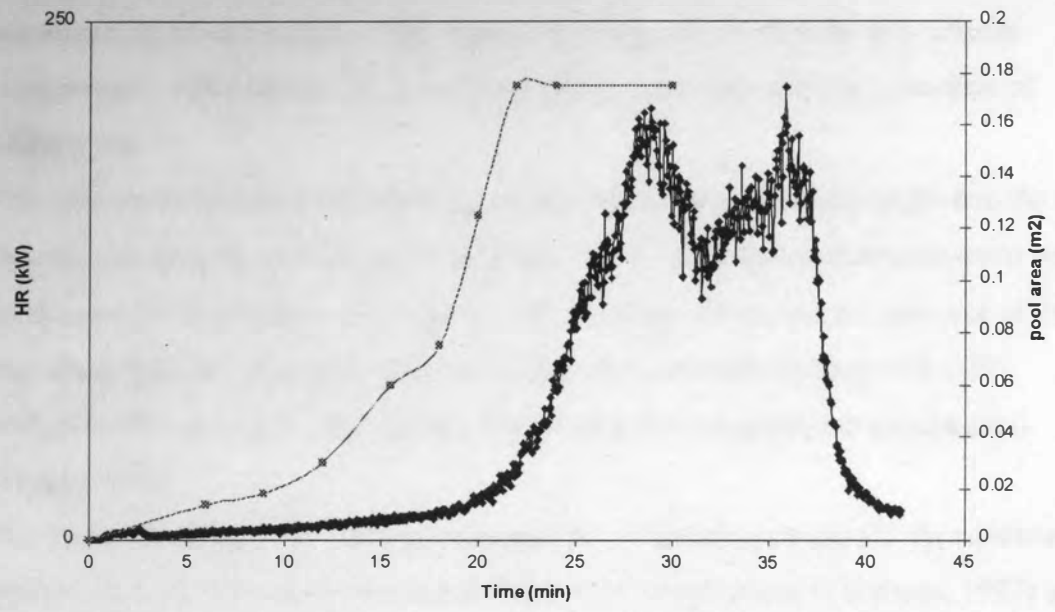

Figure 4-40. Comparison of HR and pool area over the test onto plywood

4.5 Main points for further discussion

The flooring substrate has no influence over early fire growth for a melting plastic. However, after this phase flooring properties have a significant influence on melt temperature (one of the main viscosity determining parameters), and surface contact resistance to flow of the spreading liquid pool. These factors, along with temperature dependent MW determine the burning rate and extent of potential pool area. Importantly, the fire flowing onto steel liberated more heat than onto wood, which produced ~ double the heat of the fire onto concrete. This shows that flooring material is a controlling parameter for the potential fire hazard posed by a melting plastic.

A detailed discussion is undertaken in Chapter 6.

5 Theoretical Model

5.1 Background Review

There have been previous studies related to melting behaviour, although not polymer specific, and not related to fire. For example, Stefan studied the melting of a polar ice cap in the 1850's, and developed the 'ablation' model (D'Alelio, 1971). This method assumes that phase change, in this instance melting, occurs directly at a 'critical temperature', often termed T_p. T_p is then a model parameter and not a function of heating rate.

The ablation technique was further developed when mathematically applied to the thermal conductivity of melting ice (Landau, 1950). Ablation models have since been used to model volatisation of a heated solid (Whiting, 1992), and are now one of the two main approaches employed in the section of fire models dealing with solid surface volatisation (the other being a finite rate kinetic degradation mechanism) (Staggs, 1994).

The model developed for this study incorporates an ablation model for the volatising surface, with T_p defined as the measured firepoint[i] temperature, (Thomson, 1987) as shown in Table 5-A.

The model is intended to define the depth of melt front, variation in properties through the front and gravity driven flowrate of plastic available to fuel a potential pool. The radiant heat supplied to the surface is taken as the experimentally measured plastic flame flux (Tewarson & Pion, 1976).

Table 5-A. Thermoplastic Material Parameters from Literature

Thermoplastic	Ignition Temp (K) (Thomson, 1987)	Flame Flux (kW/m^2) (Tewarson, 1976)	Melt Temperature (K) (Brandrup, 1975)
polyethylene	636	32.6	403 – 408
polypropylene	607	28	459
polystyrene	639	61.5	513
PMMA	583	38.5	433

[i] 'Firepoint temperature' - minimum surface temperature at which sufficient flow of volatiles and a piloted ignition source allow a surface flame to persist. (Drysdale, 1999)

5.2 Basic Model

Modelling melt-flow behaviour is problematic for several reasons:

- *the location of the interface is not known 'a priori'*
- *the interface between solid and liquid phases moves as latent heat is absorbed or liberated*
- *the thermal properties of solid and liquid are different*

The problem is non-linear (Ozisik, 1989) and so exact solutions are difficult. However, an exact solution was developed by Neumann (Carslaw, 1959), for the solidification of a semi-infinite region as a result of 1-D heat flow (*outlined in the Appendix, A.2, at the rear of this thesis*). This similar problem has a semi-infinite region, initially at a temperature, T_i, which is greater than the melt temperature. After time $t = 0$, the boundary surface is kept at $T = 0$, resulting in liquid solidification normal to the surface. This yields a complicated exact solution, which has been adapted for melting but is almost impossible to apply to more complex geometry. The problem was then approximated[ii] (Goodman, 1958), using the integral heat conduction method to solve the 1-D melting problem. Goodman's approach is the basis of the model presented here, preferred over the exact solution since it is more adaptable for future development. The model attempts to locate the solid-liquid interface, where the effect of the temperature distribution in the solid region is small. This addresses the first two points made above. The third point, relating to molten plastic properties is investigated in Section 5.3, but has not been fully addressed by this thesis.

5.2.1 Locating the solid - liquid interface using Goodmans Solution

Simplification: it is assumed that the solid is initially at the melt temperature, T_m, and for times, $t > 0$, a constant temperature T_o, greater than the melting temperature (*i.e.* $T_o > T_m$) is applied at the boundary surface $x = 0$.

NB T_m represents the end point of the crystal melt phase, not the point at which the polymer starts to flow.

[ii] the method is approximate since the local heat flux or temperature calculated may not be wholly accurate, although the heat balance is satisfied.

Due to T_o, the solid melts and the solid – liquid interface moves in the x direction as shown in Figure 5.1.

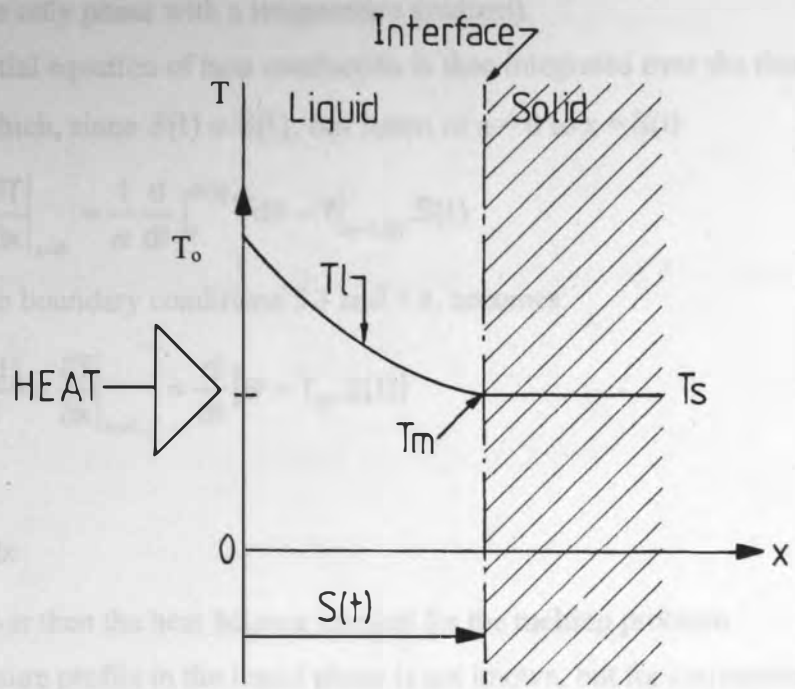

Figure 5-1. Solid-liquid interface for the 1-D melting problem.

A thermal layer thickness is defined, $\delta(t)$, beyond which the temperature gradient is zero. The location of $\delta(t)$ is identical to the location of the solid-liquid interface, so that:

$$\delta(t) = S(t) \qquad 5.0$$

With the solid initially at T_m, there is no solid phase temperature gradient. The only temperature gradient then exists in the liquid phase, so ignoring liquid convection, heat transfer in the liquid phase is purely conductive. The boundary value problem for liquid phase conduction is then:

$$\frac{\partial^2 T_l}{\partial x^2} = \frac{1}{\alpha}\frac{\partial T_l}{\partial t} \qquad \text{in } 0 \le x \le S(t), \quad t > 0 \qquad 5.1$$

$$T_l = T_o \qquad \text{at } x = 0, \quad t > 0 \qquad 5.2$$

$$T_l = T_m \qquad \text{at } x = S(t), \quad t > 0 \qquad 5.3$$

$$-k_l \frac{\partial T_l}{\partial x} = \rho L \frac{dS(t)}{dt} \qquad \text{at } x = S(t), \qquad t > 0 \qquad 5.4$$

(where L is latent heat and the subscript $_l$ refers to liquid phase, which can be omitted since it is the only phase with a temperature gradient).

The differential equation of heat conduction is then integrated over the thermal layer thickness, which, since $\delta(t) = S(t)$, has limits of $x = 0$ to $x = S(t)$.

$$\left.\frac{\partial T}{\partial x}\right|_{x=S(t)} - \left.\frac{\partial T}{\partial x}\right|_{x=0} = \frac{1}{\alpha}\frac{d}{dt}\int_0^{S(t)} T dx - T|_{x=S(t)}.S(t) \qquad 5.5$$

Which due to boundary conditions 5.3 and 5.4, becomes:

$$-\alpha\left[\frac{\rho L}{k}\frac{ds(t)}{dt} + \left.\frac{\partial T}{\partial x}\right|_{x=0}\right] = \frac{d}{dt}[\Theta - T_m.S(t)] \qquad 5.6a$$

where:

$$\Theta = \int_0^{S(t)} T.dx \qquad 5.6b$$

Equation 5.6 is then the heat balance integral for the melting problem.

The temperature profile in the liquid phase is not known, but for convenience is assumed to be a 2nd degree polynomial:

$$T = a + b(x-S) + c(x-S)^2 \qquad 5.7$$

where $S \equiv S(t)$, $a = T_m$, and the two unknown coefficients determined from the following conditions:

$$T(x, t)|_{x=0} = T_o \qquad 5.8$$

$$T(x, t)|_{x=S(t)} = T_m \qquad 5.9$$

$$-k\left.\frac{\partial T(x,t)}{\partial x}\right|_{x=S(t)} = \rho L \frac{dS(t)}{dt} \qquad 5.10$$

However 5.10 is unsuitable, as the resulting temperature profile involves a dS(t)/dt term, which will produce a 2nd ODE when substituted into the heat balance integral. Goodman (1958) instead differentiated Equation 5.9 with respect to time:

$$\frac{\partial T}{\partial x}\frac{dS(t)}{dt} + \frac{\partial T}{\partial t} = 0 \qquad 5.11$$

rewriting 5.4 as:

$$\frac{-\partial T}{\partial x} = A\frac{dS(t)}{dt} \qquad 5.12a$$

where:

$$A = \frac{\rho L}{k} \qquad 5.12b$$

(with all properties liquid phase). Eliminating dS(t)/dt between 5.11 and 5.12:

$$\left(\frac{\partial T}{\partial x}\right)^2 = A\frac{\partial T}{\partial t} \qquad 5.13$$

where the $\partial T/\partial t$ term can be eliminated by using 5.1 to obtain:

$$\left(\frac{\partial T}{\partial x}\right)^2 = \alpha A\frac{\partial^2 T}{\partial x^2} \qquad \text{at } x = S(t) \qquad 5.14$$

(5.8), (5.9) and (5.14) can then be used to find the unknowns in 5.7:

$$T-T_m = b(x-S) + c(x-S)^2 \qquad 5.15a$$

where:

$$b = \frac{A\alpha}{S}[1-(1+\mu)^{0.5}] \qquad 5.15b$$

$$c = \frac{bS + (T_o - T_m)}{S^2} \qquad 5.15c$$

and:

$$\mu = \frac{2(T_o - T_m)}{A\alpha} \qquad 5.15d$$

If the temperature profile, Eq 5.15a, is then substituted into Eq 5.6a, the heat balance integral, the following ODE is obtained for S(t), the location of the solid - liquid interface.

$$S\frac{ds}{dt} = 6\alpha\left[\frac{1-(1+\mu)^{0.5}+\mu}{5+(1+\mu)^{0.5}+\mu}\right] \qquad 5.16a$$

with $S = 0$ for $t = 0$ 5.16b

The solution for Eq 5.16 is then:

$$S = K\sqrt{t} \qquad 5.17a$$

where:

$$K = \left[12\alpha \frac{1-(1+\mu)^{0.5}+\mu}{5+(1+\mu)^{0.5}+\mu} \right]^{0.5} \qquad 5.17b$$

Goodman (1958) has compared results of this approximation with the exact solution as shown in Figure 5-2, improving accuracy by incorporating a cubic temperature profile. It should be emphasised that the boundary conditions are very important in determining the model accuracy. This approach allows determination of the depth of melt front for a model with no moving liquid.

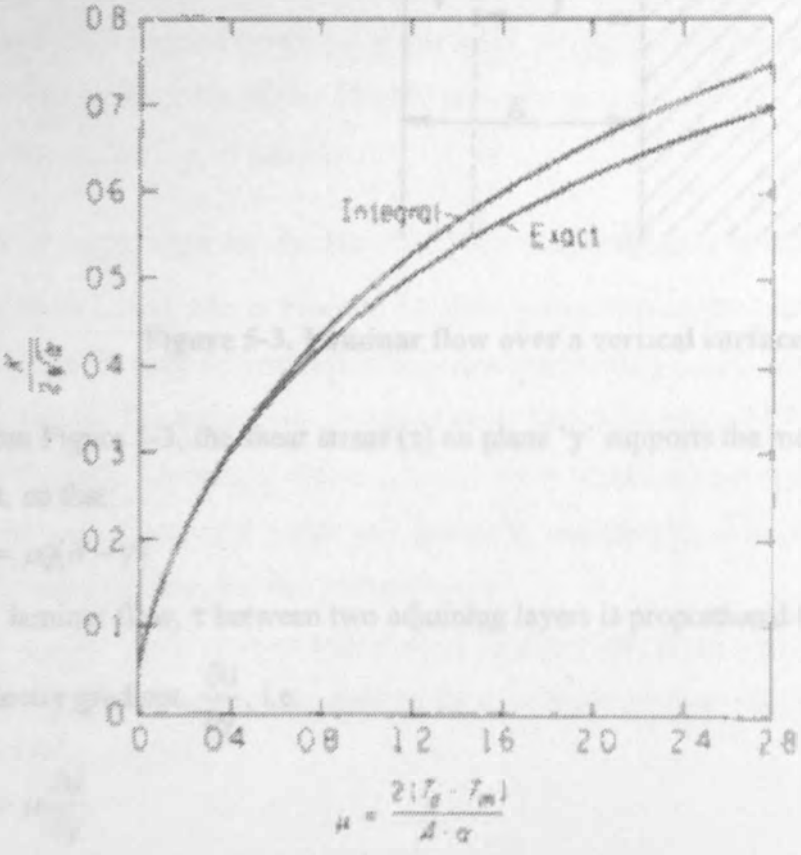

Figure 5-2. Comparison of exact & approximate integral solutions for the melting constant, K, for a semi-infinite region (Goodman, 1958)

5.2.2 Establishing flow characteristics through the heated layer

For the semi-infinite solid, downward gravity driven flow on a vertical surface can be assumed to be laminar due to low velocity of the melt. The basic solution to this problem is found in a standard text (Kay & Nedderman, 1988), and described as follows.

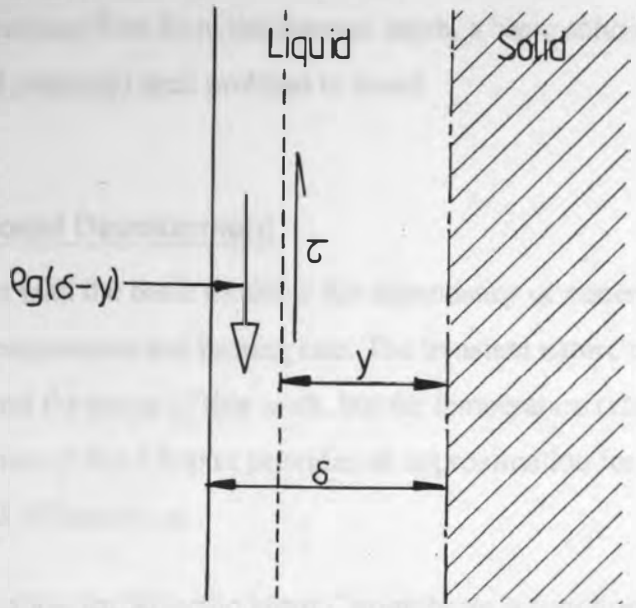

Figure 5-3. Laminar flow over a vertical surface

From Figure 5-3, the shear stress (τ) on plane 'y' supports the mass of fluid to the left, so that:

$$\tau = \rho g(\delta - y) \qquad 5.18$$

for laminar flow, τ between two adjoining layers is proportional to the perpendicular velocity gradient, $\frac{\partial u}{\partial y}$, i.e:

$$\tau = \mu \frac{\partial u}{\partial y} \qquad 5.19$$

(μ = viscosity)

where there is a boundary condition of: at $y = 0$, $u = 0$

therefore eliminating τ, applying this boundary condition and integrating yields:

$$u = \frac{\rho g}{\mu}\left(\delta y - \frac{y^2}{2}\right) \qquad 5.20$$

which when integrated, produces the volume flow rate per unit width:

$$Q = \int_0^{\delta} u.dy = \frac{\rho g \delta^3}{3\mu} \qquad 5.21$$

Therefore, using Equation 5.17 to define the depth of liquid layer, and then Equation 5.21 to generate volume flow from the thermal depth, a basic solution to the (constant material property) melt problem is found.

5.3 Further Model Development

The main problem with the basic model is the dependency of material properties of plastics on both temperature and heating rate. The transient nature of plastic thermal properties is beyond the scope of this work, but the temperature related functions are not. The next section of this Chapter provides an approximation for temperature dependant thermal diffusivity, α.

5.3.1 Approximation for Specific Heat Capacity as a function of temperature

As previously shown in Figure 3.10, there are some published data (Brandrup, 1975) available for pure polymer specific heat – temperature functions intended for use in processing. The temperature range is lower than that required for a fire model, but the melt effect is clearly visible. The effects of branching and crystallinity are also significant. According to this plot, before T_g and after T_m, there is no discernible difference between the two polymer types.

Since commercial plastics tend to be at least partially crystalline with some degree of branching and possibly copolymerisation, published values for pure polymers are not wholly appropriate.

It has been suggested (Van Krevelen, 1976) that the curves for molar heat capacity for solid & liquid polymers are approximately linear, other than for solids below 150K. Therefore, if the gradients are known, the heat capacity at an arbitrary temperature can be calculated from its value at 298K. The slopes of some of the

curves, related to 298K are listed in Table 5-B. Van Krevelen found that the solid polymer curves show a mean value of;

$$\frac{1}{C_p^{\,s}(298)}\frac{dC_p^{\,s}}{dT} = 3x10^{-3} \qquad 5.22$$

with a standard deviation of 5%.

Similarly, for liquid polymers,

$$\frac{1}{C_p^{\,l}(298)}\frac{dC_p^{\,l}}{dT} = 1.2x10^{-3} \qquad 5.23$$

but the standard deviation is much higher at 30%.

Table 5-B. Heat capacities & temperature functions of heat capacities (K^{-1})

	T_m K	$C_p^{\,s}(298)$ J/kg K	$C_p^{\,l}(298)$ J/kg K	$\frac{1}{C_p^{\,s}(298)}\frac{dC_p^{\,s}}{dT}$	$\frac{1}{C_p^{\,l}(298)}\frac{dC_p^{\,l}}{dT}$
PE	419	1550-1760	2260	3×10^{-3}	1×10^{-3}
PMMA	433	1380	1800	3×10^{-3}	1.5×10^{-3}
PS	513	1220	1720	3.4×10^{-3}	1.2×10^{-3}
PP	451	1630-1760	2140	2.9×10^{-3}	1.4×10^{-3}

Therefore, heat capacity can be approximated as a function of temperature from:

$$C_p^{\,s}(T) = C_p^{\,s}(298)[1 + 3x10^{-3}(T - 298)] = C_p^{\,s}(298)[0.106 + 3x10^{-3}T] \qquad 5.24$$

$(T<T_m)$

$$C_p^{\,l}(T) = C_p^{\,l}(298)[1 + 1.2x10^{-3}(T - 298)] = C_p^{\,l}(298)[0.64 + 1.2x10^{-3}T] \qquad 5.25$$

$(T>T_m)$

5.3.2 Thermal Conductivity as a function of temperature

There is no widely accepted theoretical approach to derive conductivity (λ) as a function of temperature for polymer melts. Most theories are based on the equation (Debye, 1914);

$$\lambda = \Lambda c_v \rho u L \qquad 5.26$$

where Λ is a constant, c_v is specific heat capacity at constant volume, ρ is density, u is the velocity of elastic waves and L is the average free path length. An example of the development is a similar equation, (Sakiadis, 1956),

$$\lambda \approx c_p \rho u L \qquad 5.27$$

where **L** is the distance between molecules in 'adjacent thermal layers' (assumed constant and independent of temperature). However it is difficult to develop a λ - T function from this approach.

Instead, it has been found experimentally that for amorphous polymers and polymer melts, conductivity at temperatures above T_g, is found to decline gradually and approximately linearly with increasing temperature. This is shown in Figure 5-4, produced from experimental data (Hands, 1973).

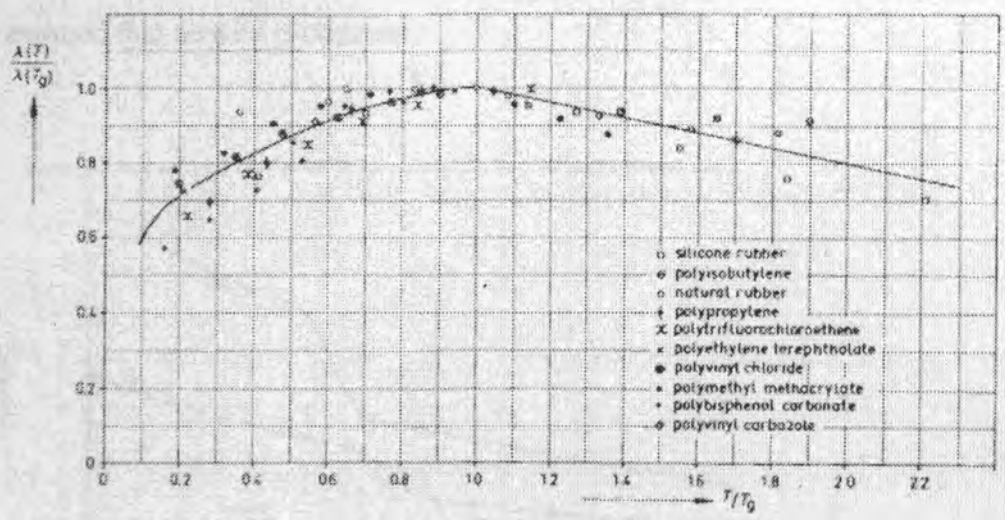

Figure 5-4. Generalised curve for the thermal conductivity of amorphous polymers (Hands, 1973)

NB *simplification:* Conductivity is highly dependent on crystallinity, but during melting the crystal phase dissolves and this dependency can be neglected for $T > T_m$.

Using published values for conductivity at 298K (Drysdale, 1999), and $298/T_g$ for each polymer, thermal conductivity at glass transition is shown in Table 5-C.

Table 5-C. Thermal conductivity parameters

	λ at 298K W/mK	T_g K	$298/T_g$	$\lambda(298)/\lambda(T_g)$	$\lambda(T_g)$ W/mK
PE	0.44	195	1.528	0.95	0.47
PP	0.24	263	1.133	0.99	0.24
PS	0.11	235	1.268	0.97	0.11
PMMA	0.19	310	0.961	1	0.19

From the plot;

$$\lambda(T)/\lambda(T_g) = -0.1(T/T_g) + 1.1 \qquad T \geq T_g \qquad 5.28$$

allowing assessment of λ as a function of temperature.

5.3.3 Thermal Diffusivity – Temperature Function

The heat capacity and conductivity – temperature functions can then be used to derive thermal diffusivity, α, as a function of temperature as shown in Figure 5-5 if it is assumed that density is constant.

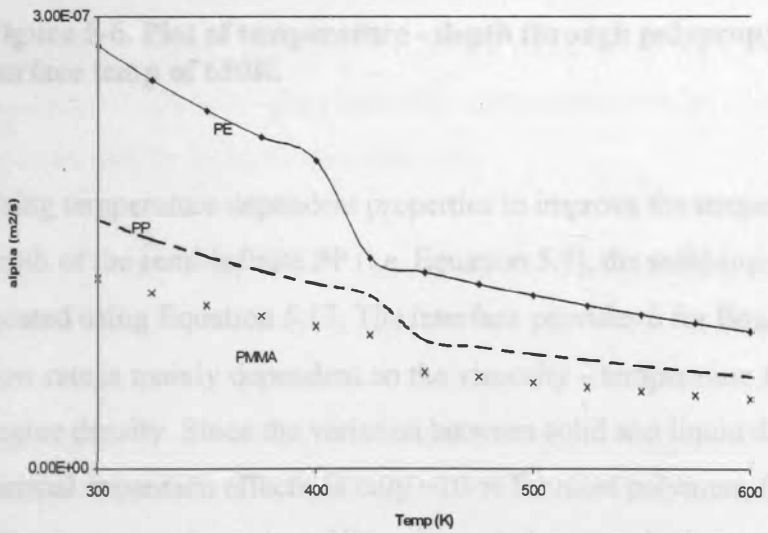

Figure 5-5. Model Thermal diffusivity - temp functions

5.3.4 Improved Temperature Gradient

Therefore, taking an arbitrary surface temperature of 650K to represent a burning surface temperature, (assuming steady state) the temperature through the PP is plotted in Figure 5-6, from which a trend fitted 2nd order polynomial is found to be:

$$T = 2.2355x^2 - 54.852x + 650.61 \qquad (R^2 = 0.992) \qquad 5.29$$

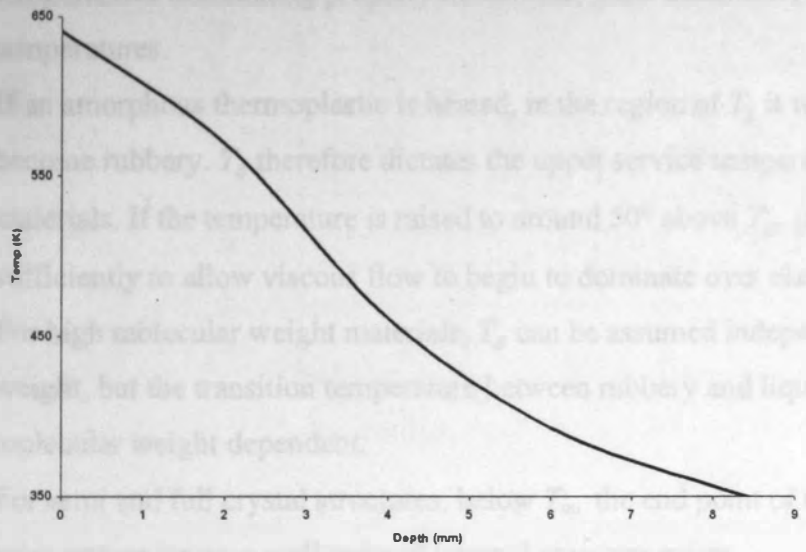

Figure 5-6. Plot of temperature - depth through polypropylene with a surface temp of 650K.

Using temperature dependent properties to improve the temperature through the depth of the semi-infinite PP (i.e. Equation 5.7), the solid-liquid interface is then located using Equation 5.17. The interface provides δ for Equation 5.21, which finds flow rate is mainly dependent on the viscosity – temperature function and, to a lesser degree density. Since the variation between solid and liquid densities, ignoring thermal expansion effects, is only ~10 % for most polymers, (as shown in Figure 3-12) it is assumed constant. Viscosity must however be input as a direct function of temperature.

5.4 Viscosity

5.4.1 Overview of deformability & viscosity

The physical properties of thermoplastics are dependent on their degree of molecular conformity or crystallinity (Beyler, 1995), so thermoplastics are usually classified as amorphous, semi-crystalline or crystalline structures. There are two critical temperatures dominating property transitions; glass transition (T_g) and melt (T_m) temperatures.

If an amorphous thermoplastic is heated, in the region of T_g it will start to soften and become rubbery. T_g therefore dictates the upper service temperatures for amorphous materials. If the temperature is raised to around 50° above T_g, μ decreases sufficiently to allow viscous flow to begin to dominate over elastic deformation.

For high molecular weight materials, T_g can be assumed independent of molecular weight, but the transition temperature between rubbery and liquid states is very molecular weight dependent.

For semi and full crystal structures, below T_m, the end point of the crystal melt temperature range, a well ordered internal structure exists.

Above T_m, the polymer can be liquid, visco-elastic or rubbery, depending on molecular weight, whilst below it, a high molecular weight polymer will be leathery and tough down to its glass transition temperature, whilst a low molecular weight material will be more like a brittle wax.

One of the major parameters controlling the melt flow behaviour, or rheology, of a thermoplastic, is the relationship between viscosity (a function of force per unit area and time), and temperature. Unfortunately, the only published data on polymer viscosity is for processing, which is conducted at temperatures lower than those which will produce thermal degradation, as shown in Figure 5-7 (ICI, 1985).

From Figure 5-7 (where viscosity has been measured with a capillary rheometer), viscosity is a logarithmic function of temperature, and there is a temperature dependency to the ranking order of material viscosities. Unfortunately, measurement of viscosity produces results with a high equipment dependency, which are useful only as relative comparators. Therefore, a different approach is taken for this model.

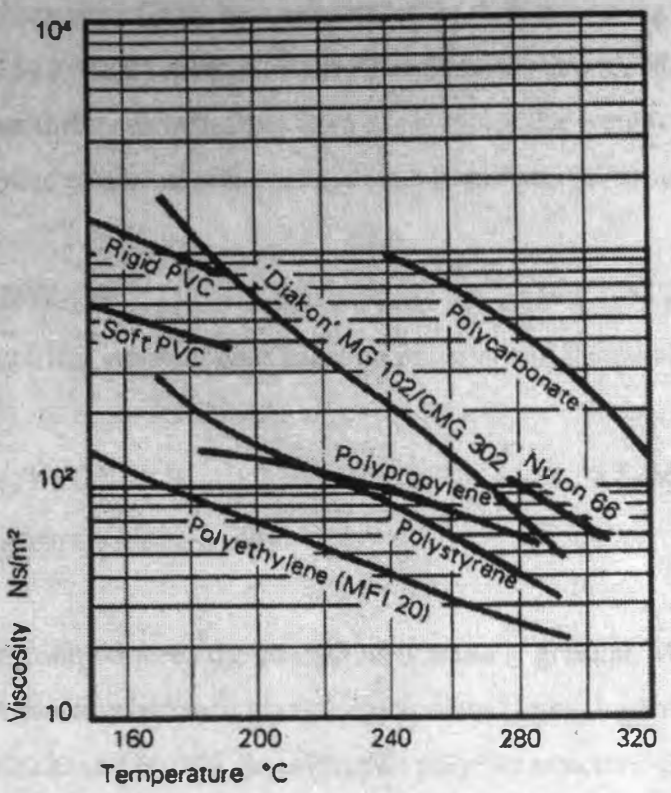

Figure 5-7. Variation of melt viscosity with temperature for various thermoplastics (shear rate 1000s-1) (ICI, 1985)

5.4.1.1 Viscosity Dependency Arguments

It is widely accepted that the principal parameters controlling melt-flow rheology are shear and extensional viscosities (Cogswell, 1981).

Shear viscosity is the ratio between applied shear stress and rate of shear, whilst extensional viscosity is the ratio of tensile stress and rate of extension.

Shear viscosity within the processing temperature range, is a function of average molecular weight, molecular weight distribution, temperature, shear stress (and rate), and hydrostatic pressure, whilst extensional viscosity is dependant on average molecular weight, temperature tensile strain and rate of extension.

For many liquids, defined as a 'Newtonian melts' (η_o) viscosity is a material constant, affected only by temperature and pressure. Steady state polymer melts at low rates of shear approximate Newtonian conditions, but generally viscosity is a function of deformation conditions, producing a melt showing some recoverable elastic effects at lower temperatures, defined as a 'viscoelastic melt'.

Predictably, the viscosity of polymer melts increases with increasing molecular weight, and there is a widely accepted 'critical molecular weight', M_{cr}, above which the melt behaviour differs significantly from a low molecular weight polymer. This has lead to published empirical relationships (van Krevelen, 1976) such as:

$$\log \eta_o = 3.4 \log MW + A \qquad (MW > M_{cr}) \qquad 5.30$$

where A is an empirical constant dependant on polymer and temperature

$$\log \eta_0 = C_1 (MW)^n + C_2 \qquad (M_{cr} > MW) \qquad 5.31$$

where $n \approx 0.5$, C_1 and C_2 are constants.

Although the transition between the conditions is actually gradual, M_{cr} is usually defined as the intersection between the two extrapolated linear logarithmic functions, varying between 2000 and 60,000, dependent on polymer structure. Some published values for M_{cr} for the model polymers are shown in Table 5.D. Theoretically, M_{cr} has been correlated with molecular dimensions as a function of radius of gyration and specific volume for the polymer chain (Fox, 1964).

(NB. These functions have been derived from polymers with initial molecular weights of above or below M_{cr} rather than degraded over the transition condition).

If Newtonian viscosity at critical molecular weight is denoted by η_{cr}, Eqs 5.30 & 5.31 can be written as:

$$\log \eta_0 = \log \eta_{cr} + 3.4 \log \left(\frac{MW}{M_{cr}} \right) \qquad (MW > M_{cr}) \qquad 5.32a$$

$$\log \eta_0 = \log \eta_{cr} - \log \left(\frac{M_{cr}}{MW} \right) \qquad (MW < M_{cr}) \qquad 5.32b$$

Table 5-D. Published polymer properties for η_o and critical molecular weight

	MW	T (K)	η_o (Ns/m^2)	M_{cr} (g/mol)
PP	3×10^5	493	3×10^3	7000
HDPE	10^5	463	2×10^4	3500
PS	2.5×10^5	493	5×10^3	35000
PMMA	10^5	473	5×10^4	30000

Non-Newtonian flow is more pronounced with higher molecular weight polymers (Cogswell, 1981), probably because the greater the average number of entanglements per chain, the greater the probability of a region of intense chain entanglement which will break down under a lower average stress. This is the main argument used to support chain entanglements not being an important flow control parameter if MW < M_{cr}.

A further argument related to this work, was first proposed by Andrade in 1930, and developed by Eyring (Glasstone, 1941). The 'hole theory of liquids' suggests that a liquid contains unoccupied sites, which move randomly through the liquid as they are filled and emptied by molecules jumping from one site to another. Each jump is achieved by overcoming an energy barrier, E_η. This activation energy is related to the heat of vapourisation of the (low molecular weight) liquid, since molecule removal is part of both processes.

In polymers, however, E_η levels off at a value independent of MW, which is translated as the extent of long chain flow being much smaller than the complete molecule. Viscous flow is thought to be successive jumps of small segments eventually moving the complete chain. E_η has been found to decrease with increasing temperature, probably due to extra free volume created by thermal expansion. This theory was used to develop the relationship (Glasstone, 1941):

$$\eta = B \exp \frac{E_\eta}{RT} \qquad (T >> T_m) \qquad 5.33$$

(B = constant)

More recent work has been published (McLeish, 1999) which concentrates on the time dependency of flow behaviour, suggesting flow has still to be fully explained in

terms of molecular topology, before large scale flow of molten polymers can be understood.

These arguments have been used to develop various viscosity functions, sadly none of which describe the full extent of viscosity – temperature dependency for plastics undergoing molecular weight degradation. However, an approach based on experimental results has been developed, (Van Krevelen & Hoftyzer, 1976) which can be adapted to this problem.

5.4.2 Model Approach for viscosity

A general η-T correlation is found by plotting $\frac{\eta_o(T)}{\eta_0(1.2T_g)}\left[=\frac{\eta_{cr}(T)}{\eta_{cr}(1.2T_g)}\right]$ as a function of T_g/T, as shown in Figure 5-8 for various polymers at zero shear viscosities.

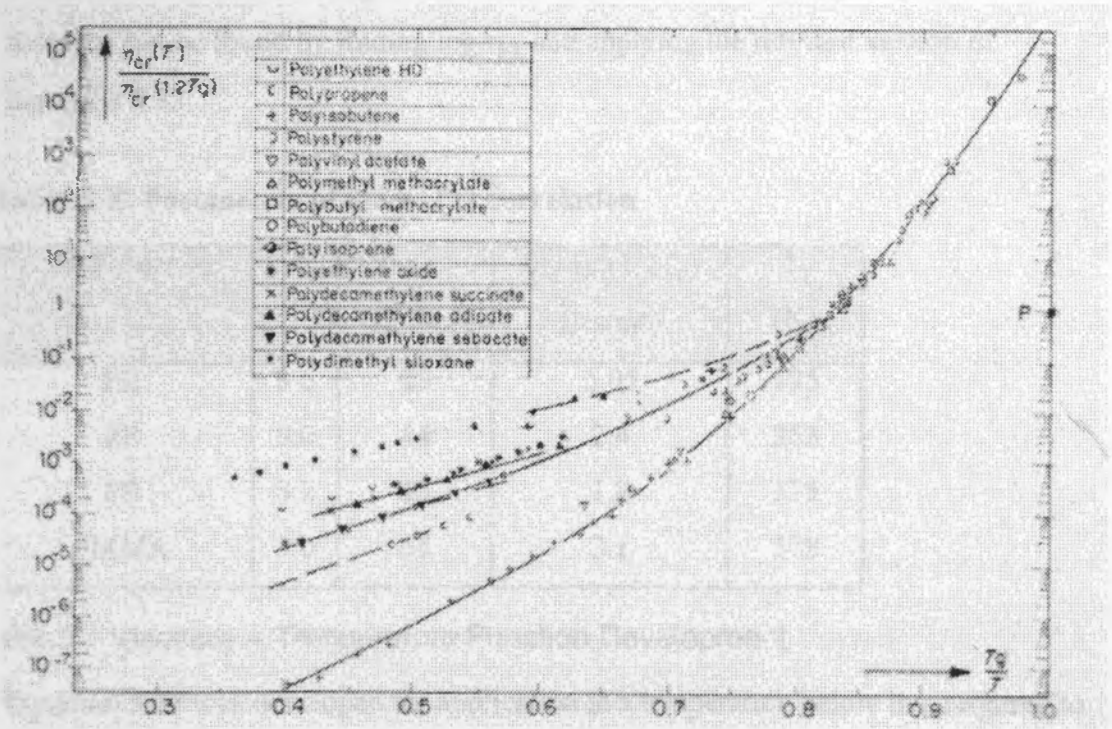

Figure 5-8. Graphical correlation of critical viscosity - temp data (Van Krevelen & Hoftyzer, 1976)

From this plot, for T_g/T values of greater than 1/1.2, all points lie on a straight line. At higher temperatures (lower values of T_g/T), different polymers produce different

curves, which approach linear approximations at high temperatures. If these are extrapolated to the right (lower T), all converge at point 'P' on the plot.

The general formula of these curves is found to be:

$$\log\frac{\eta_0(T)}{\eta_0(1.2T_g)} = \log\frac{\eta_{cr}(T)}{\eta_{cr}(1.2T_g)} = A\left(\frac{T_g}{T} - 1\right) \qquad 5.34$$

which, when compared to Equation 5.33, shows that;

$$E_\eta(\infty) = 2.3ART_g$$

or

$$A = \frac{1}{2.3}\frac{E_\eta(\infty)}{RT_g} \qquad 5.35$$

This permits log η_{cr} at a given temperature to be estimated if E_η and log $\eta_{cr}(1.2T_g)$ are known. The available published data are shown in Table 5-E.

Therefore, if molecular weight is known, the Newtonian viscosity – temperature function can be found by finding log η_{cr} and applying the relevant version of Equation 5.32.

Table 5-E. Parameters of the $\eta_{cr}(T)$ correlation

Polymer	A	$E_\eta(\infty)$ (kJ/mol)	log $\eta_{cr}(1.2T_g)$ (Ns/m^2)	T_g (K)
PE	8.5	25	5.05	195
PP	9.0	44	2.4	253
PS	8.2	65	1.8	373
PMMA	9.0	65	3.1	378

5.4.3 Viscosity – Temperature Function Development

Equation 5.32 was developed for application at a temperature below that required to produce molecular weight degradation in the polymer. Molecular weight has low temperature stability, with the molecular weight degradation temperature providing a natural upper limit for processing temperatures.

Degradation and rate of degradation are temperature dependent, but the temperature ranges are not generally published. Thermogravimetric analysis (TGA), where a

sample is exposed to a constant heating rate with decomposition measured over time, depends largely on the heating rate, therefore a rate and range appropriate to a fire model are not easily obtained.

Degradation rate will also be dependent on decomposition mechanism, which for a polymer capable of melt-flow, must be either end chain (ECS) or random scission (RS). ECS will be a slow degradation rate, since the chains break from the ends only, so there is no increase in the number of chain ends. In comparison, RS, where the chains break at weak points will result in a rapid degradation rate and corresponding increase in the number of chain ends.

Since PMMA is the only polymer in this study exhibiting ECS, it is assumed that molecular weight degradation will be linear and of low rate, and that the reduction from initial MW will not be sufficient to cross the M_{cr} barrier.

In contrast, RCS is represented by a faster reduction rate, crossing the M_{cr} barrier differentiating Equations 5.32a & 5.32b.

When added into a spreadsheet for polypropylene (initial molecular weight = $3x10^5$), the results of degradation rate on the viscosity-temp function shown in Figure 5-9.

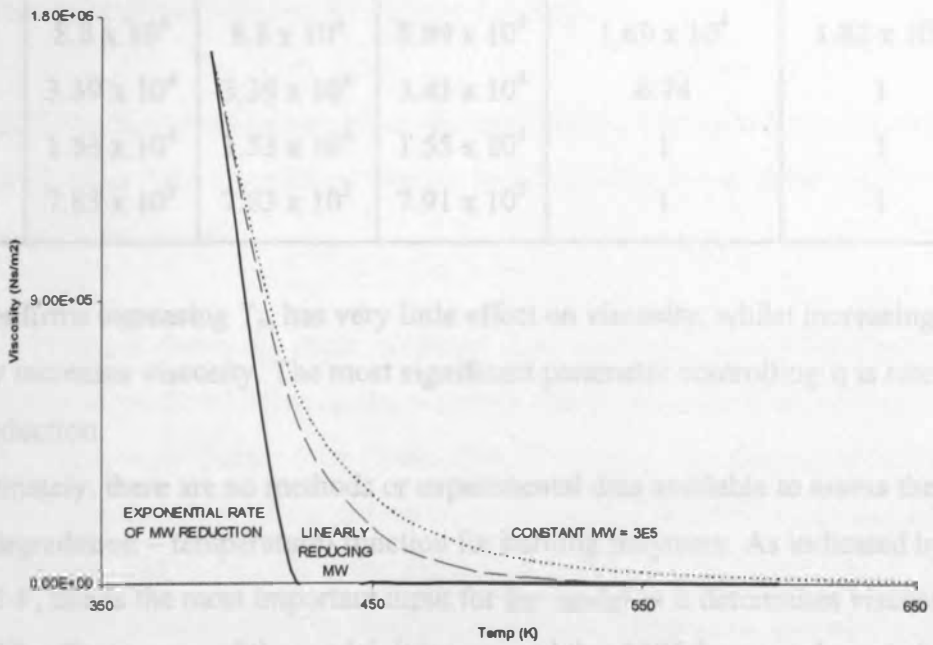

Figure 5-9. Effect of rate of MW Degradation on viscosity

5.4.3.1 Viscosity Model Sensitivity

A brief sensitivity analysis was conducted on the viscosity model to investigate whether MW was the most significant parameter. The predicted viscosities for PP calculated over 6 arbitrarily selected temperatures are tabulated below. The initial degradation temperature selected was the maximum recommended processing temperature for polypropylene (Cogswell, 1981).

Control parameters:

$MW = 3x10^5$; $\rho = 850$ kg/m^3; $T_g = 263K$; $T_m = 450K$; $T_{deg} = 423K$;

$\eta_{cr} = 0.02236$ Ns/m^2

Table 5-F. Viscosity model sensitivity

		viscosity (calculated varying the identified parameter) (Ns/m^2)			
TEMP (K)	Control η (Ns/m^2)	T_m + 20K	T_g + 20K	Linear MW red (MW>M_{cr})	Exp MW red
400	1.21×10^6	1.21×10^6	1.22×10^6	1.21×10^6	1.21×10^6
450	2.82×10^5	2.82×10^5	2.85×10^5	1.77×10^5	2.72×10^3
500	8.8×10^4	8.8×10^4	8.89×10^4	1.69×10^4	1.82×10^1
550	3.39×10^4	3.39×10^4	3.43×10^4	6.74	1
600	1.53×10^4	1.53×10^4	1.55×10^4	1	1
650	7.83×10^3	7.83×10^3	7.91×10^3	1	1

This confirms increasing T_m has very little effect on viscosity, whilst increasing T_g slightly increases viscosity. The most significant parameter controlling η is rate of MW reduction.

Unfortunately, there are no methods or experimental data available to assess the (MW degradation – temperature) function for burning polymers. As indicated by Table 5-F, this is the most important input for the model as it determines viscosity. To enable effective use of the model, it is assumed that MW does not degrade before attaining the maximum processing temperature, and degrades to a minimum value over the range ($T_{deg} < T < T_{vap}$). The minimum values are assumed to be 1 for RCS and M_{crit} for ECS. This produces the model functions shown in Figure 5-10.

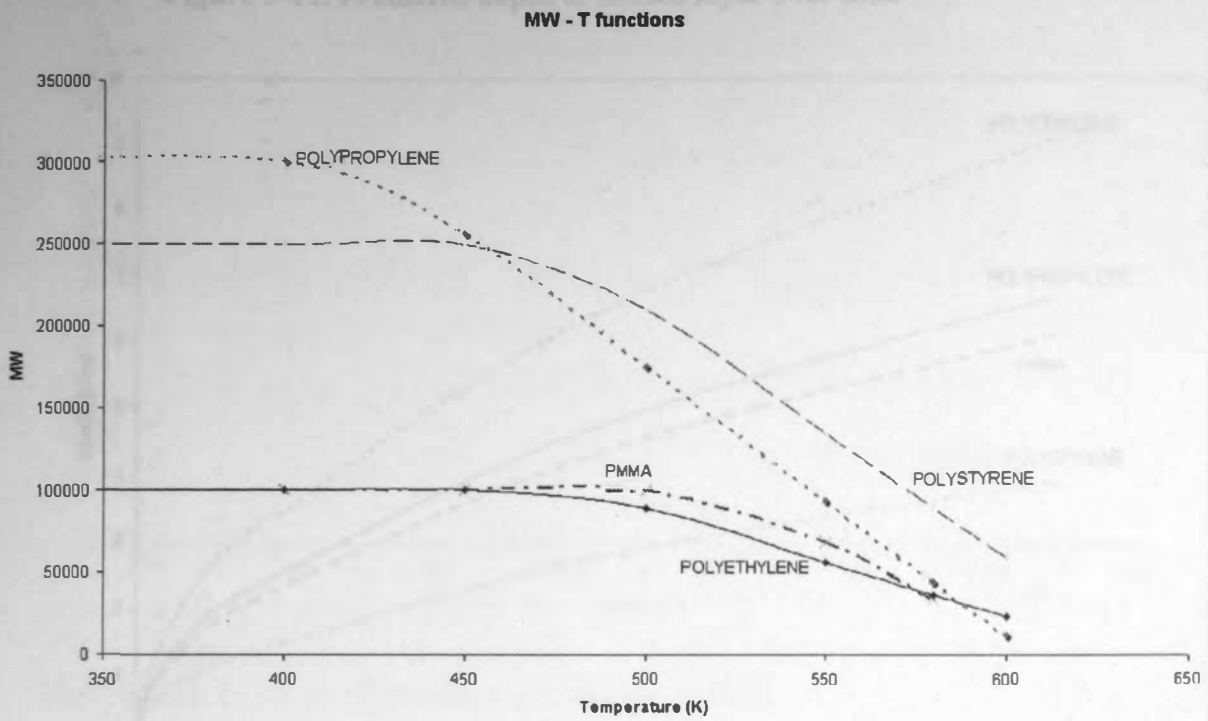

Figure 5-10. MW - Temperature functions used in the flow model

Inspection of Figure 5-10 predictably shows that the extent of MW degradation is dependant upon initial MW and the range (T_{vap}-T_{deg}).

The model was then constructed as two distinct sections (depth of heated layer and mass flow) using VBA spreadsheet macros in MS EXCEL 97, with the results shown over the following pages.

Figure 5-11 which shows the depth of heated layer over time, shows that there is little difference predicted between the polymers modelled, none of which will produce a liquid layer deeper than 10mm after 20 minutes. The ranking order reflects the thermal conductivities of the polymers, as shown in Table 5-C. Since one of the base assumptions of this model is that the heated (i.e. liquid) layer remains stationary, these results cannot be used to predict flow behaviours, and so the next section of the model is required.

Figure 5-11. Predicted depth of heated layer over time

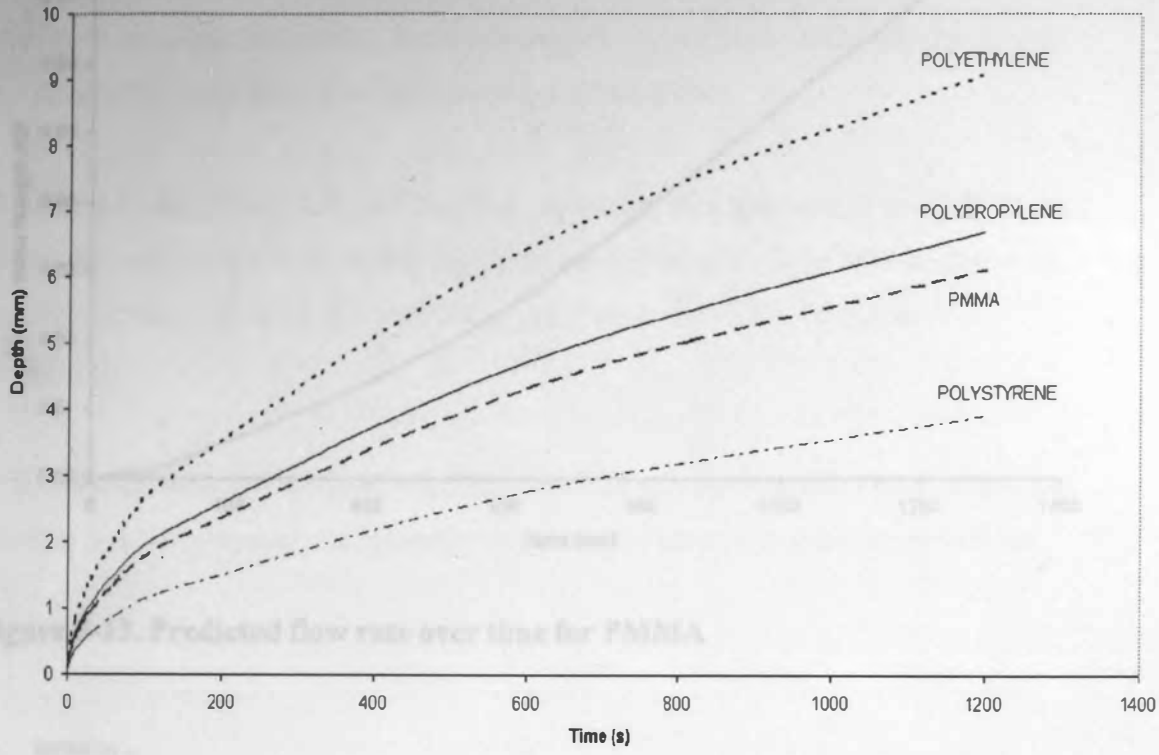

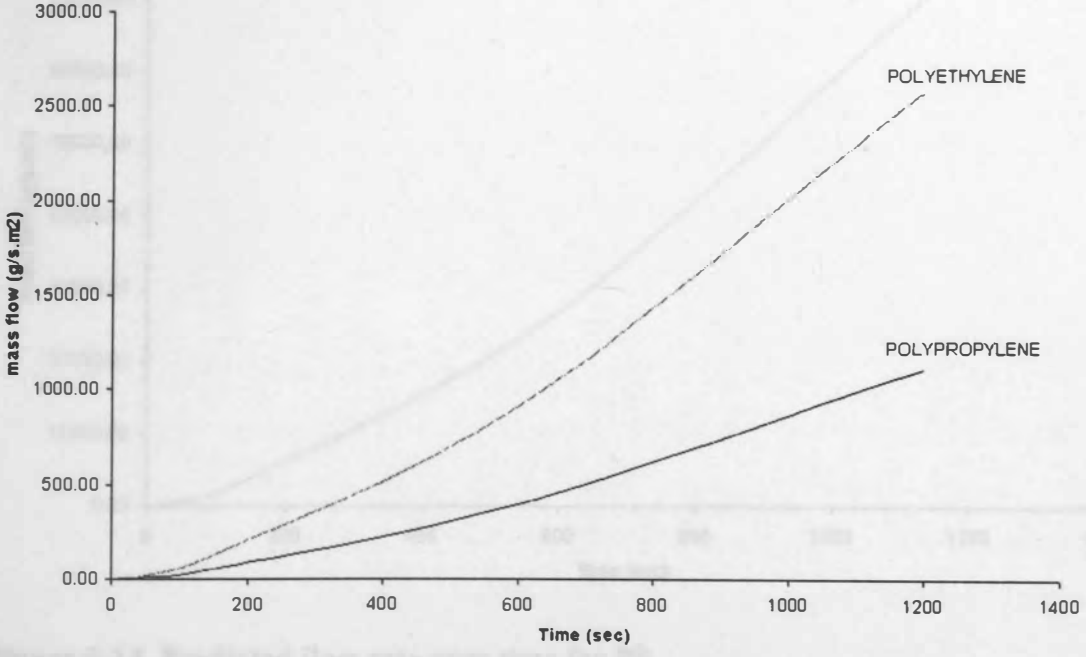

Figure 5-12. Predicted mass flow rate over time for PE and PP

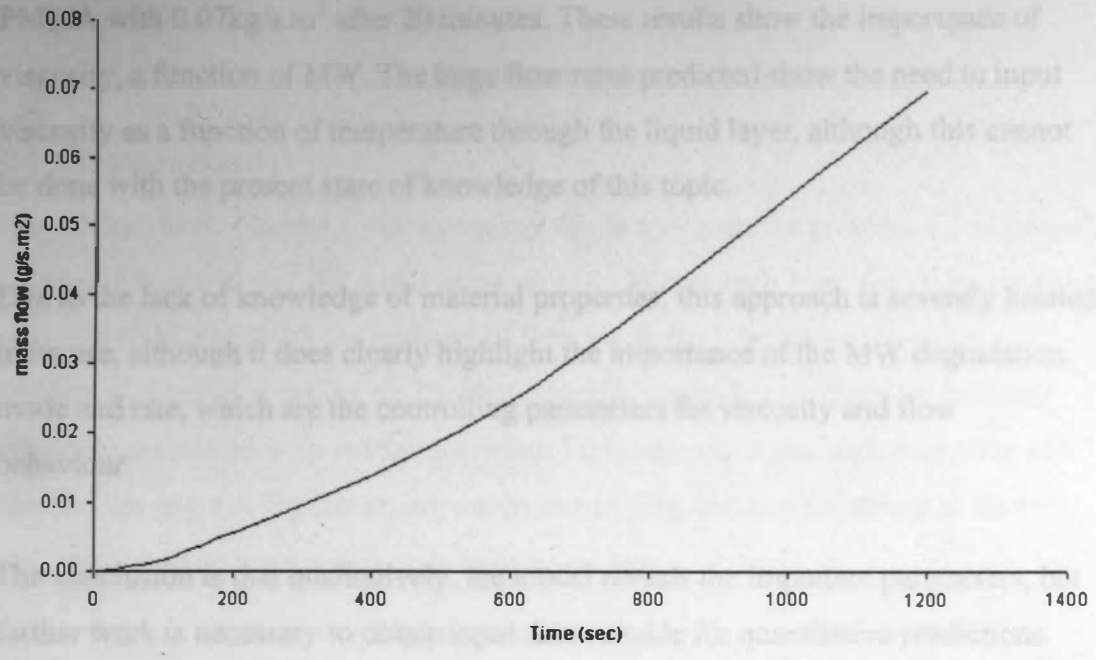

Figure 5-13. Predicted flow rate over time for PMMA

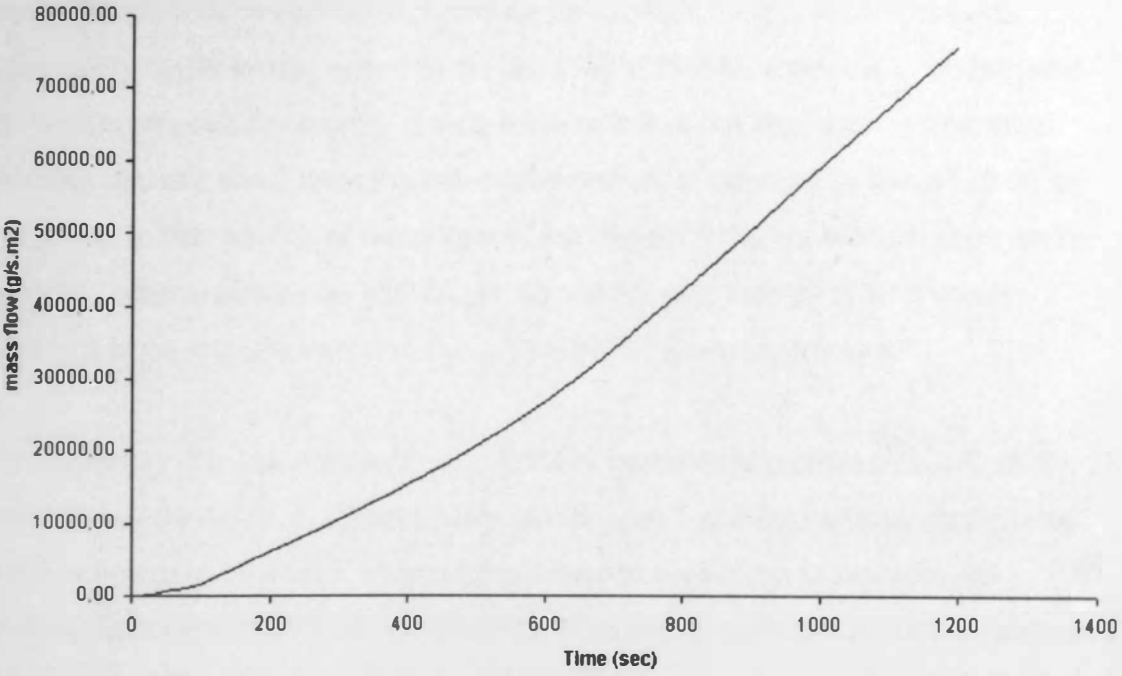

Figure 5-14. Predicted flow rate over time for PS

Comparison of Figure 5-12 to 5-14 shows a huge variation in predicted flow rates between PS, with 80kg/s.m^2, PP and PE which are similar at 1 and 2.5kg/s.m^2 and

PMMA with 0.07kg/s.m^2 after 20 minutes. These results show the importance of viscosity, a function of MW. The huge flow rates predicted show the need to input viscosity as a function of temperature through the liquid layer, although this cannot be done with the present state of knowledge of this topic.

Due to the lack of knowledge of material properties, this approach is severely limited in its use, although it does clearly highlight the importance of the MW degradation mode and rate, which are the controlling parameters for viscosity and flow behaviour.

The conclusion is that qualitatively, the model reveals the important parameters, but further work is necessary to obtain input data suitable for quantitative predictions.

6 Discussion

6.1 Introduction

It is evident from Chapter 1 that unwanted fire is an expensive problem for society, causing 679 deaths in 1998 and costing up to £1 billion each year. According to the statistics (HMSO, 1999) the majority of fires involving life loss occur within residential dwellings, whilst the greatest financial losses from individual fires are generally associated with storage facilities. To reduce the costs, both economic and human, fire engineering has an important role to play, but in comparison to other engineering disciplines is still in its relative infancy.

The focus of fire engineering research on material behaviour has been traditionally involved with construction materials. However because a particular polymer (PMMA) had repeatable, reproducible behaviour which could be exposed to the same test methods as traditional materials, for example timber, the fire research community began testing with it in the late 1960's. PMMA continues to be favoured by the fire research community mainly because it does not drip, melt or flow when burning, and as a result there is a substantial amount of information published on its behaviour in fire. Models of flame spread, burning mechanisms, thermal degradation rates and other attributes for PMMA are commonly encountered in the literature, indeed it is the material specified for calibrating the Cone Calorimeter.

Unfortunately, PMMA represents only 0.8% of commercial plastics (Dufton, 1998), used mainly for lighting diffusers, bullet proof "glass" and fire research applications. Since it unzips to monomer, remaining geometrically stable as is degrades, its burning behaviour is different to that of the most common plastics so extrapolation to the fire behaviour for other plastics cannot be made. According to Chapter 1, Tables 1-A and 1-B, over 75% of commercial plastics will undergo melt-flow behaviour in a fire, making this a significant problem overlooked to date by the fire research community. The problems associated with plastic fires are frequently documented in incident reports, and cover issues ranging from blocked drains to burning rivers of molten material advancing over everything in their path.

6.1.1 Current approach to deal with the hazard posed by melting plastic

To anticipate the problems and reduce the level of potential fire hazard to a level accepted by society, several agencies are involved. Of these, the HSC is focused on life safety, whilst the insurance industry is concerned with protection of property (both premises and stock). Input from both, along with other parties including industry, the trade unions, the Fire Brigade and society at large, is used to define acceptable workplace conditions. The acceptable level is then monitored by ensuring compliance with legislation such as the Fire Precautions Act (HMSO, 1993) and the Management of Health & Safety at Work Regulations (HMSO, 1992).

The traditional approach of the US insurance industry toward fire protection is to classify stored products according to potential hazard as Class I, II, III or IV as tabulated overleaf (NFPA, 1990). The fire hazard posed by Group I commodities is then less than that posed by Group II and so on. Plastics are then further divided from Group IV into Groups A, B and C also according to hazard potential, as shown in Table 6-B. These classifications along with factors such as storage height and quantity are then used to specify the level of fire protection required, for example sprinkler density and distance between storage and sprinklers.

NB the NFPA classification system makes no distinction between melting plastics such as PP and PE, and non-melting PMMA.

These groupings show that plastics generally are considered to represent a high fire hazard in the US. This reflects work (Heskestad, 1982) which found the fire development rates of most fires approximate parabolic growth after an incubation period (i.e. the 't^2' fire). This is the basis of the equation;

$$\dot{Q} = \alpha_f (t - t_0)^2 \qquad 6.1$$

Where: α_f = fire growth coefficient (kW/s^2)

t_0 = length of the incubation period (s)

(α_f varies from ~10^{-3} kW/s^2 for very slow developing fires to ~1 kW/s^2 for very fast fire growth)

Table 6-A. NFPA Classification of Storage Products

Class	Typical Products
I	Non-combustible food stuff Glass products Metal products Gypsum board Bags of cement
II	Incandescent/fluorescent lightbulbs Cartons or reels of thinly coated fine wire Class I products in slatted wooden crates
III	Wood Products Paper Products Natural fibre cloth Leather Products
IV	Class I, II or III products with an appreciable amount of Group A plastics Group B plastics Free flowing* Group A plastics metal products in foamed plastic cocoons in a corrugated carton synthetic thread & yarn vinyl floor tiles

** free flowing refers to plastics which will fall out of their container and create a smothering effect on a fire such as random packed small objects, rather than exhibit melt flow behaviour*

Table 6-B. NFPA Classification of plastics

Group	Typical Plastics
A	ABS
	PMMA
	Acetal
	(Expanded) natural rubber
	PET
	PBT
	Polycarbonate
	PE
	PP
	PS
	Polyurethane
	PVC
	SAN
B	Chloroprene rubber
	Fluoroplastics
	Natural rubber (not expanded)
	Nylon
	Silicone rubber
C	PTFE
	Melamine
	Phenolic
	UPVC
	PVDC

The incubation period (t_0 in Equation 6.1) is a function of several factors including the size and location of the ignition source, and location and material properties of the first item ignited. Examples of different growth rate fires are shown in Table 6-C.

Table 6-C. Parameters used for 't^2' fires (Drysdale, 1999)

Description	Typical Scenario	α_f (kW/s^2)
SLOW	Densely packed paper products	0.003
MEDIUM	Traditional armchair	0.012
FAST	PE pallets stacked 1m high	0.047
ULTRAFAST	High rack storage	0.188
	PE rigid foam stacked 5m high	

The UK situation is different, in that according to the Fire Protection Association (private communication, Lewis, 2001) there are no British Standards related specifically to storage of thermoplastics, and no specified insurers requirements. Thermoplastics are considered as hazardous materials when applying the BS sprinkler requirements (BS 5306, BSI), but other than that are not targeted for special consideration.

It should be emphasised that (as shown in Chapter 3) the level of fire hazard for melting plastics varies over the plastic life cycle. This is indicated by the annual statistics, but they are not detailed enough to further analyse. The level of fire hazard is a product of many factors including quantity and geometry of plastic, availability of ignition sources and probability of detection and extinction at an early stage. An illustration of various levels of fire hazard posed by a common commodity (beer crates) are shown in Figures 6-1 and 6-2.

Although the individual crates are the same, changes in quantity, environment and security of the location are combined to increase the overall fire hazard from the pub cellar to the warehouse. Fire hazard is then combined with frequency of occurrence to produce the overall fire risk rating.

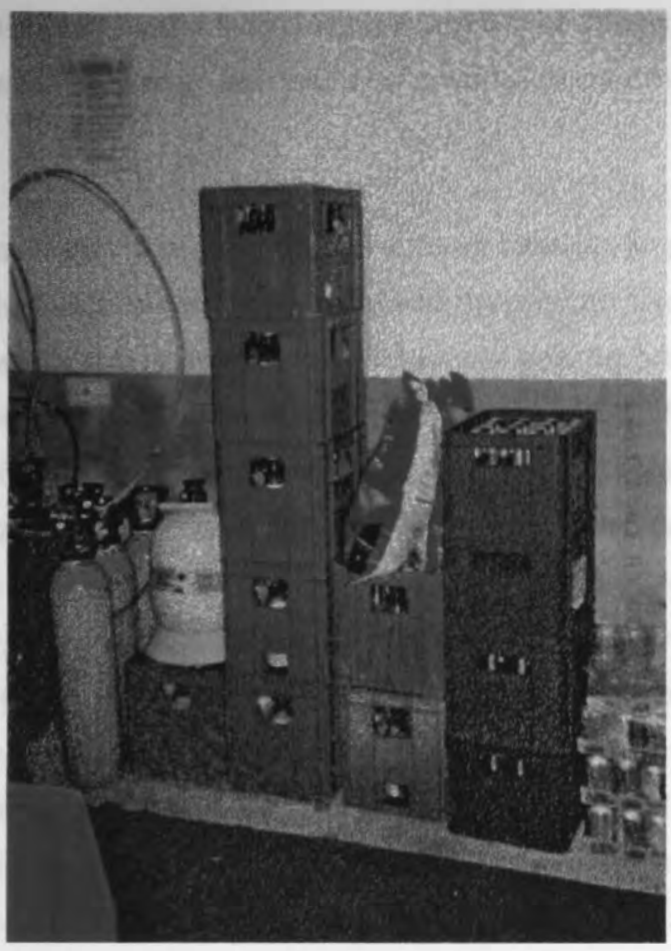

Figure 6-1. Beer crates, as found in a typical small pub cellar

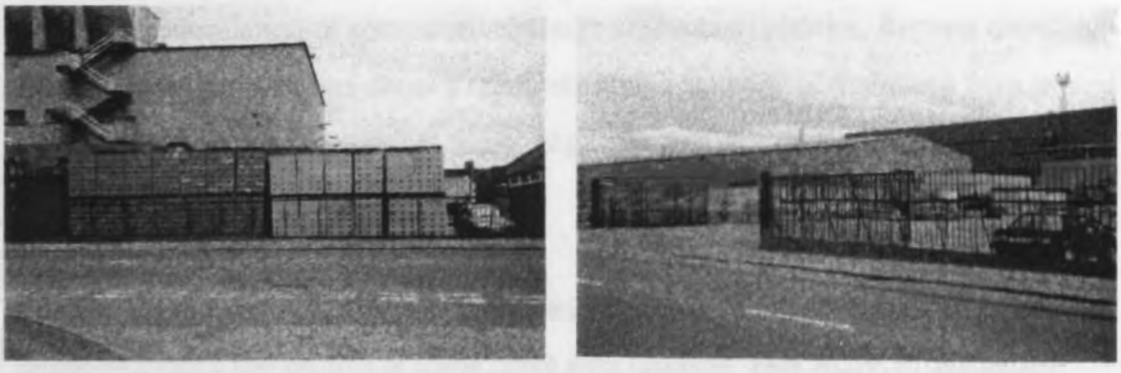

Figure 6-2. Front & side views of red, yellow and blue beer crates stacked against a warehouse in Edinburgh

Polymer production (normally in the form of granules) is considered a high risk as large volumes of chemicals are undergoing reaction processes, although mandatory

COMAH compliance (HMSO, 1999) requires this risk to be stringently controlled so that the frequency of occurrence and severity of potential consequences are minimised.

The polymer granules are then transported to different locations for processing, where any required additives are incorporated with the polymer. There are reduced quantities at these locations compared to the location of polymer production. However, manufacture of the end product requires plastic to be worked at elevated temperature and pressure. In this process, the frequency of fire occurrences is relatively high, as the increased polymer temperature reduces the time to ignition, but high staffing levels generally provide the capability to detect and deal with the fires at an early stage, so the number which grow to become serious[iii] fires is relatively small. With the plastic products, as the plastics enter the warehousing system the quantities increase and staffing levels reduce presenting a significantly increased risk. Finally, plastics are sent into the warehouses of retail chains where fire safety becomes the joint concern of local authority and fire brigade, eventually entering shops, to be purchased by their end user. End use tends to involve much smaller quantities than elsewhere in the chain, and if the end use is domestic, then the workplace based health and safety legislation does not apply.
At the end of the product lifespan, the plastic may then enter a recycling chain, again with the accumulation of comparatively large amounts of plastics. Reports detailing fires in recycling premises show a relatively high frequency of malicious fires in poorly secured outdoor premises, involving large amounts of stock with no firebreaks.

Clearly large quantities of plastic increase the level of fire hazard, and are capable of producing rapid fire growth at some point after ignition. This study, in agreement with other research (Zhang, 1997) has found the 'ignition to growth' phase (i.e. t_o in Equation 6.1) for melting plastics to be very long in comparison to non-melting

[iii] "Serious fires" are defined by Fire Prevention magazine as fires involving fatalities or losses of £50,000+

plastics (primarily PMMA). This is due to different mechanisms of vertical flame spread.

The flame spread mechanism over vertical PMMA is similar to that over a vertical wooden surface, neglecting charring. (The char behaviour of wood requires an additional heat flux to be imposed on the surface to sustain flaming). The growth rate is exponential as the flame preheats the zone above the burning area, raising the temperature and reducing the time required to produce volatiles from that area. A vertical flame spread model representing this process is illustrated in Figure 6-3 (Grant & Drysdale, 1995).

Figure 6-3. Upward flame spread model (with burnout) (Grant & Drysdale, 1995)

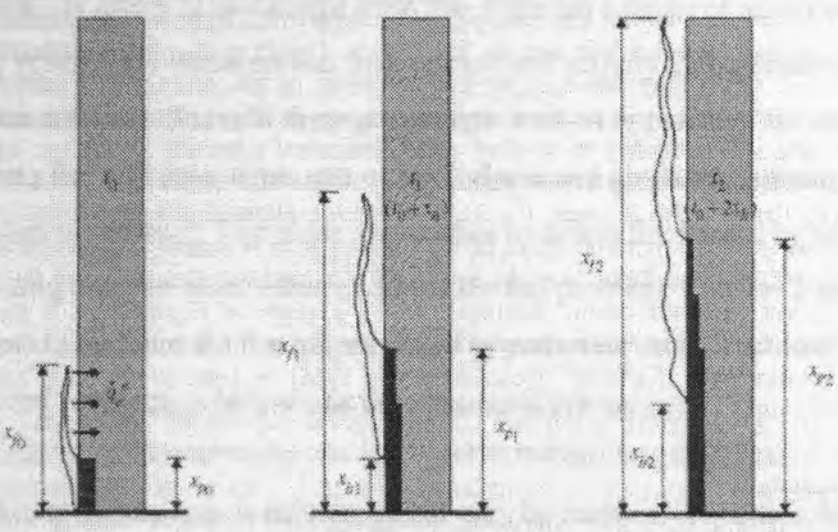

(t_0, t_1, t_2 = timesteps; x_f = flame height; x_p = pyrolysis height; x_b = burnout height)

In contrast, the preheating effect for a melting plastic creates downward flow into the burning area, maintaining a slow flame growth rate until a burning pool is eventually formed by the melt.

NB This implies that high rates of burning at the vertical surface cannot be achieved for melting plastics as the material flows away (downwards) at $T < T_{steady\ burning}$.

Due largely to asymmetric air entrainment deflecting flame from the pool fire against the wall, the pool fire will then dominate vertical fire growth. In this mode, melting

is the main cause of fuel depletion from the original plastic structure. The tests in the 'Sedan' rig, and also the 'Kebab' tests have shown that only 20 – 25% of plastic is lost from the vertical surfaces to burning, the remaining 75 - 80% entering a pool at the base of the material.

Since the mechanisms are completely different, and the flame spread models found in the literature (Grant & Drysdale, 1995; Gamal, 1994) e.g. as shown in Figure 6-3, are based on results from PMMA or wood products, current models for predicting upward flame spread (and hence fire growth rates) cannot be applied to melting plastics.

6.1.2 Difficulties with assessing the fire hazard of melting plastic

The actual term 'fire hazard' represents a complex problem. Defined (BSI, 1997) as the potential for injury to or damage from fire, there are a range of issues covered including ignitability, flame spread, heat release and toxicity and corrosivity of combustion products. Some of these parameters work in opposition, for example a smouldering fire will have a low rate of heat release and no flame, but may produce a large amount of 'smoke'. Therefore, approaches to define fire hazard by use of a single ranking order or index cannot address the full problem. Chapter 2 investigated the attempts to measure the fire hazard posed by materials using 'standard' tests, and found several problems which are further discussed below.

Fire behaviour of materials is influenced not only by material properties, but also by environmental[iv] parameters. Unfortunately, the two areas are difficult to separate experimentally and every test investigated suffers some degree of apparatus dependency. The influence of both environmental and material factors are fundamental to the fire development process: for example the influence of enclosure on the burning rate of PMMA is illustrated in Figure 6-4.

[iv] "environmental parameters" refer to the immediate surroundings of the burning item, including geometry, thermal properties of adjacent surfaces, ventilation sources, size and location of ignition source, proximity of compartment boundaries etc.

This makes the results test, and in many cases, laboratory specific. The problem was clearly demonstrated (Emmons, 1973), with an investigation of six European standard tests which give only ranking orders, producing Figure 2-2. This showed that the hazard ranking given by tests designed to assess the fire hazard of wall lining materials varied significantly as described in Section 2.3.1.

Figure 6-4. The effect of enclosure on the rate of burning of a 0.76m x 0.76m PMMA slab (Friedman, 1975)

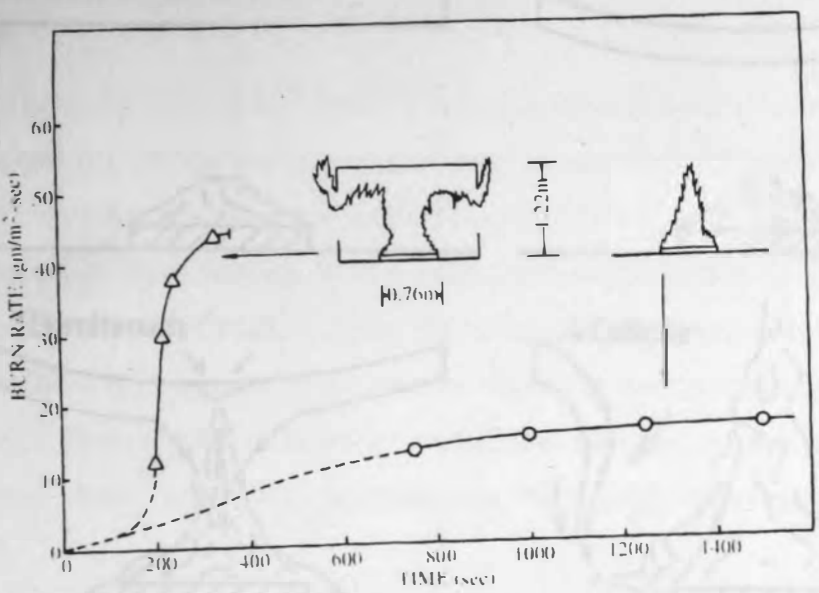

For the case of melting plastics the problems of hazard assessment are even greater. As discussed in Section 2.4, no test was found which is capable of accounting for the effect of a burning melt on fire hazard, which has been shown to be (see Chapter 1 and Chapter 4) a controlling parameter for fire growth. Observational work (Hinkley, 1966; Hirschler, 1997) confirms that horizontal flame spread and fire growth mechanisms for melting plastic differ from those for geometrically stable materials. A stable material, such as wood, exposed to a (mainly convective) flame heat flux from below, will deflect flame across the lower face, resulting in edge burning of the wood, which will begin to spread across the upper surface from the sides. This mechanism was described in Hirschler's stacked wooden chair tests. Eventually, the material may burn through, but initially edge burning will be the main fire growth mechanism. In contrast, melting plastic will behave in a manner similar to that

illustrated in Figure 6-5. (Development into the third and fourth stages illustrated depend upon the plastic staying in position in stage two). The only exception found by Hirschler was for PP incorporated in an asbestos matrix, where the PP melted away, but the matrix stayed in place deflecting flame toward the edges.

Figure 6-5. Burning behaviour of a melting plastic exposed to heating from beneath the sheet.

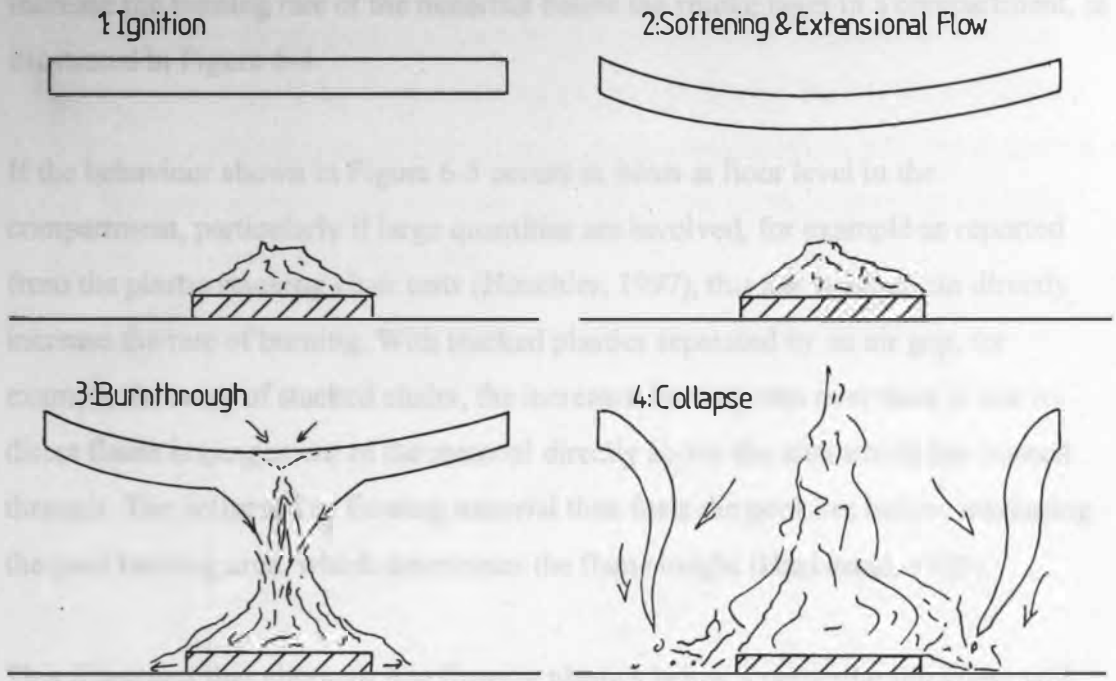

These stages may act to reduce the overall fire growth rate, as outlined in Section 2.3.6 (Abbott, 1984), where EPS panels retracted and fell away from the roof. This behaviour can be used beneficially as a fire venting mechanism, and was tested for this purpose by FRS (Hinkley, 1966). Experiments with rigid PVC rooflights in single storey buildings showed that they fell out of their mounts when heated to ~200°C, although the effectiveness of this venting requires a larger potential venting area than for a mechanical ventilation system.

Predictably the effect of the behaviour illustrated in Figure 6-5 depends partly on the polymer involved. It was reported in some of the incident reports detailed in Chapter 1, (specifically the BASF warehouse fire) that PMMA skylights fell from their mountings in flaming mode, providing additional areas of ignition away from the

original fire. (PMMA softens at ~160°C, and undergoes (piloted) ignition at ~ 310°C).

If the plastics used in roof construction provide a means of heat venting, then the volume and temperature of hot gas available to re-radiate heat downward are reduced. The re-radiation from the upper zone of the compartment would otherwise increase the burning rate of the materials below the smoke layer in a compartment, as illustrated in Figure 6-4.

If the behaviour shown in Figure 6-5 occurs in items at floor level in the compartment, particularly if large quantities are involved, for example as reported from the plastic stacking chair tests (Hirschler, 1997), this mechanism can directly increase the rate of burning. With stacked plastics separated by an air gap, for example the seats of stacked chairs, the increased burning rate over time is due to direct flame impingement of the material directly above the area which has burned through. The collapsed or flowing material then fuels the pool fire below, increasing the pool burning area, which determines the flame height (Heskestad, 1983).

This illustrates that although free flowing plastics below a particular thickness will undergo this behaviour, its effect on fire growth is largely dependent on quantity of plastic and the nature of the surrounding environment.

The first three chapters showed that melt flow is an important problem, which although recognised, has not been studied quantitatively. Table 1-B demonstrated the most common plastics are based on PE, PP, PVC and PS. PVC chars instead of melting when heated, and since time and resources limited the amount and extent of work possible in this study, the work is focused mainly on PE, PP and PS. Figure 1-2 showed that the most common usage of plastics is in packaging, and so the experiments have looked mainly at the fire behaviour of packaging, using mainly polypropylene beer, bread and milk crates. However, an important area for further examination is how the fire behaviour of packaging changes when fully laden, compared to for example, empty crates. Due to the lack of previous work on material

fire behaviour, environmental factors have been largely neglected, although the effect of flooring material on pool fire development was discussed in Chapter 4.

6.1.3 General factors affecting fire development

Following ignition of any combustible material, there are three possible courses of fire development (Drysdale, 1999):

1. the fire will burn out without spreading
2. if ventilation is restricted, the fire may self extinguish or continue to burn at a slower rate dictated by the availability of air (which may lead to 'backdraught');
3. if there is sufficient fuel and ventilation, the fire may continue to grow to a stage of full room involvement, whereby all combustible surfaces are burning. This course is illustrated in Figure 6-6.

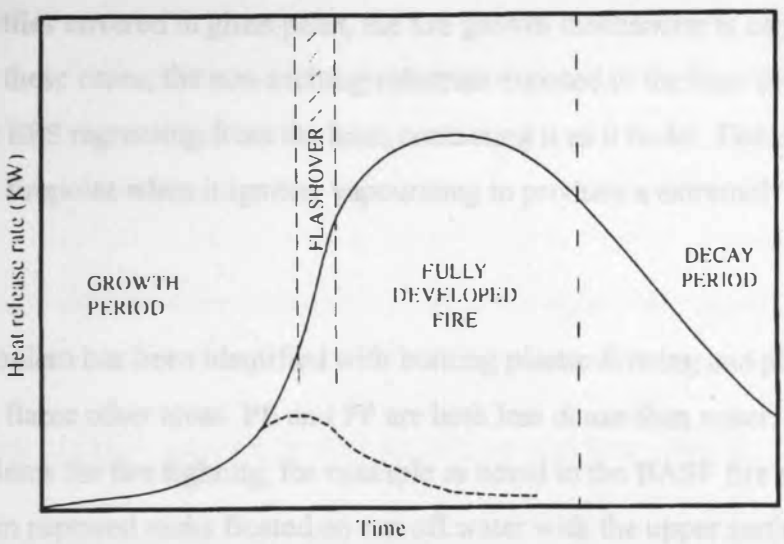

Figure 6-6. Course of a well ventilated compartment fire, expressed as the rate of heat release over time. The broken line shows the effect of fuel depletion prior to flashover (Drysdale, 1999)

The melt flow process can influence the first and third courses described above. For example, if a material melts and flows away from a heat source, the level of radiant heat flux received on a surface reduces rapidly as the surface moves away from the source. Therefore the surface radiant flux can reduce to a level below that required to produce surface volatiles in a short distance. This happens for example with some expanded thermoplastic foams, such as 'flo pak' polystyrene granules or loose

packed polyester wadding ($\rho \approx 10$ kg/m^3) (HSL, 1992). The material melts and rapidly regresses on heating, and sustained flaming conditions are difficult to achieve without the use of an accelerant.

NB the same material in a vacuum packed form ($\rho \approx 85$ kg/m^3) (HSL, 1992), will expand when the containment packaging fails, forcing more material into contact with the ignition source. This produces a rapidly developing fire, with a pool fire formed at the base of the material. The rate of increase in pool size is then determined partly by the degree of confinement, with ignition between two bales producing a much more rapidly developing fire.

Alternatively, if foam is bonded to a non melting substrate, such as EPS panels bonded to aluminium foil in order to gain a BS 476 Part 7 rating (Abbott, 1984) or EPS ceiling tiles covered in gloss paint, the fire growth mechanism is completely different. In these cases, the non-melting substrate exposed to the heat source prevents the EPS regressing from the heat, containing it as it melts. The liquid is then heated to its firepoint when it ignites, vapourising to produce a extremely fast growth fire.

A further problem has been identified with burning plastic flowing and physically transporting flame other areas. PE and PP are both less dense than water, and this has caused problems for fire fighting, for example as noted in the BASF fire where granules from ruptured sacks floated on run off water with the upper surface of the granule flaming. In this case, the separation distance required to consider the plastic as 'isolated' in terms of fire spread risk is increased compared to a geometrically stable material. .

The rate of burning, as described in Section 4.1.8, is found from:

$$\dot{m}'' = \frac{\dot{Q}''_F + \dot{Q}''_E - \dot{Q}''_L}{L_v} \qquad 6.2$$

Therefore, if the upper layer of smoke and hot gas in a compartment radiates back onto the fuel surface, increasing Q''_E, the burning rate will increase. (The increased compartment burning rate shown in Figure 6-4 is in this case about three times

greater than burning in the open. This is ultimately self limiting as fuel vapours rising from the surface attenuate the amount of radiation reaching the fuel surface).

The other major non-material influence on fire development is the amount of ventilation available. If a fire is well ventilated, then the rate of heat release is a function of burning surface area and heat of combustion of the fuel. The burning process is usually over ventilated, with between four and ten times the stoichiometric requirement of air available and the fire is 'fuel controlled'. This excess air acts to cool the flames; for a fire burning in the open, the temperature on the centreline may be as low as 800°C (M^{c}Caffrey, 1979).

If the amount of ventilation is reduced, the burning rate becomes a function of the size of ventilation opening (Kawagoe, 1958), with heat release rate dependent on rate of airflow into the compartment. The amount of excess 'diluent' air available is reduced, and the higher temperatures can be reached (e.g. 1100°C), with the fire being 'ventilation controlled'.

To focus specifically on material behaviour, all of the experiments carried out for this study were conducted under well ventilated, non-compartmentalised conditions.

6.2 Melting plastic behaviour and its effects on fire growth

6.2.1 Factors determining melt tendency

6.2.1.1 Basic Polymer Chemistry

Most polymers can be described in terms of their repeating unit: $(CWX\text{-}CYZ)_n$, where C is carbon, W, X, Y and Z are substituent groups, and n is the number of repeating monomers. The composition of the base polymers in this study is shown in Table 1-C, Chapter 1. From this, some general behaviour patterns are evident (Hirschler, 1992). End chain scission (ECS) is the decomposition mechanism if W and X are hydrogen, but not Y or Z. In this case breakdown can be dominated by elimination of a repeat unit, resulting in a large amount of monomer yield. This degradation mechanism results in a slowly decreasing MW. Random chain scission

(RCS) is exhibited by polymers where W, X, Y or Z are H atoms or hydrocarbon groups, and breakdown occurs at the weakest link, producing a wide range of MW compounds. Monomer yield for random scission is usually low, and MW falls rapidly during degradation.

If W, X, Y or Z is a halogen, this can result in chain stripping, which eliminates the halogen combined with a hydrogen atom. For PVC, this will produce hydrogen chloride, a flame inhibitor. Similar behaviour is found if W,X,Y,or Z is a hydroxyl or acetate group.

The capability to generate a melt-influenced fire is therefore shown by either RCS or ECS combined with a low initial MW.

These generalities apply to pure polymers, but in this study commercial plastics have been used. These often contain additives, the amounts and types of which are unknown, protected by commercial sensitivity. Additives can change the thermal decomposition mechanisms and "flammability" of the polymer, obviously this is the intention of flame retardants. It was confirmed that there were no flame retardants added to any of the thermoplastics tested, but the Cone Calorimeter database results presented in Appendix A clearly show that variations in molecular weight or non fire-retardant additives for the same base polymer can significantly effect the burning behaviour.

The only generalisations for the effects of additives refer to effects on viscosity as shown in Figure 3-16 (Cogswell, 1981). It must be emphasised however, that even inert non-combustible fillers will influence plastic flow and fire behaviour, as their physical presence reduces the amount of flammable polymer in the material, and may obstruct or resist flow. More specifically, the reduction of flammable polymer when combined with mineral fillers implies that the overall fire load (MJ/kg) of the plastic is less than the base polymer. It was also shown in Hirschler's chair tests that if the filler is a non-combustible matrix, then the flame spread mechanism may no longer

be that of the base polymer shown in Figure 6-5, but instead undertakes the edge burning route described above.

Formulation Differences

The Cone Calorimeter database was inspected for differences in behaviour due to molecular composition. The three main groupings are oxygen containing polymers (PMMA, PETG, PC), basic hydrocarbons (PE, PP & PS) and a halogenated polymer (UPVC). Inspection of Figures 4-14 to 4-17 illustrates that basic hydrocarbon polymers show higher peak heat release rates, and shorter ignition times over the fluxes tested (i.e. 20 - 60 kW/m^2) than oxygenated polymers, with the chlorinated polymer showing the lowest heat release and longest ignition times.
The RHR ranking is predictable, since the EHC values are higher for hydrocarbon plastics than for the other groups. The shorter ignition times are not expected, since the surface ignition temperatures are lower for PMMA (as recorded in Table 5-A) than for PP or PE. The shorter times are not related to the amount of heat required to produce volatiles. This, as shown by Equations 4.9a and 4.9b, is less for a non melting material than a melting plastic, (e.g. 1.62 kJ/g for PMMA, compared to 2.03 kJ/g (PP) and 2.32 kJ/g for PE (Tewarson, 1976)). The shorter ignition times may be related to variation in surface radiation absorptivity between the materials.

Molecular Weight Influences

Comparison of the high and low MW PMMA results show that increased molecular weight, which is associated with a higher melt viscosity, lowers peak RHR and also the MLR. Therefore, a lower molecular weight polymer burns faster and, for the low molecular weight PMMA samples shown in Section 4.1.11, has a higher rate of heat release of a shorter duration.

With PMMA, which decomposes by ECS, this is likely to be due to the availability of more ECS sites for the low MW material which will undergo faster kinetic degradation reactions. Possibly opposing this effect, is the formation of a liquid phase below a 'critical' molecular weight, due to the coupling with viscosity (private communication, Robinson, 1999), which is proportional to MW (i.e. $\eta \propto MW^{3.4}$).

This requires a significant heat input to compensate for the increased heat capacity during the phase change, reducing the amount of energy available for thermal degradation, and probably slowing the reactions.
Due to the comparatively slow rate of ECS, the reduction in molecular weight is more gradual and high molecular weight samples tend not to degrade to the critical molecular weight required to produce a melt.

The melt temperature is lower than the degradation temperature, and the time interval between the two temperature-dependant phases is a function of applied flux. Therefore, difference in burning rate between the different molecular weight samples is predicted to be greater at higher levels of applied flux, where the rate of production of flammable vapours will be greater.

For relevance to other materials, particularly those degrading via RCS, a reduction in molecular weight is faster than that from ECS. This results in more rapidly decreasing chain lengths and a greater probability of liquid phase formation. In contrast, a char formation would increase molecular weight, eliminating any possibility of a liquid phase. Therefore, for polycarbonates, a liquid phase could be formed under low applied fluxes, prior to initiation of the char forming reactions. At low heating rates, some RCS may cause a rapid decrease of molecular weight. However, in the Cone Calorimeter, where typical applied fluxes are 20 – 75 kW/m^2 the decomposition will lead to cross linking, leading to char formation and a liquid phase is unlikely. However, some melt-flow behaviour was observed prior to char formation with Cyrex 200, which is a PC/PMMA blend. The PMMA, which has been added to lubricate the PC seemed to burn off at an early phase in the test, and may have been partly responsible for the melt behaviour observed.

The Cone results imply that PE, PP and PS have lower ignition resistance than the other plastics tested, and show a higher RHR. (In the cone tests, the melt effect is masked as the melt in a horizontal test is largely contained within the aluminium foil 'tray' in which it is wrapped).

6.2.2 Parameters affecting melt behaviour

Part of this project has concentrated on identifying the most significant parameters effecting fire behaviour, specifically the tendency of some plastics to form pool fires. It has been found that flow behaviour of burning plastic is complex, comprising three main separate components. Initial melting behaviour is defined as associated with the breakdown of crystal structure on heating. This structural collapse gradually releases the polymer chains, which begin to rotate and move. Depending on the length of the chains, there is an internal stress level associated with the number of chain entanglements, restricting the tendency to flow and introducing a time dependency to the problem. This flow mechanism is slow and unsteady. As the chains rotate, there is also a tendency toward bulk expansion, slowly changing the geometry of the plastic. This degree of melting is reversible since the crystal structure will reform if the plastic is cooled. Figure 5-7, and other published data relating to polymer viscosity as a function of temperature (ICI, 1985), are only related to this aspect of the flow process. If the plastic temperature is raised further, sufficient to cause thermal degradation, the chains will begin to break up. The chain breaking mechanism, e.g. RCS or ECS, is the main factor controlling the rate of decrease of the average chain length, which dominates the flow rate at this point. A schematic illustration of the flow stages and factors dominating flow rates at each stage is shown in Figure 6-7.

Therefore, a significant problem encountered by this study is that all published melt behaviour properties relate to flow influenced by crystal structure and chain mobility, shown as X_2 in Figure 6-7. However, in a fire, flow is more influenced by chain mobility and chain length shown as X_4 above. The controlling parameters and their effects are different. It was briefly discussed in Section 5.4.1.1 that current research (McLeish, 1999) is working toward understanding molecular orientation and the effects of entanglements in low temperature, stable molecular weight flow. It can therefore be assumed that any understanding of flow for molecules which are thermally degrading at high temperatures is a challenge for a future project, yet to be considered.

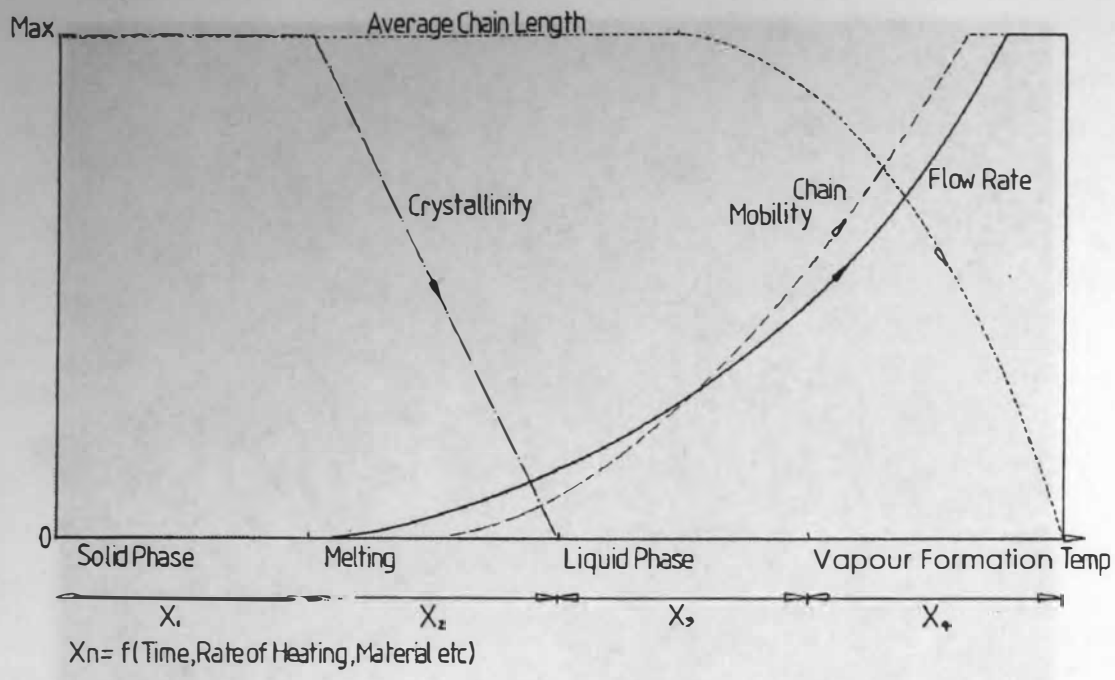

Figure 6-7. Main factors influencing flow rate of burning plastic

The situation is further complicated by the low thermal conductivity of plastics, (typical $k < 0.5$ W/mK, compared to for example, 390 W/mK for copper (Drysdale, 1999)). During the experiments carried out for this project, only superficial surface flow has been observed for PE or PP. For PP and PE, this superficial layer is generally transparent (even for coloured products), accelerating as it flows downward, faster at the edges where the flame height tends to be greater. For the opaque materials tested, beneath the transparent layer the opaque structure can clearly be seen, which remains at depth throughout the test. When the material has slumped or folded over itself, the slump is in the transparent regions of material. It appears that although the outer layer is burning, a centimetre or less below this, the structure is largely intact and resisting flow, indicating that the temperature is below that required to melt it. This is illustrated in Figure 6-8. Thus the flow rate and governing parameters change throughout the depth of burning plastic.

Figure 6-8. Photograph of PP sheet burning and slumping in the Sedan rig (flowing onto a large concrete slab)

(*The white oblong shows initial position of sheet, with arrow showing movement of upper left corner, dashed line shows current geometry*)

In contrast to the behaviour of PP and PE which degrade through a transparent 'wax' phase to a liquid, as illustrated in Figure 3-5, amorphous transparent PS was observed to degrade to a black shiny viscous liquid without a 'waxy' transition phase, which if allowed to cool was transparent and brittle. This is due to the differing decomposition products outlined in Table 1-A.

Figure 6-8 also illustrates that on a concrete substrate, a pool fire is only sustained in the area exposed to additional radiant flux from the fire in the Sedan above it. The factors contributing to this collapse mechanism are detailed in Figure 6-9.

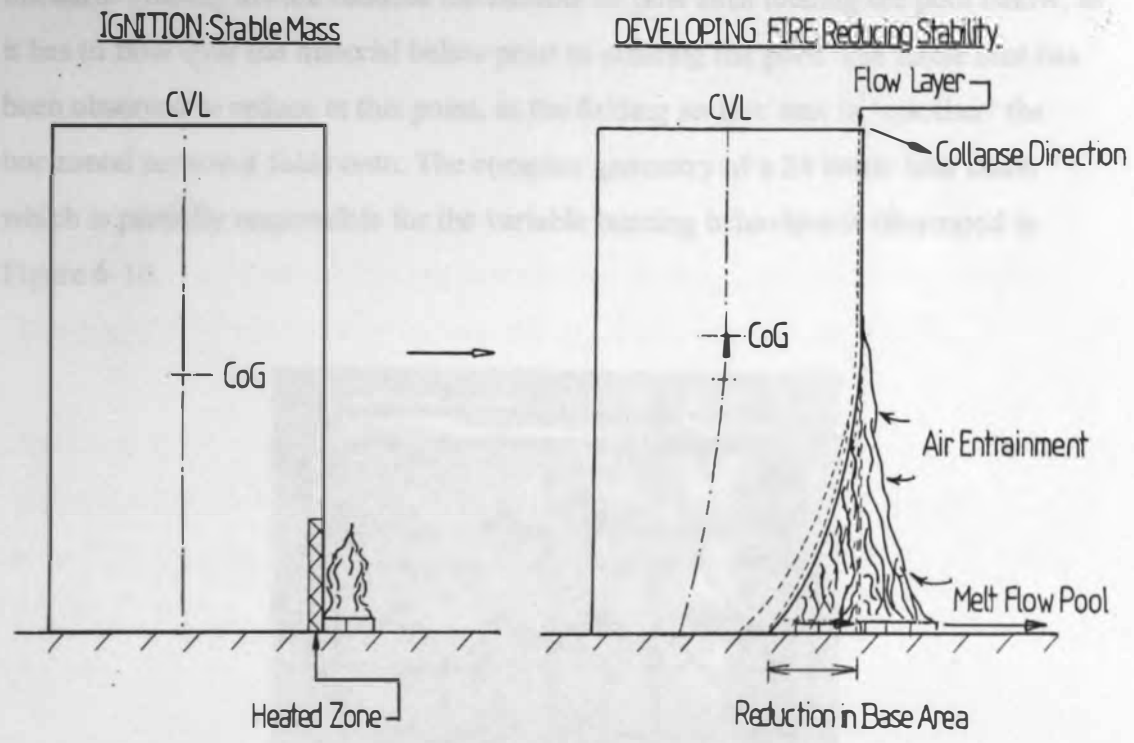

Figure 6-9. Illustration of thermoplastic melt & collapse mechanism

Comparison of Figures 6-8 and 6-9 shows the fastest flame spread to happen at the edge of the sheet. This is the area of most rapid downward flow, reducing the supporting base area, and since the centre of gravity (CoG) is the geometric centre, this becomes raised, reducing the stability. Combining a higher CoG with a reduced area of support, the eventual outcome is slumping. For the test shown in Figure 6-8, the sheet was ignited across the width of the front face, and so there is a 2-D collapse occurring, forwards and to the left. This increases the area of radiant flux exposure on the pool fire below, which then increases the burning area, shown at the

maximum pool fire size in Figure 6-11. The peak HR of this experiment was 117 kW.

For thinner walled products (e.g. beer crates), the fire behaviour consists of dripping in the early stage, until the initially ignited section has dripped and burned away. The number of flow sites then increases, as material elongates downward from each site to either rupture and form a stream of drips, or contact with the floor. The burning crate then folds in the general direction of the elongating flows, either in on itself or outward. Folding inward reduces the number of flow sites feeding the pool below, as it has to flow over the material below prior to entering the pool. The flame size has been observed to reduce at this point, as the folding section acts to 'smother' the horizontal section it folds onto. The complex geometry of a 24 bottle beer crate, which is partially responsible for the variable burning behaviour is illustrated in Figure 6-10.

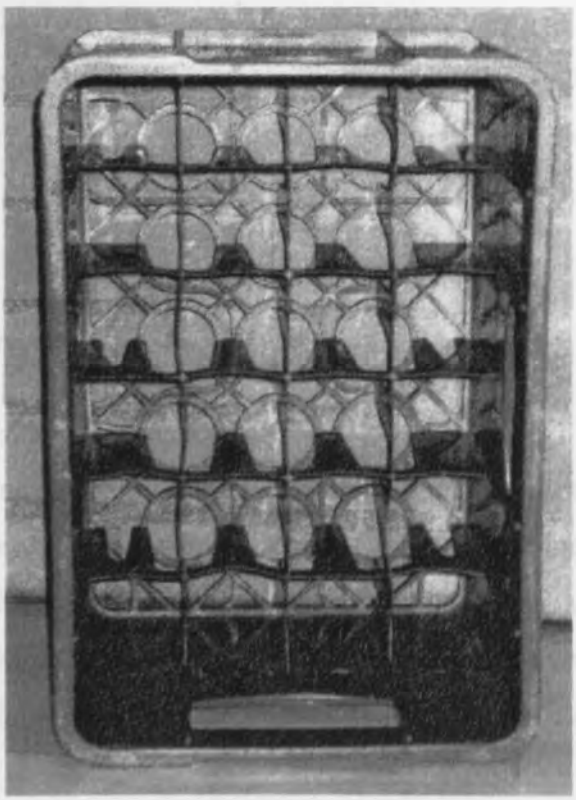

Figure 6-10. Typical 24 bottle beer crate (plan view)

Outward folding increases the number of flow or drip sites into the pool below. For flow onto concrete, the area of pool fire undergoing sustained flaming is controlled by the amount of radiation received from above. This is a function of surface area. The outward fold increases this area, and so a larger area pool fire is produced. A photograph of the same material flowing into a steel tray (peak HR of 450 kW) is shown in Figure 6-12 for comparison.

It is clear from the photographs on the following pages, and results described in Section 4.3 that the nature of the flooring substrate is an important parameter governing fire behaviour for a (medium scale) burning melt. This was investigated in Chapter 4, where it was found that the flooring material does not effect the 'ignition to growth phase' of the burning process, but when the pool fire begins to dominate the overall burning rate, floor properties are an important governing parameter. This effect is likely to be scale dependant, as a larger fire will produce a higher radiant flux which will assist pool spread less affected by the nature of flooring substrate. The size of fire required to overcome this effect is at present unknown.

Building on Equation 6.2, which describes the processes controlling burning rate, for growth to flashover conditions, the rate of increase in burning area is more significant than the increased rate of burning, (Thomas, 1981) modifying Equation 6.2 to:

$$\dot{m} = \left(\frac{\dot{Q}''_F + \dot{Q}''_E - \dot{Q}''_L}{L_V} \right) A_f \qquad 6.3$$

where A_F is the fuel surface area

Thomas was referring to the involvement of more items increasing the number of burning surfaces during fire growth. However, for the case of melting and burning plastics, each individual plastic section increases burning area due to melt spreading, increasing A_F over time. This is further complicated since the vertical burning surface flows and changes to produce an additional horizontal surface (i.e. a pool fire).

Figure 6-11. Point of maximum fire size for PP sheet burning on a large concrete slab

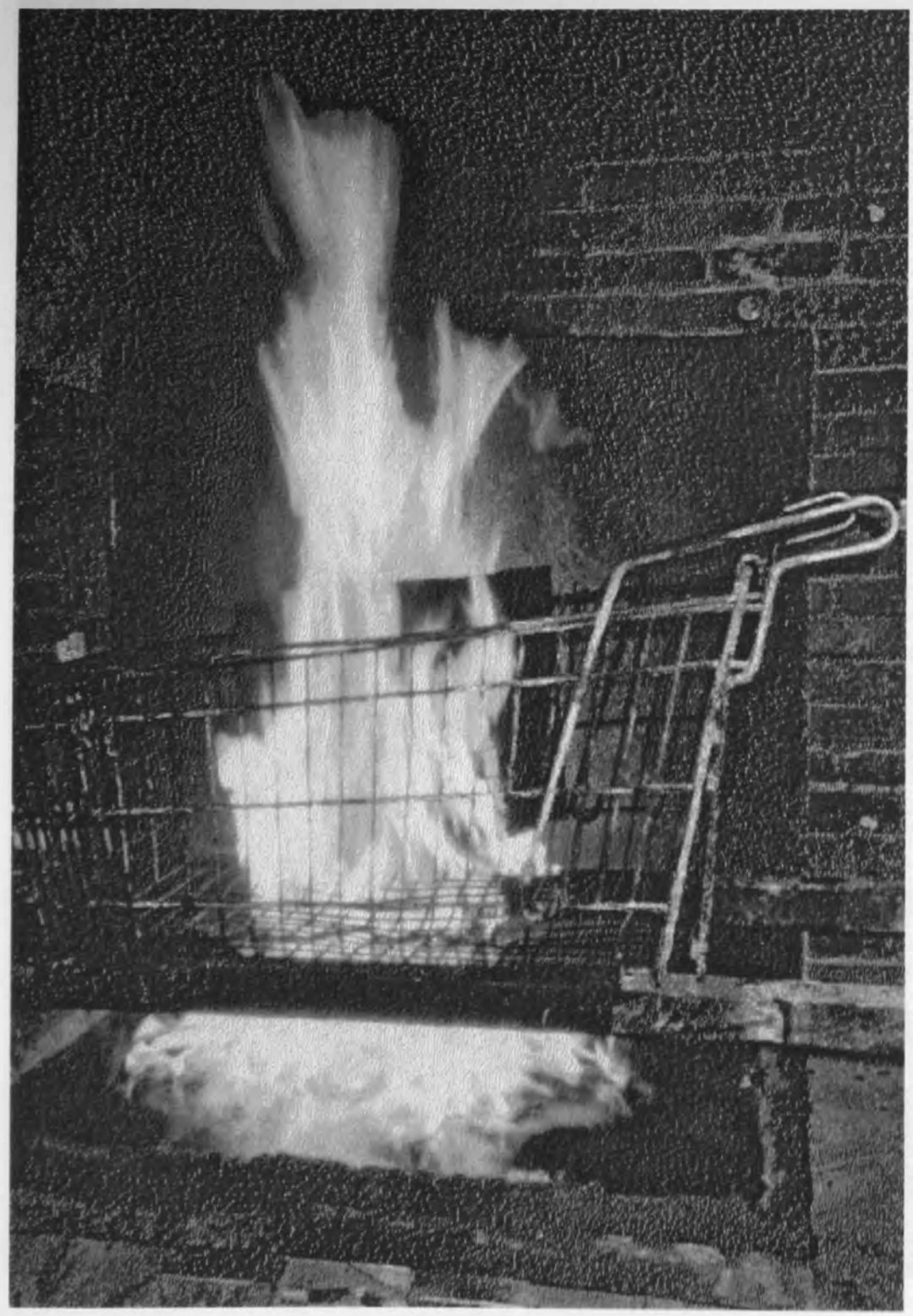

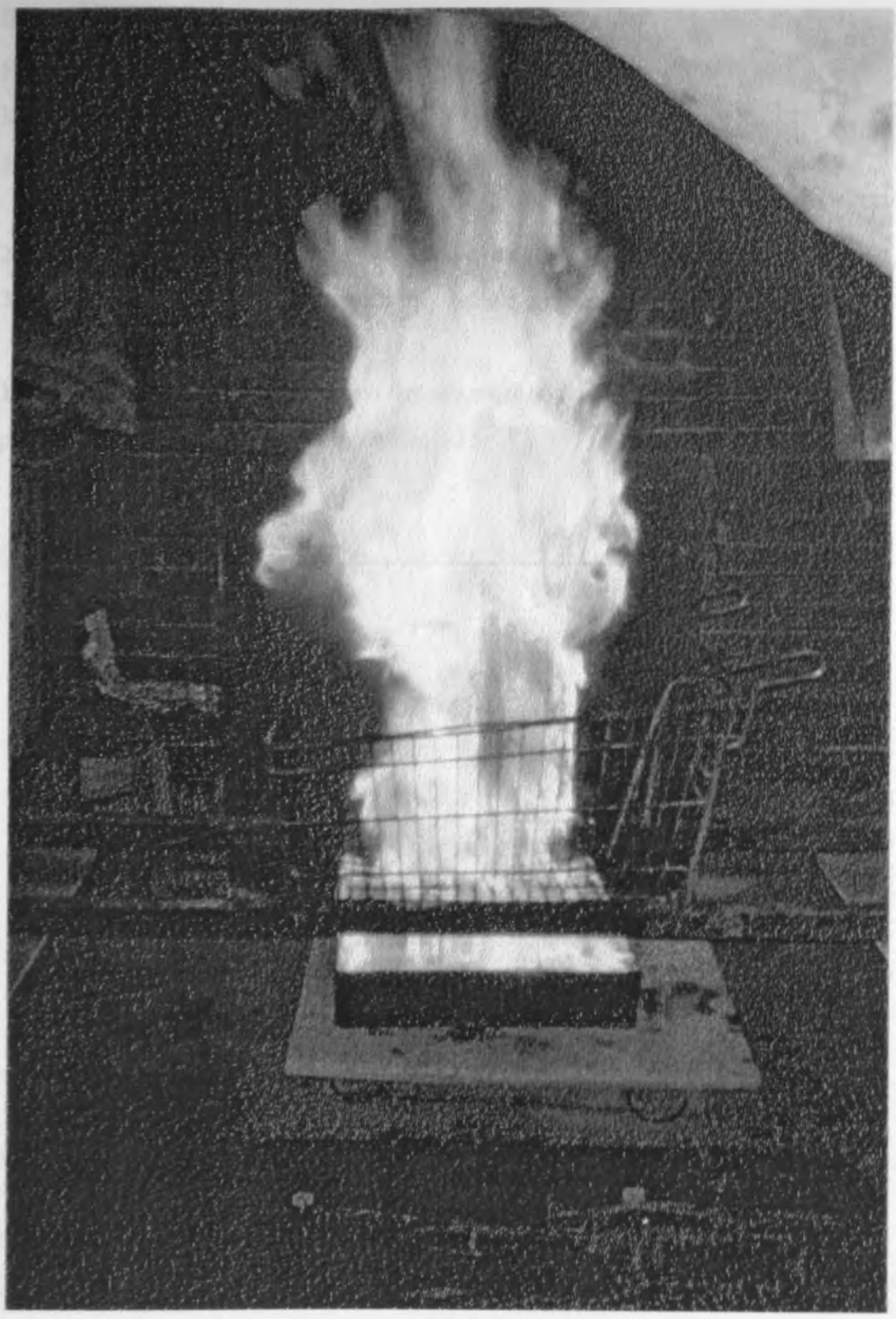

Figure 6-12. Photograph of a burning PP sheet flowing into steel tray

6.2.3 The general burning behaviour of pool fires

For a free burning liquid pool, there are three burning regimes (Blinov and Khudiakov, 1957);

1. laminar – diameter less than 0.03m, surface regression rate falls as diameter increases;
2. transitional – diameter between 0.03 and 1m;
3. turbulent – diameter greater than 1m, surface regression rate is independent of diameter.

The dependence of burning rate and flame height on pool diameter for hydrocarbon pools experimentally is shown in Figure 6-13.

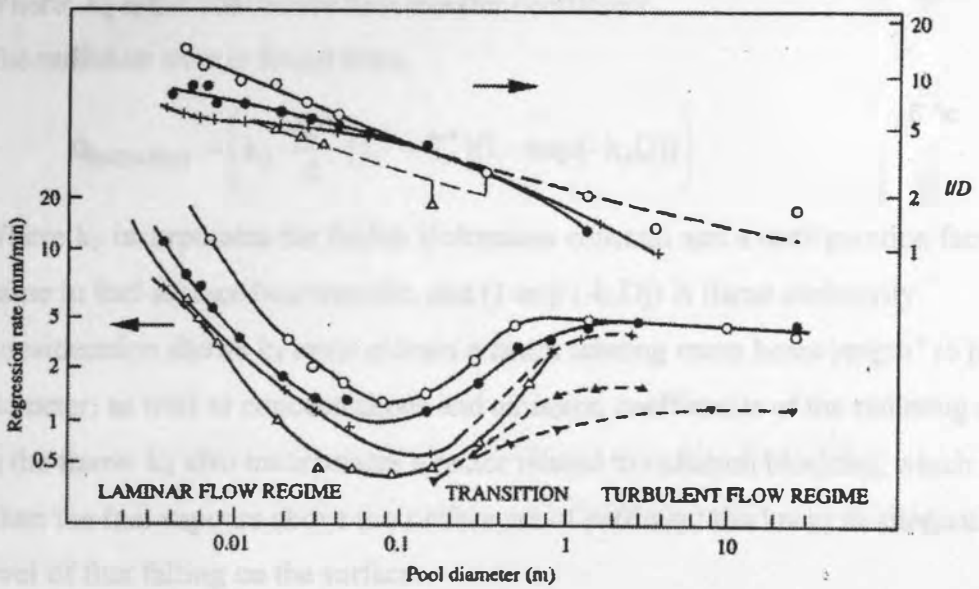

(○ gasoline, ● tractor kerosene, Δ solar oil, + diesel oil, ▲ petroleum oil, ▼ mazut oil)

Figure 6-13. Regression rates and flame heights for liquid pool fires, diameter 3.7×10^{-3} to 22.9m

These regimes are applicable to circular liquid pools heated only from the pool flames, with no external heat source and no interference with flow patterns.

The dependency on diameter is due to changes in the dominant heat transfer mechanisms from the flame to the fuel surface. The rate of burning was expressed in Equation 6.3, where the flame flux comprises three terms:

$$\dot{Q}''_F = (\dot{q}''_{CONDUCTION} + \dot{q}''_{CONVECTION} + \dot{q}''_{RADIATION}) \quad 6.4$$

(in this case, the radiation flux includes surface re-radiation)

The conduction term (relating conduction from the container rim to the liquid) is found from;

$$\dot{q}_{CONDUCTION} = k_1 \pi D(T_f - T_l) \quad 6.5a$$

Where; k_1 is a constant that incorporates a number of heat transfer terms;

T_f and T_l are flame and liquid temperatures

(*most plastic flame temperatures are ~1200K (Baubraskas, 1992)*).

For convection direct to the fuel surface;

$$\dot{q}_{CONVECTION} = \left(k_2 \frac{\pi D^2}{4} (T_f - T_l) \right) \quad 6.5b$$

Where; k_2 is the convective heat transfer coefficient.

The radiation term is found from;

$$\dot{q}_{RADIATION} = \left(k_3 \frac{\pi D^2}{4} (T_f^4 - T_l^4)(1 - \exp(-k_4 D)) \right) \quad 6.5c$$

Where k_3 incorporates the Stefan Boltzmann constant and a configuration factor for flame to fuel surface heat transfer, and (1-exp (-k_4D)) is flame emissivity. Consideration shows k_4 must contain a factor relating mean beam length[v] to pool diameter, as well as concentrations and emission coefficients of the radiating species in the flame. k_4 also incorporates a factor related to radiation blocking, which occurs when the fuel vapours above the surface are of sufficient thickness to attenuate the level of flux falling on the surface.

Dividing Equations 6-5a – 6-5c by pool surface area and substituting into Equation 6.4 finds;

$$\dot{Q}''_F = 4 \frac{k_1 (T_f - T_l)}{D} + k_2 (T_f - T_l) + \left(k_3 (T_f^4 - T_l^4)(1 - \exp(-k_4 D)) \right) \quad 6.6$$

Therefore, from Equation 6.6, if D is very small, conduction determines the rate of burning, and when D becomes large the radiative term is the dominant factor.

---

[v] mean beam length: characteristic dimension of a system used to assess the amount of radiation from a volume of gas (a function of geometry)

Further work (Zabetakis, 1961) showed the mass flux for pools greater than 0.2m diameter can be predicted from:

$$\dot{m}'' = \dot{m}''_{\infty}(1 - \exp(-k\beta D)) \qquad 6.7$$

Where kβ consists of an emission coefficient k (m^{-1}) and a mean beam length factor (β). For plastic pool fires, the only complete published data found is for PMMA (Baubraskas, 1992) where k = 1.3m^{-1}, kβ = 3.3m^{-1} and m"$_{\infty}$ = 0.02 kg/m^2s.

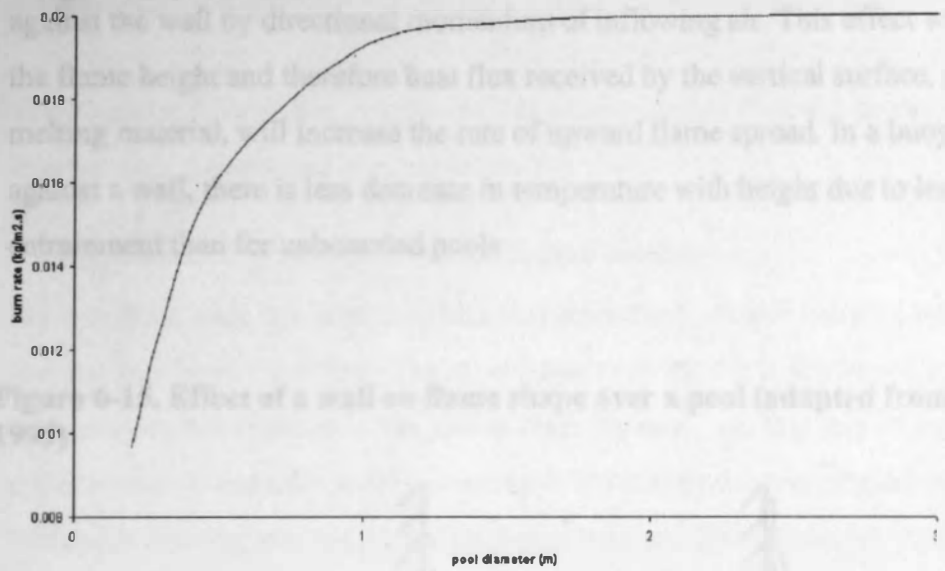

Figure 6-14. Burning rate as a function of pool diameter for PMMA

Figure 6.14 shows the limit of 20 g/m^2s is reached at a pool diameter of 1.5m for PMMA.

Considering this information with regard to melt fuelled pools, conduction losses dominate small area fires, which would represent the initial stage of a melt-fuelled pool. Therefore, the nature of flooring or any obstruction to flow spread will partially control the melt temperature. Depending partly on the flow rate into the pool, the (temperature dependent) viscosity will control the initial spread rate of the pool. Since the pools are rarely circular and there are usually drip feed sites interfering with flow patterns, creating axisymmetric conditions, turbulence will probably onset at diameters less than those shown in Figure 6.13.

The main difference between the conditions described above and a melt fuelled pool fire however, is the physical presence of the melting/burning 'wall' feeding it.

6.2.4 Effect of a wall on pool fire behaviour

6.2.4.1 Effect of a non combustible wall on pool fire development

The effect on flame profile of a non-burning wall is illustrated in Figure 6-15. From the diagram, the area through which air can be entrained against a wall is reduced compared to free burning conditions. For the fire against the wall, flame is deflected against the wall by directional momentum of inflowing air. This effect will increase the flame height and therefore heat flux received by the vertical surface, and for non-melting material, will increase the rate of upward flame spread. In a buoyant plume against a wall, there is less decrease in temperature with height due to less air entrainment than for unbounded pools.

Figure 6-15. Effect of a wall on flame shape over a pool (adapted from Drysdale, 1999)

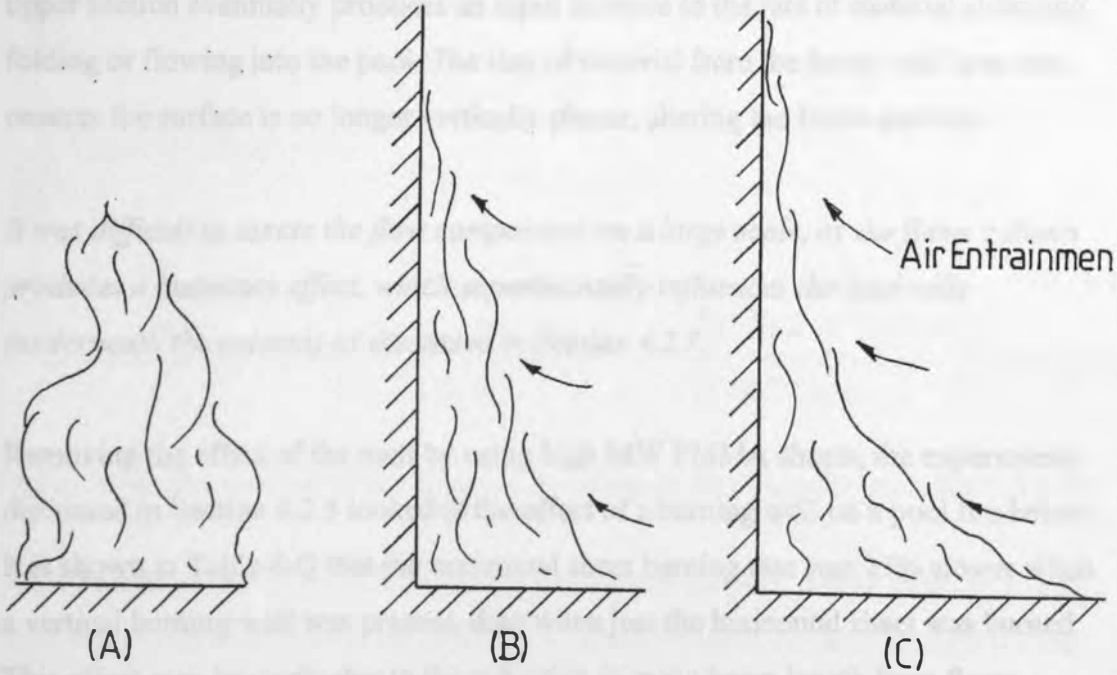

From the diagram, the presence of the wall causes flame to be deflected toward it, exposing the wall to an increased level of heat flux from the flame. As described in Equation 6.7, the pool burning rate is partially dependent upon the average mean

beam length. Considering the flame profiles sketched in Figure 6-15, the mean beam length for the free burning pool is longer than the average mean beam length for the pool burning against the wall, due to flame deflection. The average mean beam length for the deflected flame however, will be dependent on width of pool, reducing as the pool sizes increases, as shown in Figure 6-15.
Therefore, it is possible that the physical presence of the wall will effect the burning rate of the pool at its base. This will be a function of size, as the effect of the wall flames across the pool surface will reduce as the pool leading edge increases in distance from the wall.

The situation for a melting plastic wall is more complex than this as the wall material is exhibiting flowing and burning behaviour.

6.2.4.2 Effect of a combustible wall on pool burning

For a melting wall, the increased heat flux from the pool will increase the rate of melting and downward flow. The experiments carried out in the Sedan and Kebab rigs confirm that material is lost fastest from the base, and this loss of support for the upper section eventually produces an rapid increase in the rate of material slumping, folding or flowing into the pool. The loss of material from the lower wall area also ensures the surface is no longer vertically planar, altering the flame patterns.

It was difficult to assess the flow components on a large scale, as the flame column produces a buoyancy effect, which experimentally influences the load cells (underneath the column) as discussed in Section 4.2.7.

Removing the effect of the melt by using high MW PMMA sheets, the experiments discussed in Section 4.2.5 looked at the effect of a burning wall on a pool fire below. It is shown in Table 4-Q that the horizontal sheet burning rate was 25% slower when a vertical burning wall was present, than when just the horizontal sheet was burned. This effect may be partly due to the reduction in mean beam length from flame profile to the pool as shown in Figure 6-15. Comparison of Figure 6-15 (A)(B) and (C), shows the path length over the pool with a wall is very small at the leading edge, increasing to a maximum at the rear edge, whilst the free burning condition has a

maximum at the centre. A further possible limiting condition is due to the increased amount of fuel vapours from the two surface (horizontal + vertical) system attenuating the amount of radiation reaching the horizontal surface.

Support for the effect of reduction in beam length away from the burning wall is found from the Sedan tests onto concrete, where burning could not be sustained in areas not exposed to additional flux from the Sedan above.

From the experiments conducted, it seems that the presence of a burning wall actually slows the burning rate of the pool fire at its base. The melting wall may slow this further, as the melt entering the burning pool is cooler than the burning temperature of the liquid pool.

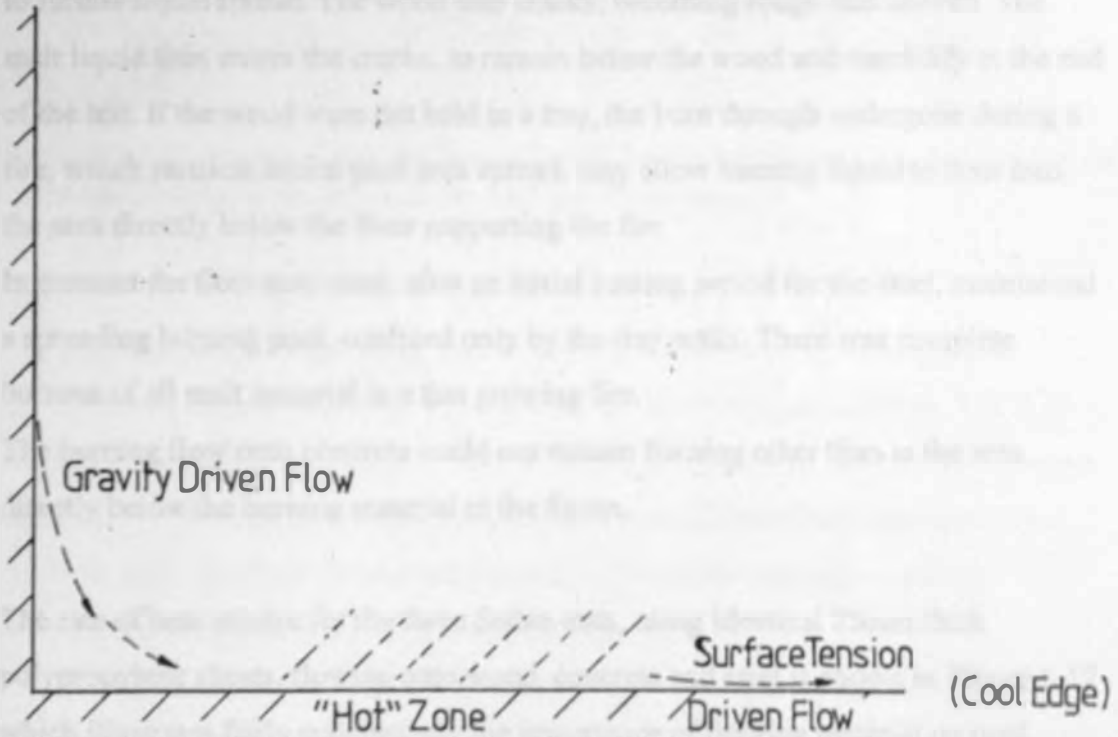

Figure 6-16. Illustration of the flow mechanisms controlling the melt fuelled pool fire

As shown in Figure 6-16, flow is gravity driven into the pool, where away from the cool entry sites a hot zone is established. A surface tension driven flow then pushes material out of the 'hot zone', toward the cooler leading edge of the pool. Depending on rates, this can result in a cyclic feed and burn out phase in the hot zone, as observed clearly in the Kebab experiments. Similarly, if the hot zone is large enough

or the feed in rate slow, then material may burn up rather than pass through it, and the surface tension flow which controls the extent of pool, may be restricted. It was observed in the experiment onto wooden flooring that because the wood burned, no material passed through the 'hot zone' and there was no enlargement of pool area due to surface driven flow. At the cool outer edges, the liquid viscosity is increased, which may re-solidify into a rim, which then physically restricts further flow spread.

6.2.5 The Effect of Flooring

Pool development is partly dependent on the flooring substrate onto which the flow is spreading. With wood, the actual floor becomes involved in the burning process, in the area exposed to the additional flux from the fire above, creating a flaming barrier to further liquid spread. The wood also cracks, becoming rough and uneven. The melt liquid then enters the cracks, to remain below the wood and resolidify at the end of the test. If the wood were not held in a tray, the burn through undergone during a fire, which restricts lateral pool area spread, may allow burning liquid to flow into the area directly below the floor supporting the fire.

In contrast the flow onto steel, after an initial heating period for the steel, maintained a spreading burning pool, confined only by the tray walls. There was complete burnout of all melt material in a fast growing fire.

The burning flow onto concrete could not sustain burning other than in the area directly below the burning material in the Sedan.

The rate of heat release for the three Sedan tests, using identical 25mm thick polypropylene sheets, flowing onto wood, concrete and steel is shown in Figure 6-17 which illustrates fairly conclusively the importance of flooring material on pool development after an initial relatively lengthy period of fire growth.

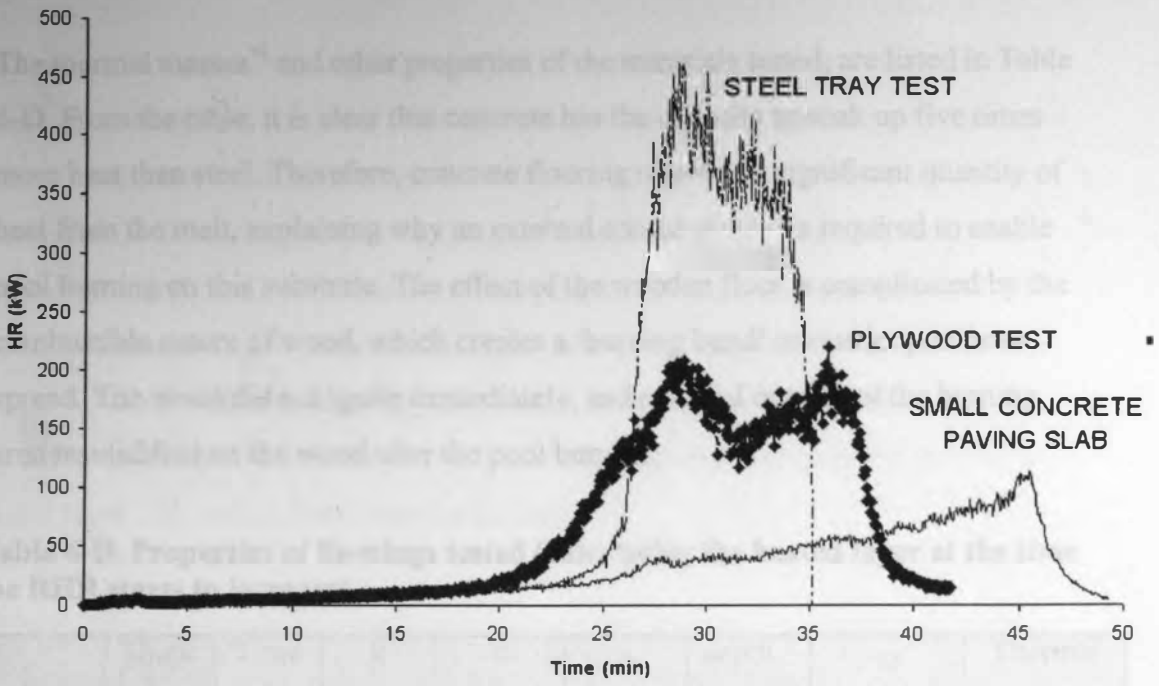

Figure 6-17. Plot comparing the heat released by polypropylene sheets tested in the Sedan and flowing onto three different floor materials

6.2.5.1 Why flooring dominates pool fire development

The potential area of a spreading pool is viscosity controlled, which is partially dependent on thermal conductivity / thermal inertia of the floor substrate. The high thermal inertia of the steel floor, ($1.6x10^8$ W^2s/m^4K^2 compared to $2x10^6$ for concrete and $3.2x10^5$ for wood (Drysdale, 1999)) shows heat will be rapidly conducted into the steel bulk. The high thermal conductivity of steel then ensures a uniform temperature is rapidly achieved through the material.

Therefore, liquid spread on steel is initially slow as the floor undergoes a heating phase, removing heat from the melt and increasing its (temperature dependent) viscosity to reduce the pool spread rate. Once a stable, uniform temperature is attained melt viscosity is kept low, enabling pool spread. In contrast, the low inertia of concrete will result in surface heating, with continual removal of heat as it is conducted slowly into the bulk, cooling the melt on the surface. Hence, early non-burning pools spread faster on wood than concrete, which allows faster spread than steel.

The thermal masses[vi] and other properties of the materials tested, are listed in Table 6-D. From the table, it is clear that concrete has the capacity to soak up five times more heat than steel. Therefore, concrete flooring removes a significant quantity of heat from the melt, explaining why an external source of heat is required to enable pool burning on this substrate. The effect of the wooden floor is complicated by the combustible nature of wood, which creates a 'burning bund' to restrict pool area spread. The wood did not ignite immediately, and material outside of the burning area resolidified on the wood after the pool burnout.

Table 6-D. Properties of floorings tested (calculating the heated layer at the time the RHR starts to increase).

	Thickness mm	Time min	k W/m K	c J/kg.K	ρ kg/m^3	depth heated layer* m	α m^2/s	Thermal Mass J/m^2.K
steel	3	23	45.8	460	7850	0.13	1.26E-05	10833
wood	20	20	0.16	2600	700	0.01	8.79E-8	18693
concrete	30	25	1.1	880	2100	0.03	5.95E-7	55220

$depth\ of\ heated\ layer = \sqrt{\alpha t}$ (t = time of heating; $\alpha = k/(\rho c)$)

** *wood and concrete can be approximated as 1-D systems, but steel has to be considered as 2-D as heat will be conducted horizontally away from the immediate vicinity of burning*

In addition to the thermal characteristics, surface texture will effect the flow rates. The textural characteristics and effects are summarised below:

Steel is non-porous and smooth offering little resistance to flow, and if the steel temperature is raised uniformly, liquid viscosity will be kept low, increasing spread rate.

[vi] thermal mass = thickness x density x specific heat capacity (assuming constant heating rate)

Concrete is porous, with its absorption of heat capability dependent on both free moisture content and water of hydration, producing specific heat capacity increases at both 100 and ~ 450°C (Marchant, 1997). The rough surface is less conducive to flow than steel, although the lower thermal inertia of the concrete will result in a reasonably high rate of rise in surface temperature, maintaining low viscosity flow. During the experiment, a layer of solid polymer eventually formed across the slab surface, which whilst fed by flaming material, sustained surface burning. Shortly after the burning flow into the pool stopped, the pool self extinguished, leaving a solid layer ~ 5 – 8 mm thick over the surface.

Wood changes properties completely during a fire. Initially flat, and moderately rough with a free moisture content, wood is a combustible material, comprising ~20 – 30% cellulose, 50 – 60% semi-cellulose, and 20 – 30 % lignin (Marchant, 1997; Drysdale, 1999). Due to the composition, which varies between species, combustion occurs in stages and produces a rough black char, breaking up the initially flat surface. During the test, it was noted that the flaming combustion of the wood restricted the possible area increase of the burning pool. This was partly due to a burning area directly below the drip feeding sites preventing build up of a smooth solidified plastic layer over which the low viscosity melt could flow, extending the pool as happened on the concrete surface. The other control mechanism was the cracked surface, slightly raised at the crack edges, which diverted liquid flow down into the crack rather than over the horizontal surface.
NB During this test, this mechanism restricted pool fire spread. However, diverting burning liquid into cracks caused by burn through, as occurred in the test, will restrict the spread area above but could possibly spread fire to the area below.

6.2.6 Effect of increased radiation on a wall fire

Having discussed the effect of the burning wall on the pool, the next consideration is the effect of the burning pool on the original thermoplastic wall. Previous work with geometrically stable materials (Fernandez Pello, 1995), has found that flame length,

flame spread velocity, pyrolysis rates and solid surface temperature[vii] are all partially dependant on external radiant flux. Experimental results (Saito, 1986) showing the dependence of pyrolysis front and flame tip upward spread rates on the level of external applied flux for wood are shown in Figure 6-18, (NB wood requires an external flux in order to sustain flaming due to char forming).

The Sedan experiments that used an oil bath to quench the melt were carried out to investigate this effect for melting plastic. The results, shown in Tables 4-P and 4-Q indicate that 75 – 80% of the original plastic enters the pool, with only 20 – 25% burning in the vertical array.

Typical results for the overall burning rates of two halves of a (Holsten Pils) beer crate burning both fully and in the sedan only (flowing into the steel tray) are shown in Figure 6-19. From the plot, the pool fire is shown to have no effect on the early fire growth phase, in this case taking around 13 minutes, after which the pool fire below increases the overall burning rate. A plot of the two Sedan burning rates is shown in Figure 6-20 for comparison.

[vii] the flame preheats the solid ahead of the flame front, and as the solid temperature, To approaches the pyrolysis temperature, Tp, flame spread rate tends to infinity

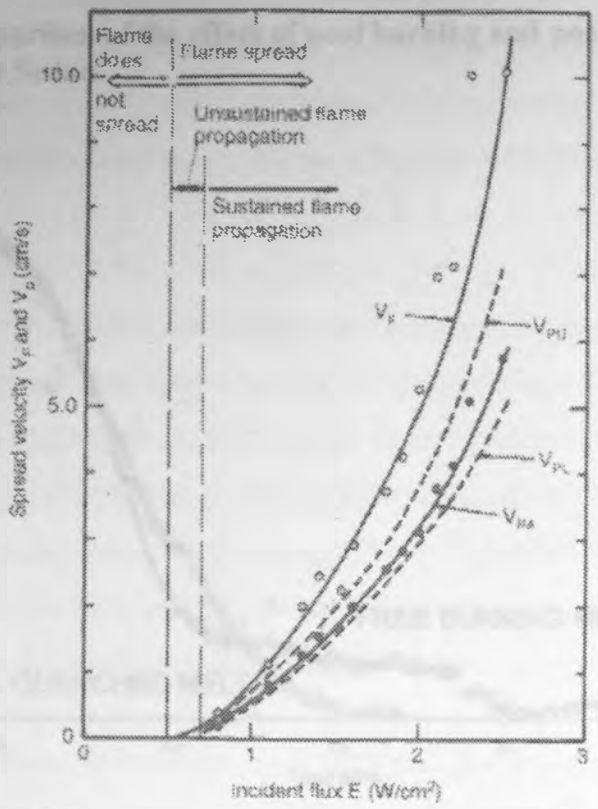

Figure 6-18. Pyrolysis front and flame tip upward flame spread rates over wood sheets as a function of external radiant flux.

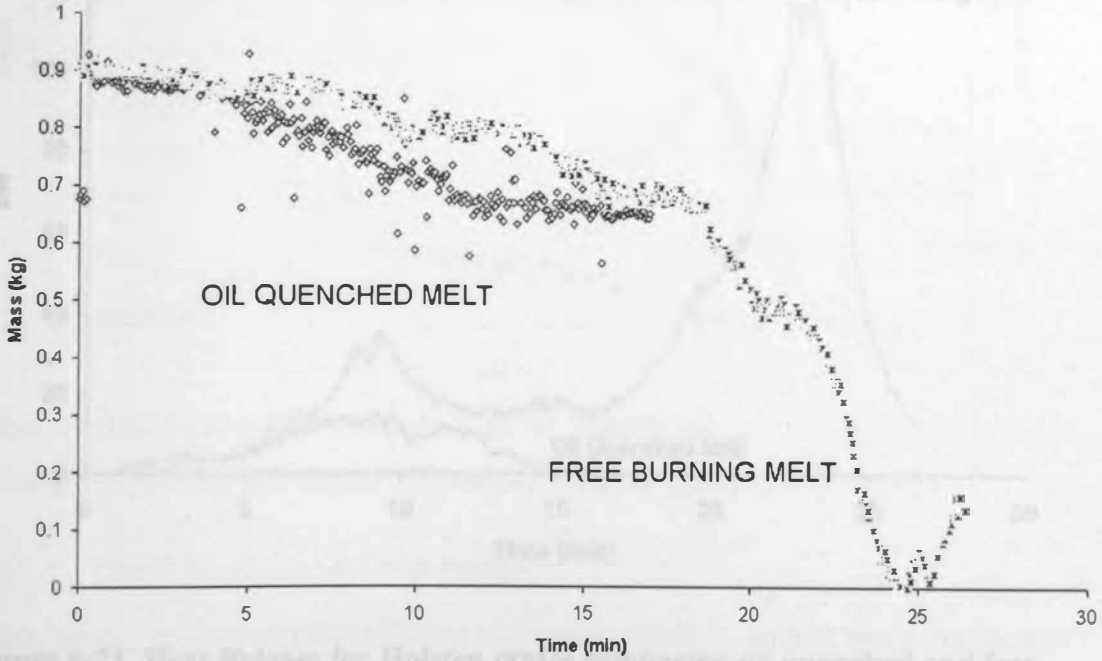

Figure 6-19. Comparison of overall burning rates for half crates burning with pool fire below, and with quenched pool

Figure 6-20. Comparison of the effect of pool burning and pool quenched on mass loss rates from the Sedan

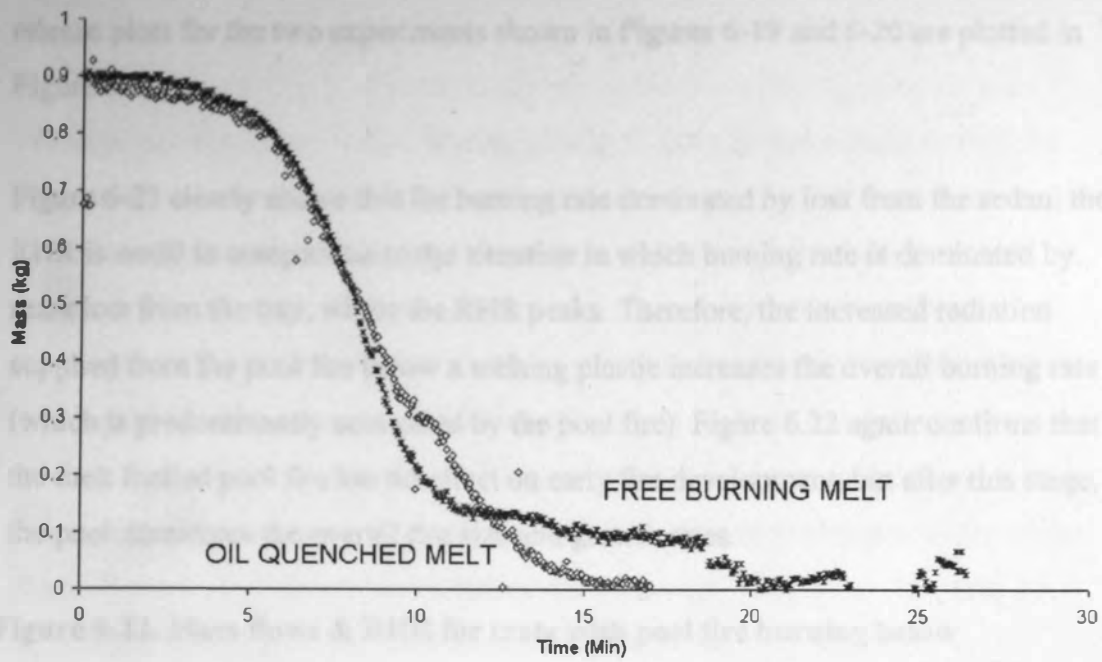

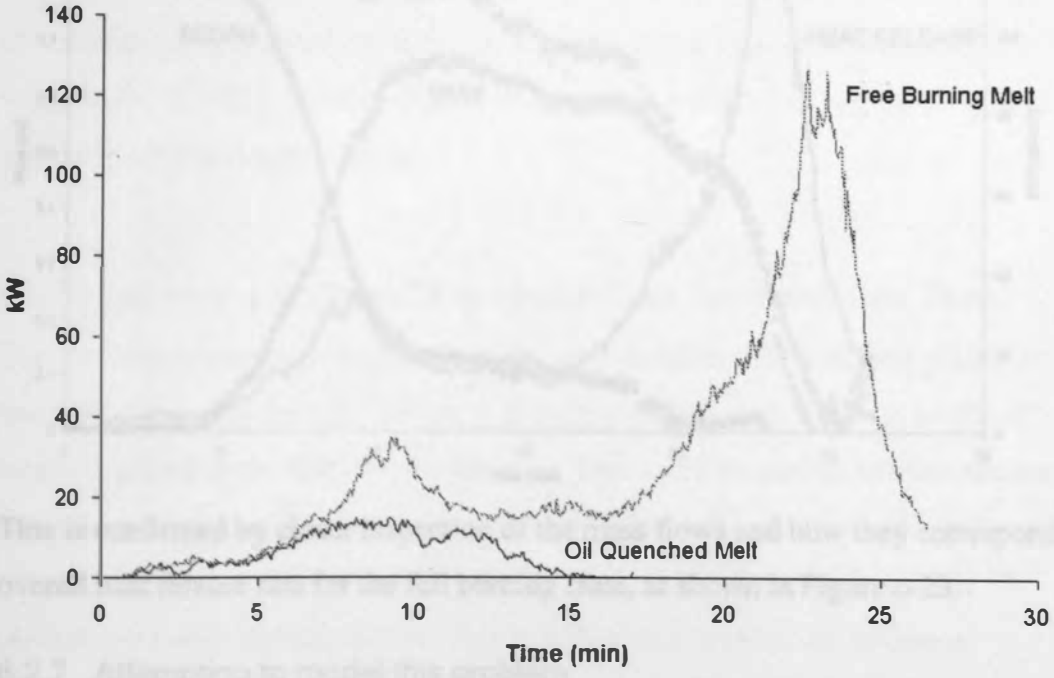

Figure 6-21. Heat Release for Holsten crates comparing oil quenched and free burning pool fires

The Sedan and Kebab experiments show less than 25% of mass lost is due to surface burning in the sedan. Most of the plastic flows downward, in thin surface layers (typically < 2cm.sec^{-1} over a vertical surface) to eventually enter the pool. The heat release plots for the two experiments shown in Figures 6-19 and 6-20 are plotted in Figure 6-21.

Figure 6-21 clearly shows that for burning rate dominated by loss from the sedan, the RHR is small in comparison to the situation in which burning rate is dominated by mass lost from the tray, where the RHR peaks. Therefore, the increased radiation supplied from the pool fire below a melting plastic increases the overall burning rate (which is predominantly controlled by the pool fire). Figure 6.22 again confirms that the melt fuelled pool fire has no effect on early fire development, but after this stage, the pool dominates the overall fire size and growth rates.

Figure 6-22. Mass flows & RHR for crate with pool fire burning below

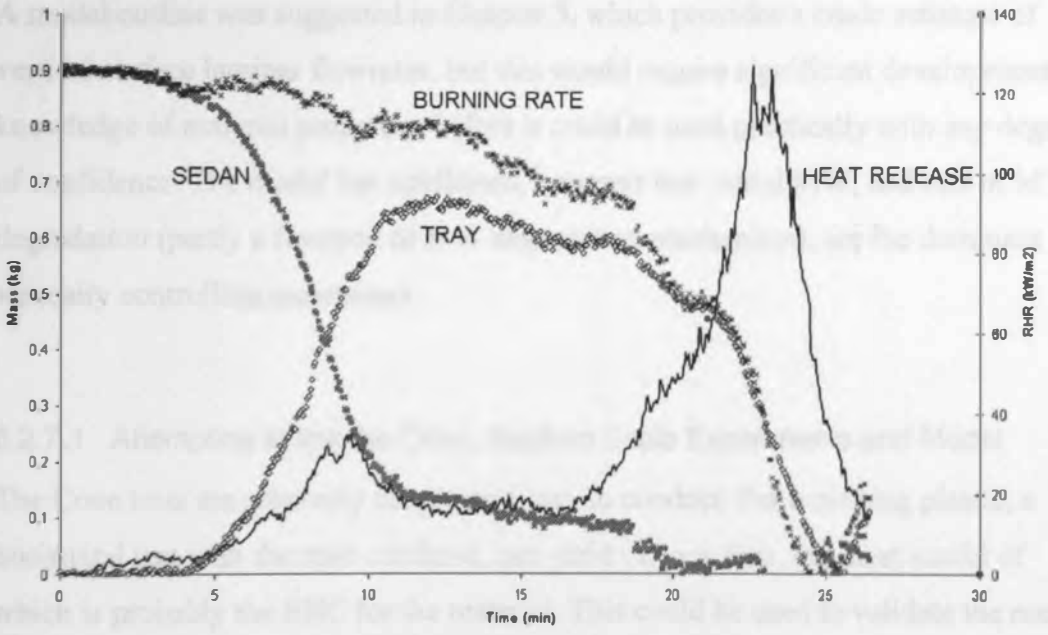

This is confirmed by closer inspection of the mass flows and how they correspond to overall heat release rate for the full burning crate, as shown in Figure 6-23.

6.2.7 Attempting to model this problem

This has proved almost impossible to tackle meaningfully, mainly due to the lack of knowledge regarding material properties for a melt controlled by MW degradation

rather than dissolution of the crystal phase. There was no way found to measure these properties effectively, in particular viscosity. However, the model has confirmed that MW and rate of MW degradation are controlling parameters for melt fuelled pool fires.

One significant problem is that burning plastic surfaces do not remain vertical for long, as a combination of bulk expansion and slumping or loss of material to melting in the lower regions of the plastic inevitably distort the initially vertical surface geometry. This then causes flow rate variation due to orientation as well as temperature. Due to the flow rate slowing over an inclined surface compared to vertical, there will be greater conduction of heat into the bulk due to the longer residence time of the surface layer. This may produce a thicker surface layer flow, and higher surface temperatures. This is likely to be very significant with regressing plastic foams, which tend to form 'caves' above the ignition source. The time dependency to this problem has not been considered further in this work.
A model outline was suggested in Chapter 5, which provides a crude estimate of vertical surface laminar flowrates, but this would require significant development of knowledge of material properties before it could be used practically with any degree of confidence. The model has confirmed, however that initial MW, and rate of MW degradation (partly a function of MW degradation mechanism), are the dominant viscosity controlling parameters

6.2.7.1 Attempting to link the Cone, Medium Scale Experiments and Model

The Cone tests are relatively simple and easy to conduct. For a melting plastic, a horizontal test with the melt confined, can yield various data, the most useful of which is probably the EHC for the material. This could be used to validate the results from the medium scale experiments. Very few other valid comparisons can be made since the Cone data is produced in a freely ventilated convection dominated environment with laminar flames. This is unrelated to a turbulent, radiation dominated natural fire. For the model, it may be possible to use (melt constrained) Cone data to measure or deduce material parameters such as Lv and specific heat capacity, using the approaches suggested in Chapter 4

6.2.7.2 General Conclusion

This research project has started an investigation into a very significant problem which has received very little previous attention. Unfortunately, previous experimental studies of geometrically stable materials cannot be readily adapted, and so there were problems developing techniques as well as obtaining results. However, a first step has been taken, abandoning traditional approaches to clamping or restraining test materials, simply utilising a supporting mesh and allowing the material to flow as it burns. The project has concentrated experimentally on a narrow range of materials. This is partly to try and devise a reproducible method so the results could be compared, and partly due to equipment limitations, e.g. the limited amount of burning material which could be successfully quenched in the oil bath (around 1kg). It was found that the burning behaviour of melts is rarely reproducible, as the material elongates and ruptures randomly, increasing or decreasing the burning surface area. This prevents any comparison on a $/m^2$ basis, which is the approach generally undertaken with geometrically stable materials. The main conclusions and recommendations for future development are listed in the following Chapter.

7 Conclusions & Recommendations for further work

7.1 Introduction & Main Problems For This Study

The objective of this research study was to investigate the effect of the melt flow process on fire growth. Foley pointed out that there had been little research on this topic, and it was discovered at an early stage that there were significant problems in three main areas;

1) Lack of knowledge of the effect of melting and burning processes on plastic material properties, which are the basic inputs for any model. Detailed published data does exist for a wide array of polymers as it is required for processing purposes. However, the data only applies to a relatively low temperature range, and does not account for thermal degradation of the polymer.

2) There are no published 'standard tests', experimental methods or industrial practices capable of measuring any of the melt properties affecting fire behaviour. It appears that melt-flow has been treated as a nuisance which can be ignored by various techniques, rather than an important material property. These 'avoidance techniques' include:

   a) standard tests: for some tests, such as BS 476 Part 7, the minimum rating can be achieved by bonding the plastic to a non-melting substrate, which stays in place during the test. The merit of this approach was clearly demonstrated by Abbott with the agricultural EPS panels. Other tests, such as the SBI, accept that melting plastics cannot meet the test criteria, and so are listed as incapable of being tested. (*It should be emphasised, however, that even for geometrically stable materials, these tests suffer a large apparatus dependency, and the results from them are of little use in predicting actual fire behaviour*).

b) experimentalists & fire researchers: who circumvent the melt problem by the almost universal adoption of high MW PMMA which doesn't melt, for both testing and modelling purposes.

c) industry has considered melting, as it is a necessary property for moulding, and produced tests intended to measure a melt viscosity type parameter as a function of temperature (e.g. MFI). These tests are all apparatus dependent, generally involving pressure driven flow through a particular size, shape and temperature die, where if the apparatus is similar to processing equipment, the data is of use in that field.

3) The published properties of polymers differ from those of plastics, and commercial sensitivity prevents manufacturers disclosing the composition of their products. Therefore, it is possible that an effect may be due to an unspecified additive or degree of copolymerisation rather than the base polymer, but this is difficult to identify or quantify

Despite the problems faced in this project, the work has produced some interesting results which lay the ground for further investigation.

7.2 Conclusions

7.2.1.1 Small scale (Cone Calorimeter) Work

The previous research focused on PMMA has generally concentrated on thermally thick PMMA, thereby allowing steady state data to be obtained, but this not representative of commodity plastics.

This study has looked at commodity plastics, although small-scale work excludes any geometrical configuration effects, covering a range of common behaviour known to have caused problems in actual fire incidents. The results show a range of factors including molecular composition and weight, additives, orientation, ventilation conditions, material thickness and applied level of flux affect the small scale fire performance of thermoplastics. The effects of some of these variables can clearly be

detected with Cone Calorimeter tests, but some, such as the effect of orientation, are apparatus dependent and not generally transferable. On the other hand, some larger scale problems such as thermal expansion, or loss of component rigidity due to softening are not apparent from a cone test.

The cone database indicates that all the plastics tested would begin to burn during flashover (defined by a radiant flux in excess of 20 kW/m^2 received at floor level). In most cases it is possible to observe melting behaviour from a Cone Calorimeter test, particularly as if commonly occurred, the material overspills the sample holder. This may indicate a thermoplastic is capable of generating a pool fire in larger scale well-ventilated conditions. (This could also be observed from simply igniting a small specimen clamped in a retort stand.).

7.2.1.2 Medium Scale work

To answer the problem of no appropriate measuring techniques, a method has been developed which is capable of assessing the influence of a melt on fire dynamics. The Sedan and Kebab rigs both operate on the principle of separating the mass flow components from vertical to horizontal. This technique seems to be moderately successful for medium scale tests.

It has been confirmed that increasing pool fire area increases overall rate of heat release, and therefore the radiant flux supplied to the material feeding the pool. This loop mechanism increases the flow rate into the pool and the burning rate of the pool. The Sedan and Kebab experiments show that for a thermoplastic exhibiting melt-flow behaviour, the fire size and rate of growth are controlled by the pool fire formed at the base of the burning flowing material.

Results from the oil quenched experiments, show 70 – 80% of the mass loss from the array will enter the pool.

Flame deflection from the pool is a significant component of the level of flux received by the vertical wall, and when the wall is no longer physically present, this will influence the burning process.

All of the plastic fires studied during this project show an initial relatively long fire growth phase. It is not yet known if this is a function of the material properties, or whether a larger ignition source or different configuration would reduce this phase, increasing the level of hazard.

It has also been found that there are two controlling mechanisms influencing pool fire development. This project has focused on gravity driven surface melting, but it has also been observed that softening followed by geometrical slumping is an important pool feeding mechanism. This is harder to predict as it is only seen on larger scale tests. It appears to be driven partly by loss of the supporting base area combined with a moving centre of gravity. It has been found impossible to separate the two mechanisms experimentally, as even thick sheets of plastic will eventually succumb to a slumping collapse.

The material properties of the flooring substrate are a major influencing parameter on the burning rate of the pool and therefore overall fire growth and development.

7.2.1.3 Modelling

Previous work by physicists and mathematicians has looked at melting ice. This has known properties, and is reversible (e.g. no chemical changes). Although burning plastic melts are not reversible, and the properties are largely uncertain beyond processing temperatures, this approach has been used as the basis for a model. Unfortunately, the only available flow data relates to a different flow mechanism to that controlling melt-flow in a fire, and it is not certain that the extrapolations and assumptions are valid.

Despite these concerns, and although basic, the model reinforces the idea that initial MW, and type and rate of MW degradation are the most significant parameters influencing gravity driven flow. It has also been confirmed that the fire models in the literature, developed based on vertical flame spread mechanisms for PMMA and timber cannot be utilised to assess the potential fire hazards of melting plastics.

7.2.2 Overall Conclusion

If a plastic undergoes RCS, then the rate of MW degradation is rapid and there is a high probability of rapid fluid formation. The level of fire hazard is probably related to the rate of MW decrease. The formation of a pool fire seems to increase the duration of the fire growth phase, lowering the overall fire hazard in comparison to non pool forming materials, but after this phase fire growth is rapid and controlled by the pool. The pool is fuelled from the vertical array by two distinct mechanisms; melting and structural collapse. The burning rate of the pool is then partly determined by the nature of flooring substrate and also the level of radiant heat feedback from the vertical array.

7.3 Recommendations for future work

The following plan for future work has been submitted to the HSE for approval.

Many thermoplastics undergo melt-flow behaviour in fires. This study has shown that as much as 75 - 80% of the original material can form a pool fire which has the potential to cause the fire to spread far beyond its original limits. It was also found that after a certain period of time, the pool fire dominates the fire growth process. This type of behaviour has been observed on numerous occasions but more data are required to enable the risk associated with the storage of significant quantities of thermoplastics to be quantified. The experiments carried out at Edinburgh University and at HSL, Buxton, were mostly on a small scale, but they provide valuable guidance on the type of work that should be done to clarify a number of relevant issues. Validation of the Sedan method is required - the most obvious method would be to compare the EHC's of plastic sections using the Cone to results from the Sedan.

The most important issue is the rapidity with which a thermoplastic fire will develop to its maximum severity. Attempts to assess the hazard of baled synthetic fabrics using the one-third scale rig (TSR) at Buxton were not wholly successful as the effect of the confining compartment began to dominate the behaviour shortly after ignition. The experiments to date indicated that there was likely to be a substantial delay between ignition and the commencement of the rapid growth stage, partly influenced by the nature of the flooring material. Indeed, it appeared that in small scale tests that a pool fire would be of limited extent on a concrete (or a wooden) floor, and would self-extinguish when the "vertical array" of material burned out or collapsed. The evidence from real fires indicates that this is unlikely to be the case when large quantities are involved. Further work is required to identify the critical conditions defining the point beyond which a plastics pool fire will become self-sustaining and not require "supporting radiation" from the remains of the original "vertical fire" as was found in the small scale tests with concrete and wooden floors. Additional work should also be undertaken to investigate whether enhanced vertical

surface burning can be achieved, using cross radiation from adjacent surfaces in the Sedan rig.

The investigation into thermoplastic fires should be continued to extend our knowledge of behaviour on a larger scale. There are many issues that need to be addressed, but the three most important appear to be:

(1) how bales of synthetic fabric behave if ignited by a range of ignition sources;
(2) how the geometrical configuration of the materials affects the rate of fire development; and
(3) what are the conditions under which a thermoplastic pool fire will continue to spread and be able to develop on a concrete floor without "supporting radiation".

These should be approached in the following manner:

(1)In the TSR, baled synthetic fabrics appeared to behave in a manner similar to standard polyurethane foam. To our knowledge, no experiments have been carried out to examine their behaviour under relatively "unconfined" conditions. A series of experiments is proposed. In the first, single bales of acrylic fabrics will be exposed to the range of BS ignition sources, primarily to observe what happens. It is not known if they will fall apart as the fire develops and the binding tape burns through, or if the material will "weld together" and preserve the form of the bale during each experiment. Selecting one ignition source, the behaviour of a bale of acrylic fabrics will be compared with a bale of "polycotton" (cotton/acrylic blend) fabrics. (In the TSR, acrylic fabrics "fail", while polycotton fabrics "pass".)

These preliminary tests will be followed by single and multiple-bale experiments in which the material is allowed to burn out. These would be carried out at HSL, Buxton. The mass-loss rate from the bales will be measured and various events noted and timed (rate at which the molten plastic spreads, rate of spread of flames over the pool, collapse (and nature of collapse) of the bale, etc.). The results will be compared with their behaviour in the TSR: this may require the materials to be tested in the TSR. If the bales retain their shape, then they can be used as the material for Part (2).

(2) Depending on the results from (1), this part of the work will be carried out using either baled synthetic fabrics or half-lengths of rolls of polythene sheeting (as used in the "Kebab" experiments). A BS ignition source (size to be determined from Part (1)) will be applied between two bales (or three rolls of sheeting) which are separated by a distance slightly greater than the width of the ignition source. Mass loss will be measured and the time to the commencement of rapid fire growth will be determined. The experiment will be repeated to determine the effect of spacing and some tests on the effect of the size of the ignition source will also be carried out. A decision whether or not to carry out larger scale tests will be taken after the results are analysed.

(3) The third series of experiments will be designed to investigate the circumstances under which a thermoplastic pool fire will become self-sustaining and enhance the rate of burning of the vertical array. There are two components, (a) the downward flow of polymer melt which "feeds" the pool, and (b) the rate of spread of the polymer melt over the horizontal surface. These are likely to be interdependent – the heat flux to the vertical surface dictating the rate of "feeding", the rate of "feeding" influencing the rate of spread of the melt, and radiation and convection from the pool fire contributing to the heat flux to the vertical array. Two approaches will be used. In the first, the Cone Calorimeter will be modified to investigate how the rate of "feeding" the pool of molten thermoplastic is affected by the imposed radiant heat flux. (Samples of polypropylene sheet 25 mm thick will be used.) This will first be carried out in the absence of flame (i.e. without igniting the fuel vapours, although spontaneous ignition may occur at the higher heat fluxes) and then with flame. In each case, the rate of mass loss from the vertical sample will be measured directly and the rate of mass gain in a partially enclosed collection tray (inerted with N_2 or CO_2 to suppress flaming) will be measured separately. The difference between the mass loss and the mass gain will be the mass lost

due to the formation of the fuel vapours. The difference between the flaming and the non-flaming tests (at the same imposed heat flux) will provide a means of estimating the additional heat flux from the flame at the surface. Additional tests will be carried out with the surface at an inclined angle (e.g. 45°) to establish if there are any significant differences in behaviour. Should such differences exist, a review of the work schedule will be carried out and appropriate adjustments made.

It would be very difficult to scale up these small-scale tests. Instead, the second approach will involve medium scale tests with bales of acrylic fabric (or 25mm thick PP sheet if the bales do not behave in a suitable manner). The bale will be ignited and the polymer melt will be allowed to burn, but the extent of the pool fire will be limited by the provision of bunded areas of different lengths normal to the burning surface. Independent tests will be carried out to determined the heat flux from the burning polymer pool to the vertical surface. (It is recognised that the "vertical" surface will be unlikely to remain vertical due to the melt-flow process, but measures will be taken to ensure that it does not slump.)

The objective of this study would be to develop a method of estimating the time available for safe egress between ignition and the onset of fast fire growth for different configurations of material. It is suggested that some tests are carried out with foamed plastics which are known to be hazardous. It is likely that these will be very difficult to work with, but the experience of working with solid thermoplastics should give an insight to methods by which useful information may be gleaned. EPS foam and standard PU foam are two obvious target materials, but as the project progresses other materials may be identified for study.

8 REFERENCES

Abbott, J.G., "Standard Laboratory Tests: How meaningful are they in assessing fire performance of insulation materials", Fire & cellular polymers, pub Elsevier Applied Science, pp. 199 – 219, 1984.

AFNOR, Epiradiateur test (NF P 92 – 501). Association de Normalisation, Paris, 1975.

Alpert, R., & Ward E.J., "Evaluation of unsprinklered fire hazards", Fire Safety Journal vol. 7 pp 127 – 143, 1984.

ASTM 84-84a Steiner Tunnel test: "Surface burning characteristics of building materials" Pub ASTM 1984

ASTM Committee E-5 on Fire Standards. "ASTM Fire Test Standards", 2nd Ed, 1988

ASTM Test Method E 1822 "Standard test method for fire testing of stacked chairs" Pub ASTM

ASTM / ANSI D 2863 –87 Standard Test Method for measuring the minimum oxygen concentration to support candle like combustion of plastics (ASTM 1977).

Atkinson, G.T., "Fire Hazards of the Polyblock scaffold system", HSE Report FR/05/001/89 Part E, February 1995

Babrauskas, V., Grayson, S.J., "Heat Release in Fires" Pub. Elsevier Applied Science, 1992.

Babrauskas, V., Peacock, R.D., "Heat Release Rate: The single most important variable in fire hazard", pp. 67 – 80, Fire Safety Developments and Testing: Toxicity, Heat Release, Product Development, Combustion Corrosivity, Fire Retardant Chemicals Association, Fall 1990 Meeting, FRCA, Lancaster, PA (1990)

Beyler, C.L., Hirschler, M.M. 'Thermal decomposition of polymers' SFPE Handbook, 2nd Ed, Section 1, Chap 7, 1995.

Blinov V.I., Khudiakov G.N., "The burning of liquid pools" Doklady Akademi Nauk SSSR, vol. 113, 1094. 1957

Brandrup, J., Immergut, E.H., "Polymer Handbook, 2nd Edition", Pub, Wiley Interscience, 1975.

Briggs, P. "New dimension testing: A review of intermediate scale testing of construction products" International Fire Protection, pp 39 – 42, 2001.

British Plastics Federation, http://www.bpf.co.uk/plaspack.htm (taken on 8/04/2000)

BS 476: Part 7: 1987 "Fire Tests on Building Materials & Structures. Part 7. Method for classification of the surface spread of flame of products." Pub BSI 1987.

BS 5306 (Fire extinguishing installations and equipment on premises) Part 2. Specification for sprinkler systems. Pub BSI

BS 5852, Part 1:1979 "Method of test for the ignitability by smokers' material of upholstered composites for seating." Pub BSI 1979

Buckinghamshire Emergency Planning Unit "Emergency Planning Report on The Milton Keynes Borough Council Materials Recycling Factory (MRF) Fire, Wed 5th June 1996"

Bucks F& RS "C.R.O.P Recycling Depot Incident Report – 5th June 1996"

Carslaw, H.S., Jaeger, J.C "Conduction of heat in solids" 2nd Ed (Chap XI), Clarendon Press, 1959

Cleveland County Fire Brigade (ADO B. Lamb) Report on Fire at 'Integral Ltd', Middlesborough (12/1/97),

Cleveland County Fire Brigade "Technical Investigation Findings, BASF South Area Stores Fire, ICI Wilton" 1996

Cogswell, F.N., "Polymer Melt Rheology, A guide for industrial practice" pub George Godwin Ltd., 1981

Control of Major Accident Hazards Regulation, (COMAH) 1999. SI 1999/743 implementing EC Council Directive 96/82 Pub HMSO SI 1999/743

Cowie, J.M.G. "Polymers: Chemistry & Physics of Modern Materials", Pub. Intertext Books, 1973

Cullis, C.F., Hirschler, M. M. "The Combustion of Organic Polymers" Pub. Clarendon Press, Oxford, 1981

D'Alelio, G.F., & Parker, J.A., "Ablative Plastics" pg. 3, pub. Marcel Dekker Inc, 1971

David, C., "Comprehensive Chemical Kinetics", (Eds. Bamford, C.H., & Tipper, C.F.H.) Vol. 14, Chap 1, p1. pub. Elsevier, 1975

DD 240: Part 1: 1997 (Draft for Development) Fire Safety Engineering in Buildings. Part 1. Guide to the application of fire safety engineering principles. Pub BSI, 1997

Debye, P., Math Vorlesungen Univ. Gottingen 6 (1914), 19.

Delichatsios, M., Panagiotou, T. et al, "The use of time to ignition data for characterising the thermal inertia and minimum (critical) heat flux for ignition or pyrolysis." Combustion and Flame, vol. 84 pp 323 – 332. 1991

DIN, Model introductory decree DIN 4102; Mitt. IfBt 9, 1978

Discussion with Dr G. Atkinson & Dr A. Tyldesley, UK HSE, June 8th 1999

Drysdale, .D.D "Introduction to fire dynamics, 2nd Ed" Pub John Wiley & Sons (1999)

Dufton, P.W. "Functional additives for the plastics industry. The effect of polymer usage on their supply and demand". ADDCON World Conference, 1998, Paper 12.

Emmons, H.W. Journal of Heat Transfer, Vol. 95, pg. 145, 1973

Encyclopaedia of polymer science & engineering. Vol. 6. Pub. John Wiley & Sons.

Federal Trade Commission; "Cellular plastic products, disclosure of combustion characteristics in Marketing & Certification;" Federal Register, Vol. 40 No 142, p 30842, July 1975

Fernandez-Pello, A. Carlos, "The Solid Phase", Chap 2. "Combustion Fundamentals of Fire", Ed Cox, G., Pub. Academic Press Ltd, 1995

FIRE "Cleveland Chemical Plant Fire", December 1995

Fire Engineers Journal, "Concern over plastic storage pallets", Nov 2000 pg. 4

Fire Investigation Report, Cressdale Ltd, Thornaby Cleveland (19/8/95), ADO S.C. Jones, Cleveland Fire Brigade

Fire Precautions Act, 1971. Guide to fire precautions in existing places of work that require a fire certificate. Factories, offices, shops and railway premises. Pub HMSO 1993

Fire Prevention No 215 "Plastic Injection Moulders, Alfreton, Derbyshire (15/3/88)" December 1988

Fire Prevention No 247 "Plastics Recycling Plant, Thetford, Norfolk 11/10/91" March 1992

Fire Prevention No 247 "Plastic Products Factory, Mansfield Woodhouse, Nottinghamshire", March 1992.

Fire Prevention No 288, "Detectors failed to operate in BASF fire", pg. 5

Fire Prevention, No 328. January 2000 Pg. 40

Foley, M., "The use of small scale fire test data for the hazard assessment of bulk materials" (PhD Thesis), University of Edinburgh (1995)

Fowell, A.J., "Fire & Flammability of furnishings & contents of buildings". Pub. ASTM, 1994

Fox, T.G & Allen, V.R., J. Chem. Phys. 41 (1964) p344

Friedman, R., "Behaviour of fires in compartments" International Symposium on Fire Safety of Combustible Materials, pp 100 – 113, Edinburgh University, 1975.

Gamal, N. Ahmed, M.A Dietenberger, Jones, W.W. "Calculating flame spread on horizontal and vertical surfaces" NISTIR 5392, Pub NIST, April 1994

Glasstone, S., Eyring H., Laidler K.J. "The theory of rate processes", Pub. McGraw Hill, 1941

Goodman, T.R. "The heat balance integral and its applications to problems involving change of phase". Trans ASME, vol. 80, No 2., pp 335 – 342 (1958)

Grant G.B. & Drysdale, D.D. "Numerical modelling of early fire spread in warehouse fires" Fire Safety Journal, vol. 24, pp. 247-278, 1995

Hands, D., Lane, K., Sheldon, R.P., J. Polymer Science, Symp No 42 (1973), pg. 717

Heskestad, G. "Luminous heights of turbulent diffusion flames" Fire Safety Journal, Vol. 5, pp 103 – 108, 1983.

Heskestad, G. "Engineering relations for fire plumes" Society of Fire Protection Engineers, Technology Report 82-8, 1982

Hiles A., "Testing the fire hazards of computer tapes", Fire Prevention 223, pp. 39–42, October 1989

Hinkley, P.L., Theobald, C.R. "PVC rooflights for venting fires in single storey buildings" Fire Research Technical Paper No. 14, (Fire Research Station) HMSO Pub. 1966

Hirschler, M.M, Trevino, J.O., "Heat release testing of stacked chairs: analysis of repeatability in a single laboratory", Fire & Materials vol. 21, pp. 85 – 93 (1997)

Hirschler, M.M., Chap 12 (a) "Heat Release in fires" Eds. Baubraskas, V., Grayson, S.J., Pub Elsevier Applied Science, London & New York, 1992

Holman, J.P., "Heat Transfer 7th Edition", McGraw Hill, 1992

Hopkins, D. Jr., "Predicting the ignition time and burning rate of thermoplastics in the Cone Calorimeter", MSc Thesis, University of Maryland, September 1995.

Horrocks, A.R., "Intumescent Additives." Notes from Polymers & Textiles in Fire Course, University of Leeds, October 1998.

HSE "Assessment of fire hazards from solid materials and the precautions required for their safe storage and use". Pub HMSO (London) 1991

HSL "Flammability testing for storage hazards: vacuum packed thermally bonded polyester wadding – LUXBOND CM" (tested March 1992)

Huggett, C., "Estimation of rate of heat release by means of oxygen consumption measurements" Pub Fire & Materials, vol. 4, No 2, pp. 61 – 65, 1980.

ICI PLC, "Diakon Technical Manual" Petrochemicals & Plastics Division, Research & Technology Division. (1985)

ISO 5660 "International Standard: Fire Tests – Reaction to Fire – Rate of Heat Release from Building Products". Pub ISO 1993

Jellinek, H.H.G. Polymer Science, Vol 4, No 13. 1949

Kandola, B.K., "An overview of flame retardency". Notes from Polymers & Textiles in Fire Course, University of Leeds, October 1998.

Kawagoe, K., "Fire behaviour in rooms", Report No 27, Building Research Institute, Tokyo 1958.

Kay, J.M., Nedderman, R.M., "Fluid Mechanics & Transfer Processes." Pub. Cambridge University Press, 1988

Kaye, G.W.C. & Laby, T.H., "Tables of Physical and Chemical constants" 14th Ed. pub. Longman 1975

Landau, G., "Heat Conduction in a melting solid" Quarterly Journal of Applied Mathematics, 8:81 (1950)

Lees, F.P. "Loss Prevention in the Process Industries: Hazard Identification Assessment and Control" 2nd Ed (3 volumes) Pub. Butterworth Heinemann 1996

Lukas, C. "Reaction to Fire Testing in Europe in 2000 & the Plastics Industry." pp. 7-14. Flame retardants 2000 Conf., Interscience Publishers, 2000

Madorsky, S.L., "Thermal Degradation of polymers" Pub. Interscience Publishers, 1964

Magee & McAlvey "The Mechanism of Flame Spread", Journal of Fire & Flammability, vol. 2, pp 271-297, 1971

Marchant, E.W., "Response of Materials & Structures to fire conditions" Fire Science & Fire Investigation Course Notes, University of Edinburgh, 1997.

Markstein, G.H. "Radiative properties of plastics fires" 17th Symposium (International) on Combustion pp 1053 – 1062, The Combustion Institute (1979)

McCaffrey B.J., "Purely buoyant diffusion flames: some experimental results" National Bureau of Standards, NBSIR 79-1910.

McLeish, T.C.B., Milner, S.T. "Entangled Dynamics and Melt Flow of Branched Polymers", Advances in Polymer Science, Vol. 143, pp 195 – 256. 1999

Messerschmidt, B. "Prediction of SBI Test Results by means of Cone Calorimeter Test Results." Interflam '99, Pub Interscience Communications, p13, 1999

Mills, N.J. "Plastics: Microstructure, Properties & Application" Edward Arnold Pub. 1986

Milovancevic, M., "Fire Behaviour of flammable products in plastic bottles and aerosol cans" Interflam 99, Volume 2 pp. 865 – 872. Interscience Communications Ltd., 1999.

National Materials Advisory Board "Fire safety aspects of polymeric materials Vol. 2., Test methods, specifications & standards." National Academy of Sciences, Washington 1979.

NFPA 231. "General Storage", Pub NFPA 17.08.1990

Ostman, B.A., Nussbaum, R.M., "Correlation between small scale rate of heat release and full scale room flashover for surface linings," Fire Safety Science- Proc. of the 2nd International Symposium on Fire Safety Science, pp 823 – 832 Hemisphere Publishing Co., 1988

Ozisik, M. Necati "Boundary value problems of heat conduction", Dover Publications Inc, 1989

Paul, K.T., "Cone Calorimeter: Initial Experiences of Calibration and Use", Fire Safety Journal, 1994

Paul, K.T., "Demonstration of the effect of softening and fire resistance of materials on burning characteristics", Fire & Materials pp. 83 – 86, vol. 4, No 2 (1980)

Pearson, J.R.A. "Mechanical Principles of Polymer Melt Processing" Pub Pergamon Press, 1966

Persson, B., Wetterlund, I. "Tentative guidelines for calibration and use of HF meters" NORDTEST Project No 1291-96 SP Report 1997:33

Price, D. "Fundamentals of Polymer Combustion", Paper 1, Polymers & Textiles in Fires Course, University of Leeds. 27-29 October 1998.

Private Communication from Dr I. Robinson, ICI Acrylics, 1999

Private Communication from Mr. I. McIlwee, Business Research Officer, British Plastics Federation, April 2000.

Private Communication, ADO Wilson, Staffs F& RS. (May 2000)

Private Communication – D.C.O W. R. Tucker, Director of Operations, Bucks F&RS (April 2000)

Private communication (Re: B & J Parr Ltd, Mansfield Woodhouse (6.5.91)), Stn.O. P. Sisson, Headquarters, Nottinghamshire Fire & Rescue Service

Private communication, Mr. Adair Lewis, Fire Protection Association (06/06/01)

Private communication, Mr. C. Swanson, BP Chemicals, Grangemouth

Private communication, Mr. S. Whitman, Waste Services Officer, Solihull Borough Council.

Quintiere, J. "A semi-quantitative model for the burning of solid materials", NIST 4840, June 1992

RB Hawkins & Associates, "Report Into The Contamination Aspects Of Debris Removal From The MRF Site", Plastic Recycling Plant Fire, Old Wolverton, 5 June 1996

Rogers, G.F.C., Mayhew, Y.R., "Thermodynamic & transport properties of fluids 4th Ed" Pub. Blackwell, 1993

Saito, K., Quintiere, J.G., Williams, F.A., Proceedings of the First International Symposium of Fire Safety Science, Hemisphere Publications, 1986.

Sakiadis, B.C., Coates J., A.I. Chem E., Journal (1956), 88

Staggs, J.E.J., "A discussion of modelling idealised ablative materials with particular reference to fire testing", Fire Safety Journal, 18 pg. 89 (1994)

Summary UK Annual Fire Statistics, 1998 Published 8/9/99 by HMSO, UK Home Office

Sundstrom, B., "European Classification of Building Products" Interflam 99, Volume 2 Interscience Communications Ltd., 1999.

taken from http://www.bpamoco.co.uk/polyethylene (on 04/01/01)

TARGOR Polypropylene Technology "Summary report on ICI Wilton site fire, 9 October 1995", Nov 97

Technical Investigation findings, BASF South Area Stores, ICI Wilton", Cleveland County Fire Brigade. 1997

Test video kindly supplied by Dr J. DeHaan, Fire-Ex Forensics Inc, 2000.

Tewarson, A., "Generation of heat & chemical compounds in fires", Sect 1, Chap 13, The SFPE Handbook of Fire Protection Engineering, Pub NFPA 1988

Tewarson, A., Pion, R.F., "Flammability of Plastics 1. Burning Intensity." Combustion & Flame, vol. 26 pp 85-103 (1976)

Textiles Industry Advisory Committee "Fire Precautions in the clothing and textile industries" Pub Health & Safety Commission, HSE 2000

The Construction Products Directive (CPD) 89/106/EEC (1989)

The Management of Health & Safety at Work Regulations, 1992. No. 2051 .Pub HMSO

Thomas P.H. "Testing products and materials for their contribution to flashover in rooms" Fire and Materials, Vol. 5 pp 103 – 111. 1981

Thomson, H.E., Drysdale, D.D. "Flammability of Plastics. I: Ignition Temperatures", Fire and Materials, Vol. 11, pp 163 – 172. 1987

Thomson, H.E., Drysdale, D.D., "Effect of sample orientation on the piloted ignition of PMMA" Interflam '90 Proceedings of the 5th International Fire Conference. Pub Interscience Communications Ltd., 1990

Thomson, H.E., Drysdale, D.D., "The ignitability of flame retarded plastics" Proceedings of the Fourth International Symposium on Fire Safety Science, pp 195 – 204, pub IAFSS, 1994.

Thornton, W.M. "The relation of oxygen to the heat of combustion of organic compounds." Pub Philosophical Magazine, vol. 33, pp. 196 – 203, 1917

Troitzsch, J., "International Plastics Flammability Handbook", 2nd Ed, Hanser Pub, Munich. 1990.

Van Krevelen, D.W & Hoftyzer P.J., Angew Makromol. Chem 52 (1976) 101

Van Krevelen, D.W., "Properties of Polymers: Their estimation & correlation with chemical structure.2nd Ed" Pub. Elsevier, 1976

Ward, R.B. "The warehouse scandal. Survey of large fires in sprinklered and non-sprinklered warehouses & storage areas". Fire Prevention, 177, (March 1985).

Wharton, R.K., "A medium scale test method for assessing the fire hazard of flammable solid materials" Journal of Loss Prevention in the Process Industries, vol 3 pp 349 – 354, 1990

Whiting, P., Dowden J.M., "A one dimensional mathematical model of laser induced thermal ablation of biological tissue", Lasers in medical science, 7 pp 357 – 368 (1992)

Woolley, W.D, Raftery, M.M., Ames, S.A., "The behaviour of stacking chairs in fire tests", BRE Current Paper CP 10/79, Building Research Establishment 1979.

Zabetakis M.G., Burgess D.S. "Research on the hazards associated with the production and handling of liquid hydrogen" US Bureau of Mines RI5707, Pittsburgh, PA (1961)

Zhang, J., Shields, T.J, Silcock, G.W.H., "Effect of melting behaviour on flame spread of thermoplastics" Fire & Materials Vol.21, No. 1, Jan - Feb 1997 pp 1 - 6

Material	Applied Q	tIgnition	Test Time	Total HR	Original Mass	Pk RHR	t(Pk RHR)	Rec Mass Loss	EHC(kJ/g)	MLR50	TEST ID
CYREX200	20	206	570	8.81E-02	51.49	368.603	320	32.9729	22.6	0.1528	6792003
CYREX200	20	217	535	7.41E-02	50.94	413.397	320	30.0728	23.5	0.1638	6792002
CYREX200	20	224	565	6.89E-02	51.36	451.137	325	31.5683	26.6	0.1576	6799200
DUROLON PC	20	228	755	0.13984	55	268.675	495	51.5085	30.4163	0.0367	7799dpc2
DUROLON PC	20	631	980	0	53.89	298.688	755	52.76285	22.7381	FALSE	7799dpc1
DUROLON PC	20	NO	620	0.16441	55.11	9.119	245	55.11	16.2835	0.0046	7799dpc3
HDPE LUPOLEN	20	259	600	7.49E-02	39.41	330.691	415	38.6391	17.8	0.0646	6799l2
HDPE LUPOLEN	20	288	560	0.05705	39.62	253.17	425	25.71515	18.2	FALSE	6799l1
HDPE LUPOLEN	20	293	645	7.62E-02	39.33	283.426	440	38.6422	16.3	0.0454	6799l3
HMW PMMA	20	196	965	0	55.75	424.297	440	54.8791	25.4402	0.1333	7799hmw2
HMW PMMA	20	211	985	0	57.6	424.603	465	56.586	25.0981	0.1523	7799hmw3
HMW PMMA	20	225	1000	0.20186	60	412.992	495	58.7943	24.9692	0.1604	7799hmw1
PETG	20	315	485	0	53.25	218.69	330	52.5514	5.29	FALSE	6799pet2
PETG	20	361	505	3.08E-02	53.53	231.56	385	52.1189	5.56	FALSE	6799pet3
PETG	20	NO	600	0.13243	52.79	1.338	240	52.79	0.76	0.0094	6799pet1
POLYMAN PS185K	20	199	485	0	45.78	521.058	300	45.2808	23.7	0.1174	6799p1
POLYMAN PS185K	20	203	510	7.81E-02	46.58	558.863	300	12.4565	32.3	0.1366	7799p2
POLYMAN PXC 31	20	NO	605	0.16085	51.8	6.539	5	51.8	26.66	0.0006	7799311
POLYMAN PXC 31	20	NO	575	0.15176	52.02	6.899	5	-8.686848	40.2681	0.0046	7799312
POLYMAN PXC 31	20	NO	1060	0.28307	51.23	5.164	5	-6.704201	12.6726	1E-05	7799313
POLYMN PCXP41RS	20	NO	490	0	56.5	7.173	330	56.5	15.3856	0.0273	7799411
POLYMN PCXP41RS	20	NO	975	0	51.01	10.626	5	51.01	34.5386	0.0011	7799413
POLYMN PCXP41RS	20	NO	580	0	49.74	7.206	10	49.74	24.8228	0.0011	7799412
POLYSTROL HI NT	20	207	590	0	41.98	689.502	295	41.12715	32.0767	0.2191	7799phn3
POLYSTROL HI NT	20	235	650	0.1065	41.97	652.928	325	32.0738	32.6415	0.2025	7799phn2
POLYSTROL HI NT	20	245	615	9.28E-02	42	682.407	345	28.3476	32.8117	0.2013	7799phn1
PP NOVOLEN 1100H	20	168	580	0	38.02	368.833	315	37.6226	24.4	0.1802	6799n2
PP NOVOLEN 1100H	20	175	985	0	37.13	374.703	320	36.58335	26.2	0.057	6799n3
PP NOVOLEN 1100H	20	184	1035	0.18574	37.57	219.17	305	36.9509	43.5	0.0193	6799n1
PS MUSTER	20	151	575	0.10856	44.7	563.967	290	24.0991	27.8063	0.3056	7799mus1
PS MUSTER	20	196	550	0.09111	44.34	530.689	305	29.9722	24.8933	0.1766	7799mus3
PS MUSTER	20	198	575	0.0974	44.26	572.377	295	29.41634	25.6802	0.3187	7799mus2
UPVC	20	NO	585	0	61.69	4.505	580	0	0	0.0127	6799pvc1
UPVC	20	NO	590	0	61.18	5.875	590	61.18	2.08076	0.0695	6799pvc2
UPVC	20	NO	1175	0.25951	61.74	7.661	1160	22.5772	0.76388	0.0474	6799pvc3

Material	Applied Q	tIgnition	Test Time	Total HR	Original Mass	Pk RHR	t(Pk RHR)	Rec Mass Loss	EHC(kJ/g)	MLR50	TEST ID
CYREX200	25	165	910	1091.27	52	363.356	250	47.2131	22.2346		7E+07
CYREX200	25	168	840	1032.31	51.5	368.454	245	45.22625	22.1085		7E+07
CYREX200	25	178	915	0	53	358.818	300	0	22.1147		7E+07
DUROLON PC	25	0	1170	2.94655	56.3	5.984	10	1.5839	2.81027		121dpc18
DUROLON PC	25	0	1695	19.8719	56.35	5.105	10	2.088749	4.25962		1101dpc7
DUROLON PC	25	0	990	13.5667	54.74	2.913	10	1.410751	4.62752		1101dpc6
HDPE LUPOLEN	25	188	690	356.285	38.5	205.498	335	30.72095	15.1141		1201l17
HDPE LUPOLEN	25	196	1260	434.235	37.5	223.136	310	26.9201	15.1995		1201l18
HDPE LUPOLEN	25	212	715	375.973	37.8	250.328	350	25.4232	15.805		1201l16
HMW PMMA	25	139	980	1679.64	73	408.29	410	74.16705	21.6964		701HMW18
HMW PMMA	25	142	1105	1654.13	72.3	401.364	400	74.55605	21.3139		701HMW17
HMW PMMA	25	143	1085	1605.73	72	401.889	470	72.1499	21.5145		701HMW16
lmw pmma	25	147	870	1586.12	71	456.912	445	67.9593	22.3884		701LMW18
lmw pmma	25	150	835	1547.84	69	455.595	435	66.2657	22.6436		701LMW16
lmw pmma	25	157	1020	1581.65	69	431.626	450	67.6081	22.1962		701LMW17
PETG	25	282	495	288.101	52.1	359.483	335	30.98895	4.60827		701PET17
PETG	25	285	750	341.187	51.6	241.466	320	36.6271	7.98056		701PET16
PETG	25	321	545	146.641	53	201.503	355	30.9612	2.1196		701PET18
POLYMAN PS185K	25	157	700	922.277	44.5	610.403	250	35.4533	25.196		1201p17
POLYMAN PS185K	25	163	905	820.751	44.52	530.708	280	28.098	28.1667		1201p16
POLYMAN PS185K	25	171	770	800.285	43.94	521.08	245	20.74115	32.3351		1201p18
POLYMAN PXC 31	25	0	1870	0.64285	52.55	5.907	10	2.5858	2.1894		1.1E+07
POLYMAN PXC 31	25	0	990	0	51.66	5.894	10	0	1.75069		1.1E+07
POLYMAN PXC 31	25	0	985	50.745	51.58	8.123	940	2.2416	6.60184		1.1E+07
POLYMN PCXP41RS	25	0	585	0.17698	50.44	1.946	10	1.701401	0.19791		1241117
POLYMN PCXP41RS	25	11	885	4.57795	51.5	6.662	765	1.40155	1.47283		1214116
POLYSTROL HI NT	25	181	865	1150.77	42.5	610.591	280	39.30845	27.914		701PHN16
POLYSTROL HI NT	25	191	775	1196.04	42.7	599.496	295	41.9219	27.5383		701PHN17
POLYSTROL HI NT	25	194	835	1148.98	43.03	605.161	295	40.687	27.6413		701PHN18
PP NOVOLEN 1100H	25	116	660	557.628	36.9	268.967	235	15.4555	37.2321		12n18
PP NOVOLEN 1100H	25	118	690	487.669	37.6	256.787	240	17.7489	31.255		121n17
PP NOVOLEN 1100H	25	123	830	498.31	36.9	261.238	250	22.0682	24.7135		121p16
PS MUSTER	25	160	640	720.305	43.6	553.247	290	27.1969	25.968		12mus18
PS MUSTER	25	164	520	845.165	44.4	597.408	285	30.4182	20.4104		12mus16
PS MUSTER	25	173	675	680.917	45.5	450.767	305	22.7444	29.1221		12mus17
UPVC	25	0	985	23.9738	60.92	5.023	10	33.6208	2.31994		121pvc18
UPVC	25	0	3580	171.364	62.22	9.733	2600	47.6346	0.72562		701PVC17
UPVC	25	214	2005	52.4564	61.36	19.319	225	37.77	1.1068		701PVC16

CONE CALORIMETER DATABASE: COMPLETE RESULT SET

Material	Applied Q	tignition	Test Time	Total HR	Original Mass	Pk RHR	t(Pk RHR)	Rec Mass Loss	EHC(kJ/g)	MLR50	TEST ID
CYREX200	30	101	730	0.16263	52.74	441.777	180	51.6832	23.3055	0.0582	8.8E+07
CYREX200	30	103	685	0	53.14	448.305	290	0	23.9896	0.0926	8.8E+07
DUROLON PC	30	218	1110	1.02E+03	56.2	367.333	395	42.61625	20.9945	0.0201	9799dpc4
DUROLON PC	30	299	1050	8.68E+02	55.71	412.728	375	38.0012	21.3395	0.0709	9799dpc5
DUROLON PC	30	365	825	7.05E+02	55.15	389.193	470	35.88645	21.5668	0.1825	9799dpc6
HDPE LUPOLEN	30	130	740	4.64E+02	38.87	336.153	265	31.48635	15.2801	0.0177	9799l4
HDPE LUPOLEN	30	131	940	4.81E+02	39.01	328.944	260	40.3135	10.0357	0.0079	9799l6
HDPE LUPOLEN	30	142	1095	5.12E+02	51.75	408.834	255	36.2815	15.0967	0.0077	9799l5
HMW PMMA	30	87	655	0.14725	52.99	539.669	300	52.2473	24.0127	0.1539	8799hmw5
HMW PMMA	30	88	715	0.16051	52.99	533.878	300	52.381	24.0692	0.0605	8799hmw6
HMW PMMA	30	91	605	0.12903	51.35	535.168	300	48.6903	24.0256	0.2206	8799hmw4
PETG	30	160	645	1.26E-01	52.3	288.719	215	28.02505	7.42676	0.0254	8799pet6
PETG	30	174	550	9.89E-02	53.41	275.594	215	44.73255	5.9956	0.0752	8799pet4
PETG	30	197	675	0.00E+00	52.31	298.884	225	49.8345	5.08987	0.0168	8799pet5
POLYMAN PS185K	30	93	545	0.11549	44.76	661.298	185	35.0358	24.8868	0.1088	8799p4
POLYMAN PS185K	30	104	510	0.10517	44.68	668.968	195	35.1599	25.0395	0.1259	8799p5
POLYMAN PS185K	30	107	565	0.11698	44.26	646.96	190	36.5485	24.4612	0.0692	8799p6
POLYMAN PXC31	30	215	1000	0.20391	50.95	365.413	340	49.1263	19.1265	0.0143	8799315
POLYMAN PXC31	30	245	1325	0	51.06	307.444	320	49.5122	19.1069	0.0162	8799316
POLYMAN PXC31	30	258	995	0	53.22	413.206	420	51.9579	21.194	0.3297	8799314
POLYMN PCXP41RS	30	157	1330	3.18E-01	50.21	439.564	305	50.3891	27.1501	0.0151	9799415
POLYMN PCXP41RS	30	205	1015	2.16E-01	50.39	440.311	330	32.8883	27.4891	0.0438	9799414
POLYMN PCXP41RS	30	218	990	2.08E-01	49.94	408.263	315	7.1251	35.9685	0.9142	9799416
POLYSTROL HI NT	30	103	540	1.11E-01	42.38	734.068	195	35.4805	29.8315	0.117	8799phn6
POLYSTROL HI NT	30	108	600	1.28E-01	41.96	778.813	215	41.3718	30.906	0.0736	8799phn4
POLYSTROL HI NT	30	109	560	1.15E-01	42.22	763.031	210	34.3183	30.3532	0.1091	8799phn5
PP NOVOLEN 1100H	30	75	710	517.001	37.66	403.001	185	25.8603	20.2377	0.0101	9799n4
PP NOVOLEN 1100H	30	75	700	526.61	37.63	410.681	190	28.0822	18.7851	0.0126	9799n6
PP NOVOLEN 1100H	30	80	955	571.45	37.72	421.743	195	32.0807	17.5099	0.007	9799n5
PS MUSTER	30	88	665	0.15282	44.67	733.828	190	33.38395	26.3865	0.0695	9799mus6
PS MUSTER	30	91	1175	0.00E+00	43.73	741.113	185	43.1137	25.777	0.0042	9799mus4
PS MUSTER	30	91	865	0.00E+00	44.74	759.267	185	44.3819	26.4193	0.0285	9799mus5
UPVC	30	109	600	1.33E-01	64.23	60.482	115	62.96731	1.30118	0.0879	8799pvc5
UPVC	30	129	590	0.00E+00	62.08	33.676	135	59.1091	1.37859	0.0821	8799pvc4
UPVC	30	590	590	0.00E+00	61.16	71.008	250	61.16	14.5638	1E-05	8799pvc6

Material	Applied Q	tignition	Test Time	Total HR	Original Mass	Pk RHR	t(Pk RHR)	Rec Mass Loss	EHC(kJ/g)	MLR50	TEST ID
CYREX200	40	60	615	1.16E+03	50.36	570.961	130	49.3798	23.1791	0.0309	9.8E+07
CYREX200	40	62	685	1.25E+03	53.32	543.846	230	53.0003	22.6942	0.0376	9.8E+07
DUROLON PC	40	110	1005	1.08E+03	55.06	412.146	285	43.72895	21.9093	0.0201	197dpc7
DUROLON PC	40	114	805	9.63E+02	54.91	386.665	295	40.27185	21.747	0.0253	197dpc8
DUROLON PC	40	130	990	1.13E+03	55.83	439.476	310	46.4046	21.3265	0.0177	197dpc9
HDPE LUPOLEN	40	75	890	5.44E+02	39.4	403.12	180	36.0849	14.4443	0.0052	207l7
HDPE LUPOLEN	40	80	925	5.91E+02	39.35	378.433	180	31.85085	18.2335	0.0138	207l9
HDPE LUPOLEN	40	82	845	5.81E+02	38.99	442.354	190	34.0839	15.7684	0.0061	207l8
HMW PMMA	40	46	700	1.40E+03	57.39	664.938	220	58.0609	24.3183	0.0468	9799hmw8
HMW PMMA	40	47	675	1.34E+03	52.31	671.48	205	52.6124	25.0395	0.0366	9799hmw7
HMW PMMA	40	47	670	1.34E+03	54.29	641.522	230	57.8713	22.7884	0.0533	9799hmw9
PETG	40	105	505	4.03E+02	52.97	427.118	185	44.5529	8.4471	0.0706	197petg7
PETG	40	106	440	4.49E+02	52.92	464.517	150	41.0182	10.0395	0.067	197petg9
PETG	40	114	340	2.24E+02	52.61	347.069	145	32.3529	6.55107	0.2168	197petg8
POLYMAN PS185K	40	50	605	8.86E+02	44.84	729.849	160	38.3484	23.8068	0.0162	197p7
POLYMAN PS185K	40	64	910	9.76E+02	45.75	763.746	130	41.0106	25.6916	0.0063	207p9
POLYMAN PS185K	40	65	540	9.34E+02	46.85	717.138	135	39.7841	24.1447	0.0377	197p8
POLYMAN PXC 31	40	119	910	1.10E+03	53.11	442.582	295	47.3293	22.4326	0.0217	2E+07
POLYMAN PXC 31	40	122	995	1.04E+03	52.67	515.946	220	42.791	36.6421	0.0153	2E+07
POLYMAN PXC 31	40	123	620	9.06E+02	51.5	481.125	255	39.6773	34.9998	0.6694	2E+07
POLYMN PCXP41RS	40	22	840	9.17E+02	49.85	365.363	230	40.6903	15.5189	0.0122	2E+07
POLYMN PCXP41RS	40	103	875	9.50E+02	50.57	401.832	240	40.4243	20.7339	0.1602	2E+07
POLYMN PCXP41RS	40	105	945	9.46E+02	49.82	381.922	270	39.1549	21.9175	0.0129	2E+07
POLYSTROL HI NT	40	59	565	9.97E+02	41.77	760.151	150	35.6798	27.5475	0.0306	197phn8
POLYSTROL HI NT	40	61	585	1.06E+03	42.14	719.89	160	38.309	27.1423	0.0375	197phn9
POLYSTROL HI NT	40	66	475	1.14E+03	41.57	779.782	160	39.3461	28.4918	0.0989	197phn7
PP NOVOLEN 1100H	40	49	670	6.20E+02	37.12	495.944	145	31.9172	20.4695	0.0186	207n8
PP NOVOLEN 1100H	40	51	940	6.09E+02	36.55	478.959	150	26.4407	24.2909	0.0014	207n7
PP NOVOLEN 1100H	40	51	915	6.74E+02	36.62	521.721	150	30.068	21.95	0.0079	207n9
PS MUSTER	40	56	620	9.97E+02	44.58	782.729	140	40.17149	25.888	0.0396	197mus8
PS MUSTER	40	58	745	1.08E+03	44.5	791.447	150	41.5404	26.5465	0.0163	197mus7
PS MUSTER	40	61	700	1.02E+03	44.54	780.717	150	40.31315	25.3386	0.0119	197mus9
UPVC	40	47	585	9.95E+01	61.74	89.829	85	43.2424	2.3264	0.0916	19799pv8
UPVC	40	86	585	1.54E+02	62.11	166.055	240	36.6089	3.37014	0.0771	19799pv7
UPVC	40	152	585	2.17E+02	61.11	117.476	250	29.7546	7.76618	0.0831	19799pv9

Material	Applied Q	tignition	Test Time	Total HR	Original Mass	Pk RHR	t(Pk RHR)	Rec Mass Loss	EHC(kJ/g)	MLR50	TEST ID
CYREX200	50	40	670	1.17E+03	51.4	517.949	110	50.1984	22.1312	0.036	2.1E+07
CYREX200	50	47	500	1.13E+03	49.98	540.005	105	47.1892	23.026	0.0703	2.1E+07
DUROLON PC	50	85	985	1.01E+03	53.48	387.794	250	45.3596	19.2962	0.0164	207dpc12
DUROLON PC	50	88	750	9.50E+02	55.72	394.234	250	42.5218	20.0745	0.0213	207dpc10
DUROLON PC	50	92	985	1.17E+03	54.04	442.326	260	49.5229	20.1633	0.0182	207dpc11
HDPE LUPOLEN	50	53	700	5.62E+02	37.55	450.73	145	23.228	23.1857	0.0122	217l10
HDPE LUPOLEN	50	53	530	5.17E+02	37.93	562.209	150	17.28525	26.0183	0.001	217l11
HMW PMMA	50	33	475	1.28E+03	61	559.002	215	61.8957	20.5024	0.2002	207hmw11
HMW PMMA	50	35	540	1.09E+03	50.75	578.32	175	52.0785	20.7999	0.0744	207hmw10
HMW PMMA	50	35	460	1.00E+03	48.55	565.305	165	50.1483	19.842	0.1011	207hmw12
PETG	50	72	445	3.89E+02	53.27	457.168	115	29.0061	12.6647	0.0306	217pet10
PETG	50	74	550	3.12E+02	53.03	319.536	115	40.21265	6.87322	0.0288	217pet11
PETG	50	75	695	3.02E+02	53.5	282.757	110	40.3398	6.59841	0.023	217pet12
POLYMAN PS185K	50	41	600	1.10E+03	45.51	689.407	115	41.7271	26.7569	0.0322	217p11
POLYMAN PS185K	50	42	860	8.81E+02	46.42	636.849	130	36.2578	28.1351	0.0204	217p12
POLYMAN PS185K	50	43	720	1.01E+03	45.27	709.844	125	38.6849	27.4836	0.0232	217p10
POLYMAN PXC 31	50	79	590	9.83E+02	53.43	438.325	180	43.6238	30.7128	1.9246	2073110
POLYMAN PXC 31	50	80	895	1.04E+03	52.29	508.629	180	44.3411	33.4157	0.0175	2073111
POLYMAN PXC 31	50	83	905	1.12E+03	52.47	461.951	180	47.8925	24.7831	0.0189	2073112
POLYMN PCXP41RS	50	69	1005	1.26E+03	50.02	617.667	180	51.01115	43.3398	0.0212	2174112
POLYMN PCXP41RS	50	74	985	9.95E+02	50.46	366.927	170	44.4321	21.4702	0.0169	2074110
POLYMN PCXP41RS	50	75	745	9.29E+02	49.47	398.995	230	43.1681	33.1901	0.0255	2074111
POLYSTROL HI NT	50	40	455	1.09E+03	41.77	765.68	125	41.8338	26.1957	0.0566	207phn11
POLYSTROL HI NT	50	40	820	1.10E+03	42.09	736.119	115	44.27015	25.3087	0.0127	507phn12
POLYSTROL HI NT	50	43	895	1.12E+03	42.48	811.946	120	42.3102	27.0274	0.0072	207phn10
PP NOVOLEN 1100H	50	32	760	7.22E+02	37.35	518.976	130	26.9423	31.1489	0.0446	217n10
PP NOVOLEN 1100H	50	34	655	7.34E+02	37.46	630.58	130	27.3159	29.5994	0.0162	217n12
PP NOVOLEN 1100H	50	36	995	8.52E+02	36.7	531.949	125	76.5988	32.0541	0.0113	217n11
PS MUSTER	50	40	410	9.26E+02	44.53	694.954	110	37.9674	25.0551	0.0675	217mus11
PS MUSTER	50	43	905	1.06E+03	44.19	750.358	115	42.5717	26.9732	0.0195	217mus10
PS MUSTER	50	43	1065	1.05E+03	44.85	744.28	115	42.8825	29.1524	0.0228	217mus12
UPVC	50	31	985	5.55E+02	62.95	165.165	145	52.33595	8.97053	0.0375	217upvc0
UPVC	50	54	985	2.78E+02	62.33	100.583	65	51.1737	2.16238	0.0366	217pvc12
UPVC	50	56	1185	5.88E+02	62.3	155.697	95	51.2521	9.62864	0.018	217pvc11

Material	Applied Q	tignition	Test Time	Total HR	Original Mass	Pk RHR	t(Pk RHR)	Rec Mass Loss	EHC(kJ/g)	MLR50	TEST ID
CYREX200	60	24	870	1.02E+03	52.35	475.758	100	54.301	17.6296	0.0095	2.4E+07
CYREX200	60	25	610	1.15E+03	51.39	540.36	90	51.5999	20.7918	0.0203	2.4E+07
DUROLON PC	60	54	1185	1.18E+03	54.88	469.416	200	46.514	22.7723	0.0204	267dpc13
DUROLON PC	60	66	1335	1.46E+03	53.63	585.684	210	52.9831	22.8247	0.0195	267dpc14
DUROLON PC	60	91	1185	1.47E+03	57.16	599.106	225	51.6391	23.8823	0.0189	267dpc15
HDPE LUPOLEN	60	48	1770	1108.07	36	710.666	155	36.8009	30.7146		601LC
HDPE LUPOLEN	60	48	935	791.911	40	688.199	150	29.3582	25.2161		601LA
HDPE LUPOLEN	60	49	1260	750.973	40	471.324	150	28.9561	24.5844		601LB
HMW PMMA	60	24	775	1696.34	69.8	896.899	230	74.8406	22.0186		601HMWA
HMW PMMA	60	27	630	1557.32	66	887.887	230	66.55775	22.496		601HMWC
HMW PMMA	60	27	880	1764.64	72.5	885.132	240	75.1628	22.1419		601HMWB
low mw pmma	60	29	495	1571.04	69	863.824	225	66.7488	22.3494		601LMWC
low mw pmma	60	30	545	1576.44	68	860.236	225	67.8532	22.1678		601LMWB
low mw pmma	60	30	565	1656.36	6	808.046	260	70.8945	22.0918		601LMWA
PETG	60	50	985	6.00E+02	53.6	378.359	105	33.8959	15.4389	0.0131	267pet15
PETG	60	53	600	5.78E+02	53.29	632.788	120	46.4547	11.7263	0.0255	267pet14
PETG	60	56	985	6.06E+02	53.03	487.167	105	31.9343	16.4848	0.0167	267pet13
POLYMAN PS185K	60	35	1220	1148.92	45.3	955.493	145	43.81355	25.5459		601PB
POLYMAN PS185K	60	35	1185	1225.95	45.8	973.299	160	46.4613	25.6914		601PA
POLYMAN PS185K	60	38	640	1146.35	46.3	993.618	135	44.4576	25.6357		601PC
POLYMAN PXC 31	60	59	1105	1.07E+03	52.38	490.385	155	46.6833	18.4875	0.0191	2373113
POLYMAN PXC 31	60	61	985	1.01E+03	52.8	464.174	160	44.6991	19.2124	0.0166	2373114
POLYMAN PXC 31	60	68	1005	1.01E+03	53.12	458.101	175	45.3429	18.9046	0.0214	2373115
POLYMN PCXP41RS	60	48	1185	1.23E+03	50.68	549.145	155	43.12155	26.3974	0.0205	2674114
POLYMN PCXP41RS	60	58	985	9.01E+02	49.76	413.637	150	40.8965	18.4533	0.0204	2374113
POLYMN PCXP41RS	60	61	1460	1.30E+03	51.67	557.651	175	45.1508	25.4829	0.0096	2674115
POLYSTROL HI NT	60	27	835	7.44E+02	41.9	559.911	90	38.863	18.2012	0.0098	237phn13
POLYSTROL HI NT	60	32	925	7.55E+02	42.81	502.551	90	40.5475	17.7058	0.0062	237phn14
PP NOVOLEN 1100H	60	28	1115	1132.41	37	700.595	150	32.8416	33.6236		601NB
PP NOVOLEN 1100H	60	30	1985	1010.32	36.6	564.21	130	31.4555	31.5175		601NC
PP NOVOLEN 1100H	60	30	685	629.373	36.5	475.186	125	22.7434	28.9538		601NA
PS MUSTER	60	35	1195	1184.85	44.6	1024.469	145	43.5046	26.0292		601MUSC
PS MUSTER	60	35	1220	1162.74	44.5	791.191	145	43.573	25.8192		601MUSB
PS MUSTER	60	35	1195	1056.97	43.9	899.738	150	42.6179	25.1113		601MUSA
UPVC	60	28	985	5.66E+02	62.36	188.225	80	53.794	7.58354	0.0325	267pvc14
UPVC	60	32	1185	6.31E+02	60.93	201.11	65	54.5004	9.67396	0.0166	267pvc13
UPVC	60	47	990	5.83E+02	63.2	165.024	215	54.2434	8.68528	0.0274	267pvc15

CONE CALORIMETER DATABASE: COMPLETE RESULT SET

Material	Applied Q	t ign	Test Time	Total HR	Original Mass	Pk RHR	t(Pk RHR)	Rec Mass Loss	EHC(kJ/g)	MLR50
DUROLON PC	20	0	987.5	25.372485	51.62	7.0085	475	1.1208	4.176263333	#DIV/0!
HDPE	20	64	778.3333333	385.1749746	48.14666667	206.3996667	351.6666667	14.13713367	9.861582778	#DIV/0!
PS MUSTER	20	88.6666667	658.3333333	0.145593633	52.44333333	536.2383333	300	51.1062	24.03584333	0.145018333
PS 185K	20	102	707.5	0.08131565	52.94	445.041	235	25.8416	23.647535	0.075405
PETG	20	105	2120	74.6067	58.7	160.8993333	1000	45.94216667	8.538255	0.04168
CYREX200 PC ALL	20	133.666667	720	568.7610667	39.36666667	357.0906667	260	22.338	27.31213778	#DIV/0!
POLYPROPYLENE	20	140.666667	841.6666667	340.7488771	54.02666667	419.1383333	288.3333333	31.43315	22.76318667	0.056976667
HMW PMMA	20	167	756.6666667	967.5497667	40.87666667	491.208	275	32.68813333	30.80388111	#DIV/0!
POLYSTYROL	20	208.666667	835	550.1473667	44.34333333	351.43	331.6666667	35.89543333	15.62753667	0.069376667
PC XP41 RS	20	NO	726.6666667	516.6851167	50.27333333	351.066	200	28.9278	17.284145	#DIV/0!
PXC 31	20	NO	623.3333333	0.07495409	52.67333333	287.7323333	218.3333333	40.86403333	6.170745667	0.039123667
UPVC	20	NO	540	0.112547067	44.56666667	659.0753333	190	35.5814	24.79584	0.101303333
POLYPROPYLENE	25	119	726.6666667	514.5355333	37.13333333	262.3306667	241.6666667	18.4242	31.066825	
HMW PMMA	25	141.333333	1056.666667	1646.496	72.43333333	403.8476667	426.6666667	73.62433333	21.50826333	
LMW PMMA	25	151.333333	908.3333333	1571.868333	69.66666667	448.0443333	443.3333333	67.2777	22.40940722	
PS 185K	25	163.666667	791.6666667	847.7710333	44.32	554.0636667	258.3333333	28.09748333	28.56593611	
PS MUSTER	25	165.666667	611.6666667	748.7955	44.5	533.8073333	293.3333333	26.7865	25.166835	
CYREX200 PC ALL	25	170.333333	888.3333333	707.861	52.16666667	363.5426667	265	30.81311667	22.15256833	
POLYSTYROL	25	188.666667	825	748.7955	42.74333333	605.0826667	290	40.63911667	27.69786389	
HDPE	25	198.666667	888.3333333	388.8312667	37.93333333	226.3206667	331.6666667	27.68808333	15.372865	
PETG	25	296	596.6666667	258.6426667	52.23333333	267.484	336.6666667	32.85908333	4.902807778	
UPVC	25	NO IGNITION	2190	82.59795	61.5	11.35833333	945	39.67513333	1.38412	
PC XP41 RS	25	NO IGNITION	735	2.37746195	50.97	4.304	387.5	1.5514755	0.835366667	
PXC 31	25	NO IGNITION	1281.666667	17.1292729	51.93	6.641333333	320	1.609133333	3.513974444	
DUROLON PC	25	NO IGNITION	1285	12.12837967	55.79666667	4.667333333	10	1.694466667	3.899136111	

Material	Applied Q	t ign	Test Time	Total HR	Original Mass	Pk RHR	t(Pk RHR)	Rec Mass Loss	EHC(kJ/g)	MLR50
POLYPROPYLENE	30	46.6666667	681.6666667	1361.680333	54.66333333	659.3133333	218.3333333	56.18153333	24.04871333	0.045581667
PS 185K	30	59.3333333	636.6666667	1188.806667	51.08666667	553.7416667	191.6666667	50.7311	22.79001667	0.034008333
UPVC	30	59.6666667	685	931.8101667	45.81333333	736.911	141.6666667	39.71436667	24.54766333	0.020061667
HMW PMMA	30	76.6666667	788.3333333	538.3534333	37.67	411.8083333	190	28.6744	18.84422667	0.009899
POLYSTYROL	30	79	886.6666667	571.9037333	39.24666667	407.969	183.3333333	34.00655	16.14875	0.008385
PC XP41 RS	30	90	901.6666667	0.050938667	44.38	744.736	186.6666667	40.29318333	26.19425667	0.03407
HDPE	30	106.666667	566.6666667	0.1178232	42.18666667	758.6373333	206.6666667	37.05686667	30.36354333	0.099876667
PS MUSTER	30	108.333333	428.3333333	358.5521	52.83333333	412.9013333	160	39.308	8.345887333	0.118125
PXC 31	30	118	933.3333333	1057.9816	55.26666667	412.7623333	296.6666667	43.46846667	21.66092667	0.02099
DUROLON PC	30	193.333333	1111.666667	0.247270833	50.18	429.3793333	316.6666667	30.13416667	30.20258333	0.324397333
CYREX200 PC ALL	30	239.333333	1106.666667	0.0679701	51.74333333	362.021	360	50.1988	19.80914667	0.120092333
PETG	30	276	593.3333333	0.044393233	62.49	55.05533333	166.6666667	61.07880333	5.747869333	0.056661667
PXC 31	40	40	560	1137.216333	50.24	525.84	108.3333333	48.50896667	22.45607333	0.062246667
POLYSTYROL	40	46.3333333	568.3333333	786.7338	45.49333333	523.9803333	170	34.13631667	23.23545333	0.071119
POLYPROPYLENE	40	47.3333333	481.6666667	827.0400333	50.85666667	533.5976667	151.6666667	43.7443	17.76884667	0.068691667
HMW PMMA	40	50.3333333	841.6666667	634.2952333	36.76333333	498.8746667	148.3333333	29.4753	22.23682	0.009299667
UPVC	40	54.6666667	723.3333333	958.5298333	48.37333333	595.006	145	39.52216667	28.77716667	0.656068667
PETG	40	58.3333333	688.3333333	1033.514133	44.54	784.9643333	146.6666667	40.67501333	25.92435667	0.022585
HDPE	40	62	541.6666667	1064.739433	41.82666667	753.2743333	156.6666667	37.7783	27.72723333	0.055655
PS MUSTER	40	63.3333333	615	570.0122	50.68	430.5666667	113.3333333	40.75985	13.40952167	0.028031667
DUROLON PC	40	76.6666667	886.6666667	937.7019	50.08	383.039	246.6666667	40.08983333	19.39008667	0.061766667
PC XP41 RS	40	88.3333333	906.6666667	1043.8304	54.41333333	408.118	253.3333333	45.80143333	19.84467	0.018637667
PS 185K	40	95	585	157.0598967	61.65333333	124.4533333	191.6666667	36.5353	4.487573667	0.083925
CYREX200 PC ALL	40	121.333333	841.6666667	1015.686933	52.42666667	479.8843333	256.6666667	43.26586667	31.35816667	0.235452

Material	Applied Q	t ign	Test Time	Total HR	Original Mass	Pk RHR	t(Pk RHR)	Rec Mass Loss	EHC (kJ/g)	MLR50
PXC 31	50	24.3333333	766.6666667	1050.7773	51.65666667	496.714	95	53.10683333	18.51706333	0.013046
POLYPROPYLENE	50	26	761.6666667	1672.765	69.43333333	889.9726667	233.3333333	72.18705	22.21884889	#DIV/0!
PS MUSTER	50	29.6666667	535	1601.282667	47.66666667	844.0353333	236.6666667	68.49883333	22.20302	#DIV/0!
HMW PMMA	50	34	803.3333333	769.1306667	37.17	560.5016667	128.3333333	43.619	30.93413333	0.024023667
HDPE	50	41.5	857.5	1109.8575	42.285	774.0325	117.5	43.290175	26.16803	0.00994
PETG	50	42	793.3333333	1010.3599	44.52333333	729.864	113.3333333	41.14053333	27.06021667	0.036606333
PS 185K	50	47	1051.666667	474.1179	62.52666667	140.4816667	101.6666667	51.58725	6.920512667	0.030707667
POLYSTYROL	50	48.3333333	1321.666667	883.6514	38.66666667	623.3963333	151.6666667	31.70506667	26.83835111	#DIV/0!
UPVC	50	53	856.6666667	594.6307333	53.30666667	499.438	110	37.4283	14.55002	0.018420667
DUROLON PC	50	63	728.3333333	1003.9476	47.23333333	510.534	175	43.14466667	26.95198333	0.032974667
PC XP41 RS	50	70.3333333	1235	1370.919333	55.22333333	551.402	211.6666667	50.37873333	23.15974667	0.019596667
CYREX200 PC ALL	50	77.3333333	935	1140.506333	51.59333333	529.4156667	180	47.74825	33.84616667	0.019179
HMW PMMA	60	26	761.6666667	1672.765	69.43333333	889.9726667	233.3333333	72.18705	22.21884889	
PC XP41 RS	60	29	958.3333333	876.9635	40.57	587.6856667	110	37.41736667	23.17684778	0.008003
POLYPROPYLENE	60	29.3333333	1261.666667	924.0344667	36.7	579.997	135	29.0135	31.36498056	
LMW PMMA	60	29.6666667	535	1601.282667	47.66666667	844.0353333	236.6666667	68.49883333	22.20302	
PXC 31	60	31.6666667	1288.333333	941.5141333	39.23333333	687.955	133.3333333	32.56783333	28.83353444	#DIV/0!
POLYSTYROL	60	35	1207.5	1109.8555	44.2	845.4645	147.5	43.09545	25.46523917	#DIV/0!
PS MUSTER	60	35	1203.333333	1134.852667	44.33333333	905.1326667	146.6666667	43.23183333	25.65323111	
UPVC	60	35.6666667	1053.333333	593.292	62.16333333	184.7863333	120	54.17926667	8.647593333	0.025513
CYREX200 PC ALL	60	36	1015	1173.74	45.8	974.1366667	146.6666667	44.91081667	25.62432833	#DIV/0!
PS 185K	60	36	1015	1173.74	45.8	974.1366667	146.6666667	44.91081667	25.62432833	
HDPE	60	48.3333333	1321.666667	883.6514	38.66666667	623.3963333	151.6666667	31.70506667	26.83835111	
PETG	60	55.6666667	1210	1142.319367	50.70333333	506.811	160	43.05628333	23.44451667	0.016836
DUROLON PC	60	68	1005	1006.776	53.12	458.101	175	45.3429	18.90456	0.021352

A.2 The exact solution for melting of a semi infinite slab (Carslaw, 1959)

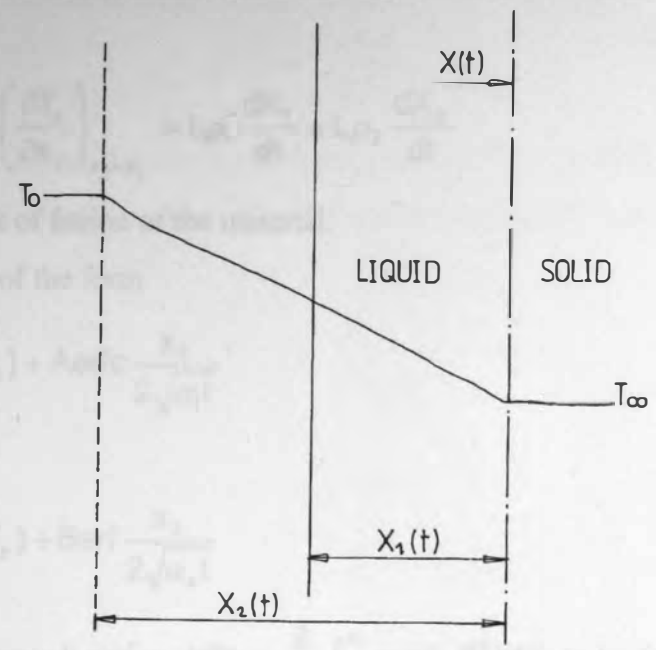

Figure 1. Diagram of exact solution for semi infinite melting plate

A semi-infinite plate is exposed to a heat flux, which causes it to melt. As shown above, the melt front moves from left to right, as does the plate surface owing to the density difference between solid and liquid phases. The problem is assumed to be 1-D and transient. To the left of the melt front, ($x < X(t)$), the material is liquid with properties k_l, α_l, ρ_l, C_{pl}. The heat balance is written as:

$$\frac{\partial^2 T}{\partial x_1^2} - \frac{1}{\alpha_1}\frac{\partial T}{\partial t} = 0 \qquad 1$$

at the left hand surface, $T = T_0$ at $x_l = 0$.

To the right of the melt front ($x > X(t)$), the material is solid with properties k_s, α_s, ρ_s, C_{ps}. The heat balance is written:

$$\frac{\partial^2 T}{\partial x_2^2} - \frac{1}{\alpha_s}\frac{\partial T}{\partial t} = 0 \qquad 2$$

and far away from the surface $T = T_\infty$ at $x_2 \rightarrow \infty$.

Because the density of the material changes with phase

$$\frac{X_1}{X_2} = \frac{\rho_s}{\rho_l} = \beta \qquad 3$$

At the interface where $x_1 = X_1(t)$ or $x_2 = X_2(t)$, $T_0 = T_\infty = T_p$, where T_p is the temperature at which the material melts. A heat balance at the interface yields:

$$k_l\left(\frac{\partial T_l}{\partial x_1}\right)_{x_1=X_1} - k_s\left(\frac{\partial T_s}{\partial x_2}\right)_{x_2=X_2} = L\rho_1\frac{dX_1}{dt} = L\rho_2\frac{dX_2}{dt} \quad (4)$$

where L is the heat of fusion of the material.

Assume solutions of the form

$$T_l - T_0 = (T_0 - T_p) + A\,\mathrm{erfc}\frac{x_1}{2\sqrt{\alpha_l t}} \quad (5)$$

and

$$T_s - T_0 = (T_\infty - T_p) + B\,\mathrm{erf}\frac{x_2}{2\sqrt{\alpha_s t}} \quad (6)$$

where erf z is the error function $\mathrm{erf}z = \frac{2}{\sqrt{\pi}}\int_0^{z_0}\exp(-\beta^2)d\beta$ and erfc = 1 erf z (Drysdale, 1999). At the interface:

$$T_p - T_0 = A\,\mathrm{erfc}\frac{X_1}{2\sqrt{\alpha_l t}} \quad (7)$$

and

$$(T_p - T_\infty) = B\,\mathrm{erf}\frac{X_2}{2\sqrt{\alpha_s t}} \quad (8)$$

Equations (7) and (8) must hold for all values of X_1 and X_2, which must therefore be proportional to $\sqrt{t}$. Therefore, using equation (3):

$$X_1 = k\beta\sqrt{t}, X_2 = K\sqrt{t} \quad (9)$$

where K is a constant.

Applying the results of equations (5),(6)and (9) to equation (4):

$$\frac{Ak_l}{\sqrt{\pi\alpha_l}}\exp\left(\frac{-K^2\beta^2}{4\alpha_l}\right) + \frac{Bk_s}{\sqrt{\pi\alpha_s}}\exp\left(\frac{-K^2\beta^2}{4\alpha_s}\right) = \frac{1}{2}L\rho_l K\beta \quad (10)$$

Then using equations (7) and (8):

$$\frac{(T_p - T_0)k_1 \exp\left(\frac{-K^2\beta^2}{4\alpha_1}\right)}{\sqrt{\pi\alpha_1}\,\mathrm{erfc}\left(\frac{K\beta}{2\sqrt{\alpha_1}}\right)} - \frac{(T_\infty - T_p)k_s \exp\left(\frac{-K^2}{4\alpha_s}\right)}{\sqrt{\pi\alpha_s}\,\mathrm{erf}\left(\frac{K\beta}{2\sqrt{\alpha_s}}\right)} = \frac{1}{2}L\rho_1 K\beta$$

This equation then has to be solved numerically to find K in terms of the temperatures and thermal properties of the material, and hence the values of A and B.

THE EFFECT OF THE MELT-FLOW PROCESS ON THE FIRE BEHAVIOUR OF THERMOPLASTICS

Jo Sherratt & Dougal Drysdale
Fire Research Group
School of Civil & Environmental Engineering
University of Edinburgh

ABSTRACT

An area largely overlooked by the fire research community to date is the effect of the melt-flow process on the potential for fire spread in situations involving substantial quantities of thermoplastic material. If a vertical array of items made of a typical thermoplastic such as polypropylene (e.g. plastic crates) becomes involved in fire, a polymer melt will form, flowing downward as a burning liquid to form a pool fire at the base of the array. Although the consequences of this behaviour have been observed and are known to be potentially serious, the effect has never been quantified. The absence of any standard procedure makes it impossible to assess the magnitude of the fire hazard posed in locations where large quantities of thermoplastics and thermoplastic goods are stored. This paper presents an experimental method to quantify the effect of the melt fuelled pool fire on the overall fire development process, and also some results showing the importance of flooring material on pool fire development.

INTRODUCTION

Previous work undertaken at the University of Ulster[1], investigating upward flame spread behaviour over vertical sheets of thermoplastics, found the mechanism differed between melting and non-melting materials. The thermoplastic sheets, 2.2m (high) x 0.8m x 0.003m were screwed onto an insulating mounting board, and ignited using a standard BS No 7 crib[2]. For a non-melting thermoplastic, polymethylmethacrylate (PMMA), flame spread was driven by the fire plume attached to the vertical surface. The rate of upward flame spread was extremely rapid over the PMMA panel, which burned out at 7 minutes. This is in sharp contrast to the flame spread rate over a melting material, e.g. polypropylene. After the polypropylene was ignited combustion was confined to a small area, and the fire grew slowly from the base of the panel where molten polymer fed a growing pool fire. From this stage, flame spread on the vertical panel was controlled by the height and width of the fire plume from the pool fire, rather than the flame produced at the vertical surface. The height and width of the fire plume of the pool fire are functions of pool area, which depends on the entry flow rate of material feeding it. The duration of the pool fire was around 55 minutes, lasting around 8 times longer than the fire from the non-melting panel.

To investigate further the role of the melt-flow process in the burning of thermoplastics, including plastic crates and polypropylene sheets, a series of experiments has been carried out at Edinburgh University. An apparatus (known as the 'Sedan Chair') has been developed which allows burning on the vertical surface to be studied in the absence of the pool fire that would normally develop. This provides data on the proportion of the total mass lost from the vertical array that enters (or has the potential to enter) a developing pool, i.e. how much fuel is available to form a pool fire at the base of the burning material. The apparatus is also used

to examine the effect that the burning pool has on the burning of the vertical array. In comparison to the rate of burning of a vertical array without the formation of a pool fire, the pool fire significantly increases both the rate of flow of molten polymer into the pool and the rate of burning at the vertical surface. It is the pool fire at the base that dominates the fire size and the rate at which it grows, after an initial phase during which molten fuel flows downwards to start the formation of a pool. It is suggested that the latter process is important in determining the magnitude of the fire hazard and that proper assessment will require a deeper knowledge of the melt-flow process and the properties of the melt. The hazard is influenced to some extent by the nature of the flooring material which can affect the rate of development of the pool fire.

This paper forms part of a three-year study into the fire behaviour of thermoplastics commissioned by the Health and Safety Executive. A significant objective is to develop a method by which the fire hazard associated with these materials in storage may be assessed on the basis of measurable material properties. In view of the large quantities of these materials that are found in warehouses and other storage facilities, such a method of assessment is long overdue.

METHOD

Rate of heat release ($\dot{Q}_c$) is the main variable used to characterise fire size[3], given by[4]:

$$\dot{Q}_c = \chi \dot{m}'' A_f \Delta H_c \qquad [1]$$

where $\dot{m}''$ is the rate of burning (g/m^2 s);
A_f is fuel surface area (m^2);
ΔH_c is the heat of combustion of volatiles (kJ/g); and
χ is a factor (< 1) accounting for incomplete combustion.

Therefore, heat release rate is dependant on rate of burning, generally expressed as[4]:

$$\dot{m}'' = \frac{\dot{Q}_F'' + \dot{Q}_E'' - \dot{Q}_L''}{L_v} \qquad [2]$$

where; $\dot{Q}_f''$ represents the heat flux supplied by the flame (kW/m^2);
$\dot{Q}_E''$ represents any additional external heat flux (kW/m^2)
$\dot{Q}_L''$ indicates the surface heat loss term (kW/m^2); and
L_v is the latent heat required to produce volatiles (kJ/g).

Using these equations, if the mass loss components for a melting and burning thermoplastic are separated, then the component contributions to overall rate of heat release can be assessed. Experimentally, it has been found that any attempt to hold a specimen of thermoplastic in a vertical orientation during a test will inevitably result in failure as the material softens and liquifies.

A system was therefore developed, in which an unrestrained specimen was placed in a wire mesh basket as shown in Figure 1. The basket was welded to two steel bars, the ends of which rested on load cells, allowing the melt to flow downward through the grid supporting the specimen and be collected in a tray (0.5m x 0.5m x 0.1m deep) located directly below. When

it was required to extinguish the burning melt, the tray was ¾ filled with high flashpoint oil, ('TERESSO 100', flashpoint 529K), which acted to quench the burning flow. However, it was necessary to stir the oil during the test to prevent formation of a 'raft' of burning melt, which would eventually result in ignition of the oil. Although polypropylene is denser than the oil, ($\rho_{polypropylene} \approx 940 kg/m^3$ compared to $\rho_{oil} \approx 885 kg/m^3$) and should therefore sink, the polypropylene melt produces a lower density 'wax', which floats on the oil. This technique was very successful, providing that no more than ~1 kg of plastic was allowed to collect in the tray

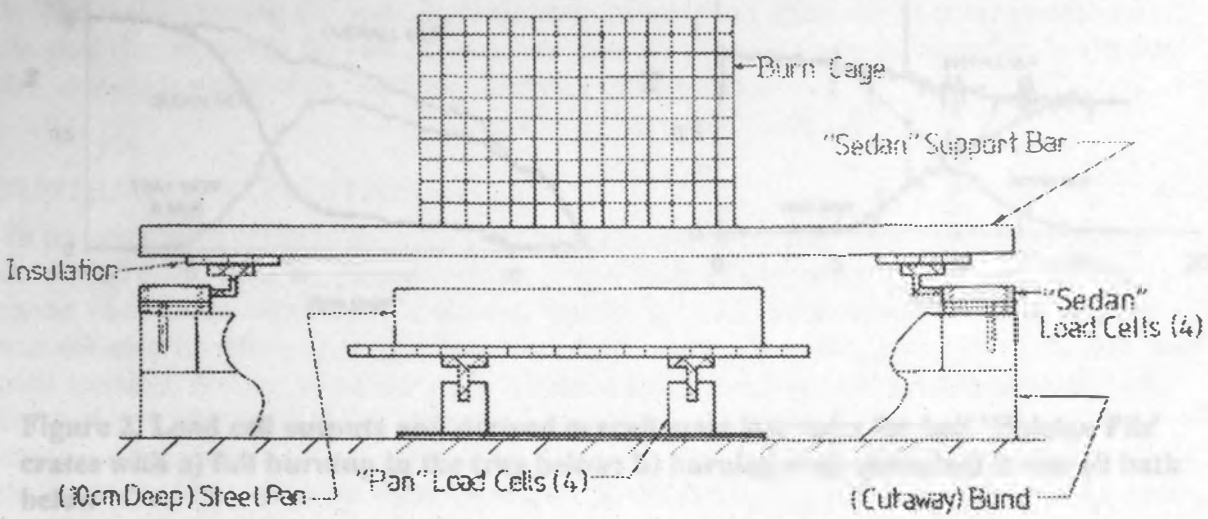

Figure 1 Schematic illustration of the 'Sedan Chair' rig (not to scale)

As shown in Figure 1, two independent load cell systems were used to measure the total mass loss from the sedan, and the mass gain into the pan below.

Considering the load cell outputs;

$$\frac{dm}{dt}(\text{sedan}) = \left[\frac{dm}{dt}(\text{sedan burning}) + \frac{dm}{dt}(\text{pan gain})\right] \qquad [3]$$

where; $\frac{dm}{dt}(\text{sedan})$ is the rate of mass loss measured by the sedan load cells;

$\frac{dm}{dt}(\text{sedan burning})$ is the rate of mass loss due to burning in the sedan;

$\frac{dm}{dt}(\text{pan gain})$ is the rate of mass change measured by the pan load cells, e.g.

$$\frac{dm}{dt}(\text{pan gain}) = \left[\frac{dm}{dt}(\text{flow from sedan}) - \frac{dm}{dt}(\text{tray burning})\right] \qquad [4]$$

Therefore, the total burning rate in the sedan rig can be derived from the two load cell outputs, and compared for both burning and non-burning conditions in the pan below, as illustrated overleaf.

SOME EXPERIMENTS

A 'Holsten Pils' yellow beer crate, (overall dimensions 33 x 39.5cm x 25cm high), was halved and burned in two tests; a full burn followed by quenching the burning melt for comparison. During the tests, carried out in the Edinburgh University Fire Calorimeter, mass losses, duct pressure, temperature and O_2, CO_2 and CO concentrations were monitored at a 3 second sample frequency.

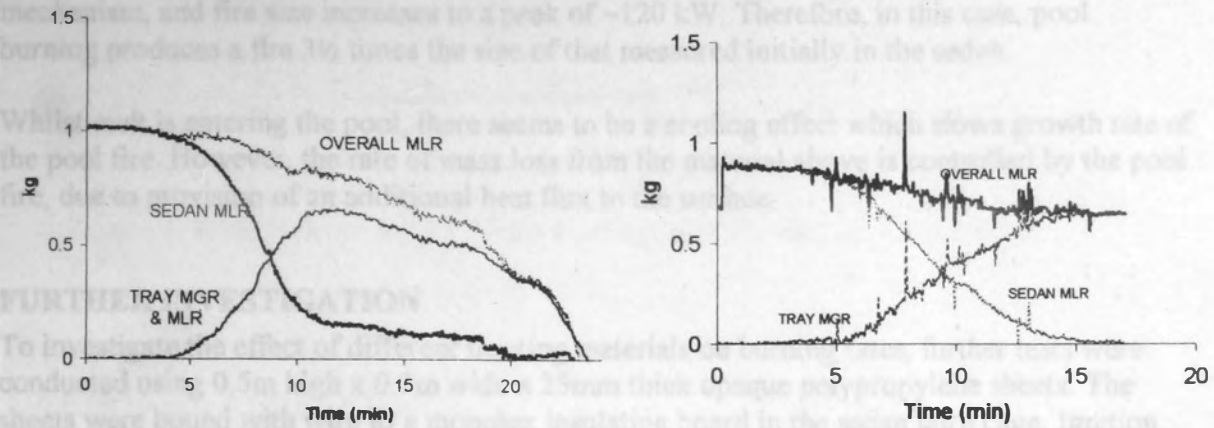

Figure 2. Load cell outputs and derived overall mass loss rates for half 'Holsten Pils' crates with a) full burning in the tray below; b) burning melt quenched in the oil bath below

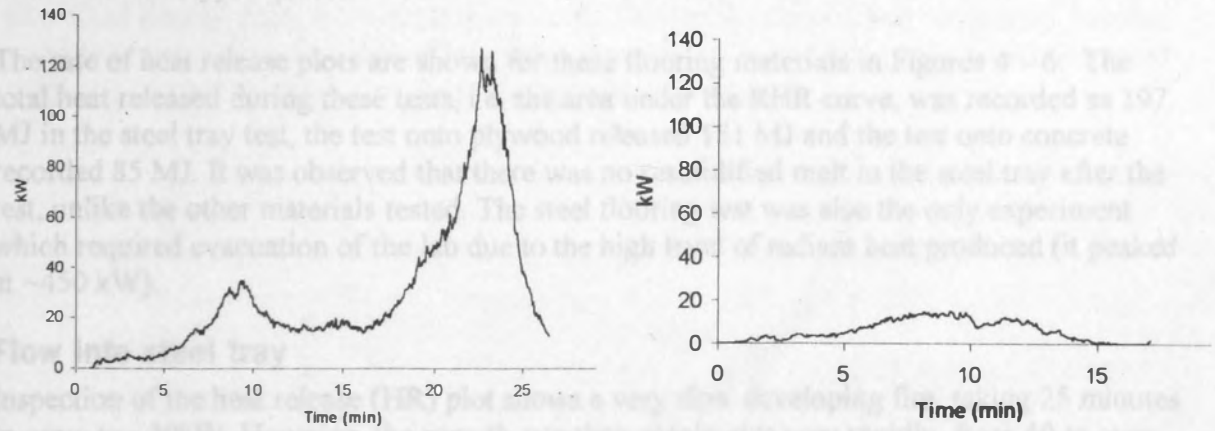

Figure 3. Heat release rates (HRR) (from oxygen depletion) for half 'Holsten Pils' crates with a) full burning in the tray below; b) burning melt quenched in the oil bath below

Figures 2 and 3 above show the mass flows and measured heat release rates for the two half crate tests a) full burning in sedan & tray; and b) burning in sedan, burning melt quenched by oil in the tray. The load cell outputs for the second case illustrates that ~80% of the mass lost from the sedan enters the tray, as potential fuel for a pool fire. Comparison of the HRR plots show clearly that most of the heat release is from the pool fire in the tray beneath the sedan.

(It was found that in most of the experiments conducted during this project 75 – 80 % of the original mass flowed into the quenching tray.)

Closer inspection of the data from the full burning tests shows a first peak of around 35 kW on the heat release curve, corresponding to a region dominated by mass loss from the sedan. Fire size remains constant for a time as the volume of molten feed into the pan is reducing, at ~20 kW. Then, as the pan fuel feed stops, pool burning becomes the dominant mass loss mechanism, and fire size increases to a peak of ~120 kW. Therefore, in this case, pool burning produces a fire 3½ times the size of that measured initially in the sedan.

Whilst melt is entering the pool, there seems to be a cooling effect which slows growth rate of the pool fire. However, the rate of mass loss from the material above is controlled by the pool fire, due to provision of an additional heat flux to the surface.

FURTHER INVESTIGATION

To investigate the effect of different flooring materials on burning rates, further tests were conducted using 0.5m high x 0.3m wide x 25mm thick opaque polypropylene sheets. The sheets were bound with wire to a monolux insulating board in the sedan burn cage. Ignition was achieved by slowly passing a blowtorch flame across the width, 10cm above the slab base until sustained flaming was observed. Below the sedan, the 'flooring' substrates tested were the steel tray referred to above, a concrete paving slab measuring 0.45m x 0.45m x 0.03m thick, and a 0.49m x 0.49m x 0.02m thick plywood sheet, both of which were placed inside the steel tray. These flooring materials were selected as a review of fire incident reports such as 'Plastics Products Factory'[5] in 'Fire Prevention' found them to be the three most common industrial floor types quoted.

The rate of heat release plots are shown for these flooring materials in Figures 4 – 6. The total heat released during these tests, i.e. the area under the RHR curve, was recorded as 197 MJ in the steel tray test, the test onto plywood released 151 MJ and the test onto concrete recorded 85 MJ. It was observed that there was no resolidified melt in the steel tray after the test, unlike the other materials tested. The steel flooring test was also the only experiment which required evacuation of the lab due to the high level of radiant heat produced (it peaked at ~450 kW).

Flow into steel tray

Inspection of the heat release (HR) plot shows a very slow developing fire, taking 25 minutes to grow to ~30kW. However, the growth rate then accelerates very rapidly, from 40 to over 450 kW in just four minutes.

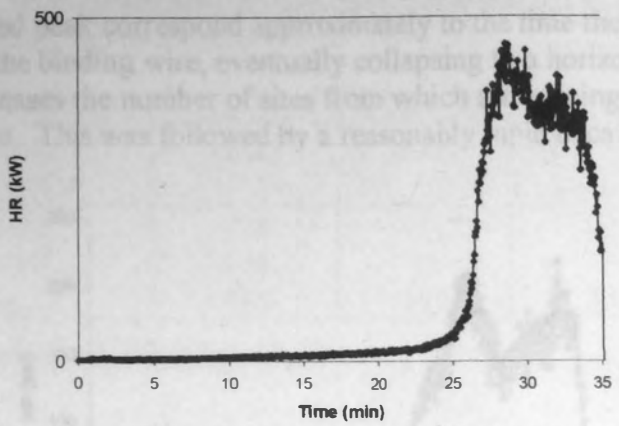

Figure 4. Heat Release for PP Sheet burning and flowing into a steel tray

Flow onto the concrete slab

Inspection of the HR plot (Figure 5) shows a slow, steadily growing fire taking 45 minutes to reach a peak of 112 kW, followed by a rapid decay over 4 minutes. Around a quarter of the initial mass accumulated on the slab as re-solidified melt by the end of the test. Some adjustment of the sheet was required as the sheet slumped to the side and melt was overshooting the slab area below. A burning pool below the sedan was only sustained when exposed to radiation from the burning material in the sedan cage above the pool. Burning melt which had flowed away from directly under the flaming feed area could not sustain flaming conditions and eventually resolidified. When the material in the sedan had flowed or burned away, the fire on the slab below immediately self extinguished.

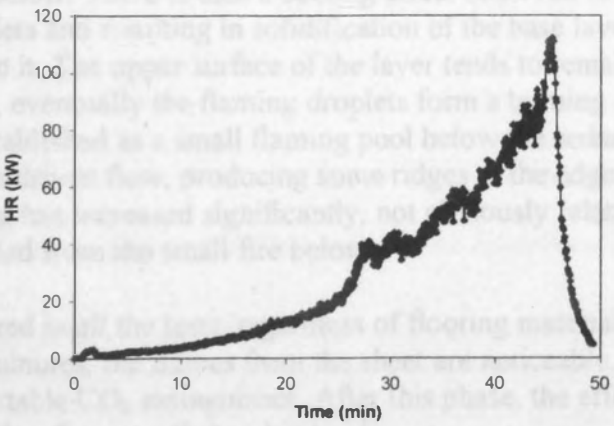

Figure 5. Heat Release for PP Sheet burning and flowing onto a concrete slab

Flow onto plywood sheet

The heat release plot in Figure 6 shows a very slowly developing fire, taking 20 minutes before accelerating over 8 minutes or so to a first peak of ~200 kW. The fire then decays over 3 minutes to ~ 130kW, before growing over to ~ 190 kW over the next four minutes. This

increase and the second peak correspond approximately to the time the remaining solid material folded over the binding wire, eventually collapsing to a horizontal position in the sedan. This then increases the number of sites from which the burning melt entered the pool, increasing the fire size. This was followed by a reasonably rapid decay rate to extinction.

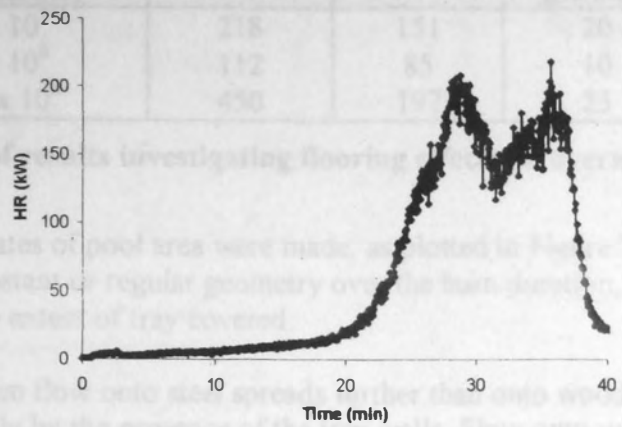

Figure 6. Heat Release for PP sheet burning & flowing onto plywood

DISCUSSION OF FLOORING EFFECT ON FIRE GROWTH

The results are summarised in Table 1. In all the tests the polypropylene sheet undergoes a relatively long incubation period after ignition before significant fire growth occurs. The sheets, which were ignited 10 cm above the base, all exhibited initial slow downward flame spread, taking up to 10 minutes to cover the 10cm or so with stable flame. The downward spread mechanism is caused by movement of the surface layer the flame is attached to. This moving layer then drips sporadically from the base of the sheet, the droplets flaming as they fall onto the substrate below. There is then a cooling effect observed in all the tests, extinguishing the droplets and resulting in solidification of the base layer, which builds up as other droplets land onto it. The upper surface of the layer tends to remain liquid, as the dripping rate increases, eventually the flaming droplets form a burning liquid stream, which eventually becomes established as a small flaming pool below the sedan rig. This pool exhibits surface tension driven flow, producing some ridges at the edge. By this time, the area of sheet surface flaming has increased significantly, not obviously related to any increase in surface heat flux supplied from the small fire below.

This early phase occurred in all the tests, regardless of flooring material, and for practical purposes, for over 10 minutes, the flames from the sheet are noticeable, and easily extinguished with a portable CO_2 extinguisher. After this phase, the effect of flooring becomes a factor affecting fire growth development.

Comparing results, flow into the steel tray after the ignition to growth phase, produces the fastest growing and largest fire of the floorings tested. The total heat released is ~ double that of the fire with the wooden substrate, and almost four times that of the fire developing onto concrete. The peak HR is 25% greater than for a wood base, and four times greater than that on the concrete slab. The fire onto steel has the longest incubation period, followed by the fastest growth rate and the shortest fire duration. It was also the only test where the entire

'floor' was covered in flaming material, no polymeric melt was left after the test, and the level of radiant heat necessitated lab evacuation.

Flooring material	Thermal inertia[4] of floor (W^2s/m^4K^2)	Peak RHR (kW)	Total HR (MJ)	Time (min) (ignition to growth)	Time (min) (growth to peak RHR)
Wood	3×10^5	218	151	20	8
Concrete	2×10^6	112	85	10	35
Steel	1.6×10^8	450	197	23	4

Table 1. Summary of results investigating flooring effects on overall burning behaviour

During the tests estimates of pool area were made, as plotted in Figure 7. The pools formed tend not to exhibit constant or regular geometry over the burn duration, so the areas quoted are estimated from the extent of tray covered.

From the results, molten flow onto steel spreads further than onto wood or concrete, and the pool area is limited only by the presence of the tray walls. Flow onto wood spreads faster initially than onto concrete, which is faster than onto steel, but both the wood and concrete pool burning areas were self-limiting.

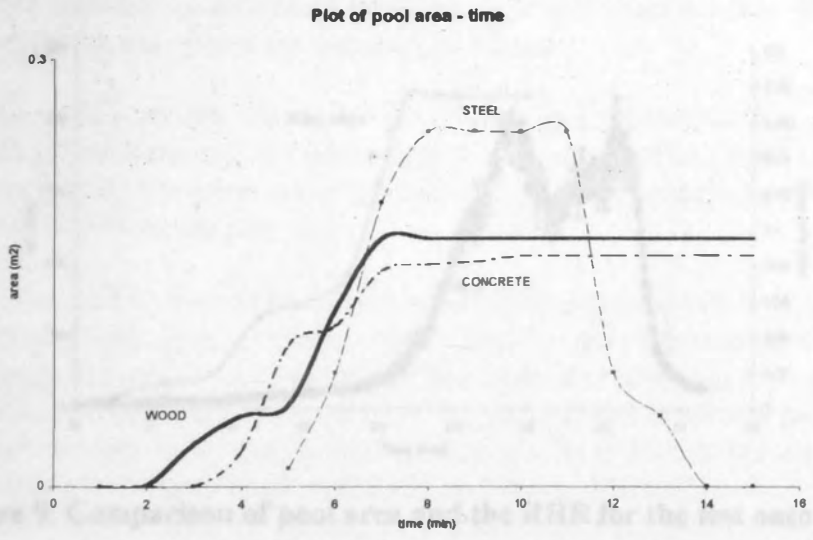

Figure 7. Estimated pool area - time correlations

The pool spread rate onto steel shows a slow initial phase, followed by a smooth rapid acceleration to maximum possible area. This is compared to the measured RHR in Figure 8. The plot shows that the acceleration to peak of fire growth corresponds to full area burning of the pool. This trend is also found on the plot comparing HR and pool area for the plywood base, shown in Figure 9.

Figure 9 shows the molten pool spreading onto a wooden base increases area gradually over the first 10 minutes or so, and then more rapidly followed by a slowing, and finally a much faster spread rate which is ultimately self-limiting. The end of the gradually increasing phase approximately corresponds to the start of the molten material burning, and the faster spreading rate corresponds to the time the wood began to burn.

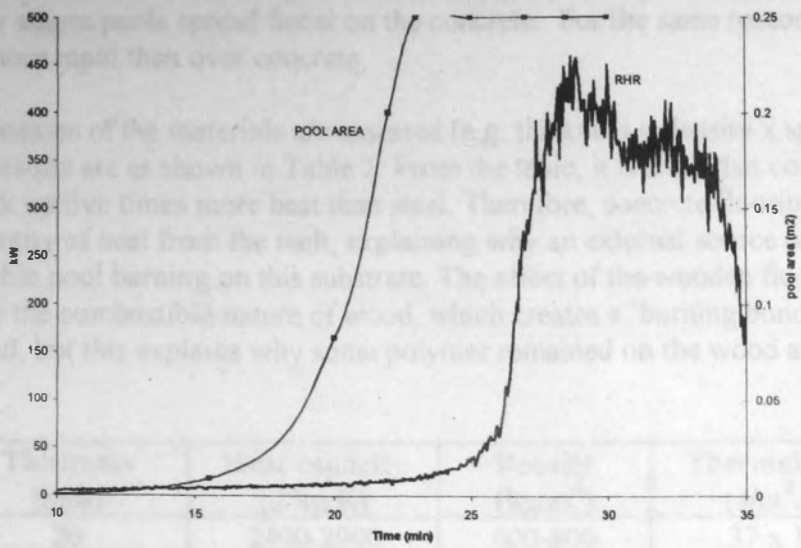

Figure 8. Comparison of pool area and the RHR during the steel tray test

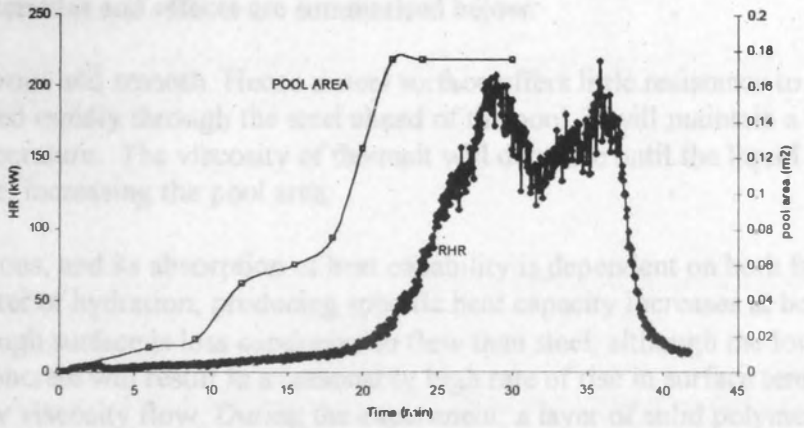

Figure 9. Comparison of pool area and the RHR for the test onto wood

These tests indicate that for a pool formed on a steel base, the extent of spread is controlled by either the amount of material available, or physical containment barriers. In contrast, a combustible wooden substrate may limit spread, whilst a concrete substrate enables spread, but will not sustain burning after the external flame flux has been removed.

CONSIDERATIONS

The spreading pool potential area is controlled by viscosity, which is partially dependent on thermal conductivity / thermal inertia of the floor substrate. The high thermal inertia of the steel floor, shown in Table 1 indicates that heat will be rapidly conducted into the steel bulk. The high thermal conductivity of steel (45.8 W/mK compared to 0.8 – 1.4 for concrete and 0.14 – 0.17 for wood[4]) then ensures a uniform temperature is rapidly achieved through the material. Therefore liquid spread on steel is initially very slow as the floor cools the melt thus causing its viscosity to increase and reduce the pool spread rate. Once the steel has reached a

uniform high temperature, the melt viscosity is remain low thus enabling rapid pool spread. In contrast, the lower thermal inertia of concrete will result in less rapid cooling of the melt so that in the early stages pools spread faster on the concrete. For the same reason, initial spread over wood is more rapid than over concrete.

If the thermal masses of the materials are assessed (e.g. thickness x density x specific heat capacity), the results are as shown in Table 2. From the table, it is clear that concrete has the capacity to soak up five times more heat than steel. Therefore, concrete flooring removes a significant quantity of heat from the melt, explaining why an external source of heat is required to enable pool burning on this substrate. The effect of the wooden floor is complicated by the combustible nature of wood, which creates a 'burning bund' to restrict pool area spread, but this explains why some polymer remained on the wood after the pool burnout.

Floor	Thickness (mm)	Heat capacity (J/kg.K)	Density (kg/m^3)	Thermal mass ($J/m^2.K$)
Wood	20	2400-2900	600-800	37×10^3
Concrete	30	880	1900-2300	55×10^3
Steel	3	460	7850	10×10^3

Table 2. Thermal masses of flooring materials tested.

In addition to the thermal characteristics, surface texture will effect the flow rates. The textural characteristics and effects are summarised below:

Steel is non-porous and smooth. Hence a steel surface offers little resistance to flow and as heat is conducted rapidly through the steel ahead of the pool, it will maintain a uniform but increasing temperature. The viscosity of the melt will decrease until the liquid flows rapidly over the surface, increasing the pool area.

Concrete is porous, and its absorption of heat capability is dependent on both free moisture content and water of hydration, producing specific heat capacity increases at both 100 and ~ 450°C[4]. The rough surface is less conducive to flow than steel, although the lower thermal inertia of the concrete will result in a reasonably high rate of rise in surface temperature, maintaining low viscosity flow. During the experiment, a layer of solid polymer eventually formed across the slab surface, which whilst fed by flaming material, sustained surface burning. However, shortly after the burning flow into the pool stopped, the pool self extinguished, leaving a solid layer ~ 5 – 8 mm thick over the surface.

Wood changes properties completely during a fire. Initially flat, and moderately rough with a free moisture content, wood is a combustible material, comprising ~20 – 30% cellulose, 50 – 60% semi-cellulose, and 20 – 30 % lignin[4]. Due to the composition, which varies between species, combustion occurs in stages and produces a rough black char, breaking up the initially flat surface. During the test, it was noted that the flaming combustion of the wood restricted the possible area increase of the burning pool. This was partly due to a burning area directly below the drip feeding sites preventing build up of a smooth solidified plastic layer over which the low viscosity melt could flow, extending the pool as happened on the concrete surface. The other control mechanism was the cracked surface, slightly raised at the crack edges, which diverted liquid flow down into the crack rather than over the horizontal surface.

NB During this test, this mechanism restricted pool fire spread. However, diverting burning liquid into cracks caused by burn through, as occurred in the test, will restrict the spread area above but could spread fire to the area below.

Conclusions

It has been confirmed that increasing pool fire area increases overall rate of heat release, and therefore the radiant flux supplied to the material feeding the pool. This loop mechanism increases the flow rate into the pool and the burning rate of the pool.

These experiments show, in agreement with Zhang *et al.*[1], that for a thermoplastic exhibiting melt-flow behaviour, the fire size and rate of growth are controlled by the pool fire formed at the base of the burning flowing material.

Results from the oil quenched experiments, show 70 – 80% of the mass loss from the array will enter the pool.

After an initial relatively long growth phase, the material properties of the flooring substrate are influencing parameters on the burning rate of the pool and therefore overall fire growth and development.

ACKNOWLEDGEMENTS

The authors are pleased to acknowledge the financial support of the UK Health & Safety Executive during this research project.

REFERENCES

[1] Zhang, J., Shields, T.J., Silcock, G.W.H., "Effect of melting behaviour on flame spread of thermoplastics" Fire & Materials, Vol. 21, No 1. Jan – Feb 1997 pp 1 - 6

[2] "BS 5852: 1990. Methods of test assessment of the ignitability of upholstered seating by smouldering and flaming ignition sources", BSI London, 1990.

[3] Baubraskas V., Peacock R., "Heat Release Rate: the single most important variable in fire hazard" Fire Safety Journal, Vol.18, pg 255 - 272

[4] Drysdale, D.D., "An introduction to fire dynamics, 2nd Ed", Pub Wiley 1999

[5] "Plastics Products Factory, Mansfield Woodhouse, Nottinghamshire" Fire Prevention No 247 March 1992